LIQUID BIOPSY USING THE NANOTUBE-CTC CHIP

By

Seyed Masoud Loeian

A Dissertation

Submitted to the Faculty of the

WORCESTER POLYTECHNIC INSTITUTE

In partial fulfillment of the requirements for the

Degree of Doctor of Philosophy

in

Mechanical Engineering

April 2019

APPROVED:

_____

Professor Balaji Panchapakesan, Advisor

_____

Professor Jamal Yagoobi, Committee Member

_____

Professor Nikhil Karanjgaokar, Committee Member

_____

Professor Shesh N. Rai, Committee Member

_____

Dr. Amy Heintz, Committee Member

_____

Professor Raghvendra V. Cowlagi, Graduate Committee Representative

ABSTRACT

Liquid Biopsy using the Nanotube-CTC Chip

Seyed Masoud Loeian

Worcester Polytechnic Institute 2019

In this work, we describe the development of the nanotube-CTC-chip for capture and enumeration of circulating tumor cells (CTC) in breast cancer patients. The nanotube-CTC-chip is a new 76-element microarray technology that combines carbon nanotube surfaces with microarray batch manufacturing techniques for capture and isolation of tumor-derived epithelial cells.

Using a combination of red blood cell (RBC) lysis and preferential adherence, we demonstrate the capture and enrichment of CTCs with 5-log reduction of contaminating WBCs. EpCAM- MDA-MB-231/Luciferase-2A-Green Fluorescent Protein (GFP) cells were spiked in the blood of wild mice and enriched using an RBC lysis protocol. The enriched samples were then processed using the nanotube-CTC-chip for preferential CTC adherence on the nanosurface and counting the GFP cells enabled anywhere from 89-100% capture from the droplets. Electron microscopy (EM) studies revealed strong focal adhesion with filaments from the cell body to the nanotube surface. The preferential adherence strategy of CTC capture compared to collagen adhesion matrix (CAM) scaffolding method, which in the past reported as a viable strategy for CTC capture in patients. The CAM scaffolding on the device surface yielded 50% adherence with 100%

tracking of cancer cells (adhered and non-adhered) versus carbon nanotubes with >90% adherence and 100% tracking for the same protocol.

The nanotube-CTC-chip successfully captured CTCs in the peripheral blood of breast cancer patients (Stage 1-4) with a range of 4–238 CTCs per 8.5 ml blood or 0.5-28 CTCs per ml. CTCs (based on CK8/18, Her2, EGFR) successfully identified in 7/7 breast cancer patients, and no CTCs captured in healthy controls (n=2). CTC enumeration based on different markers using the nanotube-CTC-chip enables dynamic views of metastatic progression.

ACKNOWLEDGMENTS

This thesis describes a small selection of experiments from a wide range of highly interdisciplinary and collaborative research projects I pursued with others. First and foremost, I would like to thank my thesis advisor Professor Panchapakesan. He consistently allowed this investigation to be my work, but steered me in the right direction whenever he thought I needed it. His persistent and enthusiasm regarding research and scholarship has been an inspiration for me throughout my Ph.D and his advice in the past few years have been priceless. Besides my advisor, I would like to thank the rest of my thesis committee: Prof. Rai and Dr. Heintz who have been our collaborators in this work, and Professor Yagoobi, Professor Cowlagi, and Professor Karanjgaokar for their encouragement and insightful comments.

My sincere thanks go to our collaborators at University of Louisville James Graham Brown Cancer Center: Dr. Aqil, Dr. Mandadi, Dr. Chesney, and Dr. Rai for their input and for providing us the breast cancer patient blood samples. I also would like to thank our collaborators at University of Massachusetts Medical School, Dr. Mark Johnson, Dr. Hongwei Yang, Dr. Rona Carroll, and Dr. Karl Simin for their valuable training and advise through my internship. I gratefully acknowledge the funding sources by the Office of Vice-Provost for Research at Worcester Polytechnic Institute and StrandSmart Inc., and its executive team, Adrianna Davies, Mark Myslinski, and Don Howard that made my Ph.D. work possible. I should also thank Dr. Lambert, Dr. Timko, and Dr. Geoffrey at the Department of Chemistry and Chemical Engineering.

I want to express my special appreciation to my family: my parents and my brother Mahdi who have encouraged me through my life toward greatness and I have been blessed with their prayers and continue love along with my life journey. I thank my fellow labmates especially Sadegh Aghaei for their help. Additionally, I thank my friends Ramin, Adel, Pejman, and Ali for accepting nothing less than excellence from me.

Finally, I must express my very profound gratitude to my wife, Farzaneh for providing me with unfailing support and continuous encouragement throughout my years of study and through the process of researching and writing this thesis. This accomplishment would not have been possible without you. I am looking forward to sharing many more success stories and lovely moments with you.

TABLE OF CONTENTS

LIST OF FIGURES

LIST OF TABLES

ABBREVIATIONS

CTC	circulating tumor cells
DTC	disseminated tumor cells
CNT	carbon nanotubes
SWCNT	single wall carbon nanotubes
FET	field effect transistor
RBC	red blood cell
WBC	white blood cell
FISH	fluorescence in situ hybridization
PCR	polymerase chain reaction
EpCAM	epithelial cell adhesion molecule
PSMA	prostate specific membrane antigen
HER-2	human epidermal growth factor receptor 2
CK	cytokeratin
EDTA	ethylene diamine tetra acetic acid
SES	Socioeconomic status
MWCNT	multi-walled carbon nanotubes
PBS	phosphate-buffered saline
EMT	epithelial mesenchymal transition
McTN	Microtentacle
CAM	collagen adhesion matrix

Chapter 1

INTRODUCTION

A primary tumor is created due to abnormal growth of the cells in major body organ like breast, lung, colon, prostate, ovary and cervix. This primary tumor is treatable in most of the cases. However, cancer takes a deadly turn when it becomes a systemic disease called metastasis. As an example, from every five metastasis breast cancer patients, only one survives [1].

Cancer is the second leading cause of death in the US and metastasis tumors are the main cause of cancer related deaths. Only in the US, there will be approximately 4800 new cancer cases diagnosed each day during 2019 [2]. The early detection of cancer is the key to increase the chance of the patient to survive. However, there is not any general standard test as a routine procedure for different cancer diagnosis.

The imaging techniques do not have the sensitivity and specificity for detecting solid tumors especially in the early stages in most of the cases while the mass is small [3]. Also, these techniques can be the cause of cancer themselves in some cases. Based on the estimations, 1.5-2 % of cancers in the US is caused by computed tomography [3]. Diagnostic ultrasound is a harmless method. however, its capability is limited in organs that contain gas like lung and its resolution is fairly low. Optical detection technologies are useful in cases that the mass is visual like stomach and oral cancers, but it cannot be used for many cancer types and the tumor should be large enough to be observed. Detecting cancer biomarker (i.e., Prostate-specific antigen (PSA) for prostate cancer [4]

and ctDNA [5]) is another option, but this technique is not still accurate and sensitive in many cases.

Currently, most of the cancer diagnosis is taking place when symptoms of the tumor become evident. This means that the lump should be large enough to be noticed. At this point, a biopsy is the gold standard for cancer diagnosis. Surgically, a sample of tissue is taken from the tumor and based on the report of the pathologist from that sample; the final decision can be made on the status of the patient. At that point, it may be already late for treating the patient. According to the American Society of Clinical Oncology (ASCO), 5-6 % of women with breast cancer are still diagnosed at metastasis and final stages.

The mechanism of switching local cancer tumor into the distant metastasis site is very complicated, and it is still under study [6, 7]. However, it has been established that circulating tumor cells (CTCs) are the main component of this process. Since these cells are carrying tumor information in the blood vessels, isolating them in blood samples would be an effective approach for early detection of cancer. Furthermore, isolating CTCs in body fluids during the treatment can provide more information effect of treatment on the disease and its dissemination.

1.1. Circulating tumor cell

CTCs are released from a primary tumor into body fluids, and they are carried around the body in blood or lymph vessels. Studies have shown that individual or cluster of cells are released continuously from the primary tumor amid early stages of cancer and they

are spread all over the body using body vessels [8, 9]. CTCs have attracted a lot of attention since they have the genetic information of tumors and based on seed and soil hypothesis [10], they are mainly responsible for metastasis. The global CTC market has been estimated to be almost $9 billion in 2018, and it includes 400 on-going clinical trials worldwide [11].

Thomas Ashworth, an Australian physician noticed CTCs in the blood of cancer patient [12]. In 1869, he suggested that there should be a connection between multiple tumors in the patient organs and the present of various tumor cells in his blood. Since then, extensive research has been conducted to get more information about these cells. Only in Web of Science database, more than 400 different techniques have been published for isolating CTCs.

Cancer dissemination is very complicated and multiple elements contributing to this process. Figure 1 1 shows the schematic operation of metastasis cascade [6]. The official marks of cancer comprise six biological capabilities acquired during the multistep development of human tumors: sustaining proliferative signaling, evading growth suppressors, resisting cell death, enabling replicative immortality, inducing angiogenesis, and activating invasion and metastasis [13]. Tumor cells obtain these capabilities through several steps.

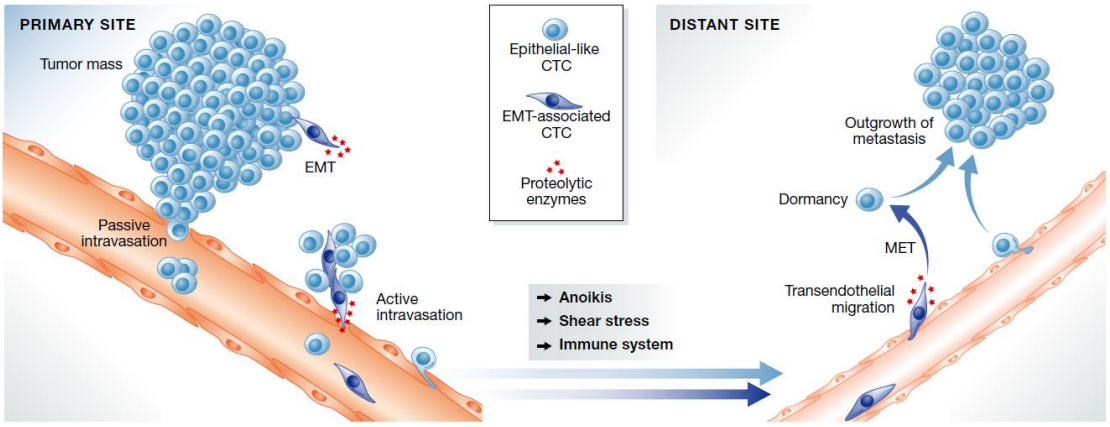

Figure 1. Schematic image of dissemination of CTCs into blood stream and their contribution into creating a metastasis tumor in distant site [6].

First, the CTC should be able to separate themselves from primary mass and enter the lymphatic system alive. The timing of CTC separation is still an unresolved question. It is still not clear if the cell separation from tumor starts as early as the creation of the primary mass itself or it takes some time till these cells evolve and gain the capability of leaving the primary tumor. This step is taking place in two different ways, active and passive [14], depending on tumor type, blood vessel structure, and conditions occurring in the tumor microenvironment [15].

Motile cells are those who are shedding into bloodstream actively. For carcinomas (80% of all cancer cases diagnosed), which are solid tumors derived from epithelial tissues, the transition of tumor cells from Epithelial to mesenchymal is an essential step for the development of motile CTCs. Epithelial-mesenchymal transition (EMT) is a process which epithelial cancer cells from the primary tumor lose their polarity and cell-cell adhesion [6]. During EMT, epithelial cells gain migratory and invasive estate, and they turn into mesenchymal stem cells [16]. At this point, CTCs lose their ability to show epithelial biomarkers like Epithelial cell adhesion molecule (EpCAM) and instead,

mesenchymal biomarker expression will be up-regulated [17]. This mechanism entails alteration of cell morphology, nearby tissue, and position [6].

It should be noted that EMT is a common feature of embryogenesis and it is a part of wound healing and organ development [17]. Although most of the motile cells are separated individually, there may be a few which would be observed as strand, cluster, and single Indian files. EMT cells could have the capability of moving through the surrounding tissue and extracellular matrix, penetrating basement membranes and endothelial walls upon intravasation and extravasation, and entering the lymphatic or blood vessels [6].

Mobile CTCs are the second group of the cells that migrate into body fluids passively. This suggests that an external force like the growth of the tumor, mechanical forces, and friction may be dragging the cells into the vessels [6]. There are still a lot of questions about mobile CTCs, and there is not a lot of information about them. Although these cells may not have the capability of starting a new metastasis site like EMT cells, their genetic information and properties are identical to the primary tumor. This means that isolating these cell can provide us the necessary information on primary mass without an invasive biopsy. This can provide an opportunity to diagnose cancer in the early stages with a simple blood test. Figure 2 shows the schematic of active versus passive migration of CTCs into a blood vessel.

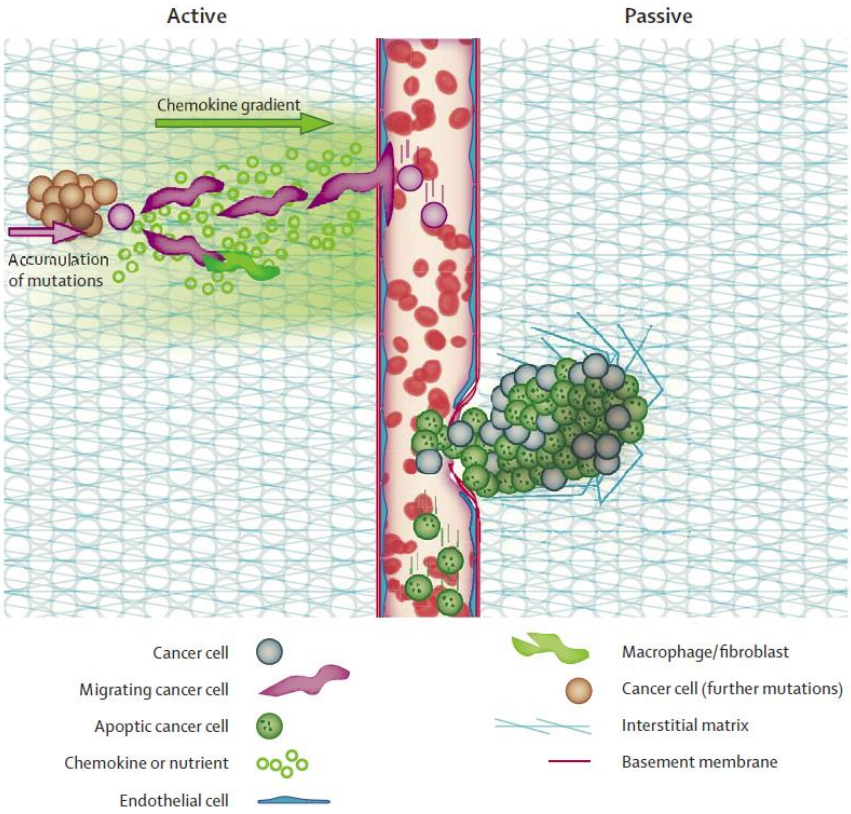

Figure 2. Schematic image of active versus passive movement of CTCs into a blood vessel [18].

Leaky vessels due to angiogenesis [19] and micro-tracks created by other tumor cells [20] are two examples of how passive CTC shedding is happening. High compression of solid tumor on vessels due to uncontrolled growth is the main reason for creating mobile CTCs. These accidental CTCs are mostly epithelial, and epithelial-based biomarkers like EpCAM would be a good choice for identifying them.

The second step for CTCs after entering vessels is surviving against several natural obstacles. Thanks to these obstacles, almost all of CTCs cannot start a new malignant distant tumor. First of all, the large shear forces of bloodstream and collision to normal blood cells can destroy most of CTCs. However, EMT cells which have gone through EMT transition and are more plastic have a higher resistance to these forces, and this is

one of the reasons that EMT cells have a better chance to start a new metastasis site [6]. The second obstacle is anoikis which is a process that triggers apoptosis due to lack of cell-matrix interactions. However, activated tropomyosin-related kinase B (TrkB) helps CTCs to survive in liquid suspension [21]. The other important obstacle for CTCs is the immune system.

The third step for CTCs to create a new metastasis tumor is leaving the vessel and become dormant. The dissemination process will start when the shear forces are decreased in small capillaries like regional lymph nodes, peripheral blood, and in bone marrow. Disseminated tumor cells (DTC) can be found at early stages of tumor progression in cancer patients using proper methods in bone marrow (BM) [22]. DTCs have been found in cancer patients even after several years of primary tumor removal [23]. Having a dormant state gives DTCs the capability of evading systematic therapy, and this makes it even harder to eliminate them entirely [23].

The final step for CTCs to create a distant mass is a mesenchymal-epithelial transition (MET). This process is the reverse of EMT process, and it favors growth and proliferation. This step is essential for the rapid growth of a solid tumor and this new site can itself be a new source of CTCs and dissemination of cancer in the body.

The purpose of discussing the journey that CTCs are going through for creating a new metastasis site is to know how we may be able to separate them among many normal cells in the blood. For healthy human males, the red blood cell (RBC) count is from 4.19 to 5.54 million per microliter while this number for females is 4.00 -5.09 [24]. The normal white blood cell (WBC) count for males is 3.7-9.5 thousand cells per microliter,

and this number for females is 3.9-11.1 [24]. This means that in each milliliter of blood, we are looking for a few CTCs among 4.7 billion normal cells. Many scientists have tackled this problem with a different perspective. However, a viable solution has been elusive during the past century.

Currently, for almost all of carcinoma cancer cases, the prognosis of the patient is determined by blood-borne dissemination of tumor cells [25]. Even for small primary tumors, DTCs in BM, liver, lungs, or brain are identified specific assays [26]. BM is accessible by needle aspiration through the iliac crest, and it has played the most successful role as an indicator organ for minimal residual disease [27]. BM also can be a reservoir for DTCs with the capacity to reenter other distant organs [28]. Continuous monitoring of treatment progress in a cancer patient is crucial in successful survival. Unfortunately, BM needle aspiration is a painful and inconvenient method for the patient and, it makes it difficult to increase the sampling frequency to the desired rate.

Multiple reports have highlighted the CTCs potential as a biomarker for diagnosis and prognosis of cancer [29-36]. Still, there are doubts whether CTCs can be used for early detection of cancer. Interestingly, studies had shown that pancreatic cells with mesenchymal phenotype have been noticed in mice blood even before the primary tumor was found in the liver [8, 37]. This has created a new research field called liquid biopsy. This field has been expanded significantly in the past few decades, and any technology for capturing CTCs should consist of two major steps, enrichment of CTCs from body fluid and identification of CTCs using known biomarkers. Detecting CTCs needs high-

level sensitivity and specificity. In the next section, different techniques for isolating CTCs in blood are being reviewed.

1.2. CTC enrichment methodology

As it was mentioned above, there are a few CTCs among billions of normal cells in each milliliter of blood and the difference between CTCs as the target and other cells is where it makes it possible to separate them. There are two categories for the techniques that are designed for isolation of CTCs, one based on CTCs biological aspects, and one based on physical properties of CTCs. There is another category which detects CTCs through direct analysis, but it can also be included in the first category since it is using biological properties of CTCs to label them in the blood. Figure 3 summarizes different approaches for CTC enumeration. Here we are going to discuss these approaches further.

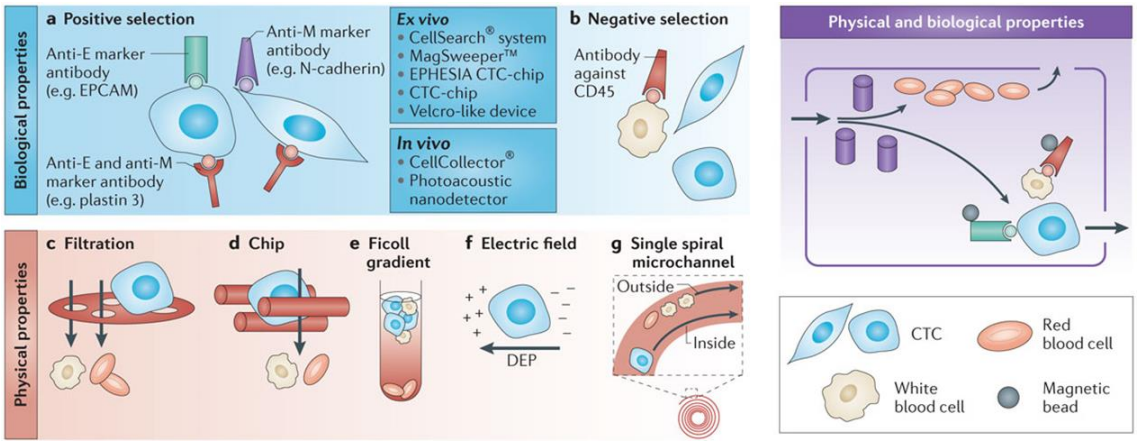

Figure 3. Main approaches of enumeration and detection of CTCs in blood samples [37].

1.2.1. Enrichment of CTCs based on their biological properties

The biological characteristics of CTCs are unique, and there is a distinct difference between CTCs specific antigens and other cells in the blood. This provides an opportunity to isolate CTCs based on their reaction with appropriate biomarkers. There would be a specific binding between an antibody and its counterpart antigen expressing on the surface of CTCs. This ideology can be used both in positive and negative selection depending on the utilized biomarker.

The most common type of cancer is carcinoma, and since this cancer type has epithelial nature, the most prevalent biomarker for CTC isolation is EpCAM [38] that generally expressed with almost all of the tumor cells with epithelial origin [39]. Many technologies have reported successful isolation of CTCs using EpCAM for breast, colon, lung, and prostate, esophagus, liver, rectum, head, neck, and pancreas cancer [40-55]. It should be noted that when EpCAM reacts with CTCs' surface antigen, it might induce cytotoxicity and this will lead to a change in CTC original state and it makes it unreliable to do further biological characterization on the isolated CTC [56]. Cytokeratin (CK) is another epithelial marker that is utilized for identification and in some cases isolation of CTCs. However since CK is an internal architectural protein and it is not always on its external surface, it is not as popular as EpCAM [57].

Although EpCAM is useful for some of the epithelial CTCs, it is not able to bind with all of CTCs [58]. As it was discussed before, CTCs go through several biological changes in their journey to create a new metastasis site, and the most dangerous CTCs are EMT cells since they have the capability of surviving in a dormant site for a long time. Since

EMT cells have mesenchymal characteristics, their epithelial characteristics are down-regulated, and there is a high chance that they will not bind to epithelial markers like EpCAM. There are other biomarkers that can be used for different types of CTCs including human epidermal growth factor receptor 2 (Her2) [59], prostate specific antigen (PSA) [60], CD133 [61], etc. There are a lot of variations in the mutation biological properties of CTCs from one cancer type to another, one patient to another, and even within a single patient sample. Therefore, it is naive to think that one universal biomarker can be used to bind with all CTCs in a blood sample. A cocktail of antibodies may be more feasible for better CTC capture yield but selecting the right mixture of antibodies and production of such mixture is a challenge itself. Table 1 has summarized some of the popular surface antibodies that have been used for isolation and identification of CTCs. This is a positive selection of CTCs based on the reaction between CTCs and their antibodies.

Table 1. Some of the popular surface antibodies for isolation and detection of CTCs.

Target	Cancer Types	Reference
CD133	colorectal cancer	[61]
CEA (carcinoembryonic antigen)	Breast, Gastric, Pancreatic	[62, 63]
EGFR (epidermal growth factor receptor)	Colon, Breast, Gastric	[63-65]
Melanoma-associated antigen (HMW-MAA)	Melanoma	[66]
PSA	Prostate	[67]
HER-2 (human epidermal growth factor receptor 2)	Breast, Gastric	[59]
MUC-1 (mucin 1)	Colorectal, Ovarian, Breast, Prostate	[68, 69]
cadherin-11	Breast, Prostate	[43]
CSV (cell-surface vimentin)	Sarcoma	[70]
prostate-specific membrane antigen (PSMA)	Prostate	[71]

It is also possible to use Immunoaffinity approach by negative selection. Using the antibodies that bind to normal cells specially WBCs will be used to remove them from blood with minimum disturbance of CTCs. This makes it possible to enrich CTCs label-free and complication for selecting the right antibody for positive selection and complication for cytotoxicity and post-processing to be resolved. The most popular antibody for negative depletion of WBCs is CD45 [71-74]. The problem with this technique is that there is a chance to lose CTCs in the "sea" of WBCs [75].. As an example, in a series of studies, density-gradient centrifugation and subsequent immunomagnetic separation by using anti-CD45 coated superparamagnetic beads and a magnetic column were utilized to remove CD45+ cells and enrich for CTCs in head and neck squamous cell carcinoma, colorectal cancer and renal cell carcinoma patients [76-79]. These two-step studies lead to 1.4 depletion of nucleated cells (260,000 cells/ml blood) with 40-90% sensitivity [80]. Other antibodies like CD66 and CD14 have also been used for negative depletion of WBCs [80, 81].

Using aptamers which also can be called "chemical antibodies" is another approach for isolation of CTCs. Aptamers consist of short RNA or single-stranded DNA oligonucleotides that can bind to their target with high specificity. Due to their low molecular weights, they are stable in solutions for a long time and penetrate tissue barriers and are rapidly internalized in tumor cells [82]. Aptamers are being produced through simple chemical processes which make them easy to be synthesized and less expensive in comparison with protein antibodies. Also, aptamer-based reagents can be reused [83]. Because of their high sensitivity and affinity, fluorophore-labeled aptamers

can be used as imaging probes for detecting CTCs in a simple, sensitive and versatile manner [84].

Counting on capturing all of CTCs in a sample solely based on using an antibody is going to result in many false-negative diagnosis cases and even using several antibodies together is not going to fix the issue since there are a lot of variations between different cancer types, mutations, stages of cancer, and biological conditions. Following the biological properties of CTCs is like going after a moving target and it is safe to say that there would always be reasonable doubt that some CTCs will be lost in the process.

1.2.2. Enrichment of CTCs based on their physical properties

This category of enumeration techniques is label-free. They are not depending on any biomarkers or limited to any cancer type or CTC phenotype. Heterogeneity is not a challenge when physical properties are being chosen for isolation of CTCs from hematopoietic cells. The physical properties can include size, mass, electrical property, and deformability.

Methods that differentiate CTCs from normal cells in blood sample based on their size and mass have overlap in some cases. Initially, it was assumed that the diameter of CTCs is larger than 8-12 μm [37, 85-87]. However, later studies proved that this is not the case. Isolating CTCs solely based on assuming that the diameter of CTCs is larger than 8 μm will lead into two consequences, losing some of the CTCs that are smaller and having a large portion of white blood cells as impurity [88]. There is also some overlap between

the mass of CTCs and WBCs so in these methods is also a chance to lose some CTCs or collect a high number of WBCs.

Electric charge is another property of CTCs that can be used for their enumeration. Electrophoresis is a process that applies a force on a dielectric particle which is subjected to a non-uniform electric field. In the case of CTCs, the total plasma membrane capacitance and conductance by using alternating field gradients can be measured, and its total capacitance can be used to separate tumor cells from white blood cells [89].

Another interesting property of CTCs that can separate them from normal cells in the blood sample is deformability. Studies have shown that the nuclear to cytoplasmic ratio (N/C) for CTCs is higher in comparison to WBCs which means that CTCs are stiffer than WBCs. N/C ratio can be used to have relative deformability, and Meng et al. measured this ratio . for CTCs around 0.8 and for WBCs around 0.5 [90]. This means that CTCs are less deformable than WBCs. Deformability of CTCs is also more than non-cancerous cells [91-93]. However, there is not much data on the deformability of CTCs isolated from patient samples since most of the technologies fix the cells during the process and the cells are not viable after enumeration. Vazquez et al. also observed that the cells with the higher metastatic potential are more deformable [94] among CTCs.

1.2.3. Enrichment of CTCs based on their function

When the process of metastasis development studies as it was shown in Figure 1, it can be observed that half of the process is biological transitions in CTCs, but the other half is mechanical actions of CTCs. This fact and the unique mechanobiological behavior

of CTCs can be a distinct parameter for isolating them from many hematologic cells in the blood sample. The way EMT cells invade the vessels to complete the intravasation, their mechanobiology technique for attaching to the interior wall of vessels endothelium, CTCs infiltrating a new organ at a distant site, and how CTCs traverse through the vessels are some examples that can be studied. This field has been noticed recently in CTC community, and recently, there have been a few new technologies that are using this concept to validate the viability of cells and their potential to start a new metastasis [95, 96].

1.3. Identification of CTCs

After enrichment of CTCs, identification, and confirmation of isolated cells is the final step. No matter which approach is being used for enumeration of CTCs; there would be other cells in the final product including WBCs or tissue epithelial cells that their appearance, morphology, and size have overlap with CTCs. In that case, biological and genome characterization of collected cells is necessary. This step is not only for identification of CTCs, but also for extracting more information about their nature, origin, mutation, and phenotype. Some of the specific biomarkers that bind to the surface of CTCs were mentioned earlier for isolation of CTCs. In addition to those biomarkers, other biomarkers bind to proteins and receptors inside the CTCs. CK is one that can be used for identification of CTCs with epithelial nature.

Fluorescence in situ Hybridization (FISH) is a category of biomarkers that fluorescent probes bind to only those parts of the chromosome with a high degree of sequence

complementarity. The HER2 oncogene which is seen in 20% of breast cancer patients was the first target for a successful FISH bioassay [97]. This quantitative assay is measuring the expression level of Her2 in breast cancer patient samples. The results can lead to selecting trastuzumab therapy [98].

There are also a few technologies that do not isolate the CTCs but label them with the fluorescent biomarker and observe them in the blood sample. This technique is called a direct analysis of CTCs. Cells are labeled using biomarkers of interest for positive or negative selection and using a high-throughput assay, the population of CTCs will be counted.

1.4. Major platforms and highlighted technologies for isolation of CTCs

In the previous section, various properties and behaviors of CTCs that can be used to separate them from billions of normal cells in a blood sample were described. In this section, the major platforms that utilize these properties to isolate and identify CTCs in blood samples are introduced.

1.4.1. Magnetic beads

Using magnetic beads in isolation of CTCs is one of the most popular methods in this field. In this platform, magnetic particles are coated with the antibody of interest. When the antibody binds to CTC's surface receptors, magnetic bead attaches to the target cell, and it can be separated from hematologic cells using a magnetic field. The only technology that is cleared by US Food and Drug Administration (FDA) based on the

enumeration of CTCs for partial and conditional prognosis of cancer patients is CellSearch® instrument (Veridex, LLC, Raritan, NJ, USA) [99]. CellSearch® is using CTC count as a threshold for predicting the outcome of treatment for breast [100], prostate [101], and colon [102] patients with metastasis potential. Magnetic particles covered with EpCAM are separating the CTCs with epithelial origin from a 7.5-mL blood sample, and collected cells are stained with a nucleic acid dye (DAPI), anti-CD45 with Allophycocyanin (APC) conjugate and anti-cytokeratin 8/18/19 with Phycoerythrin (PE) conjugate. These stains are being used to identify the WBCs and CTCs in the final product.

In an extended study that was carried out in multiple institutions, increased progression-free survival and overall survival were correlated with falling below a cutoff of 5 CTCs in 7.5mL of blood sample [99]. During this study, blood was drawn from 177 patients before a new line of therapy was administered and of 3 to 4 weeks after initiation of therapy. There have been more than 7000 studies published on CTC isolation using CellSearch®, and this technology is a breakthrough in this field. However, there is still a lot of room for improvement, and it suffers from a lack of high sensitivity. Also, during the process, the cells are fixed, and therefore, they are not viable to be used for further investigation. Another limitation for this technology is that it only targets CTCs with epithelial nature and it loses the cells that are EpCAM down-regulated including EMT and MET cells that are extremely important in creating a new metastasis tumor. Figure 4.a shows the schematic of the CellSearch process [103].

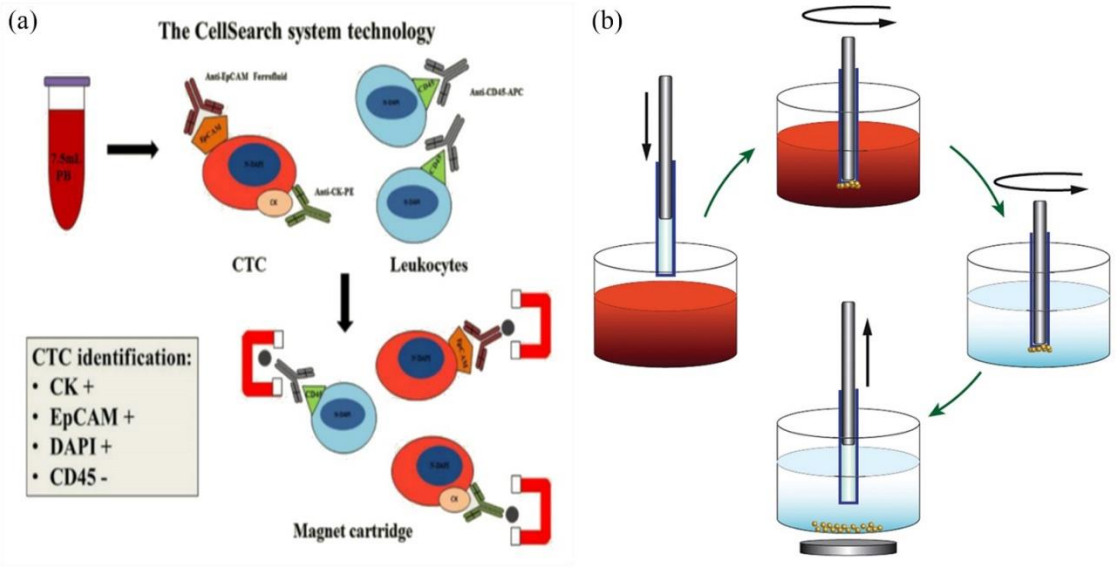

Figure 4. (a) Schematic diagram of CellSearch technology concept [103], (b) Schematic image of Magsweeper [104].

Another immunomagnetic CTC isolation method that was invented by Jeffrey's group at Stanford is MagSweeper. This technology can process 9 ml of blood in an hour using EpCAM coated magnetic beads, and it has a high purity output. However, its capture efficiency is only 60% [105]. One of the advantages of this technology is that it does not fix the cells and isolated cells are viable for downstream processing like reverse transcription polymerase chain reaction (RT-PCR) [104].

Adnatest® (Adnagen AG, Langenhagen, Germany) is another technology that uses functionalized magnetic particles to isolate CTCs. It uses a cocktail of antibodies to improve the sensitivity in contrast to CellSearch technology (only EpCAM). Adnatest magnetic particles are covered with EpCAM and MUC1 antibodies [106, 107]. Overexpression of MUC1 is associated with epithelial CTCs in colon, breast, ovarian, lung and pancreatic cancers [108]. The second step in this test is identifying the CTCs and their genomics using (RT-PCR). The Adnatest is enabling the physicians to target

CA15-3, Her2, estrogen (ER) and progesterone (PR) receptors biomarkers. The assay was also used to identify CTCs expressing three EMT markers from 502 primary breast cancer patients [109].

MACS is one of the oldest immunomagnetic technics that is using a magnetic field in a column to separate the CTCs [79, 110]. It uses both positive (EpCAM) and negative (CD45) selection and high area to volume ratio to increase its efficiency. Earhart et al. have used the same concept to create a magnetic sifter containing a dense array of magnetic pores [111]. The high magnetic fields around the edges of 40 μm holes lead to efficiency of more than 91% in a vertical flow configuration in spiking experiments. The processing speed for this technology is 10 ml/hour.

1.4.2. Microfluidics

Microfluidics is the other popular platform for isolating CTCs. Microfluidics is the science of controlling and monitoring small volumes of fluids (Micro liter to Pico liter). The channels of these devices are in the range of submillimeter, and it has applications in biochemistry, physics, nanotechnology, and biotechnology.

One of the critical aspects of this platform for CTC enumeration is that it is a dynamic process and the sample is flowing. Therefore, all components of blood have the chance to interact with the device and improve the selection process independent the preferred criteria. Microfluidics also enables the user to utilize two or more properties of cells to separate CTCs from normal cells, and it is compatible with almost all of the enrichment

approaches that were mentioned in the previous section. On the other hand, microfluidic devices are slow and complicated to design.

1.4.2.1. Microfluidics with micro posts

Toner's group at Harvard and Massachusetts general hospital introduced one of the first technologies that incorporated Immunoaffinity, microfluidics, and microfabrication called CTC-chip for enumeration of CTCs [54]. This device consists of 78000 micro posts functionalized with EpCAM. The reason for creating the micro posts was to increase the surface of the functionalized area to processed volume. It could process 2.5 ml/hour, and it resulted in capture efficiency of 60% and purity of 50% [54]. Figure 5-a shows the SEM image of an isolated CTC among the micro chip posts.

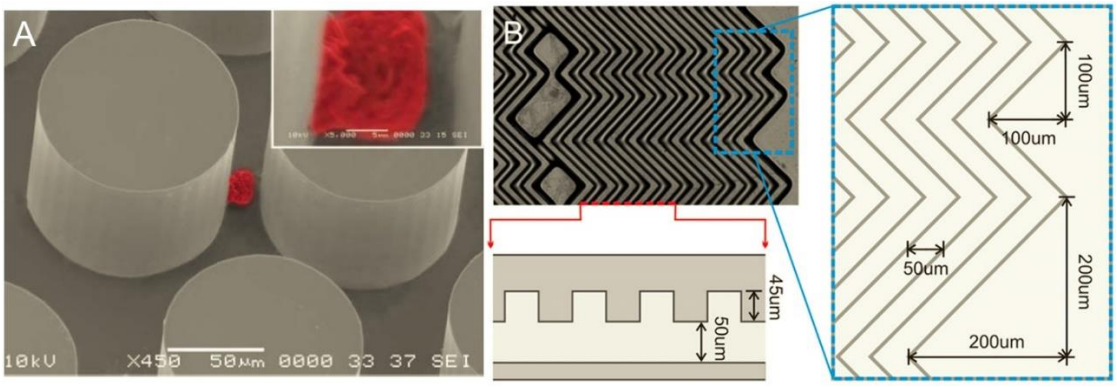

Figure 5. (a) An isolated CTC next to a micro post in CTC chip [112], (b) The architecture of herringbone chip [113].

The second generation of CTC-chip called "herringbone chip" was introduced by the same group in 2010 [113]. With an easier fabrication and better mixing using micro vortices, new design improved cell to surface contact. Herringbone chip was able to deliver 91.8% capture efficiency, and it captured the CTC cluster in 14 out of 15 prostate

cancer patients. This chip also used EpCAM to isolate CTCs, and it could process 4.8 mL/hour.

Geometrically enhanced differential immunocapture (GEDI) is using a similar concept and micro-posts to isolate CTCs. However, they have adjusted the distant of micro-posts to use the larger size of CTCs induce particle trajectories that maximize CTC–wall interactions while minimizing the interactions of other blood cells [114]. Another difference between GEDI and CTC-chip is in the antibodies that they have used to isolate CTCs. Prostate-specific membrane antigen (PSMA) [114] for prostate cancer and Her2 [59] for breast cancer are two biomarkers that were used in GEDI to isolate CTCs. The capture efficiency of 85%, the sensitivity of 90% (18 out of 20 prostate patients) and purity of 68% was reported for GEDI [114].

OncoCEE is another microfluidic device that is using the combination of Immunoaffinity and micro-posts to isolate CTCs [58]. However, they show that by using a cocktail of antibodies including EpCAM and TROP-2 they can increase the capture efficiency in spiking experiments and isolate CTCs that are EpCAM or CK negative.

1.4.2.2. Microfluidics with magnetic beads

Another set of microfluidic devices have utilized immunomagnetic beads along with the micro posts to improve their sensitivity. The third generation of a microfluidic device in Toner's group named "CTC-iChip" is among them. The first step for this technology is discarding RBCs, platelets, plasma proteins, and free magnetic beads using size-based sorting and hydrodynamic focusing. The nucleated cells including WBCs and CTCs were presented to the second stage for inertial focusing. This device was designed in two

configurations, negative depletion of WBCs using magnetic beads coated with CD45 antibody or positive selection of CTCs using magnetic beads coated with EpCAM. They reported capture efficiencies of 98% although their sensitivity in patient samples was smaller (37 out of 42 prostate cancer patients) [71, 80]. CTC-iChip can process up to 8 ml/hour. Figure 6-a shows the schematic of the CTC-chip process.

IsoFlux microfluidic cartridge is also using magnetic beads covered with EpCAM with three reservoirs [115]. This system showed a high purity in CTC isolation, and it is possible to do molecular profiling on the final product. IsoFlux showed 95% sensitivity in prostate cancer patients and 87% sensitivity in colorectal cancer. Figure 6-b shows the configuration of the IsoFlux system. Ephesia is another technology based on microfluidics and magnetic beads, and it uses Self-assembly of magnetic beads into columns. Ephesia can process 3 ml of blood per hour [116].

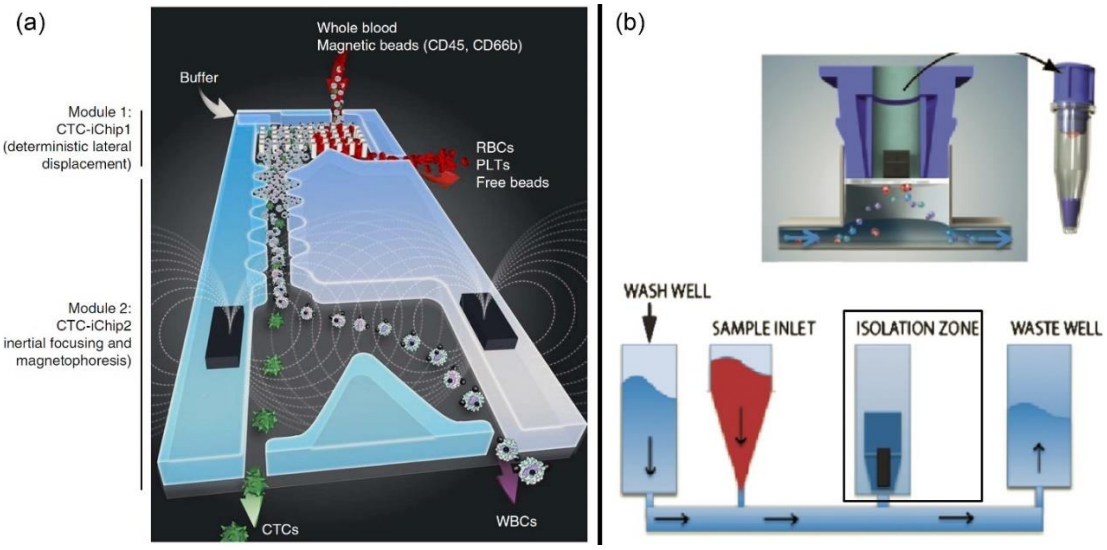

Figure 6. (a) Schematic of CTC-iChip [71], (b) Configuration of IsoFlux [115].

1.4.2.3. Microfluidics with inertial forces

This category of technologies is using a larger size of the CTCs for isolating them from the rest of the blood sample. The challenge in this ideology is that there is a huge overlap between the size of the CTCs (7-25 μm) [87, 117, 118] and the size of WBCs (6-20 μm). This means that whether we have to collect a lot of WBCs or lose some CTCs in the final product. Vortex is the most famous device that uses inertial forces to affect the positioning of target cells within the fluid channels [87]. Vortex was able to collect CTCs with diameters of 12-25 μm and WBCs with a diameter of 8-14 μm. The number of WBCs was about the number of CTCs, and it would result in low contamination (>50%) outcome. This technology does not perform RBC lysis, and the collected cells are viable.

ClearCell® FX also uses spiral microfluidics to separate larger CTCs from smaller normal cells in blood [119, 120]. Using a trapezoidal cross-section, smaller cells are trapped in the Dean vortices pushed toward the waste output while larger CTCs are lifted due to inertial forces and send toward the product outlet. This process is speedy (1 ml of blood per minute), very sensitive, and its purity is relatively good (~4 log depletion WBCs). However, it needs RBC lysis.

Spiral design is another approach that can use hydrodynamic forces to separate larger CTCs from the smaller cell-like WBCs and RBCs. Sun et al. created a double spiral microfluidic channel to reported capture efficiency of 88.5% from spiked cells in diluted blood [121, 122]. MCF-7 and Hela cells spiked into whole blood were collected at the inner and the middle outlet of the device while hematologic cells exit through outer outlet [121]. Lim et al. also used a spiral microfluidic channel to isolate CTCs (individual and

clusters) from blood samples [86]. Centrifugal forces collect the CTCs for an inner outlet while RBCs and WBCs are going through the outer outlet. They were able to isolate CTCs in all 20 metastatic lung cancer patient samples [86].

1.4.2.4. Microfluidics with electrophoresis

ApoStream® is the first technology that isolates CTCs based on their electrical signature [123-125]. The presence of an electric field generated by the interdigitated gold electrodes attracts tumor cells by positive dielectrophoresis (DEP), while other cells flow past and move toward the waste outlet. After completing the process, the collected CTCs would be released by removing the electric field [124]. The capture efficiency for this method was 95% for spiked breast cancer cell lines [123]. This technology can process 10 ml of blood per hour [126]. Figure 7.a shows a schematic of ApoStream process.

DEPArray™ also uses the same label-free approach to sort the cells and put the isolated CTCs in separate cages using their dielectric signature [127]. Since the cells are viable, it is possible to recover and do further downstream post-processing on them including genomics. The disadvantage of this technology is that it needs pre-enrichment using density gradient centrifugation. The purity of this technic is 100%, but it could only reach to 52% sensitivity in the isolation of CTCs in colon cancer patients [128].

1.4.2.5. Microfluidics with acoustophoresis

Using ultrasonic resonances is another label-free method for isolation of CTCs. Figure 7.b shows a schematic of using ultrasonic waves to concentrate the larger cells in the center while red and white blood cells are leaving the outlet. When the spiked prostate

cancer cells in blood were fixed, this technology could deliver more than 93% capture efficiency. However, if the cells were not fixed, capture efficiency was decreased to 72.5%.

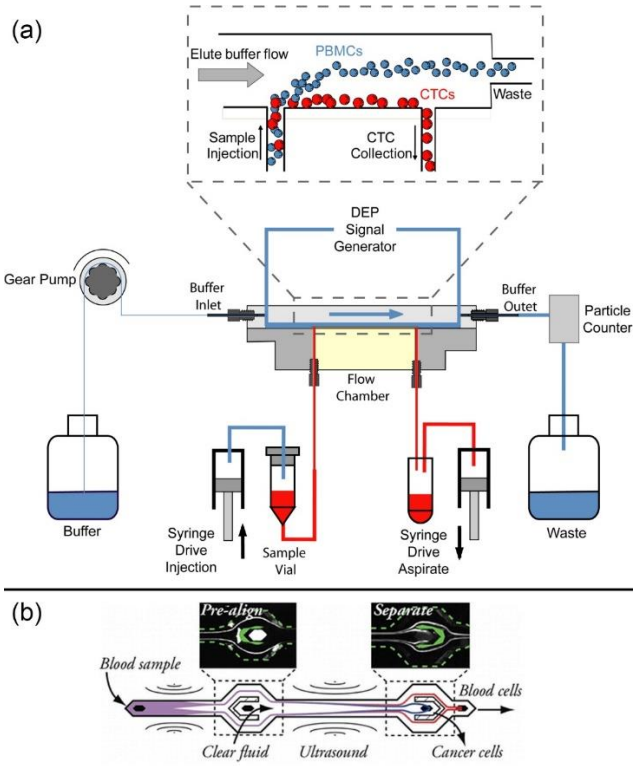

Figure 7. (a) Schematic of electrophoresis process [124], (b) Schematic of acoustophoresis concept [129].

1.4.2.6. Microfluidics-based on migration behavior of CTCs

CTC migration is a part of tumor cell dissemination [130], and recently, this behavior is in the focus of a few new technologies for isolation and characterization of CTCs. Toner's group have proposed a new technology that separates EMT CTCs based on their migration capability [131]. They used polydimethylsiloxane (PDMS) micropillars to scatter individual cell. They were able to show that EMT cells can migrate through these pillars. Also, cells that encountered many neighbors migrated collectively with epithelial

biomarkers [131]. Figure 8.a shows the schematic of the migration of CTCs among PDMS micropillars.

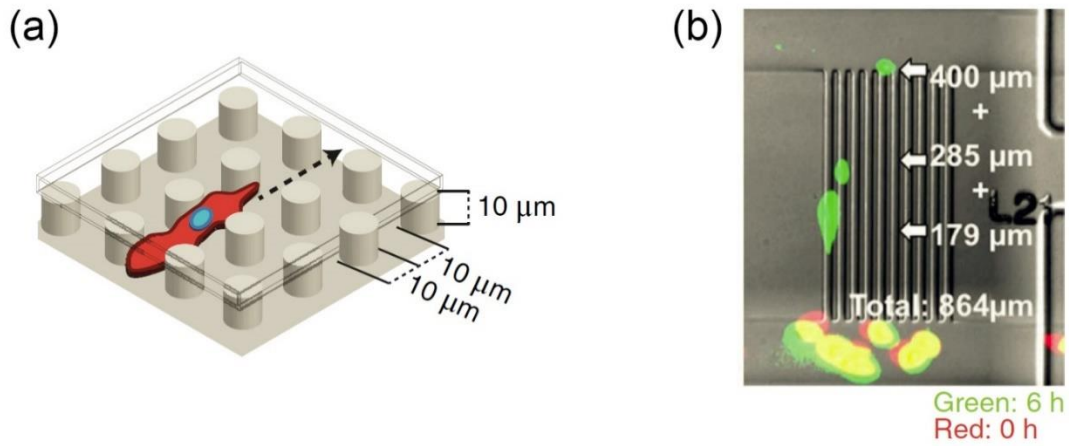

Figure 8. (a) Schematic of PDMS micropillars for studying the migration behavior of cancer cells [131], (b) Measuring the velocity and migration distant of cancer cells in microchambers [132].

Zhang et al. introduced a microfluidic device with 3120 microchambers to observe mesenchymal migration [132]. By monitoring the entire chip through advance imaging technics, they were able to evaluate velocity and percentage related to cell migratory capacity statistically. Their results show that EMT cells were migrating more aggressively in comparison with other CTCs and the CTCs that reached the highest velocities were more resistant to treatment and drugs. Figure 8.b shows the migration process of cancer cells in microchambers [132].

Toner's group utilized another microfluidic device to study the migration of CTC clusters [96]. They used ten melanoma patient samples and performed a microfiltration pre-enrichment step that its target is isolating CTC clusters [133]. Isolated cells go through 16 parallel capillary channels with a square section and dimensions of 5×5, 7×7, 7×7 μm^2. Their results confirmed that spiked cultured breast and lung cancer clusters in

blood successfully transited through capillary constrictions with over 90% efficiency [96]. Figure 9 shows how the CTC cluster is going through a capillary channel.

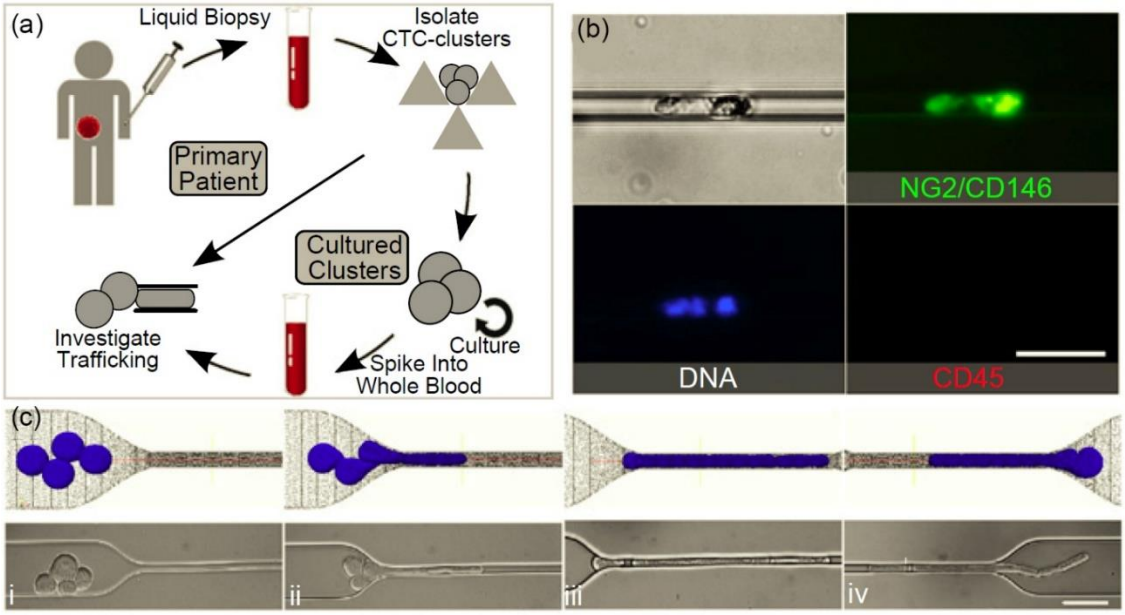

Figure 9. Cancer cell cluster is passing through a capillary channel indication of their invasive migration [96].

1.4.2.6. Microfluidics-based on deformability of CTCs

Tee and colleagues designed a microfluidic device that has crescent-shaped trap arrays with a fixed five μm gap width [134]. In this apparatus, they performed a pre-filter step and then using 5 KPa pressure, they were able to collect target cells. They could show 80% sensitivity (11 out of 15) in breast and colon cancer patient samples [134]. This microdevice was also used to isolate CTCs in 1-3 mL metastatic lung cancer patient blood samples [135]. They were able to isolate CTCs in all five metastasis lung cancer patient samples.

1.4.3. Centrifugation

Centrifugation is an easy and efficient way to separate different component of blood based on their mass. The first method for isolation of CTCs was based on centrifugation [136] in 1959. Seal reported that the specific gravity for RBCs, WBCs, and CTCs were 1.092, 1.065, and 1.056, respectively [136]. Since then, this approach has paced a long distance, and now, density gradient centrifugation is using buoyancy to separate blood components based on their density. Although it should be considered that the centrifugation method does not produce a high purity outcome and this method is usually being used as a pre-enrichment for other strategies.

Ficoll-Paque® solution was the first product that was introduced to the market for density gradient, and it could detect CTCs using an RT-PCR based assay for amplifying cytokeratin 20 expression with a resolution of 1 cell/mL of blood. The reported sensitivity for capturing CTCs colorectal cancer patients was 41% (24 out of 58) [137].

OncoQuick used a porous barrier in the middle of the centrifuge tube to use both size and density for discriminating CTCs [138]. Figure 10 shows a schematic of OncoQuick process. This centrifugation technique was used for isolating CTCs in breast [139, 140], gastrointestinal [141], colon, rectal [138], ovarian, cervical, and endometrial [140] cancer patients but in all of these experiments, the highest sensitivity they could reach was 40%. After centrifugation, OncoQuick resulted in a 632-fold enrichment (2.8 log depletion) ratio against WBCs compared to 3.8 with Ficoll-Paque [141].

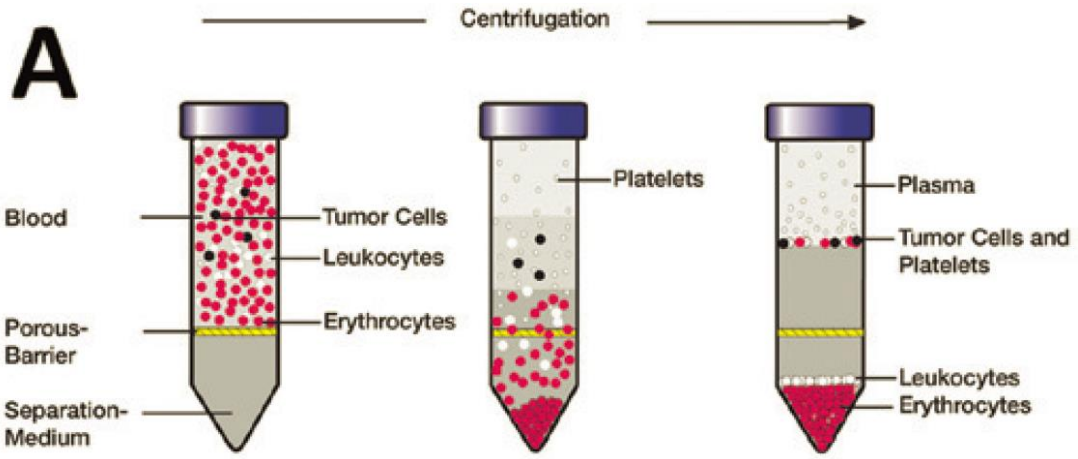

Figure 10. Schematic of OncoQuick centrifugation tube [142].

RosetteSep™ CTC Enrichment Cocktail is incorporating both Immunoaffinity and centrifugation to isolating CTCs [143]. He et al. were able to show that Antibody-labeling alters cell density and by using Ficoll-Paque, it is possible to isolate smaller CTCs. They could successfully detect CTCs in 10 out of 13 blood samples from prostate cancer patients and in blood samples of 18 out of 20 ovarian cancer patients [143].

AccuCyte™ is another technology that separates the buffy coat from red blood cells and plasma by use of a single separation tube and collector device [144]. The CyteFinder™ module uses automated scanning digital microscope for imaging stained cells. CytoFinder also uses a precise mechanical method to retrieve individual CTCs for genomic analysis. Cytesealer™ module creates a seal between separated layers, and CytePicker™ isolates individual cells for downstream processing. This technology delivered 80-90% capture efficiency. Its sensitivity was reported similar to CellSearch [144].

1.4.4. Filtration

Microfiltration is assuming that most of CTCs are larger than WBCs and RBCs and using this idea to separate them from the blood sample. Deformability of cells also is a factor in this technic unless they are fixed.

Vona et al. invented Isolation by Size of Epithelial Tumor cells (ISET) micro filters [145]. In this apparatus, track-etched circular pores with a diameter of 8 µm were created randomly in polycarbonate filters. ISET has 10-12 wells, each has 6 mm diameter membranes, and it can process up to 1 ml of liquid. They diluted the blood 1:10, and it resulted in using multiple devices for a blood sample [145]. This device was used for several clinical studies on patient samples with liver cancer [146], melanoma [147], lung cancer [148], and prostate cancer [149]. In a direct comparison between ISET and CellSearch®, among 60 patients with metastatic carcinomas of breast, prostate and lung cancers, ISET was able to find CTCs in 57 samples while CellSearch® could isolate CTCs in 42 patients [46].

Another 2D filtration technology based on track-etched filters is ScreenCell®. The hydrophilic surface improves the performance, and the cylindrical pores with diameter 6.5 or 7.5 µm can be used for isolating fixed or viable cells [150]. Blood samples from Lung cancer patients were processed with ScreenCell filter and results showed about 70% sensitivity [151].

It is also possible to use photolithography to pattern the holes in the filter membrane. CellSieve™ is a filtration system that use this fabrication technic to create 160000 holes with 7 µm diameter on a non-fluorescent 10 µm thick photoresist layer with 9 mm

diameter [88, 152]. Adam et al. could isolate CTCs in all ten patient blood samples with metastasis breast cancer. The average number of CTCs in these samples were 56 [88].

Flexible Micro Spring Array (FMSA) is also a 2D filter technology made from parylene-C polymer membrane using photolithography. This technology has the advantage of a micro spring structure which helps to avoid damaging the isolated cells and preserving the viability of cells. Using this filter, Harouaka et al. were able to isolate CTCs in 16 out of 21 breasts, lung, and colorectal cancer patients blood sample [153, 154] while CellSearch® could isolate CTCs in only 22% of samples. Because of its high porosity, FMSA does not need pre-processing while other filtration systems need centrifugation, dilution, or lysis.

3D filters are also utilized to isolate CTCs in blood samples. Zheng et al. fabricated a filter using photolithography that could have circular or oval holes on a parylene polymer membrane [155]. This filter could reach the capture efficiency of 89% [155] and 89% sensitivity in metastatic prostate, breast, colon, or bladder cancer patients [85]. The same group improved their design to have the minimum damage on the cells, by creating two layers of filters to support the structure. Figure 11 shows the schematic of this 3D filter [156].

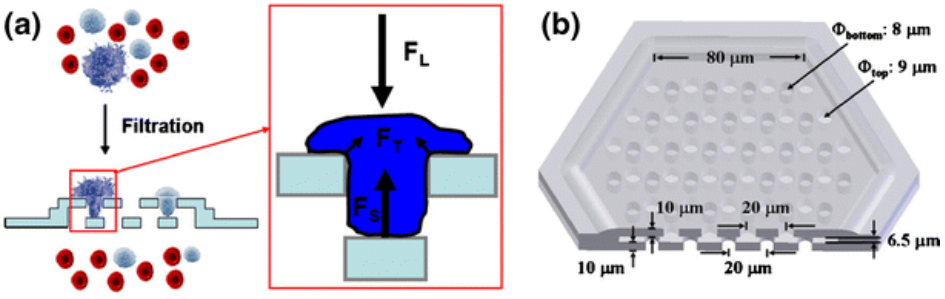

Figure 11. Schematic of a 3D filter having two-step process to reduce cell damage [156].

FactCheck is another 3D filter made of parylene-C, and it had a two-layer structure. This design intent to have viable cells trapped between two layers and reduce any damage to captured cells. They could show a capture efficiency of 78–83% and cell viability 71–74% for spiked experiments [157].

Resettable cell trap (RCT) is another 3D filter that consists of 4 groups of 32 parallelized (128 channels in total) resettable cell channels to isolate CTCs based on their size and deformability [158]. Pneumatic microvalves control the adjustable aperture which can be periodically cleared to prevent clogging. The sensitivity of RCT was 82% for 22 metastasis prostate cancer patients while CellSearch® had 41% sensitivity for the same samples.

Cluster Chip is also a 3D filter that uses a novel design with triangular pillars for isolating CTCs especially CTC clusters [133]. 'Cluster trap,' is three triangular pillars and two of them sitting side by side create a funnel that ends at the point of the third triangle. The third triangle divides the flow into two 12 mm gaps on either side of its point. Individual CTCs pass through this gap while CTC clusters are trapped by creating a dynamic force balance between the two flows [133]. It should be mentioned that other filtration technics also reported capturing CTCs [145, 153] and this could be the result of size selection approach and minimum forces applied on the clusters.

1.4.5. In Vivo

While most of the studies have been working on the blood samples after extracting it from the patient, in Vivo sampling is an interesting way of collecting CTCs in a larger

volume of blood without processing the blood. Saucedo-Zeni et al. utilized a biomedical wire that is coated with EpCAM cannula into the patient's cubital vein for 30 minutes [159]. GILUPI nanodetector® wire could potentially collect CTCs from 1.5 L of blood which is 200 time of what ex-vivo techniques are processing. This could lead to a better sensitivity of 91% [159]. The cells attached to wire could be used for down-stream processing Immunofluorescent (IF) studies. However, the blood-borne cells and invasive nature of the technology has complications that should be considered. Figure 12 shows how GILUPI nanodetector® wire was planted in a patient's vein.

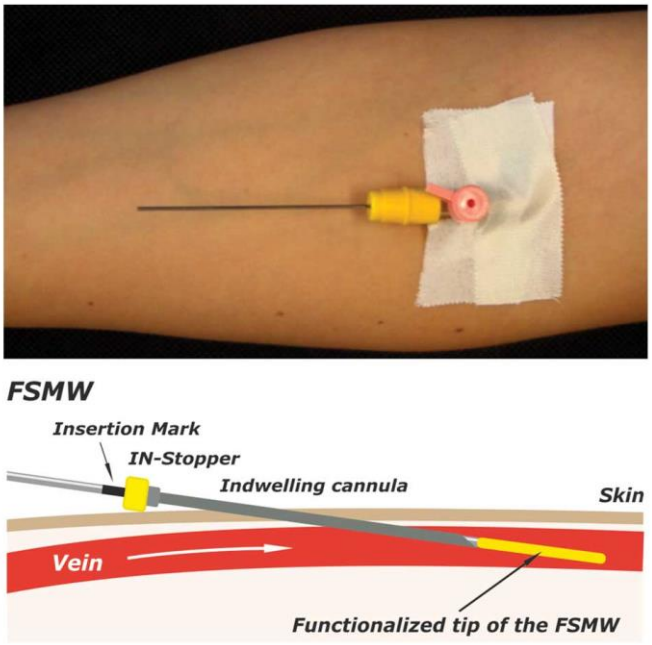

Figure 12. GILUPI nanodetector® for in Vivo collecting CTCs [159].

He et al. also used an in Vivo CTC monitoring technic by injecting fluorescent ligand-coated with EpCAM followed by multiphoton fluorescence imaging of superficial blood vessels. They were able to count the CTCs in mouse models quantitatively. However, due to the invasiveness of this method, they have not tried it on patients.

1.4.6. Direct analysis

Fiber-optic array scanning is one of these technologies that first lyse the RBCs and then it uses CD45 and CK for differentiating the WBC and CTCs, and it can count up to 300000 cells per second [160-162]. This technique has been used for different cancers including breast, prostate, pancreatic, lung and ovarian cancers [163-165]. Micro-Hall sensor is the other assay that uses magnetic nanoparticles conjugated to antibodies targeting various antigens. An array of sensors measures Hall voltages induced by the magnetic flux of each labeled cell and this was used for counting CTCs in 20 patients with ovarian cancer [166].

Epic Assay is another technology that is not isolating CTCs but rather only apply an RBC lysis step for pre-enrichment followed by microscopy. After removing the RBCs and plasma, the mixture of CTCs and WBCs are placed on a slide and using staining of remaining cells, CTCs are counted using image analysis [167].

1.4.7. Functional Assays

The technologies based on the function or action of CTCs are called functional assays. Migration of CTCs is one of its specific functions that was discussed in the technologies with microfluidic platforms. Vita-Assay™ (Vitatex) is one of the products based on one of the key functions of CTCs, preferential adherence. The first action that CTCs should do in the new site to create a new tumor is adhering to the vascular endothelium. They also invade collagenous matrices as a sign of metastasis progression [168, 169]. Vita Assay technology isolates CTCs based on their preference of digesting cell adhesion

matrix (CAM) [95]. This idea can be implemented in two configurations, culture dishes that its wells are covered with CAM and centrifuge tubes that its interior wall is covered with CAM [95]. However, Vita assay had 52% sensitivity in isolating CTCs in 28 out of 54 breast cancer patients at stage I-III. In another study, Vita assay was able to isolate CTCs in 20 treatment-naive metastasis prostate patient blood samples [170]. We will discuss this function in the next chapter in more details.

Epithelial ImmunoSPOT Assay (EPISPOT) is another technology that captures CTCs based on specific secreted/released/shed tumor-associated proteins [171]. A membrane which is covered with the antibody of interest was used for culturing cells and using a secondary antibody labeled with fluorochromes, the bound proteins to membrane can be detected [171]. Results on breast cancer patient samples showed that patients with DTC-releasing CK19 have an unfavorable outcome. Also, in prostate cancer patients, EPISPOT showed that a significant fraction of CTCs secreted fibroblast growth factor-2 (FGF2). In another study, EPISPOT was used for targeting VEGF, EGFR, and osteoprotegerin proteins in patient blood samples with colorectal adenocarcinoma [172].

1.4.8. Nanosurface

Nanomaterials have generated a new set of pharmaceutical products because of their higher sensitivity, high surface to volume ratio and close size to biomolecules [173]. Nanomaterials can be produced in different forms, and aspect ratios and their specific and distinct mechanical, optical, electrical, and chemical properties at smaller scales offer a great opportunity for cell proliferation [174], differentiation [175], and migration [176].

Here, a few nanotechnology devices that were used for isolation of CTCs are being reviewed.

Magnetic nanoparticles (MNPs) are a popular structure in this field since they can be used in most of the common platforms like centrifugation, microfluidics, and immunoreagents. Cellsearch, the only FDA approved technology for cancer diagnosis, and MACS technology are the two most famous devices that are using MNPs for isolation of CTCs. Although round MNPs with high surface area to volume ratio have proven themselves a good choice for isolating CTCs, there have been multiple studies on using high aspect ratio or one dimensional (1D) materials to provide more capabilities including electrical signaling for isolating CTCs [177-180].

Wang et al. used silicon nano pillars functionalized with EpCAM for isolating CTCs with epithelial nature [181]. Nanopillars with 100-200 nm diameter and 1-20 μm enhance local topographic interactions. Adding the 3D nanostructure improved capture yields more than 40 % [181]. Lee et al. also used vertical nanowires made of quartz using oxygen plasma etching. The immuno-functionalized nanowires improved the captured yield and enable the technology to analyze the isolated cells using laser scanning imaging cytometry [182]. Quartz nanowire device had 65% capture efficiency [182] — Zhang and colleagues electrospun TiO_2 Nanofiber (TiNFs) to fabricate a capture assay for detecting CTCs. By using horizontally packed TiNFs and extracellular matrix scaffolds, they were able to isolate CTCs from 2 out of 3 colorectal cancer patients and seven gastric cancer patient samples [183]. Graphene oxide (GO) is another exotic nanomaterial that has been used for isolation of CTCs. Yoon et al. fabricated gold flowers on silicone

substrate and GO sheet were absorbed on the gold flower. GO sheets were functionalizing with EpCAM and by adding a PDMS micro chamber, the final product as a microfluidic device could be used for CTC isolation. This device could show more than 90% capture efficiency for MCF-7 (breast cancer) cell line with high EpCAM expression with minimum flow rate (1ml/hour). However, for other cell and for higher flow rates, the capture efficiencies were not high [184]. They were also able to capture CTCs in 7 metastatic breast cancer patient samples, four lung cancer patient samples, and 9 metastatic pancreatic cancer patient samples [184].

Carbon nanotubes (CNTs) also have shown their potential as exciting material for isolating CTCs in blood samples [177, 178, 185, 186]. Vertically deposited CNTs were deposited on SiO_2 substrate. The impedance of the CNT sensor was measured before and after applying the cultured cancer cells in media on it [185]. However, this technology was limited in terms of the viability of captured cells and leukocyte contamination in case of a blood sample.

Khosravi et al. came up with a novel design to create a field-effect transistor (FET) based on CNTs which can detect the presence of CTCs in blood sample with a Yes/No signal using the specific electrical and chemical sensitivity of CNTs [177, 187]. For isolating CTCs, the CNTs were functionalized with EpCAM or Her2 antibodies using a linking molecule [178]. Figure 13 shows the schematic of CNT device and how it works as a FET.

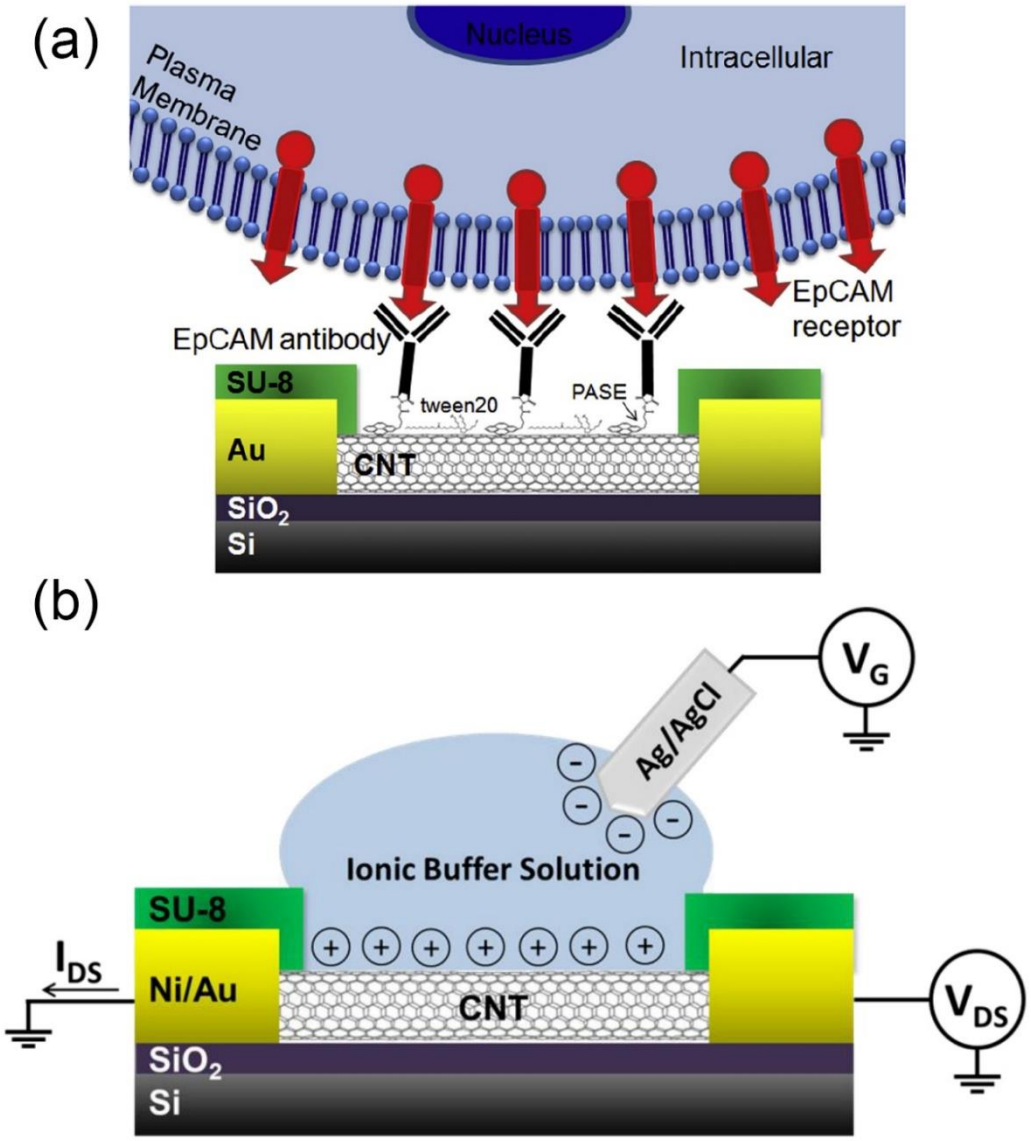

Figure 13. (a) Schematic of CNT biosensor for isolating CTCs [177], (b) Schematic of an electrolyte-gated CNT-FET [188].

1.5. Scope and outline of the thesis

In 2018, an estimated 266,120 new cases of breast cancer (BC) will be diagnosed in the United States, and 40,920 cases will die from the disease mainly due to metastasis. For example, according to the American Cancer Society, while the survival rates of BC

stages 0-1 are approximately 100% and 93% respectively, metastasized BC has only a 22% survival rate. Understanding CTCs presents a valuable opportunity for possible strategies to reduce dissemination. Currently, the only FDA-approved system (CELLSEARCH®) for prognosis enumerates merely a total number of chemically-fixed CTCs and cannot capture CTC clusters.

Microfluidics is an active field of research for isolation of CTCs. Microfluidic technologies such as CTC-Chip, Herringbone chip, CTC-iChip, Vortex, Rarecyte, Fluxion, NanoVelcro, DEP-Array, and JETTA are leading fluidic devices. Although promising, there are inherent constraints in large-scale production of complex microfluidic-based devices and surface functionalization for targeted capture. Further, the rare CTC clusters could potentially be damaged in fluidic devices due to turbulence, vortices and shear forces. Very few devices have been able to successfully capture CTC clusters with 30-40% sensitivity in metastatic patients. Further, some of the leading microfluidic technology has only 5-44% purity which makes genomic sequencing difficult. While Immunoaffinity approach for isolating CTCs suffers from varying biological characteristics of CTCs and other isolation methods based on physical properties of CTCs suffer from high leukocytes contamination. Figure 14 shows the sensitivity of some the famous technologies reviewed in this chapter in isolating CTCs.

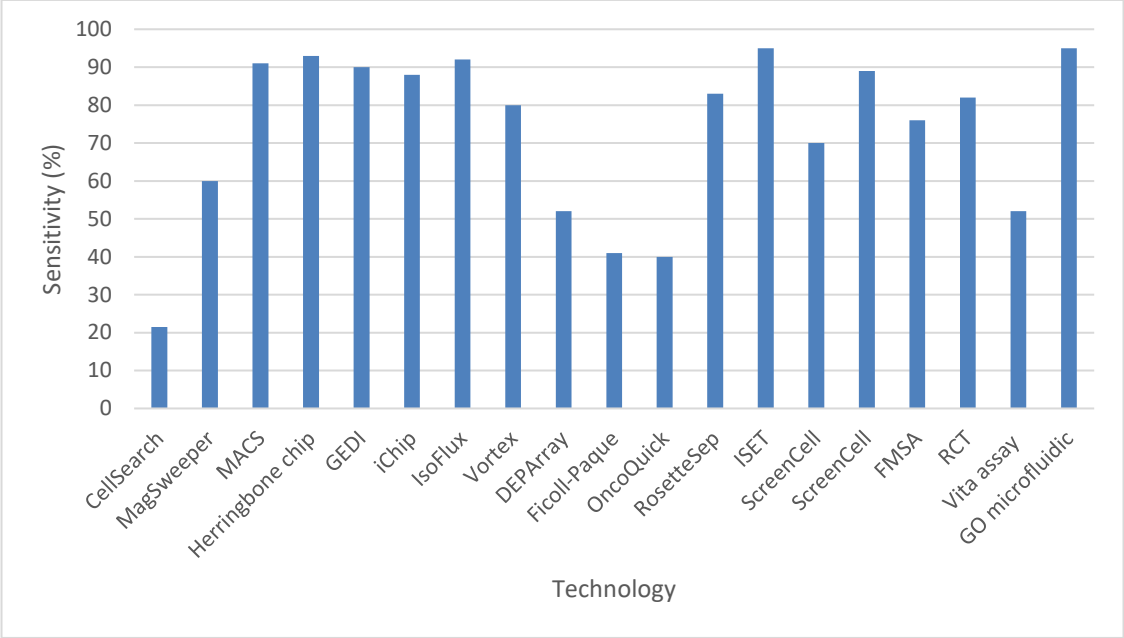

Figure 14. Sensitivity of different technologies in isolation of CTCs in patient blood samples.

Utilizing nanomaterials engineering and microfabrication technology, our group have developed a new perspective on liquid biopsies for cancer. Our group has designed and fabricated a new microarray technology called the "Nanotube-CTC-chip," for liquid biopsies. The current design is a new approach for isolating CTCs and consists of a 76-element microarray of carbon nanotube (CNT) devices on a 4-inch wafer. Advantages of the previous microarrays include:

- Microarray format enabling large volume of blood to be fractionated into smaller portion that enables better capture sensitivity.
- Variety of antibodies functionalized in the same array, resulting in CTC capture based on multiple markers from a single blood sample.

- Surface architecture lends itself to a variety of surface functionalization and instant CTC isolation for further analysis, unlike microfluidics where CTCs have to be recovered from sealed chambers and could be lost.
- Scalable manufacturing process resulting in a 99% yield.
- Improve the precision of experiments through miniaturization.
- Run multiple analyses simultaneously through automation.
- Decrease sample and reagent consumption.
- Reduce the overall costs in fabrication and utilization.

However, here in this work, we are isolating CTCs in a new and antigen independent approach which intent to improve the previous technology based on droplet biopsy. Here are the advantages of a new technology we are looking for:

- The new technology should be based on a completely new mechanism to recognize CTCs not based on their physical or biological properties but based on their specific function which also can be an indication of their viability and aggressiveness.
- It can be used to capture CTCs in all patients' blood sample regardless of cancer type, mutation, phenotype and the stage of cancer. This achievement can lead to an actual early stage diagnosis technology for cancer.
- It can process large volume of blood up to 8.5 ml.
- No transfer of cells should be necessary to do microscopy, and one can do confocal/optical microscopy on the chip.

- The isolated cells should be viable so they can be used for downstream processing. It also should make it possible to expand them in number so that they would be used for culture, genomics, and personalized medicine.
- The technology should make it possible to detect different phenotypes and EMT invasive cells for diagnosis and prognosis purposes.

To deliver such an outcome, here is what we are going to present in the next chapters:

- In Chapter 2, we review the properties of CNTs and how they directly interact with cancer cells. The mechanobiology of cancer cells adhering to CNTs will be studied. Initial assessment on the theory behind preferential adhering of CTCs to CNTs will be explored.
- In chapter 3, Detailed description of fabrication and characterization of CNT devices will be explained. Also the protocol that has been used for culturing cancer cells, immunoflourecent (IF) studies, spiking cells in blood, and how CTCs were isolated in spiked, mice and human blood samples will be explained.
- In chapter 4, the first challenge for isolating spiked cultured cancer cells in blood based on mechanobiology will be presented. A series of samples including different number of cultured breast cancer cells in blood and the capture yield for all of these experiments is explained. It details the procedure and outcome of spiked experiments and how they enlighten our path for final product for isolating actual CTCs in mice and patient blood samples.

- Chapter 5 explains how patient-derived xenografts (PDX) mice models were used to further isolate invasive CTCs. 100% sensitivity has been achieved with significant gain in EGFR and metastatic initiators in captured tumor cells. Further, using triple-negative breast cancer PDX, we have demonstrated the capture of highly invasive CTCs, CTCs with microtentacles, and the very rare CTC clusters which are metastasis-initiating cells.
- Chapter 6 describes how the large volume of patient blood samples was processed from evaluating the method of preferential adherence. CTCs were captured with 100% sensitivity in all of samples and significant EGFR gain from metastatic (Stage4) to Stage 1A cancers. These significant results show the nanotube CTC chip is useful for evaluating baseline CTCs and follow-up of recurrence in human cancers.

Chapter 2

FABRICATION AND CHARACTERIZATION OF NANOTUBE-CTC CHIP

2.1. Introduction

CNTs are cylindrical shape of a sheet or multiple sheets of carbon atoms. Since they have been discovered in 1991 by Iijima [189], there have been extensive studies on its distinctive structure, mechanical, electrical, optical, and chemical properties. In the past three decades, CNTs have found their way into many applications. Calling for compact, fast and high-performance devices around the globe, CNTs have shown their potential in actuation, communication, electronics, sensing, and biomedical devices. Lighting [190, 191], gas sensor [192], field-emission flat-panel [193] and incandescent [194] displays, X-ray generators [195], Glucose [196] and DNA sensors [197], photonic crystals [198], ion sensor [199], and optomechanical actuators [200, 201] are few applications to name here.

Single wall carbon nanotubes (SWCNT) diameter is 0.4-2.6 nm [202], and their length can be up to a few millimeters depending on their synthesis method [203]. Another type of CNTs is multi-wall carbon nanotube (MWCNT) consisting of multilayer cylinders with an interlayer spacing of 2.7 Å to 4.2 Å [204], depending on the diameter and number of cylinders [204]. The diameter of MWCNTs is in the range of 10-20 nm [205].

As can be seen in Figure 15, carbon atoms are arranged in hexagon patterns within a sheet of graphene bonded together covalently (σ bond), and a weaker van der Waals π bond stacks up the layers of graphene to form graphite The start and end of an (m,n) lattice vector in the graphene plane are used as indices of CNT when they join together to create the tube (Figure 15.a). Chirality, diameter, and properties of CNT are depending on the lattice vector. As an example, CNTs with (m,m) indices have armchair chirality, and tubes with (m,0) indices have zigzag chirality [205].

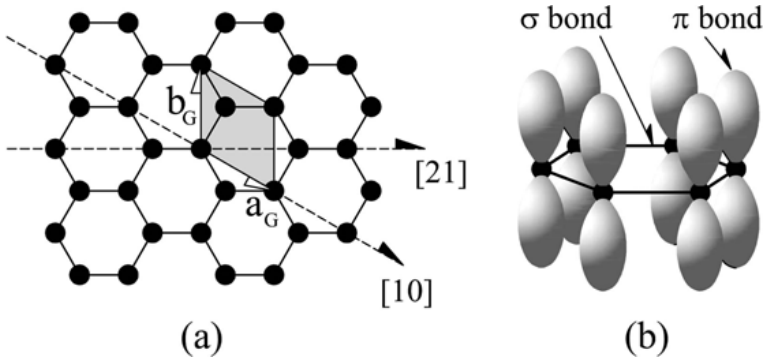

Figure 15. (a) Graphene hexagonal structure of carbon atoms which is similar in CNT. The unit cell (shaded) containing two carbon atoms and standard unit cell vectors a_G (m) and b_G (n) are shown. Two different lattice vectors, (2,1) (1,0) also are presented. (b) Schematic of the in-plane σ bonds and the π orbitals perpendicular to the plane of the sheets [206].

The chirality and diameter of CNTs determine their chemical and electrical properties. Figure 16 shows how different lattice structures create different CNTs. Figure 16.a presents an armchair nanotube (10,10). In its bottom panel, the hexagon shows the first Brillouin zone of a graphene sheet in reciprocal space and the vertical lines represent the electronic states of the nanotube. In this specific nanotube, the center-line crosses two corners of the hexagon, resulting in a metallic nanotube [205]. Figure 16. b and c both show zigzag chirality in two different CNTs with lattice indices of (12,0) and (14,0). In

Figure 16.b bottom panel, the electronic states cross the hexagon corners, but a small band gap can develop due to the curvature of the nanotube. In Figure 16.c, the states on the vertical lines miss the corner points of the carbon atom hexagon. Therefore this nanotube is semiconducting. Figure 16.d, a chiral CNT with (7, 16) lattice is also a semiconducting CNT since the corners of carbon hexagonal is not sitting on vertical lines of the electronic state [205].

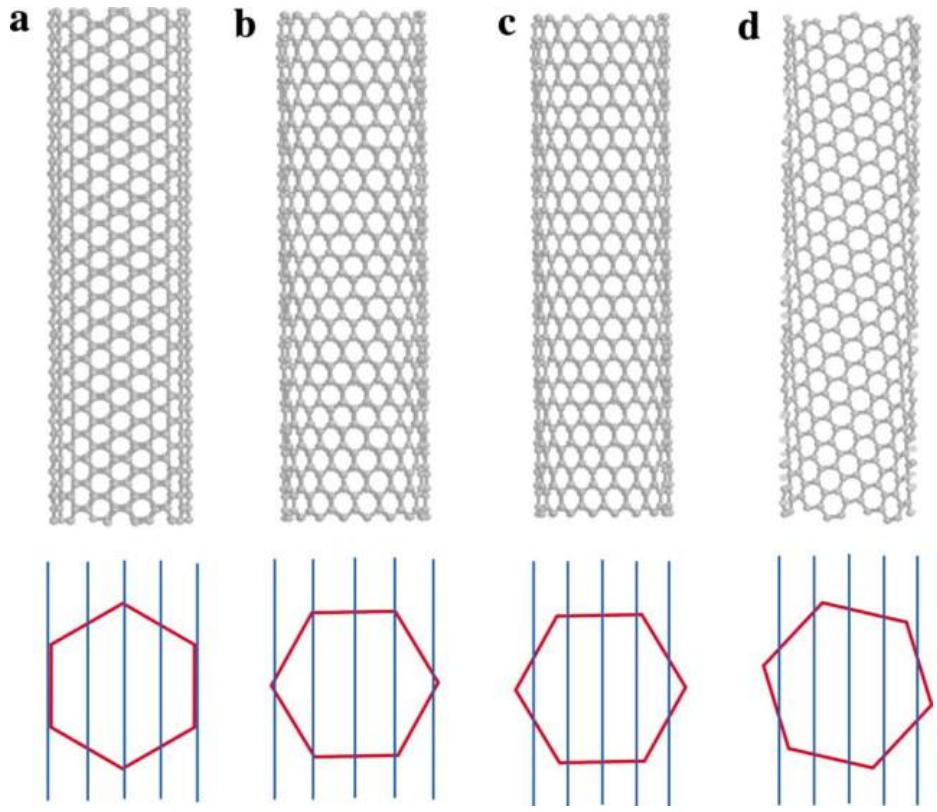

Figure 16. The structure of different types of nanotubes based on their chiralityand the diameter , a) metallic armchair CNT, b) Metallic zigzag CNT, c) Semiconductive zigzag CNT, d) Semiconductive chiral CNT [205].

CNT strength comes from a pure and ideal structure made of unbroken covalent carbon-carbon bonds. The Young's modulus of SWCNT has been estimated at 1.25 TPa [207]. MWCNTs have shown tensile strength up to 63 GPa and elongation up to 12%

[208]. It was not long ago that scientists at NASA start thinking of a space elevator to the moon made of CNTs [209]. Of course, it is still a challenge to assemble CNTs together perfectly to use their highest strength in macroscale.

Chemical, electrical and physical properties of CNTs are depending on their synthesis method. Different growth methods can determine the diameter, structure, number of walls, and the severity of defects in carbon nanotubes which leads to different properties in this nanostructure material. Arc-discharge and laser ablation methods are the first approaches for CNT growth [189, 210, 211]. Iijima discovered carbon nanotube for the first time during arc-discharge evaporation [189]. For the synthesis of SWCNTs, a metal catalyst is necessary for the arc-discharge system. Thess et al. for the first time produced high quality of SWCNTs in the form of ropes in the scale of 1-10 grams using laser ablation [212].

Chemical vapor deposition (CVD) is nowadays a popular synthesis method not only for CNTs but also for other 2D nanostructured materials [213-216]. CVD provides more control on the structure, growth direction, and properties of produced CNTs in the solid state. CNTs are produced during CVD by heating a catalyst to high temperatures (500–1000 °C) in a tube furnace while a hydrocarbon gas is flowing through the tube reactor. Dissociation of hydrocarbon molecules catalyzed by the transition metal catalyst and dissolution and saturation of carbon atoms in the metal nanoparticle lead to the tabular form of carbon.

The advantage of the CVD process is that it is possible to produce CNTs with controlled diameter size, direction, and even chirality. Aligned CNTs can be produced as

horizontal film [217], vertical forest [218, 219], cylindrical pillars [218], sheets [218], with different bundle size produced by CVD can be used for various applications including imaging and probing [220], microelectronics [221], sensor [217]. It should be mentioned that the CNTs that were grown by CVD had significant defects at first [222] and this process has been improved since by optimizing the catalyst and hydrocarbon gas conditions [223, 224].

Figure 17 is showing the schematic of Nanotube-CTC chip fabrication steps. The details of fabrication and characterization for the chips is described in this chapter. The most important step for enhancing the focal adhesion is dispersion of CNTs and transferring them onto the substrate of interest. The topography and surface chemistry of the CNTs can have a direct effect on adherence of tumor cells to CNTs. Roughness, surface energy and patchiness, defects and $I_{G/D}$, and purity of CNT dispersion are some of the important parameters during fabrication that may affecting the focal adhesion of tumor cells to CNT film.

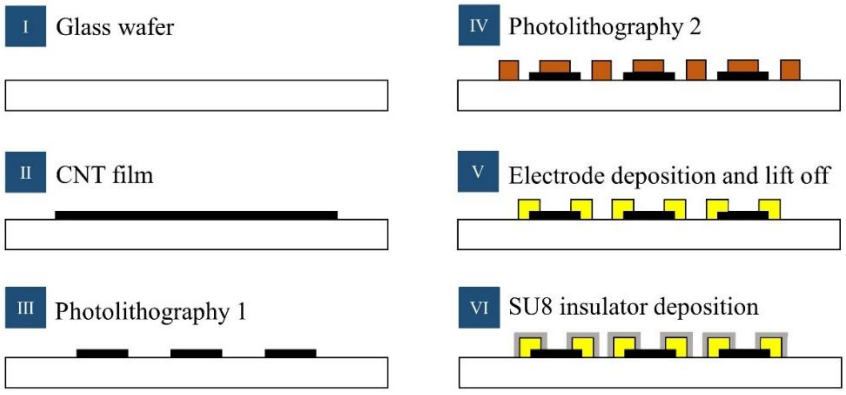

Figure 17. Schematic image of CTC- Nanotube chip fabrication steps.

All of the solvents that have been used here are purchased as ACS grade material from Sigma-Aldrich Co. unless it has been mentioned otherwise. HiPco SWCNT bulk powder was purchased from Unidym^{TM} industries (lot#SP2167). Mixed Cellulose Esters filter membranes with pore size of 220 nm that were used for fabration were purchased from Millipore-Sigma (Catalog# GSWP09000). SU-8 2075 (Fisher scientific Catalog # NC0349843) and SU-8 developer (Fisher scientific Catalog # NC9901158), MICROCHEM CORP S1813 POSITIVE PHOTORESIST (Fisher scientific Catalog # NC1165634) were purchased from Fisher Scientific Co. Borofloat 33 (ID#517) and D263 (ID#1617) glass wafers were purchased from Universitywafer. Cole-Parmer ultrasonic bath sonicator (model#08895-75), Ratio Beam Spectrophotometer Hitachi U-5100, Horiba XploRa Raman spectrometer, NaioAFM (Nanosurf Inc), and JEOL JSM-7000F Scanning Electron Microscope were used for fabrication and characterization.

2.2. Nanotube-CTC chip design and fabrication

2.2.1. HiPco SWCNT

The CNT product that has been used in this work was purchased as a dry powder of nanotubes bundled in ropes. SWCNT SPure product from Unidym^{TM} industries (lot#SP2167) is the only product that has been used throughout this dissertation. This SWCNT is synthesized by High-Pressure CO Conversion (HiPco). Smalley group at Rice University were the first that proposed to mix high pressure (1–10 atm) carbon monoxide (CO) gas that has been preheated (800-1200 ^{o}C) and an iron catalyst precursor gas (metallocene like $Fe(CO)_5$) to produce HiPco SWCNT [225]. HiPco process can run

continuously and produce SWCNT at a rate of 0.45 g/h [225]. The product of the HiPco process may need purification for especial applications, and HiPco SWCNTs are being marketed in three different substances, “Raw” with less than 35 wt% Fe catalyst impurity, “Purified” with less than 15 wt% Fe catalyst impurity, and “Super Purified” with less than 5 wt% Fe catalyst impurity. The product that has been used in here for isolating CTCs is super pure SWCNT HiPco product.

HiPco SWCNTs are a mix of metallic and semiconducting nanotubes, and they have shown different chiralities in their structures [226, 227]. Raman spectroscopy of CNT bundles in the dry form [226] and optical absorption of dispersed CNT solution in different solvents [227] can be used for structural analysis of CNTs. Individual SWCNT diameter size is 0.8-1.2 nm with a mean diameter of 1 nm from diameter distribution measured by Unidym^{TM} from TEM micrographs. Unidym^{TM} also reported in their product data sheet that the length of individual SWCNT measured by AFM is 100-1000 nm. Table 2 summarizes the properties of HiPco SWCNT SPure product from Unidym^{TM} industries.

Table 2. Properties of HiPco SWCNTs Super Pure product from Unidym^{TM} industries.

Individual SWCNT Diameter	0.8-1.2 nm
Individual SWNT Length	100 – 1000 nm
Calculated Molecular Weight	~3.4×105 – 5.2×106 Amu
Color	Black
Morphology	A dry powder of nanotubes bundled in ropes
Maximum Density	1.6 g/cm3
Bulk Density	0.1 g/cm3
Buckypaper Resistance	~0.2 – 2 Ω
Moisture Content	<5 wt%

2.2.2. Dispersion of CNTs in organic solvents

Although nano scale CNTs show great promise due to their unique properties, their aggregation is a roadblock in terms of their applications. Because of their high surface area, the attractive surfaces between CNTs are very strong, and these forces lead to aggregation. Pristine CNTs tend to entangle together and create close-packed ropes called bundles because of their high aspect ratio and flexibility [228].

HiPco SWCNTs are produced in the form of large bulk particles and in this work, we have disperse them inside organic solvents into smaller bundles to have a homogeneous film with higher quality in term of purity. There have been extensive investigations on finding the best solvents for dispersing CNTs for different applications [229-231]. Improving the dispersion of CNTs have a direct effect on their application efficiency and even after two decades, research on this topic is active. Ham et al. studied the solubility of CNTs in different organic solvents [232]. Hansen parameters are good measures to compare the solubility of CNTs in different solvents, and this method has been utilized for other nanomaterials as well [233].

Ham et al. reported that solvents with high polar (δ_p^2) and hydrogen-bonding (δ_h^2) components are good choices for dispersing CNTs. They found out that the tubes were suspended very well in solvents with dispersive component (δ_d^2) between certain boundaries (17–18 $MPa^{1/2}$). Also, organic solvents that have high polar bonding like Dimethylformamide (DMF) and 1-Methyl-2-pyrrolidone (NMP) wet the CNTs very well. However, the dispersion quality had no specific dependency on the total solubility parameter (δ_t^2) [232]. In fact, many studies have shown that NMP is one of the best

organic solvents for dispersing CNTs and show the minimum aggregation with long shelf life [232, 234, 235].

There are also other considerations for selecting the right solvent for dispersing CNTs. In our case, the compatibility of the solvent with Mixed Cellulose Ester (MCE) membrane during filtration is an important consideration. Our group has used different organic solvents like isopropyl alcohol (IPA) for other applications including photoactuation [201], profiling cancer biomarkers [236], fabricating metallic nanowires [237], and detecting breast cancer cells [238]. Dispersion and debundling, surface chemistry, and trace adsorbents could be critical to our application and cell adhesion. However, investigating the effect of dispersion process and its effect on CNT surface chemistry is outside of the scope of this dissertation.

Using surfactants is another approach for dispersing CNTs [230, 232]. Sodium dodecyl sulfate (SDS) is one of the best choices for dispersing CNTs in aqueous solutions due to its excellent stabilization and separation capabilities [239]. Khosravi et al. have used CNT dispersions in aqueous SDS solutions for fabricating biosensors that can isolate CTCs in blood samples [178]. Surfactant molecules are attached to the surface of CNTs via hydrophobic interactions, π-π stacking, hydrogen bonds or electrostatic interactions. However, due to these interactions, surfactants change the surface chemistry of CNTs and removing or washing the surfactant off the CNT surface is complicating the process.

Using acids is another option for dispersing CNTs since they can improve the wetting properties of the CNT surface via oxidizing [240]. Using strong acids like H_2SO_4 or

HNO_3 will create carboxylic moieties, preferentially on the end caps of the CNT. End caps of the nanotubes opened, there is a higher chance of further derivatization in the ends and side walls due to using acids, resulting in chain functionalized nanotubes [230]. However, using acids for dispersing CNTs will result in changing the surface chemistry of CNTs, shortening the CNTs, creating defects in their surface, and eventually changing their mechanical and electrical properties.

Considering the available methods and their outcomes for dispersing CNT particles in different solvents, we decide to use two organic solvents, IPA and NMP for dispersing CNTs. This procedure has been chosen to keep CNTs original surface properties. Therefore, we can study the direct interaction of CNTs and tumor cells and eliminate any possible chemical effect in the process. IPA was selected since its effectiveness in dispersing has been established in other applications by our group and it is compatible with MCE filter [201, 236, 238]. NMP is the best organic solvent for having the smallest bundle size and highest concentration CNT solutions. NMP is not compatible with MCE filters, but since it produces a high concentration dispersion of CNTs, it is possible to dilute it with other compatible solvents like IPA or chloroform and then filter the diluted solution to have minimal effect on the MCE filter.

Since we aim to transfer a very small amount of CNTs to the substrate, it is necessary to make a stock solution and then dilute it to the desired concentration. For making the stock solution, it should be considered that there is a limit in the bulk CNT powder that can be dispersed in that specific solvent. For both IPA and NMP solvents, about 2 mg bulk HiPco SWCNT powder was dispersed in 100 ml of each solvent inside a 125 ml

glass vial, and they were sonicated at a bath sonicator for 24 hours at 110 W power 40 KHz vibration frequency. This may be done continuously or intermittently to reach the overall time. The temperature of the sonication was maintained at room temperature (20-30 ^{o}C). If the bath sonicator was warming up due to high frequency vibration of the resonator, it was turned off to cool down and sonication was continued at a later time.

Sonication parameters like time, sonication power, and temperature have significant effects on the CNT dispersion quality in terms of purity, concentration and the ability to be transferred as a thin film to the substrate of interest. Sonication parameters also going to affect the quality of fabricated film and the defects and impurities in the film. In a study that was published by Yu et al., sonication parameters for dispersion of single-walled carbon nanotubes in surfactant were investigated.

Panthagi et al. quantified the aggregation factor of single-walled carbon nanotubes (SWCNTs) dispersion in organic solvents through a series of controlled experiments [234]. They determined the sonication energy by measuring the temperature rise in the solvent for different duration. They used $I_{G/D}$ for comparing the quality of dispersion. They reported that this ratio was decreased from 15 for the bulk powder to 5 after 30 minutes of sonication (25 kJ sonication time). They also used UV-vis absorbance spectra to compare the quality of CNT dispersions which will be discussed in the next section. One of the main hypothesis that they presented in their report was that overtime sonication with probe sonicator can lead to CNT aggregation and longer sonication necessary won't create a higher concentrated solution [234].At this point, there should be no particle in the solution, and the solution should look homogeneous. If there are still

particles in the solution, extra sonication time should be considered. After sonication, the NMP dispersed solution was centrifuged at 10000 gf for 30 minutes to remove any large bundle. Due to the larger size of CNT bundles, centrifugation of IPA dispersed solution will result in losing the sample and settling down most of dispersed CNT bundles. Since NMP solution is centrifuged at high force, it has a long shelf life, and no aggregation has been observed even after a few months. For the IPA dispersion, CNTs may intend to go back to bundle aggregation and maybe even large particles which will result in settling down at the bottom of the dispersion bottle. In this case, sonication for a few minutes will make a homogeneous solution. At this point, the solutions are ready to be characterized and used.

2.2.3. Characterization of CNT dispersions in organic solvents

A reliable and easy way to measure the concentration of CNT dispersion is measuring the optical absorbance of the solution at a specific wavelength using a spectrophotometer. Optical absorption spectroscopy is a simple but effective way to evaluate the quality and concentration of dispersions. This method measures the absorption of light as a function of wavelength due to its interaction with the sample. The most common technique is to direct a generated light beam at the solution and detect the intensity of radiation that passes through. Lambert-Beer's law as in $A/L=\alpha C$, where A/L is the absorbance per unit length, α is the extinction coefficient, and C is the concentration can be used to calculate extinction coefficients. A/L scaled linearly with C provided the α values for the different types of the solution [233].

For the CNT solutions, two peaks near 660 nm (~1.8 eV) and 1030 nm (~1.2 eV) are important, which were known as van Hove singularity transitions for metallic M_{11} and semiconducting S_{11} SWCNTs, respectively [241-245]. Pathangi et al. used absorption spectroscopy in (UV-Vis-NIR) wavelength region to quantify the aggregation factor of SWCNTs that were dispersed in different solvents for different time length and different sonication power. Figure 18 shows decreasing the wavelength of the S_{11} peak and decreasing the aggregation factor using longer sonication time for CNT dispersions in NMP [234].

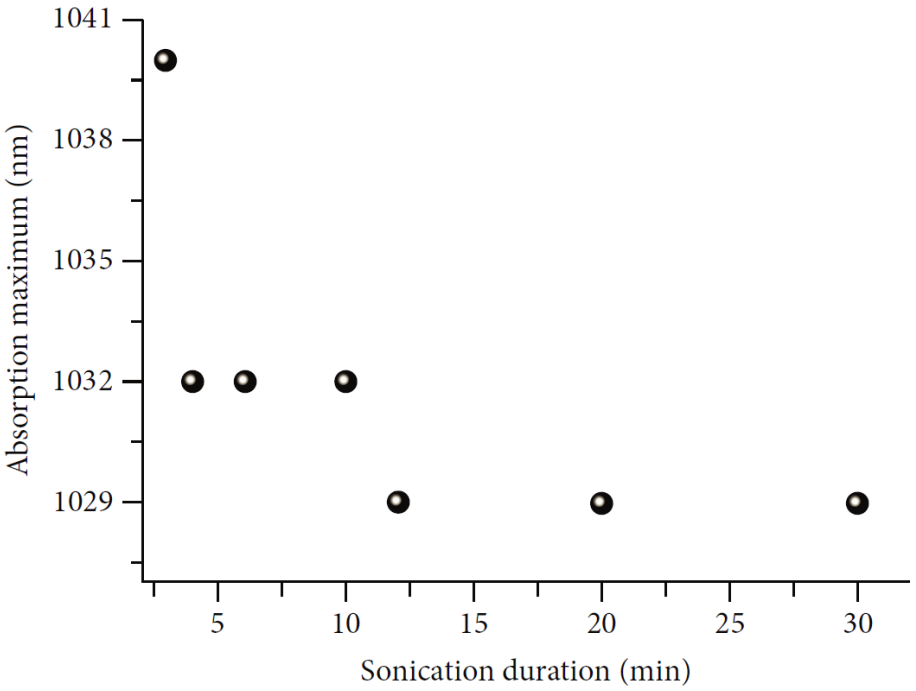

Figure 18. Decreasing the wavelength of red shift (S_{11}) peak for CNT dispersion in NMP by increasing the sonication time as an indication of improvement in dispersion quality [234].

Ratio Beam Spectrophotometer Hitachi U-5100 has been used in this dissertation for capturing optical absorption of CNT solutions. As a part of its standard configuration, the system is equipped with a 6-cell turret which accommodates up to six 10-mm

rectangular cells. The U-5100 and the standard 10 mm rectangular cell is being shown in Figure 19. Depending on the experiment, the scanning parameters can be adjusted. Here in these experiments, the scanning range for CNT solutions is selected between 300-1100 nm wavelength and the scan rate is 200 nm/min.

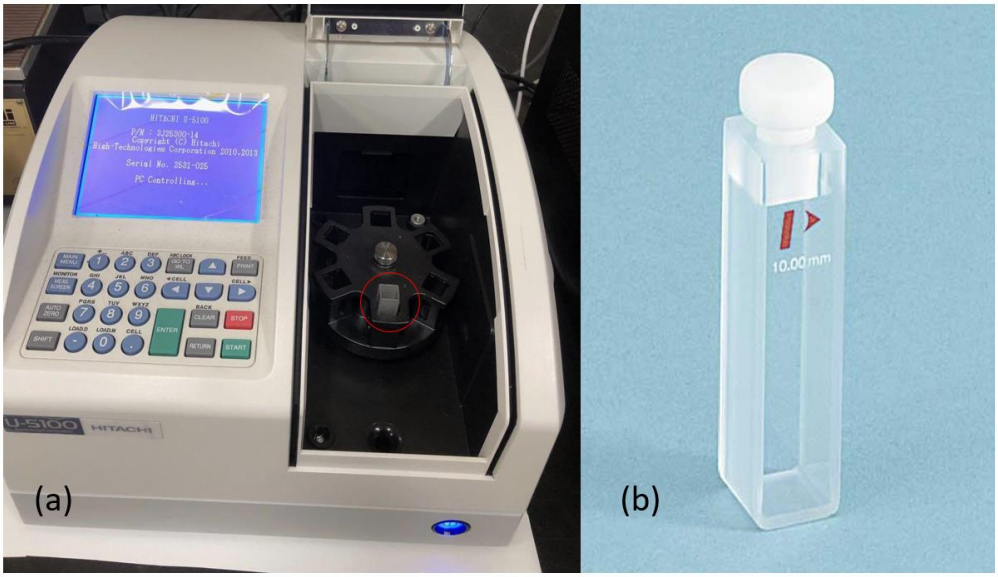

Figure 19. (a) Ratio Beam Spectrophotometer Hitachi U-5100, (b) Standard 10 mm rectangular cell.

Although the mass of bulk powder and volume of solvent are measured initially before dispersion, measuring the final concentration of dispersed solution before filtration and fabrication are necessary. The necessity of this measurement is due to losing some of the bundles during centrifugation or aggregation at the bottom of the dispersion bottle or even both. There are two ways to measure CNT solution concentration, filtration of a portion of that solution or optical absorbance of the solution at different concentration.

Filtration is the simplest way to measure the concentration of dispersed CNTs in a solution. However, the challenge is to measure the difference of filter mass before and after the filtration precisely using the minimum solution volume. The microbalance

precision and compatibility of filter and solvent are critical in this process since a small difference in measured weight can lead to a large error in concentration read out. As an example, a single Anodisc (47mm diameter, 0.02 μm pore size Aluminum Oxide) filter membrane was weighted (0.1763 gr) and then it was used to filter 50 ml of the CNT stock solution in IPA. Twenty-four hours waiting time is necessary after filtration to make sure the filter is dry in a contamination-free environment. The drying process can be accelerated by using a drying agent or by increasing the evaporation rate in vacuum. The weight of the filter was 0.1770 gr after filtration which confirms the concentration of that stock solution is 14 μm/ml.

Using UV-visible absorbance spectra, the concentration of CNT solutions can be measured. As an example, the SWCNT HiPco solution in IPA (14 μm/ml) was used for investigating its optical absorbance. A standard photo spectrometer cell containing 2 ml of IPA should be placed inside the spectrometer for establishing the baseline for the measurements. After emptying the cell, 2 ml of the stock SWCNT solution in IPA is transferred to the cell and using a spectrometer, and its absorption was measured. 5-fold, 10-fold, and 20-fold dilution of the same stock solution were also prepared and used for comparison, and their optical absorption spectra have been plotted in Figure 20. It should be mentioned that a deviation from linear relationship between the concentration and UV-Vis peak intensity can be an indication of CNT aggregation in stock solution [234].

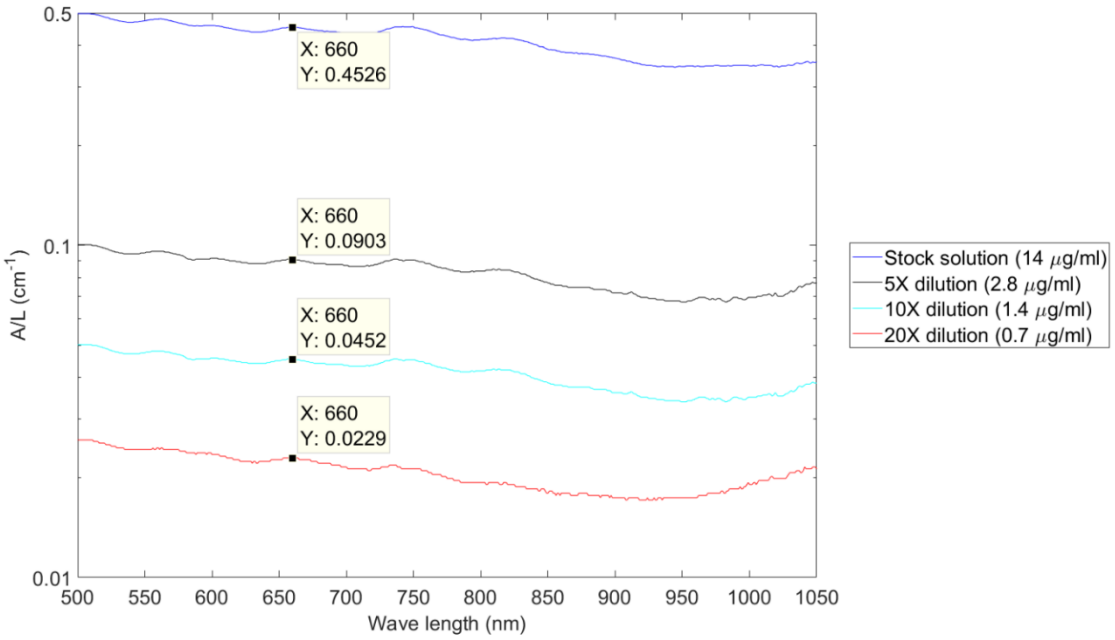

Figure 20. The optical absorption spectrum for SWCNT solutions in IPA.

Based on the above plot, there is a linear relationship between the concentration of the SWCNT in solution and the intensity of peak around 660 nm. Figure 21 shows the correlation between the concentration and M_{11} peak intensity for tested dispersions.

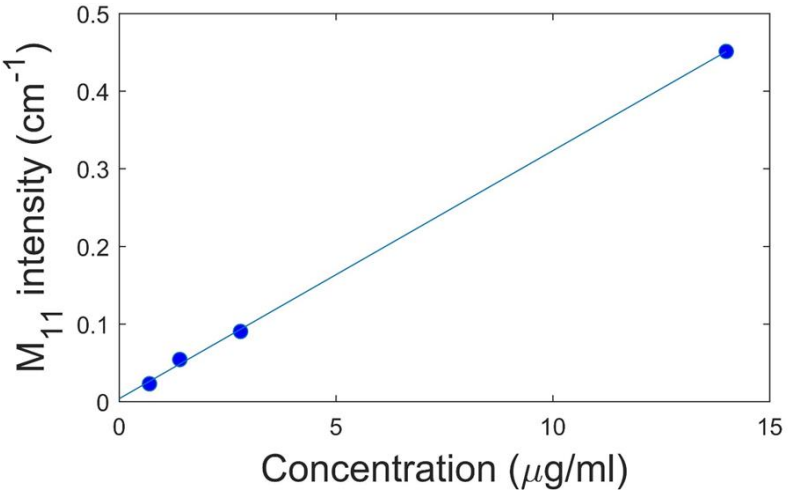

Figure 21. The linear correlation between SWCNT concentration in IPA with M_{11} peak intensity at 660 nm.

For final fabrication of devices, two stock solutions in IPA and NMP were prepared, and their concentrations were measured with a spectrophotometer. Figure 22 compares the absorbance of two stock solutions. As it can be observed, the wavelength of M_{11} peak is not the same, and it can be an indication of the final solution quality and bundle size. However, Further investigation is needed to have a better understanding of the optical absorbance spectrum.

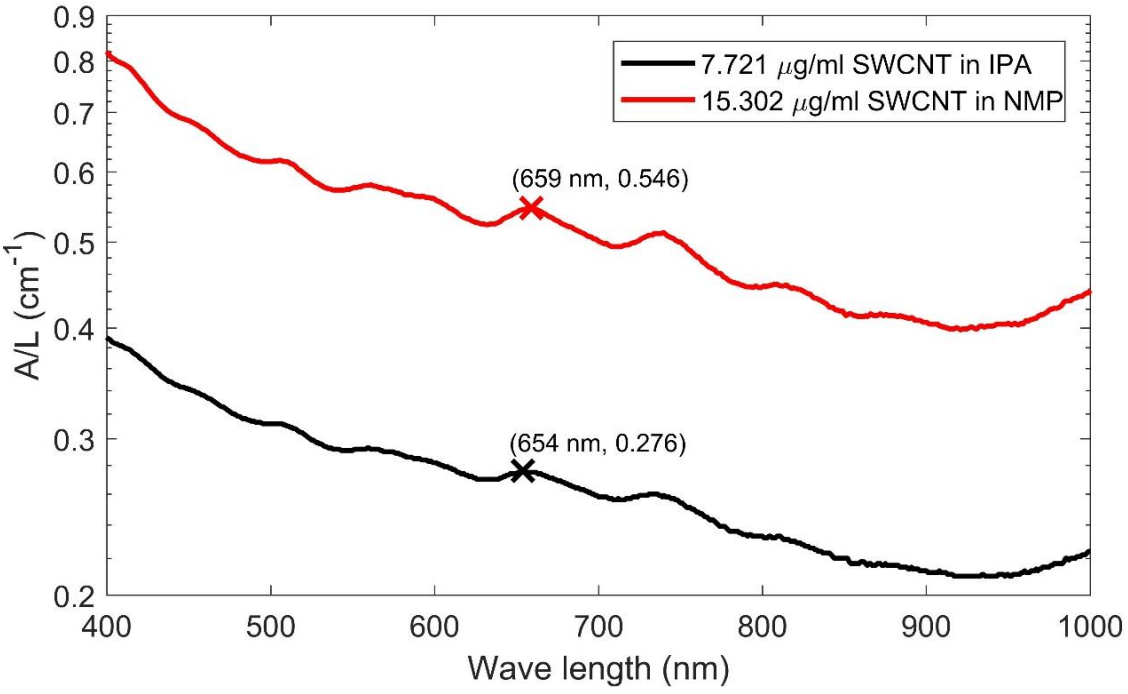

Figure 22. Comparing the optical absorbance of two CNT dispersions in IPA and NMP.

Since the wavelength of targeted peak at absorbance spectra is higher for NMP, it can be concluded that the quality of NMP solution in term of CNT defects and aggregation is better that the dispersion in IPA. The higher quality of the dispersion can be as a result of the centrifugation in case of NMP. Here in this case, CNT dispersion in NMP was centrifuged at 10000 gf for 30 minutes in order to CNT aggregates and larger

bundles settle to the bottom of the solution. In case of using surfactants and polymers in the aqueous CNT dispersions or CNT solutions in acids, centrifugation speeds up to 122000gf was used for 4 hours to make force the dispersed CNTs to the bottom of solution and removing the decant on the top [246].

2.2.4. Carbon Nanotube Film Transfer

Filtering the CNT dispersion and transferring the thin film of CNT to a substrate is an essential step of fabrication. For concentrated stock solutions, ~1 hour of sonication will be needed before the solution can be diluted reliably. Then the stock solution can be diluted to the desired concentration. From this point forward, the samples will be named with the overall mass of SWCNT transferred to each wafer. For example, to fabricate a 20 µg CNT film on a 4'' glass wafer, a 100 ml diluted CNT solution with 0.2 µg/ml concentration was prepared. Glass substrate has been used throughout this dissertation because of their ideal microscopy properties and the properties of the two type of glass wafers that have been used in this work have been described in Table 3.

Table 3. Properties of the glass substrate.

Glass material	Diameter (mm)	Thickness (µm)	R_a (nm)	Surface polish	Expansion coefficient (K^{-1})	Refraction index (n_D)	Dielectric constant
Borofloat® 33	500	500	1.5	Double Side Polished	3.25×10^{-6}	1.4713	4.6
D263 Glass Wafer	500	500	1	Double Side Polished	7.2×10^{-6}	1.5230	6.7

RCA cleaning process [247] has been applied on glass substrates, and it was followed by cleaning in acetone, methanol and DI water respectively. The substrate was dried with an air gun and dehydrated on a hot plate at 120 ^{o}C for 10 minutes. After preparing the final solution of CNT dispersion and wafer cleaning, here are the steps toward transferring the CNT film on a glass substrate:

1. The final SWCNT stock solution was sonicated for a minimum of 1 hour immediately before film transfer to ensure adequate distribution.
2. A 1000mL vacuum reservoir (Figure 23) was obtained and the vacuum filtration transfer system using an MCE nitrocellulose membrane of 0.22µm pore size and 90 mm diameter was assembled. The setup was appeared as follows:

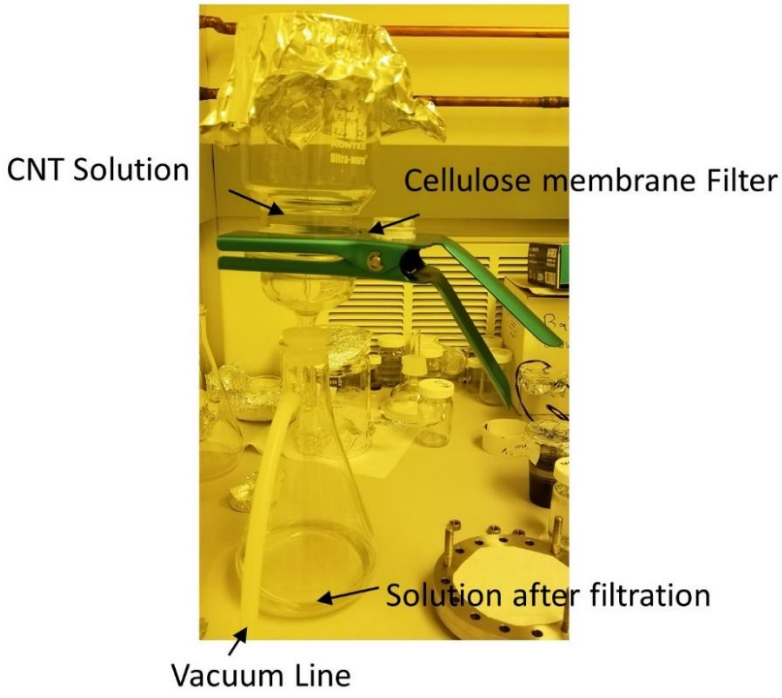

Figure 23. Vacuum filtration setup for CNT film transfer to the glass substrate.

3- The vacuum pump was switched on the filtration setup was leveled. The MCE filter membrane was wetted with 100 ml IPA, and immediately the 100mL SWCNT solution.

Note: To check that the MCE membrane has adhered well in the vacuum setup and is not leaking around the perimeter, a separate volume of ~30-50mL pure IPA was added just after turning on the vacuum and immediately before adding the CNT sample, the membrane was not allowed to dry. This could prevent a loss of carbon nanotubes and MCE membrane if a leak is present.

4- After 10 minutes, the membrane was washed with 100 mL IPA, it was followed by a washing step using100 mL DI Water and 10 minutes was waited to complete the filteration.

5- Without turning off the vacuum, the membrane was gently removed from filtration setup, diped in ethanol and it was laid down on the glass wafer without introducing any bubble between membrane and wafer.

6- After membrane transfer, a small press plate and a wipe of 100mm diameter were used to gently press the membrane onto the wafer by hand. The wafer and membrane were placed between two press plates and they were bolted together for a minimum of two hours. The wipe was placed above the membrane to allow for some cushioning and even distribution of force during this step. the nuts were hand tighten and then about an additional half turn using a wrench was added for greater force.

7- An acetone vapor bath of at least 300 mL acetone in a 1 L Erlenmeyer flask was started. The hot plate temperature was set to 80˚C and several screws were placed in the bath (to facilitate boiling, similar to a boiling chip). A large funnel was placed in the top to accommodate the diameter of the wafer and place a substitute wafer in the funnel while the boiling begins. Doing so minimizes vapor and heat loss, and allows the MCE membrane to be hydrated with acetone more rapidly after transfer. Heating the vapor bath requires around 15 minutes from the time the hotplate is turned on.

8- The wafer was transferred to the acetone bath with the membrane facing down. This was done only after the minimum two hours of pressing has elapsed and the vapor bath has established a good reflux, with acetone boiling and the vapor continuously dripping from the funnel. Also, the wafer was transferred to acetone bath quickly from the press plate before the membrane is fully dried.

9- The wafer was allowed to sit on the acetone bath only so long as required for complete dissolution of the MCE membrane. This required roughly 20-30 minutes, but care was taken not to allow the vapor bath to continue longer than required, as the thin CNT film could begin to rip and tear. The wafer was as level as possible, although occasional adjustment can help to speed up the dissolution of the film.

10- The film was carfully removed from the vapor bath and rinsed with acetone at room temperature to remove residual MCE membrane. For a thorough clean, film

was rinsed with acetone, methanol, and finally DI water. A nitrogen gun was used to dry any remaining liquid gently.

11- The CNT film was annealed in an oven at 250^{o}C for two hours under 20 inHg pressure vacuum, and it was cooled down with the oven. The oven was contaminated free.

2.2.5. Clean room fabrication of biosensors

Further processing of the fabrication process was taken place in a 100-class cleanroom facility. There were three stages of fabrication inside cleanroom:

2.2.5.1 Carbon Nanotube Patterning

For patterning CNT pads from the transferred film, Photoresist S1813 was used. Here are the steps toward etching CNT pads:

1- The CNT film and wafer was coated by a 2-micron thickness film of photoresist, and the settings of spinning parameters were set as Table 4.

Table 4. Spinner parameters for coating the CNT film with Photoresist S1813.

Step	Ramp (RPM/s)	Speed (RPM)	Time (s)
1	100 RPM/s	500 RPM	10s
2	1000 RPM/s	4000 RPM	45s
3	1000 RPM/s	0 RPM	0s

2- The wafer was affixed onto the spinner with a vacuum and the recipe was n as a trial, then the photoresist was added to cover roughly 2/3 of the wafer diameter.

3- The photoresist was soft baked at 115˚C for 60 seconds.

4- The photoresist was exposed for 7s using the SUSS Aligner.

5- The photoresist was developed in MF319 developer. Actual development time was about 45 seconds while the initial 35 seconds needed agitation.

6- The wafer was Rinsed with DI water and it was blow dried with a nitrogen gun.

7- A reactive ion etch (RIE) was run with Oxygen plasma with the following settings:

Table 5. RIE etching parameters.

Time (Sec)	Pressure (mTorr)	Oxygen	Gas (He) flow rate (sccm)
150	20	10%	2000

8- Photoresist was removed and washed thoroughly using acetone, methanol, and DI water, and wafer was blow dried with the nitrogen gun.

2.2.5.2 Electrode Patterning using Liftoff

Photoresist S1813 was used again for masking areas of the wafer that does not need electrode deposition. Here are the steps for depositing the electrodes:

1. The etched film was rinsed gently with DI water, and then it was blow dryied carefully with the nitrogen gun.
2. The wafer was placed on a hot plate at 115˚C for several minutes to remove any residual water molecules.
3. The photoresist recipe was set according to Table 4 on the spinner.
4. The wafer was affixed onto the spinner with a vacuum and the recipe was run as a trial, then the photoresist was added to cover roughly 2/3 of the wafer diameter.

5. The photoresist was soft baked at 115˚C for 60 seconds.
6. Photoresist was Exposed for 7s using the SUSS Aligner.
7. Exposed film was Developed in MF319 developer. Actual development time was about 45 seconds while the initial 35 seconds needed agitation.
8. Wafer was rinsed with with DI water and blow dried with a nitrogen gun.
9. Using Sharon E-Beam Evaporator, the entire wafer surface was coated with an adhesion layer of chromium with 15nm thickness followed by a layer of gold with 90nm thickness.
10. the underlying photoresist was removed by immersing in an acetone bath overnight or a minimum of 2 hours at room temperature.
11. After lift-off, the wafer was gently cleaned using acetone, methanol, and DI water. Metal fragments remaining on the surface was cleaned using a gentle stream of acetone from the acetone dispenser. It was critical not to rub or scrape the metal surfaces from this point onward to remove any fragments, as these forces might damage the electrodes. However, it was possible to poke the area outside of devices to help the lift-off.

2.2.5.3 Patterning SU-8 isolating layer

To cover the electrodes and avoid short-circuiting the electrodes through the liquid droplet, a 30 μm thick SU-8 later was fabricated as the final step of fabrication. A 3×3 mm^2 window was created in the center of the CNT pads for containing the target droplet. Photoresist: SU-8 2075 (Fisher scientific Catalog # NC0349843) and SU-8 developer

(Fisher scientific Catalog # NC9901158) were used in this dissertation. Here are the steps for fabricating the SU8 layer:

1. The wafer was cleaned with acetone, methanol, and finally DI water. The wafer was gently blow dried with a nitrogen gun.
2. The wafer was baked at 115˚C for several minutes to remove any residual water on the wafer, it was cooled down for 5 min.
3. The mask was cleaned with IPA and then blow dried with a nitrogen gun.
4. SU-8 2075 resist was dispensed to roughly ¾ the wafer diameter without introducing any bubbles. 4 mL for a 4" wafer was enough. The wafer was allowed to relax at room temperature for 10 min.
5. SU-8 was spun at the following conditions:

Table 6. Spinner parameters for SU8 patterning.

Step	Ramp	Speed	Time
1	100 RPM/s	500 RPM	30 s
2	300 RPM/s	6000 RPM	5 min
3	1000 RPM/s	0 RPM	0 s

6. SU8 layer was soft baked using a step process for the following times and temperatures: (ramp up-ramp down the hotplate to prevent SU-8 cracking).

Table 7. Soft baking steps for 30 μm thick SU8 layer.

Step	Ramp	Temperature	Time
1	----	75 ºC	3 min
2	120 ºC/hr	105 ºC	6 min
3	----	Room temperature	10 min

7. The wafer was exposed for 18 seconds (11 mWatts/cm^2 @ 365) total on the Karl Suss mask aligner. “Soft contact” mode was used in this work and not “vacuum contact.”
8. The wafer was allowed to relax for 1 hour.
9. A post-exposure bake (PEB) was completed at the following conditions:

Table 8. Post-exposure baking steps for 30 µm thick SU8 layer.

Step	Ramp	Temperature	Time
1		75 ºC	1 min
2	120 ºC/hr	105 ºC	5 min
3	120 ºC/hr	60 ºC	1 min
4	Let it cool down with a hot plate	Room temperature	1 hr

10. SU-8 was developed in developer/BTS-200 for about ~4 minute and 30 seconds at room temperature. Agitation was recommended for thick films.
11. When using SU-8 developer, spraying and washing the developed image with fresh solution for approximately 10 seconds was recomended, followed by a second spray/wash with Isopropyl Alcohol (IPA) for another 10 seconds. The wafer was dried with filtered, pressurized air or nitrogen.

Figure 24 shows the schematic and the actual image of a fabricated device.

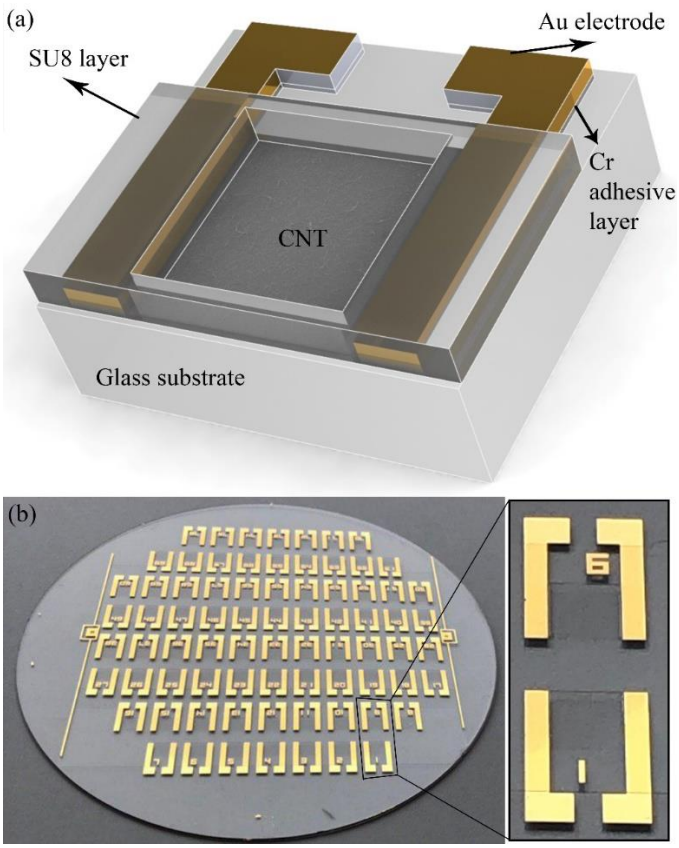

Figure 24. (a) Schematic image of CTC-Nanotube chip with different layers, (b) A fabricated wafer containing 76 micro arrays of CTC-Nanotube chips.

2.3. Characterization of CNT film on a glass substrate

Vacuum filtration of CNT dispersions is an efficient and easy way to create random or oriented films on different substrates. Our group is a pioneer in this field and more information can be found elsewhere [188, 248].

4 set of devices were fabricated and used in this dissertation: a bare 4" Borofloat®33 glass wafer without any CNT, a 4" Borofloat®33 glass wafer with a 20 µg CNT film which were dispersed in IPA, a 4" Borofloat®33 glass wafer with a 20 µg film of CNT which were dispersed in NMP, and a 4" D236 glass wafer with a 100 µg CNT film which

were dispersed in IPA. The diameter of the CNT film on the glass wafer is 75 mm, and the film transfer and fabrication were completed as it was explained in the previous section. In this section, the characterization of fabricated films will be discussed.

2.3.1. Scanning Electron Microscopy (SEM) and Atomic Force Microscopy (AFM) of CNT films

Characterization of the CNT film after its transfer to the glass substrate is a necessary step to control the quality of devices before use. Figure 25 shows the SEM image of 3 films that have been fabricated on the glass wafer. SEM images of the CNT film was obtained using a JEOL JSM-7000F instrument at 10 kV of power and under an ultra-high vacuum, 10^{-5} Pa.

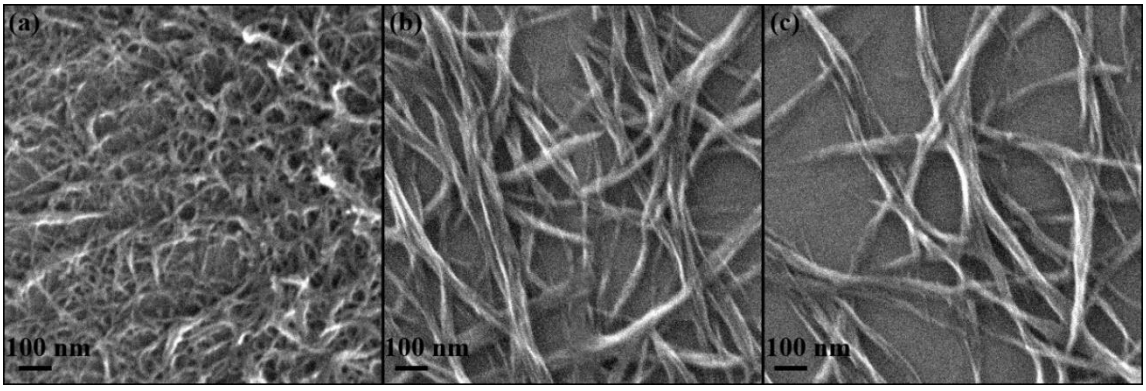

Figure 25. SEM image of HiPco SWCNT films on a glass substrate, (a) 20 µg HiPco SWCNT film dispersed in NMP, (b) 100 µg HiPco SWCNT film dispersed in IPA, (c) 20 µg HiPco SWCNT film dispersed in IPA. The diameter of every film is 75 mm.

Figure 25 shows a clear difference in bundle size when the same bulk powder is dispersed in two different solvents. Although in all CNT samples, there are bundles with a few nanometer sizes, most of CNT bundles that were dispersed in IPA are larger and

longer than the dispersed CNTs in NMP solution. Bundle size of CNTs dispersed in IPA is up to 100 nm. The average bundle size of CNTs dispersed in IPA can be estimated around 50 nm, while the average size of bundles for dispersed CNT in NMP is about 10 nm. ImageJ softwere was used to have an statistical average bundle size in these images.

Another important difference between Figure 25.(a) and (c) for the same amount of CNT (20 µg) dispersed in two different solvents can be observed is the patchiness between the CNT bundles. In Figure 25.(a), the pockets between CNT bundles are smaller a 50 nm diameter circle while in figure (c), the pockets can be as large as a 200 nm diameter circle.

Figure 26 shows a topographical image of the film that was created by transferring 100 µg HiPco SWCNTs dispersed in IPA captured using Atomic Force Microscopy (AFM). AFM images were acquired using a NaioAFM (Nanosurf Inc) in tapping mode. In this technic, the topography of the surface is captured by lightly tapping the surface with an AFM probe that is oscillated at its resonant frequency. The AFM probe that was used in this work is an HQ: NSC14 (MikroMasch) and its properties are summarized in Table 9. In this configuration, the probe cantilever substrate is excited vertically, and it reflects laser beam deflects in a regular pattern over a photodiode array, generating a sinusoidal, electronic signal or “detector signal.” Any deviation from regular cantilever oscillation can be interpreted as the topographical change in the surface.

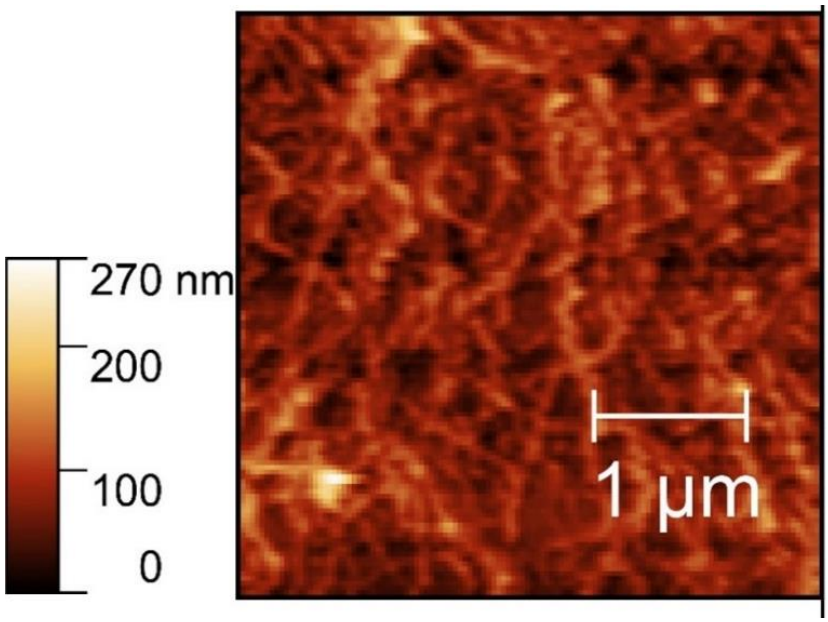

Figure 26. AFM image of CNT film made of 100 µg HiPco SWCNTs dispersed in IPA.

Table 9. Dimensions and properties of AFM probe

Probe	Resonance frequency (KHz)	Force constant (N/m)	Length (µm)	Width (µm)	Thickness (µm)	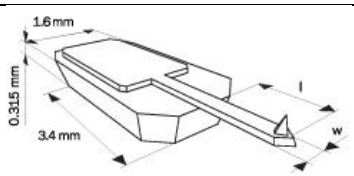
HQ:NSC14	146	4.56	125±5	25±3	2.1±0.5	

2.3.2. Raman spectroscopy of CNT film

Raman spectroscopy is another approach that can be used for measuring the bundle size of carbon nanotubes. Resonant Raman measurements provide fundamental information on the vibrational, rotational and other low-frequency modes and internal structure of the CNT bundles, and it already has proven itself as a powerful tool for

characterization of CNT films [249-252]. Here in this study, Raman spectroscopy measurements were performed using a Horiba XploRa Raman microspectrometer in the ambient environment by a green laser (excitation laser line of 532 nm) and a near infra-red laser (excitation laser line of 785 nm). A 100X objective lens was employed to focus the laser beam on the CNT film, and the measurements were conducted with 1200 gr/ mm grating, 1% ND filter and a 0.2 mW laser power to avoid any damages to the samples. For calibration, the phonon mode from the silicon substrate at 520 cm^{-1} was used.

Figure 27 shows the Raman spectra of the CNT film on the glass wafer. The first peak that is observed around 250 cm^{-1} for CNT films is called Radial Breathing Mode (RBM). RBM is due to radial expansion-contraction of the nanotube. As a result of a defect activated band in sp^2 hybridized carbon materials, D band is observed in Figure 27, and its frequency is 1338 cm^{-1}. The first-order Raman band of all sp^2 hybridized carbon materials is being observed at 1590 cm^{-1} in Figure 27, and it is called G band. G-line corresponds to the tangential vibration of carbon atoms is a Raman feature of the graphitic layers. The ratio of D and G band can give us some information about the defects in the CNTs. The large G/D band ratios suggest high-quality carbon nanotubes as also reported previously [249, 253].

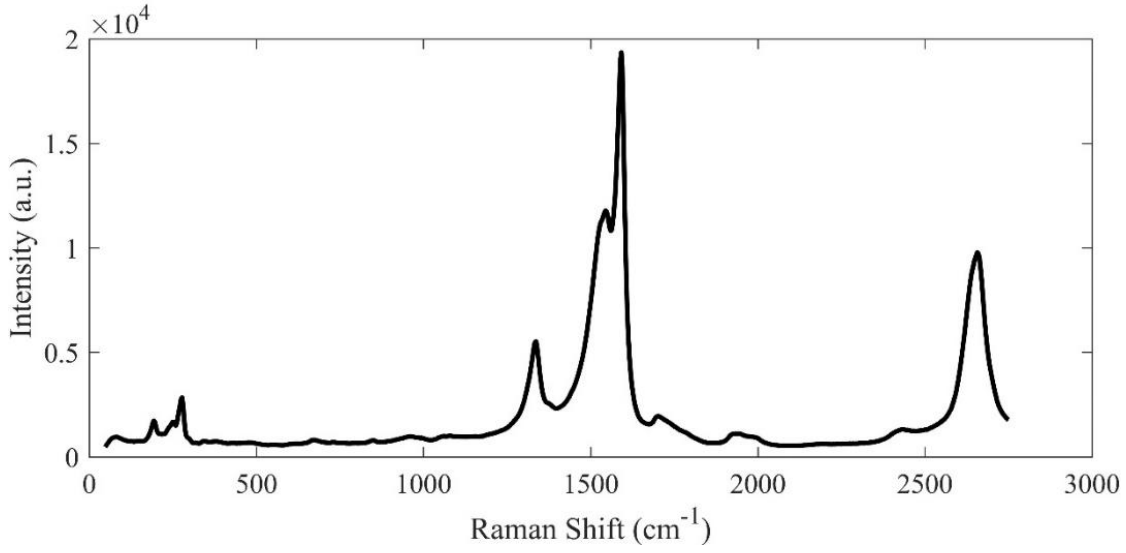

Figure 27. Raman spectra of CNT film composed of HiPco SWCNTs dispersed in IPA captured with a green laser.

In RBM mode, all the carbon atoms are moving in-phase in the radial direction. The RBM position is typically in the range of 100–350 cm^{-1}. If RBM intensity is particularly strong, its weak second overtone can be observed at double frequency. It has been suggested that the frequency of RBM (in cm^{-1}) is a function of nanotube diameter (d):

$$\omega_{RBM} = \frac{A}{d} + B \qquad \text{Equation 1}$$

where A and B are constants dependent on the preparation and environment in which the nanotube is present. For individual SWCNT, B constant can be estimated as 0. Dresselhaus et al. suggested that for typical SWNT bundles that their diameter range is 1-2 nm, A=234 cm^{-1} and B=10 cm^{-1} [254]. The B constant is due to the shift in Raman spectra as a result of tube-tube interaction. However, this formulation is for individual CNTs, and since our CNT film is consist of larger bundles, we cannot use these constants. Heller et al. was able to show that changing the CNT film from individual HiPco SWCNTs to films with larger bundles can change the Raman spectra for CNT films.

Figure 28 have shown captured Raman for different CNT bundles using 785 nm wavelength laser.

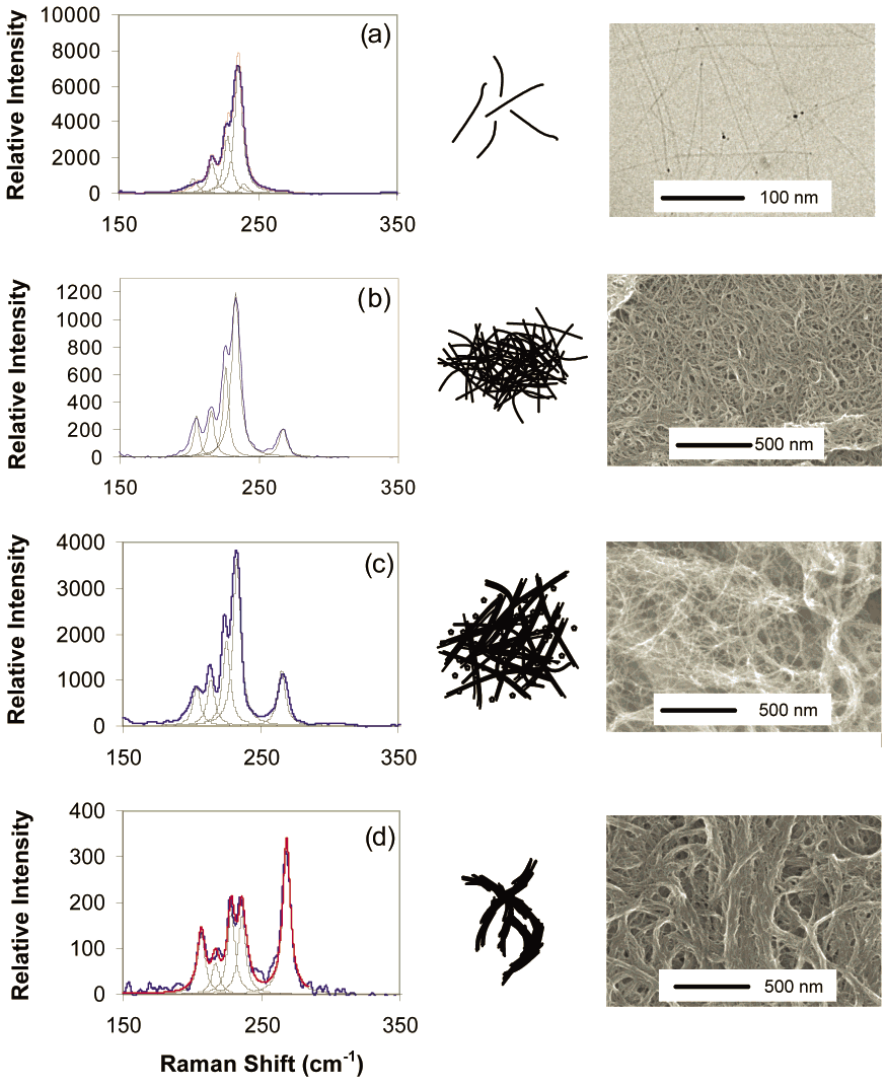

Figure 28. The effect of bundle size in Raman spectra of CNT film [226].

It can be observed that the ratio of peak intensity for 267 cm^{-1} and 234 cm^{-1} can show how the bundle size is changed [226]. For the largest bundle size in Figure 28.d, the ratio (I_{267}/I_{234}) is much larger than the same ratio with the smaller bundle size at Figure 28.b. In Figure 28.a, the peak at 267 almost vanishes from the spectrum. Figure 29 compares

the RBM mode captured with a 785 nm wavelength laser for three different CNT fabricated from 20 µg dispersed in NMP, 20 µg dispersed in IPA, and 100 µg dispersed in IPA.

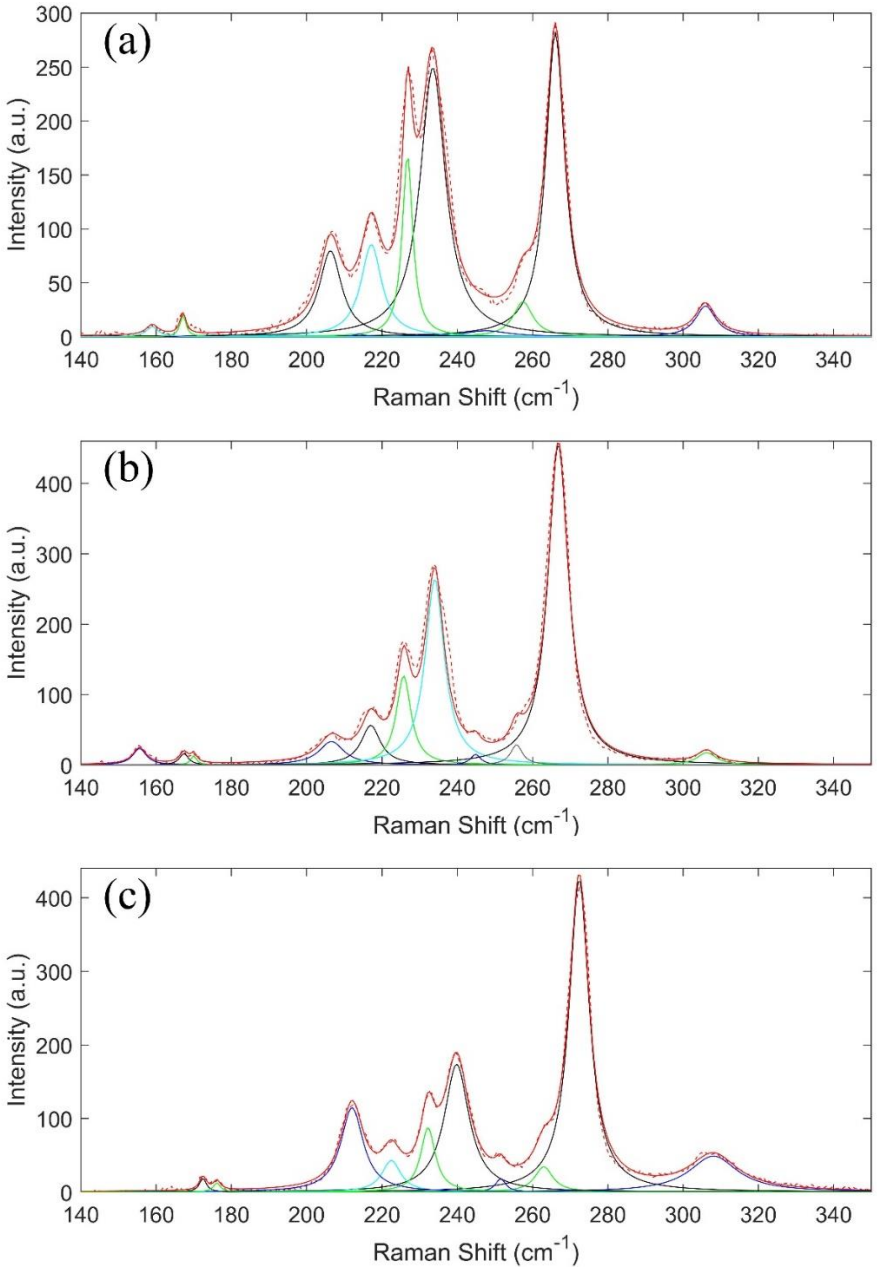

Figure 29. RBM Raman spectra (red line) of different CNT film fabricated on a glass substrate from (a) 20 µg dispersed in NMP, (b) 20 µg dispersed in IPA, (c) 100 µg dispersed in IPA. Raman spectra were fitted by Lorentzian functions.

Figure 30 is comparing the Raman spectra of three different CNT fabricated films on glass slide captured by infra-red laser focused on G and D bands in the Raman shift range of 1000-2000 cm^{-1}. As it can be observed, the highest $I_{G/D}$ belongs to 20 µg CNT dispersion in NMP ($I_{G/D}$=6.4), while this ratio for the 20 µg CNT dispersion in IPA ($I_{G/D}$=5.8) and the 100 µg CNT dispersion in NMP ($I_{G/D}$=5.78) are very close. This is an indication of less defects in carbon nanotubes in case of ultrasonic bath sonication in NMP.

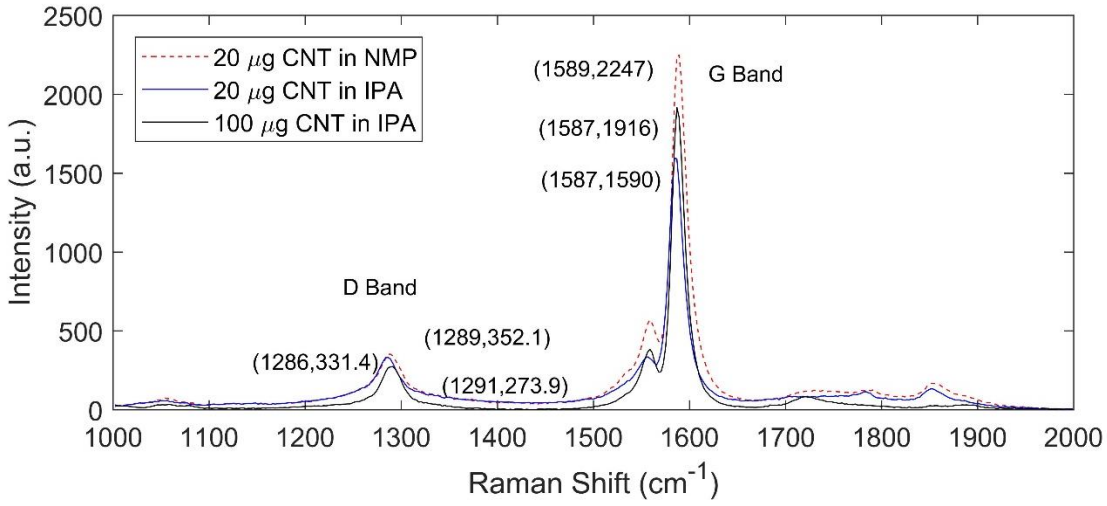

Figure 30. Comparison of D and G band intensities for three different fabricated CNT film.

Considering Figure 28, Figure 29 can qualitatively compare the bundle size in 3 different CNT films. As the (I_{267}/I_{234}) ratio increases from Figure 29.a to Figure 29.c, the bundle size is increasing as well (Figure 25). However, for quantitate measurement of bundle size larger than 2 nm, SEM is the best approach. We assumed a Cauchy distribution for each peak and Figure 29 is showing how the summation of those individual peaks can result is the final Raman Spectrum that was captured from the fabricated sample.

It is extremely hard to have a precise estimation of the structure and chirality of CNTs in the fabricated film without separating them. Tian et al. reported that 36±4% of HiPco SWCNT powder is metallic while the rest is semiconductive [255] and similar observation is reported by others [256, 257]. However, it is possible to put together the Raman spectroscopy data from fabricated films and optical absorbance of HiPco SWCNT dispersion in organic solvents (Figure 22) to recognize the dominant CNT structures in the final product.

Chapter 3

MECHANOBIOLOGY AND PREFERENTIAL ATTACHMENT OF CTCS TO CNT NETWORK

3.1. Introduction

Biomechanics is a branch of classical engineering mechanics application to biology, physiology, and medicine. Professor Y.C. Fung was the pioneer of this field in the mid-1960s, and now there is an award named after him by American Society of Mechanical Engineering (ASME) recognizing young investigators who are committed to pursuing research in the field of Bioengineering.

In 2009, the Physical Sciences-Oncology Centers (PS-OCs) Program was launched by National Institute of Cancer to use physics, and engineering concepts including mechanics to develop new tools and concepts for diagnosis, prognosis, and treatment of cancer and this was an official start for the application of mechanobiology in oncology. This concept is not new, and as a qualitative example, it has been stablished that breast cancer tumor feels stiffer than surrounding tissue. There are several aspects of cancer that can be studied and investigated using traditional mechanics including extracellular matrix stiffness, the influence of microenvironment on cell mechanics and tumor growth and progression, mechanical forces in tumor angiogenesis, mechanics of cell migration, CTC biomechanics and isolation, and developing new biomaterials for cancer study.

Here in this chapter, we will focus on focal adhesion of CTCs and how we can use Nanotube-CTC chip as a biointerface to isolate CTCs.

3.2. Mechanobiology of CTC adherence to extracellular matrix (ECM)

The cytoskeleton is the framework of every eukaryotic made of a dynamic network of multi molecular protein. The three main categories of filaments: microfilaments (actin filaments), intermediate filaments, and microtubules. The internal construction of these linkages is defining the shape of the cell. The architecture of cytoskeleton and the attraction forces between its components are determining the stability, mechanical properties, and deformability of the cell.

Microfilament is the thinnest component of the cytoskeleton, and its diameter is 5-7 nm [258]. Microfilaments are composed of actin proteins. In addition to their role for creating the skeleton of cell, they generate force when their end pushes against a barrier, such as the cell membrane and provide rigidity to the cell membrane. They also are the pathway of myosin molecules which are motor proteins best known for their roles in muscle contraction. Intermediate filaments are 8-10 nm, and they are made of a pair of two intertwined proteins that is called a coiled-coil structure [259]. Intermediate filaments are mostly bearing tension within the structure of the cell. Intermediate filaments act as the structural component of Nuclei lamina and it also anchors organelles within the cell.

Microtubules are the largest filaments in cell structure with inner diameter of 12 nm and outer diameter of 24-28 nm [260, 261]. In contrast to intermediate filaments,

microtubules are bearing the compression forces on the cell structure. Microtubules are mainly made of two polymers: α and β tubulin. The microtubule is also the passage of motor proteins that move on the surface of the microtubule transport the materials within cells. Figure 31 is an image of the three different components of the cytoskeleton.

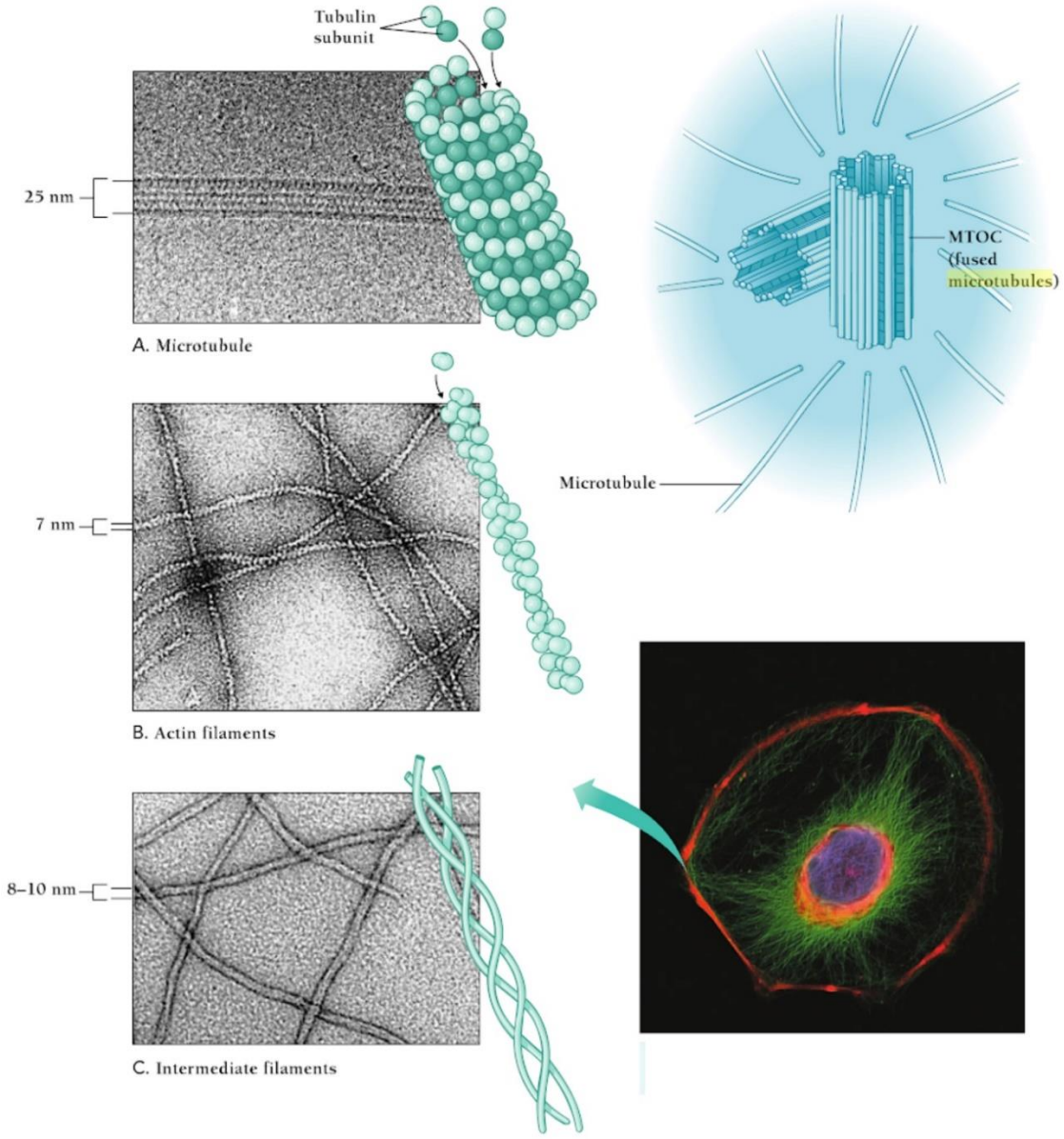

Figure 31. Different filaments on cell cytoskeleton, microtubule (green), microfilament (red) and intermediate filament [262].

One of the unique properties of microtubules is their dynamic switch between growth and shrinkage in the cell. While most of the microtubules have a half-life of 5-10 minutes, some of them can last hours [263]. Microtubules are the longest filament in cell structure with length up to 50 μm [264], and they are drawn from microtubule organizing center (MTOC) to membrane barrier. They are also extended outside of the cell and interact with ECM. To create higher order structures and more stability, microtubules are using accessories proteins to crosslink together. Not only these accessory proteins are regulating and creating larger forces, but they also facilitate mechanotransduction [265]. In fact, one of the critical roles of these accessory proteins is to transfer force, ion or other important information through signals to the core and create a signal network [266]. This is how a cell senses its 3D environment condition, the forces that are applied to its barrier, and control the filaments for adapting to different situations. Growing and shrinking the microtubules are based on the information that is transferred through the accessory proteins.

Cell protrusions which are cross-linked of multiple microtubules are called microtentacles (McTNs). McTNs are dynamic structures that promote reattachment of mammary epithelial cells to surfaces [267]. As it was mentioned in the first chapter, one of the steps in the cascade of metastasis is adherence of CTCs to the endothelium cells inside a blood vessel [268], and McTNs is the major component of CTCs contributing to this step. Filopodia is also another component that may contribute to adhesion of CTCs [269]. Filopodia are other membrane protrusions that function as antennae for cells to

probe their environment [270]. However, McTNs are tubulin-based while filopodia are actin-based and they are mechanistically distinct from each other [271].

Cytoskeleton of CTC is different from normal cells, and that unique structure is enabling tumor cells toward survival and progression. Using the McTNs is one of the main differences in CTCs that help them for better adherence to ECM. However, CTC's structural network is protecting them against the deformation caused by shear stress in the vasculature [272]. For example, in lymphatics with a typical diameter of 15-75 μm, CTCs should bear average shear stress of 0.64 dyne/cm^2 [273]. The wall shear stress at microcirculation including arterioles, capillaries, venules is 3-140 dyn/cm^2 [274]. This range is estimated based on low Reynolds number. Adhered CTCs should tolerate this shear stress at its interface with endothelium and its special cytoskeleton organization and McTNs enable them to survive and create a dormant site. Obviously, CTCs will not be able to adhere near heart due to high flow shear stress and turbulent flow. However, CTC clusters which are a series of CTCs adhered together should bear high shear stress at heart up to 520 dyn/cm^2 [275] and the created bond between CTCs' cytoskeleton in a cluster should be robust to tolerate such shear stress.

One of the most interesting mechanical properties of CTCs is their dynamic framework and alterations in its cortex stiffness [276]. While the CTCs should be stiff through the larger arteries and high blood shear stress to survive, they need to be more deformable in microvessels which allow them to squeeze through the narrow capillaries [272]. There is also the possibility of cell deformation inside microvasculature because of hemodynamic forces [277].

Focal adhesions are integrin-containing, multi-protein structures that form mechanical links between intracellular actin bundles and McTNs tips and the extracellular matrix or substrate in many cell types [278]. Cadherins are the other category of cell adhesion molecule (CAM) that contribute to the adhesion of cells [279]. Integrin and cadherin both help as physical linkages as well as sensing tools for cell interaction with its environment and neighbor cells [279]. The process of adhering cells to other cells or ECM is a very complicated process, and it involves a lot of components and chemicals [280]. There are also several theories and mechanisms including catch-bond mechanism suggested by different groups for modeling the integrin binding mechanism [280].

One of the hot topics in mechanobiology is the effect of CTCs and tumor microenvironment on cancer progression and treatment. In specific, forces between cell-cell interfaces and cell-ECM interfaces are important factors. CTCs apply forces on the biointerface they are adhered to, and their shape and response would be corresponding to shear stress and forces in their surroundings. So, by measuring these forces between the cell and its environment, it would be possible to characterize the state of the cell itself. As an example, Kraning et al. used interaction force microscopy to investigate cellular contractile force as an important role in metastasis. They reported that the metastatic cancer cell lines exert larger forces to the surface that they have adhered to. Figure 32 has plotted the said forces that cell lines from breast, prostate, and lung cancers are applying on the adhered surface.

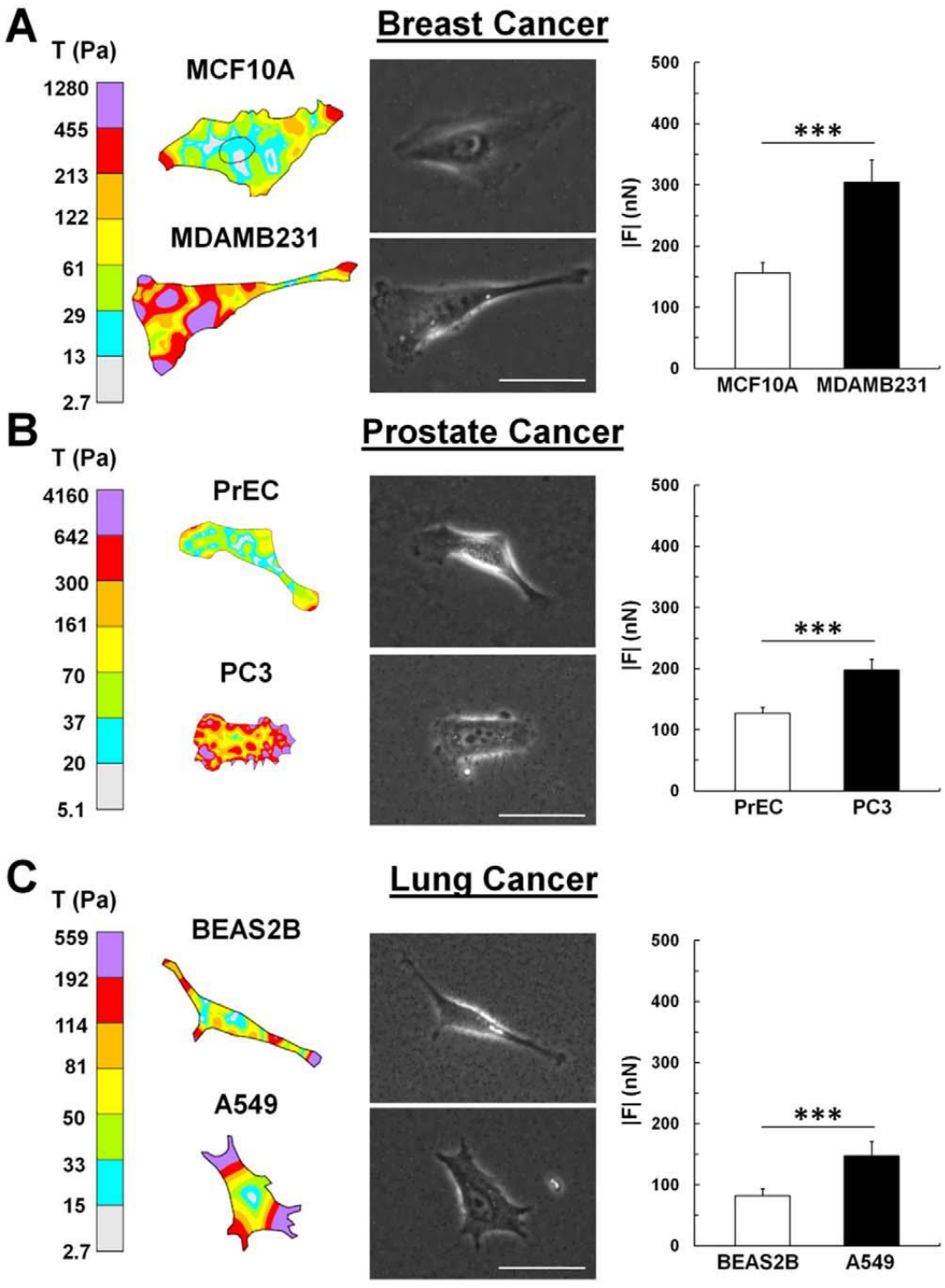

Figure 32. Larger forces of metastasis cancer cell line in comparison to non-metastasis cells [281].

Rigidity or stiffness of the surface is an essential parameter in strengthening the focal adhesion of CTCs to ECM [282]. Figure 33 shows a model that is being used to explain how rigid surfaces enhance the focal adhesion. In this figure, the black spring represents the rigidity of ECM while the green spring represents the actin-associated proteins that are functioning as a force sensor element regrouped into an integrin–cytoskeleton complex which couples the actin filaments to the adhesion protein. The purple element is a signal generator. Inside the cell, the actin filaments are pulled away by myosin which acts as the motor, generating forces on the integrin–cytoskeleton complex as well as the ECM (red arrow). When the signal generator binds to a deformed force-sensor, it would be activated or inhibited (Figure 33.a) [282]. Figure 33.b shows another configuration which the signal generator is incorporated into the force-sensor element.

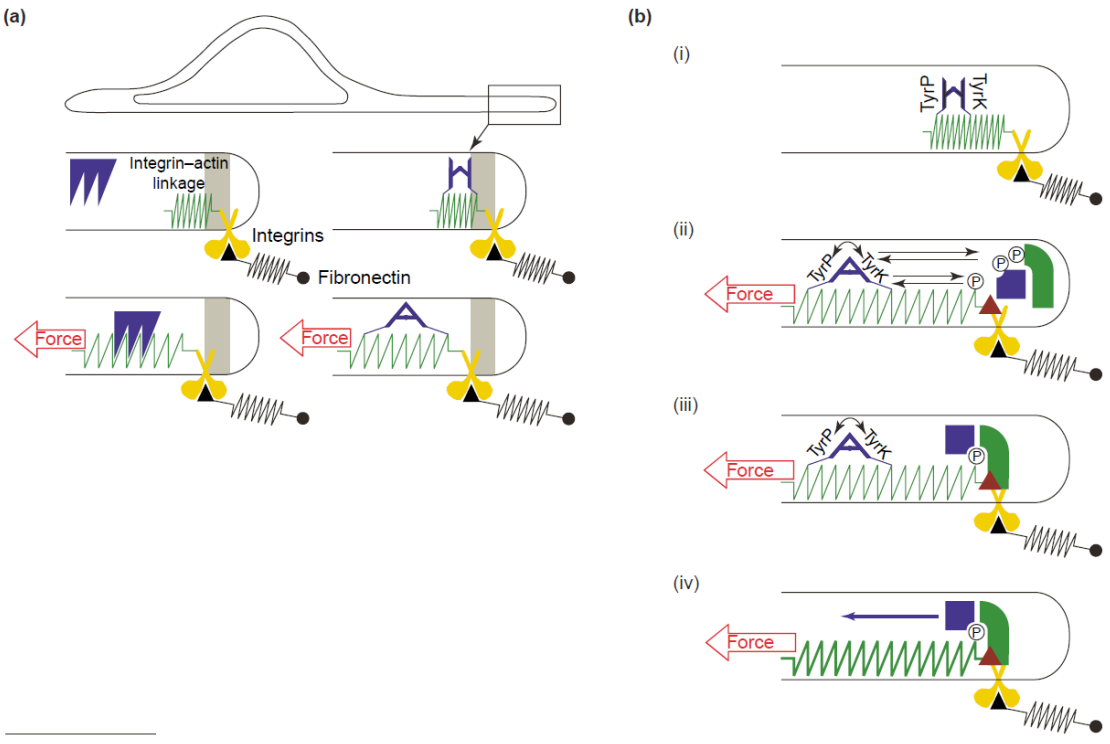

Figure 33. A schematic image for explaining how rigid surfaces enhance focal adhesion [282].

Figure 33.b.(i) shows a situation without bearing any forces which leads to inactivate the signal-generator element (blue shapes) [282]. In Figure 33.b.(ii) structural (green solid) and signaling (blue solid) proteins, which are substrates of phosphotyrosine signaling, are either cytosolic or part of the force-sensor elements. Force generated by the cytoskeleton activates tyrosine kinases and phosphatases (transition of the blue H to the blue A) and balancing the phosphotyrosine signaling (double arrows) defines the level of substrate phosphorylation. Figure 33.b.(iii) is showing the binding of structural and signaling proteins to phosphotyrosine and phosphotyrosine signaling induces changes in protein binding and/or catalytic activity. In Figure 33.b.(iv) binding and changes in activity enhance the strength of integrin-cytoskeleton linkage which is shown by thickening of the green spring. This has led to downstream signaling (blue arrow) [282].

Other groups have previously reported isolating CTCs using preferential adherence. The capture of CTCs based on CAM strategy (Vita assay) is a unique strategy and is a method of adherence [95]. The proclivity of a tumor cell to invade collagenous matrices is one of the hallmarks of metastasis. In the past, it was hypothesized that populations of CTCs that adhere and invade collagenous matrices would be invasive and exhibit the propensity of progenitor cells to metastasize [95]. With the nano-roughened glass microfluidic CTC capture device, Chen et al. was able to achieve capture yields of up to 80% for both EpCAM+ (MCF-7, SUM-149, A549) and EpCAM- (MDA-MB-231) cancer cell lines [283]. However, they lysed the RBCs before mixing the tumor cells with

blood, and they could not expand their work further. Here in this chapter, the focal adhesion of tumor cells to CNT bundles will be discussed.

3.3. Experimental setup

3.3.1. Device fabrication

Two 4" D263 glass wafers were fabricated by transferring 100 µg HiPco SWCNT dispersed in IPA on each as it was discussed in chapter 2. Two more Borofloat® 33 glass wafer glass wafers were fabricated by transferring 20 µg HiPco SWCNT dispersed in NMP or IPA on each. The devices were diced after electrode and isolation layer fabrication. It should be noted that to protect the CNT film on each device during dicing, a protective layer of S1813 photoresist was spun and deposited as it was described in chapter 2. The devices were protected in a vacuum desiccator from any surface chemical change. The day before the experiment, diced devices were washed with acetone, methanol, and DIW. Then they were dried with Nitrogen gun, and they were kept under UV light overnight.

3.3.2. Cell culture

The breast adenocarcinoma cell lines Luciferase/Green Fluorescent Protein (GFP) dual-labeled MDA-MB-231 (GenTarget # SC044) was cultured in RPMI-1640 growth medium, MCF7 breast cancer cells (ATCC® HTB-22™) were cultured in EMEM growth medium, SKBR-3 breast cancer cells (ATCC® HTB-30™) were cultured in McCoy's 5a growth medium, cervical adenocarcinoma cell line HeLa (ATCC® CCL2™) was cultured

in low glucose DMEM growth medium, and brain cancer cell lines U251, U-343, LN-229 were cultured in low glucose DMEM growth medium as per their suggested protocol by manufacturer. All media contain 10% Fetal Bovine Serum (FBS) and 1% penicillin-streptomycin. The cell lines were incubated at 37 ^{o}C 5% CO_2.

Cells were grown to reach ~80% confluence. Cells were then washed with PBS and detached from the culture dish using Gibco™ Trypsin-EDTA (Cat No. 25200056). Next, they were centrifuged at 130 gf and suspended in a specific culture media volume, and hemocytometer was used to count the cells and calculate its concentration.

3.3.3. Immunofluorescence microscopy

We were able to do the microscopy and identification of captured cells directly on the chip without further transfer. For immunofluorescent analysis, after washing the devices with PBS once, they were fixed with 4% paraformaldehyde for 10 minutes. The sample was washed with PBS and then blocked with immunofluorescence blocking buffer (cell signal #12411) for 1 hour at room temperature. The primary antibody was diluted based on the suggested concentration by the manufacturer, and then the sample was covered with it, incubated at 4 ^{o}C overnight. The sample was washed with PBS 3 times. The secondary antibody was diluted to 1 μg/ml, and the sample was covered for 1 hour at room temperature in a dark container. The final step was to stain the nucleus with DAPI, wash the devices and mount the sample with a coverslip. Table 10 has listed the antibodies that have been used in this chapter. Except for the DAPI, the other primary antibodies are reactive only to human cells.

Table 10. Utilized antibodies for immunofluorescence identification of adhered tumor cells on Nanotube-CTC chip.

Antibody	Manufacturer	Host	Clone	Used dilution
Cytokeratin 8/18	Thermofisher (#180213)	Mouse	Zym5.2 (UCD/PR.10-11)	1:100
EGFR	CellSignal (#4267S)	Rabbit	D38B1	1:50
DAPI	CellSignal (#4083S)	-------	-------	0.1 µg/ml
CD 59	BD Pharmingen (#555763)	Mouse	p282 (H19)	1:100

3.3.4. Preparation of adhered cells for electron microscopy

For this purpose, we deposited 200 breast cancer cells from SKBR3 cell line in a 10 µl droplet on a Nanotube-CTC chip. This chip was maintained in culture condition inside an incubator at 37 ºC 5% CO_2 for 48 hours. After 48 hours, the droplet was removed, and the chip was washed once with PBS.

After removing the media, the cells were fixed with freshly prepared 3% glutaraldehyde in PBS at 37 ºC for 15 min. The device with fixed cells was washed three times over 5 min with PBS. Next, the cells were fixed with 1% osmium tetroxide (OsO4) at room temperature for 30 min. The device with fixed cells was rinsed five times over 10 min with PBS. Then, the device was incubated in freshly made 1% carbohydrazide for 30 min. The device then was washed five times over 15 min with DI water. In the next step, the device was incubated in 1% OsO_4 for 30 min. The device was washed 3 times over 15 min with DI water. Dehydration was carried out sequentially in the dishes with ethanol at concentrations of 30%, 50%, 70%, 90%, and three times 100 % over 30 min. The device was then dried in Critical Point Dryer. The surface of the device was

sputter-coated with 1-2 nm thick layer of gold-palladium . SEM images were then recorded.

3.4. Attachment of CTCs to Nanotube-CTC chip

The cytoskeleton is the dynamic network of interlinking protein filaments in a cell and Microtentacles are microtubule-based membrane extension of cancer cells framework that act as linking tools for focal adhesion and aggression. Here in this work, we have used a similar concept for isolation of tumor-derived epithelial cells from peripheral blood, with high purity, by exploiting the physical mechanisms of preferential adherence of CTCs on a nanotube surface.

3.4.1. Electron microscopy of single-cell adhesion on the nanotube surface

We conducted electron microscopy studies of attached single cells to investigate the mode of how cancer cells attach to the nanotube surface. Figure 34 is the SEM image of an attached SKBR3 cell that was incubated for 48 hours on the nanotube surface. The striking image suggests that cancer cells change morphology and spread on the nanotube surface causing strong focal adhesion. The filaments from the main body of the cell extend to the nanotube surface. Many such filaments are observed to attach to the individual nanotubes/bundles directly. The diameter of these filaments is about 150 nm to 200 nm, and cannot be seen under an optical microscope. The exposure of some of these filaments under an SEM suggests, thousands of such filaments bond to the nanotube matrix from underneath the cell. Integrin receptors are vital in static in vitro cell adhesion

and spreading [32]. Specific integrin binding provides a mechanical linkage between the intracellular actin cytoskeleton and nanotube matrix [32]. The EM studies suggest that tumor-derived epithelial cells attach firmly to the CNT surface, including individual CNT bundles and exhibit active dynamics, which suggests our hypothesis. More electron microscopy images of adhered SKBR3 are shown in Appendix A.

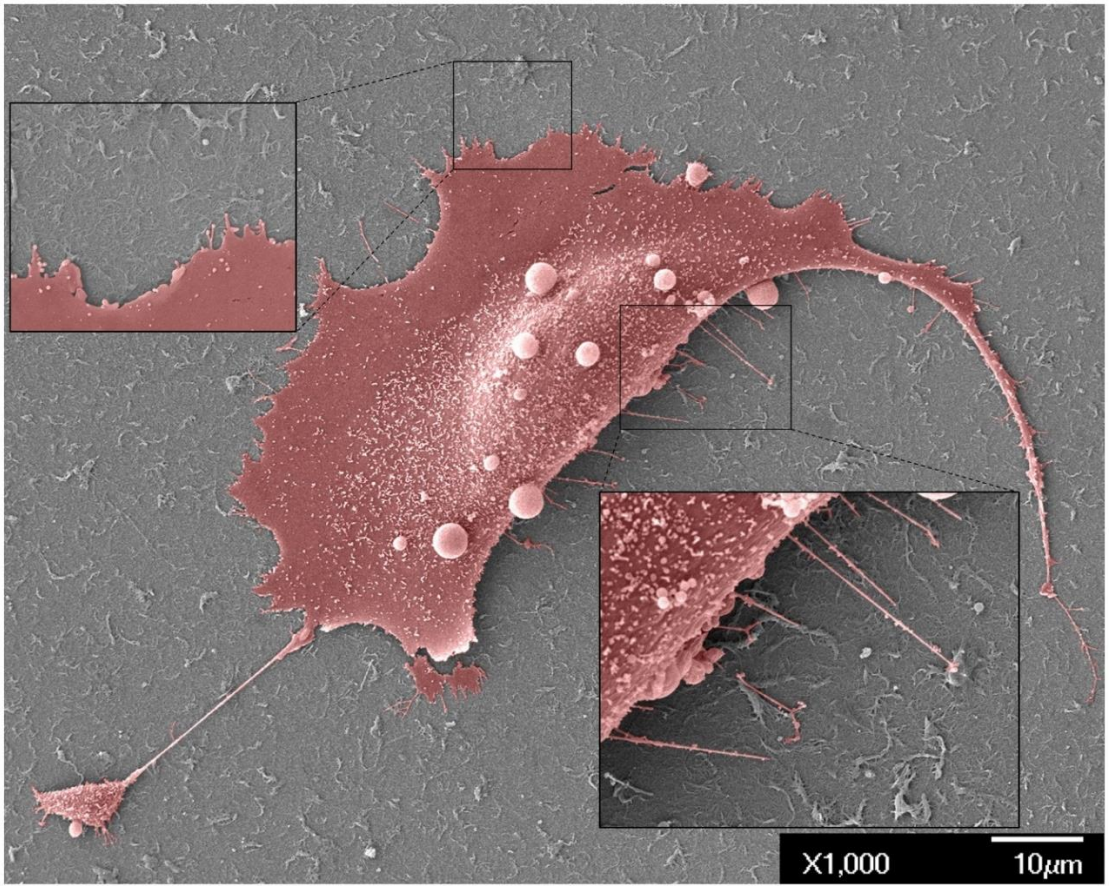

Figure 34. Electron microscopy of adhered breast cancer cell (SKBR3) on the nanotube surface.

There have been several studies that have investigated the focal adhesion of tumor cells to CNTs [284-286]. In one of the most recent studies, Imaninejad et al. investigated the process by which cells attach and spread on CNTs [284]. Considering

mechanical interaction between cells and the underlying substrate can influence cell spreading and communication, they hypnotized that focal adhesion of tumor cells on nanotubes is integrin-dependent and is facilitated by the adsorption of serum and cell-secreted adhesive proteins to the nanotubes. In a series of controlled experiments comparing two culture media with and without serum, they were able to show that cells had higher cell spreading area (per individual cell) and an elongated morphology (low shape factor) in the presence of serum in the medium and lower cell spreading area and a more rounded morphology (high shape factor) in the absence of serum. In addition, they could show that cell spreading area in the presence of serum was significantly higher than other media. Finally, they claimed that cells attached and spread via integrin binding onto all substrates in all media conditions, indicating that serum or cell-secreted adhesive proteins adsorb on the nanotubes and elicit cell attachment and subsequent spreading. It has been previously reported that proteins including fibronectin are adsorbing tightly onto the CNT surface due to π-stacking[284].

Surface properties of materials also influence the composition of the adsorbed protein layers, which subsequently regulate a variety of cell behaviors such as attachment, viability, spreading, migration, and differentiation [287]. surface roughness can also increase fibronectin expression and secretion by fibroblast cells, and that fibronectin expression is greatly enhanced in high serum conditions and minimal in low serum conditions [288].

3.4.2. Adherence of tumor cells to Nanotube-CTC chip independent of cancer type

Although the focus of the current thesis was on the breast cancer patients and cells, isolation of tumor cells using Nanotube-CTC chip is not limited to specific cancer types, and therefore could potentially capture any type of epithelial cancer cell which constitutes the four significant cancers (breast, colon, lung, and prostate) using the method of preferential adherence. Further, our method is currently the only one to track both adherent and non-adherent cells on the same chip, thus effectively tracking all the cells, a task that is of high value in CTC capture especially in early-stage cancers where the cell numbers may be meager.

Cultured cells from HeLa (Cervix), U-251 (Glioblastoma), MCF7 (Breast), LN-291 (brain), and SKBR3 (Breast) cell lines were prepared as it was explained in section 3.3.1. Several devices were prepared from a bare 4'' D263 glass wafer with 100 µg CNT film which was dispersed in IPA. 200 cells in 10 µl of culture media for each cell line were deposited on each device. After 48 hours, the number of seeded cells on each device was counted using an optical microscope. After initial count, the droplet was removed and 10 µl of PBS was deposited on the device to avoid drying. Again, the number of cells that were adhered to the surface was counted as the captured cells. Figure 35, Figure 36, Figure 37 show the captured cells for different cell lines.

Table 11 has summarized the result of these experiments. This table shows that the yield of adherence has been more than 88%. With suitable functionalization protocol, one can also capture non-epithelial cells such as lymphoma and sarcomas.

Table 11. Adherence rate of different cancer types on CNT film.

Cancer cell line	Number of seeded cells	Number of adhered cells	Capture efficiency (%)
Hela (cervix)	189	186	98.4
MCF 7 (Breast)	194	181	93.3
SKBR3 (Breast)	201	177	88.1
U-251 (Glioblastoma)	212	203	95.8
U-343 (Brain)	208	202	97.1
LN-229 (Brain)	198	195	98.5

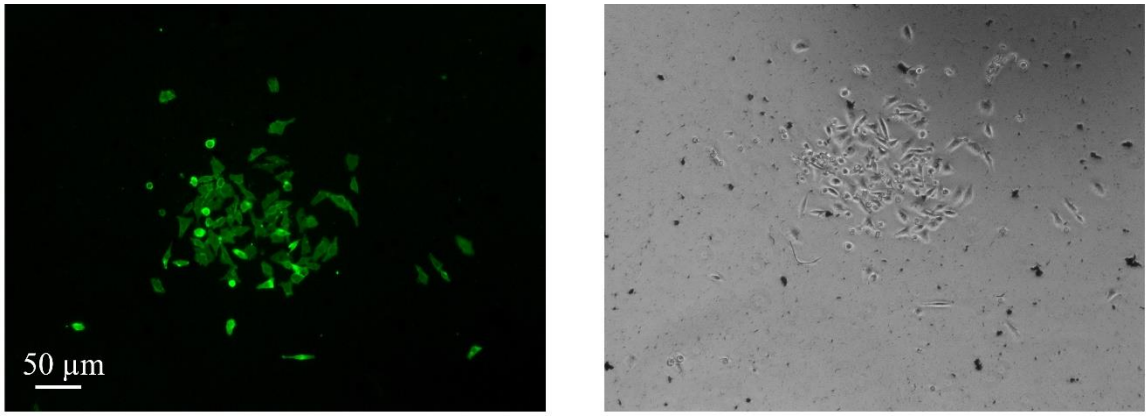

Figure 35. Stained cervix cancer cells (HeLa cell line) with CD59-FITC antibody in the right and the same cells under optical microscope on the right.

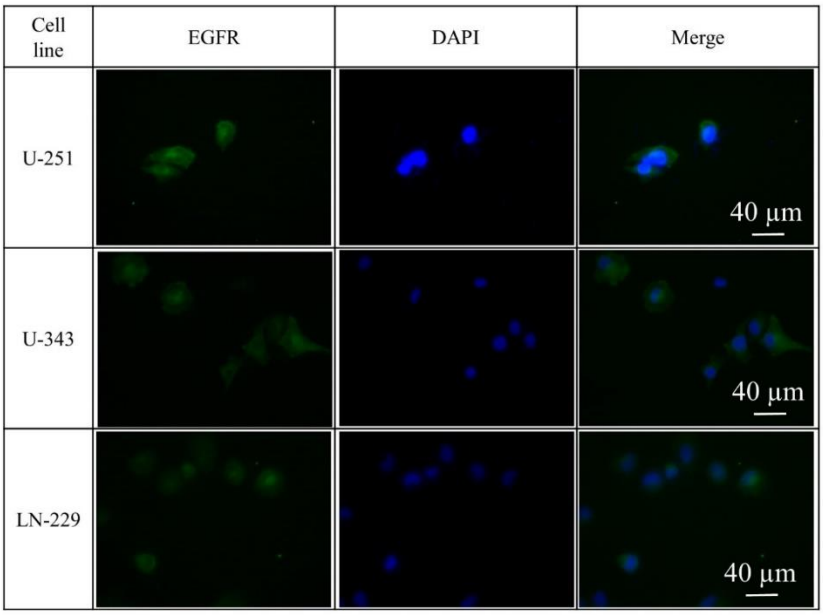

Figure 36. Stained U-251 (Glioblastoma), U-343 (Brain), and LN-229 (Brain) cancer cell line adhered to Nanotube-CTC chip.

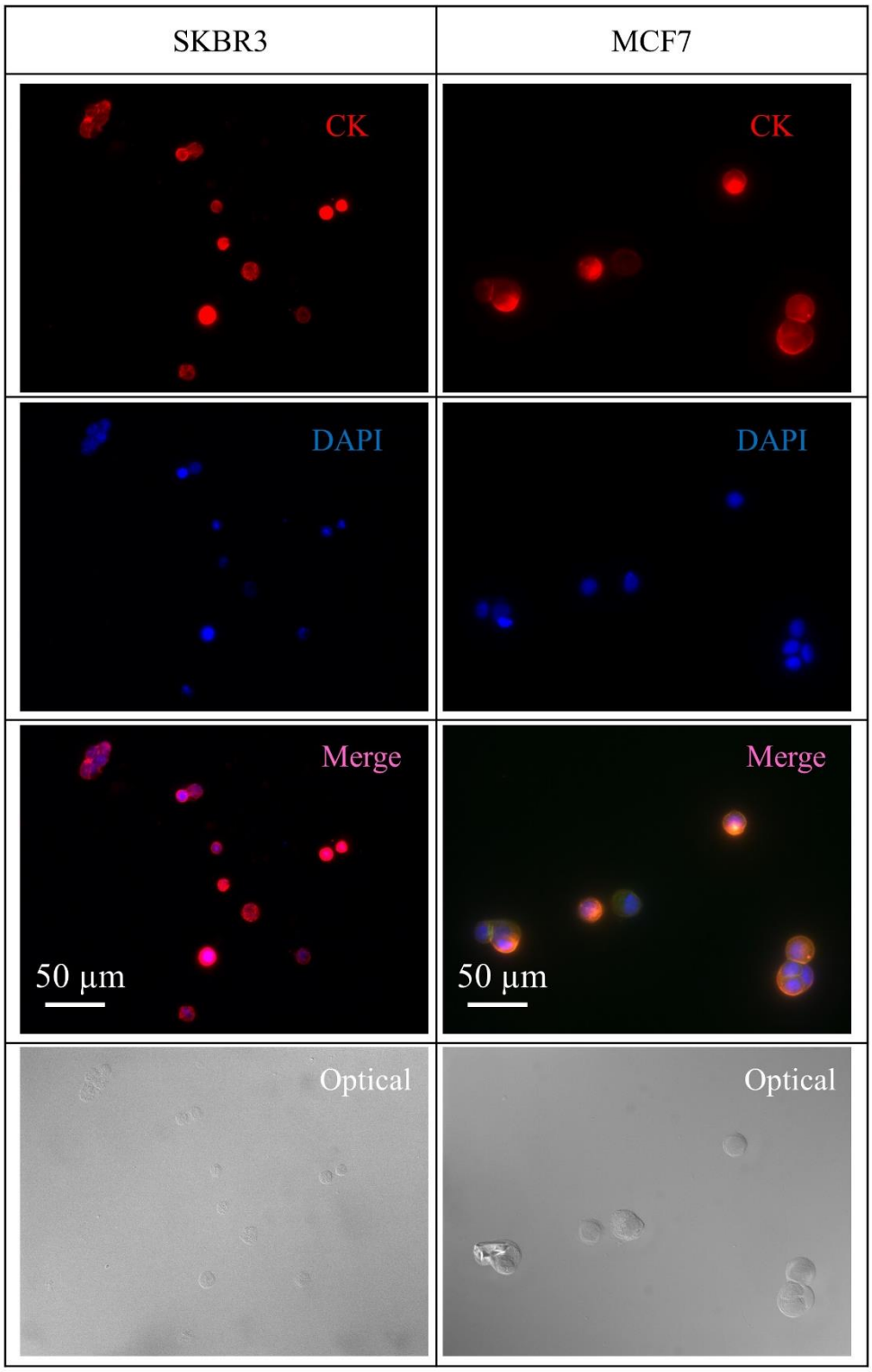

Figure 37. Breast cancer cell lines SKBR3 and MCF7 adhered to Nanotube-CTC chip stained with cytokeratin 8/18 for their epithelial membrane and DAPI for their nuclei.

It is also possible to culture tumor cells directly on the Nanotube-CTC chip. This will be very important since the expansion of captured CTCs can be very helpful for genomic and personalized treatment. Figure 38 presents how 3 cells in day 0 have proliferated into 13 cells in 6 days. Growth and shrinkage of microtubules and McTNs is the method that cells are using to expand and move around the surface [262].

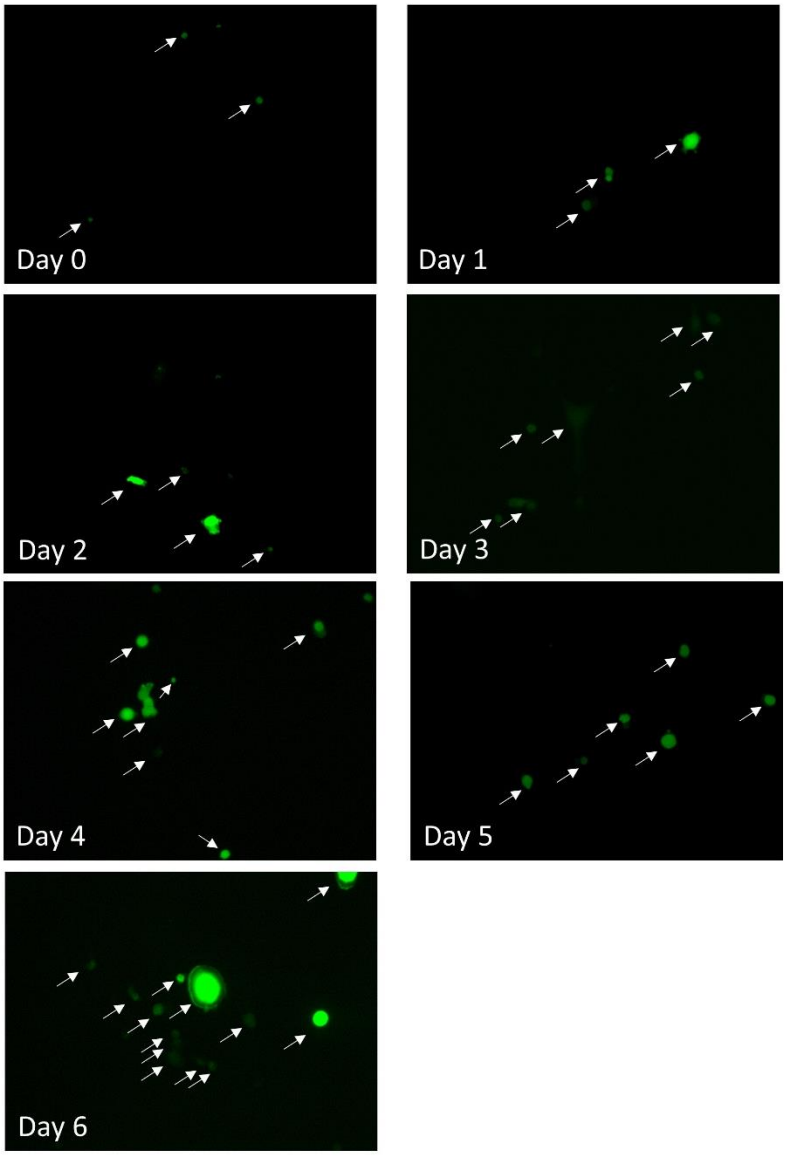

Figure 38. Expansion of MDA-MB-231 breast cancer cells cultured directly on Nanotube-CTC chip.

3.5. The correlation between CTC capture efficiency and CNT surface topography

One of the influential elements of adhering CTCs to CNTs that is confirmed with others [283] is topography and roughness of the surface. In order to investigate this theory with carbon nanotubes, the CNT powder dispersion in different solvents and its effect on CNT bundles should be discussed.

Due to the narrow distribution of CNTs and their surface attraction, CNTs are naturally forming bundles. The size of CNT bundles depends on their synthesis, environment, chemical and physical properties, and chirality. Dispersing CNTs in different organic and inorganic solvents have been studied extensively, and it is a common practice for reducing the bundle size to a few CNTs by dispersing the bulk CNT powder in solvents [232, 248]. Here we used two organic solvents, IPA and NMP. These two solvents have shown promise for dispersion of bulk CNT powder, and they have been used for fabricating CNT thin films for different applications.

It has been reported that NMP is one of the best choices for the dispersion of nanomaterials, especially CNTs [232, 234]. Other solvents also have been reported for dispersing CNTs, but there are other considerations for using them especially their compatibility with MCE filters and our fabrication process. NMP is not compatible with MCE filters, but since it produces a high concentration dispersion of CNTs, it is possible to dilute it with other compatible solvents like IPA or chloroform and filter the diluted solution to have minimal effect on the MCE filter. Bulk HiPco SWCNT powder purified grade from Unidym industries was dispersed in IPA and NMP for 24 hours using an

ultrasonic bath as it was explained in the previous chapter. At this point, there should be no particle in the solution, and the solution should look homogeneous. If you still see particles with naked eyes, extra sonication time should be considered. It should be noted that depending on the solvent and bundle size, CNTs may intend to go back to bundle aggregation which will result in settling down at the bottom of the dispersion bottle.

The bundle aggregation depends on the interactions of van der Waals forces between carbon nanotubes and the interactions between carbon nanotube threads with dispersion solvent [232]. The problem with bundle aggregation is that it interferes with concentration measurement and the final CNT film mass on the substrates. For the dispersed CNT solution in IPA, any centrifugation will result in complete aggregation and losing the sample. However, in case of NMP dispersed solution, it is possible to centrifuge it up 10000 G-force without complete aggregation., centrifugation of dispersed CNT solution in NMP at high speeds will result in a high purity CNT solution with longer stability and high-quality CNT film output without any large bundles.

Cultured cells from SKBR3 cell line were prepared as it was explained in section 3.3.1. 3 set of devices were prepared: a bare 4'' Borofloat 33 glass wafer without any CNT, a 4'' Borofloat 33 glass wafer with a 20 µg CNT film which was dispersed in IPA, and a 4'' Borofloat 33 glass wafer with a 20 µg film of CNT which was dispersed in NMP. Three devices from each fabricated wafer were selected for this experiment. 200 cells in 10 µl of culture media were deposited on each device. After 48 hours, the number of seeded cells on each device was counted using an optical microscope. After initial count, the droplet was removed, and 10 µl of PBS was deposited on the device to avoid

drying. Again, the number of cells that were adhered to the surface was counted as the captured cells. Figure 39 is showing the capture efficiency of each device for SKBR3 cell line.

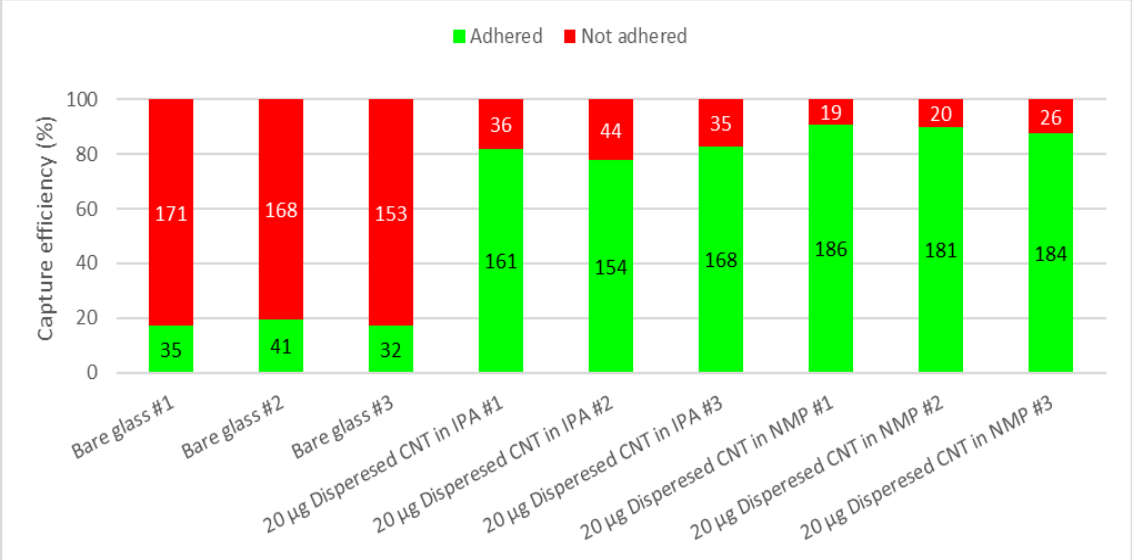

Figure 39. The capture efficiency of three different set of devices based on the mass and dispersion solution of CNTs.

The average of capture efficiency for bare glass is 17.9% while for 20 µg CNT films on the same glass wafer dispersed in IPA and NMP has been increased to 80.7% and 89.46%, respectively. This result indicates that for a glass substrate with roughness of 3 nm, the capture rate is small while adding the SWCNT film can increase this efficiency significantly.

There can be several explanations for different capture efficiency of CNT films with various morphology:

1- There was less defects in CNTs for 20 µg CNT film in NMP (higher IG/D in Figure 27) in compare to the film fabricated from the same amount of CNT

dispersed in IPA since. Enrichment in damaged CNTs can be one of the reasons for smaller capture efficiency in case of dispersed solution in IPA.

2- The purity of dispersed CNTs in NMP is higher since that sample was centrifuged and presented smaller wavelength for the targeted peak at the UV-Vis spectra graph in Figure 18)

3- Less defects in dispersed sample in NMP is an indication of higher surface energy. In addition, smaller pocket sizes between CNT bundles for NMP sample is an indication of higher surface. It is possible that having a higher surface energy is causing the higher capture efficiency for dispersed sample in NMP. Based on the electron microscopy of adhered cell on CNT film, the diameter of cells filaments are about 200 nm (Figure 34) while some of the pocket sizes in the SEM image of 20 µg CNT film in IPA is about the same size order (Figure 25). This can be a reason for having smaller capture efficiency.

4- Roughness is another reason for different capture efficiency as it was claimed elsewhere [283]. However, we did not compare the roughness of these samples and it is outside of the scope of current work.

3.6. Conclusion

Here in this chapter, we successfully demonstrated the adherence of different cancer cell lines to Nanotube-CTC chip with capture efficiency of > 90%. Three stages characterize the process of static in vitro cell adhesion: attachment of the cell body to its substrate (initial stage), flattening and spreading of the cell body, and the organization of

the actin skeleton network with the formation of focal adhesion between the cell and its substrate [289]. The deformation, mechanical stretching, and flattening are observed in our electron microscopy results.

Integrin receptors and heterodimeric transmembrane proteins play a central role in static in vitro cell adhesion and spreading [289]. Specific integrin binding provides not only a mechanical linkage between the intracellular actin cytoskeleton and nanotube matrix but also the bidirectional transmembrane signaling pathways [289]. The EM studies confirm that tumor-derived epithelial cells attach firmly to the CNT surface and exhibit active dynamics, which confirms our hypothesis.

The CNT film topography enhances the capture yield. This concept has been proven before in other studies [283, 290, 291]. Another possible contributing element in our study is the nature of CNT film. In previous studies, it has been shown that inorganic surfaces have yielded lower capture yield for CTCs [183, 291]. .

The last but not least, high stiffness of CNTs can help the focal adhesion. CNTs have the one of the highest Young modulus ever been measured in materials (1.25 TPa [207]) and Giannone et al. described how rigid surfaces stimuli the cells to produce more integrin and adhesion proteins to enhance the adherence of cell to nanotube film [282].

Chapter 4

CTC CAPTURE FROM SPIKED BLOOD SAMPLES USING NANOTUBE- CTC CHIP

4.1. Introduction

In the previous chapter, we established the fact that cancer cells intend to adhere to carbon nanotubes with very good efficiency. Different cancer types and cell lines including breast, brain, and cervical cancer cells have shown excellent adherence to the CNT film. However, in real life, the cancer cells are mixed with billions of normal cells in blood, and that can change the experimental condition significantly. Blood is a specialized body fluid that contains multiple components and elements, and each of these components would be enough to complicate the experimental condition for any biosensor technology. As a matter of fact, these elements with different functionalities make blood an excellent candidate for diagnosis and prognosis purposes and targeting each of these elements successfully can lead to better understanding of the subjects' health condition.

There are four major components in the blood: plasma, red blood cells (RBCs), white blood cells (WBCs), and platelets. The liquid part of blood is plasma, a combination of water, sugar, fat, proteins, and salts. The major role of the plasma is to carry other blood components throughout the body along with nutrients, waste products, antibodies, clotting proteins, chemical messengers like hormones, and proteins. There have been multiple technologies that have tried to use the existing DNA and proteins in blood for

cancer diagnosis [4, 5, 171]. However, these technologies are still not able to show high efficiencies for diagnosis purposes. Erythrocytes or RBCs are the most plentiful component of the blood that constitutes 40-45% of blood volume. Although RBCs are the smallest cells in blood, they are one of the heaviest components in the blood due to their high iron content. The shape of a red blood cell is a biconcave disk, and their function is to deliver oxygen to body organs and return the CO_2 back to lungs to exhale. Leukocytes or WBCs are protecting the body from infection, and they are accounting for only 1% of the blood. However, WBCs are the closest component of the blood to CTCs in term of physical or biological properties, and they are the most common contamination in CTC isolation technologies. Platelets are not cells but rather small fragments of cells that help the blood in clotting process (or coagulation) by gathering at the site of an injury. There are other cells that may be present in blood samples including tissue epithelial cells and CTCs. Figure 40 shows the concentration of different components in blood including CTCs.

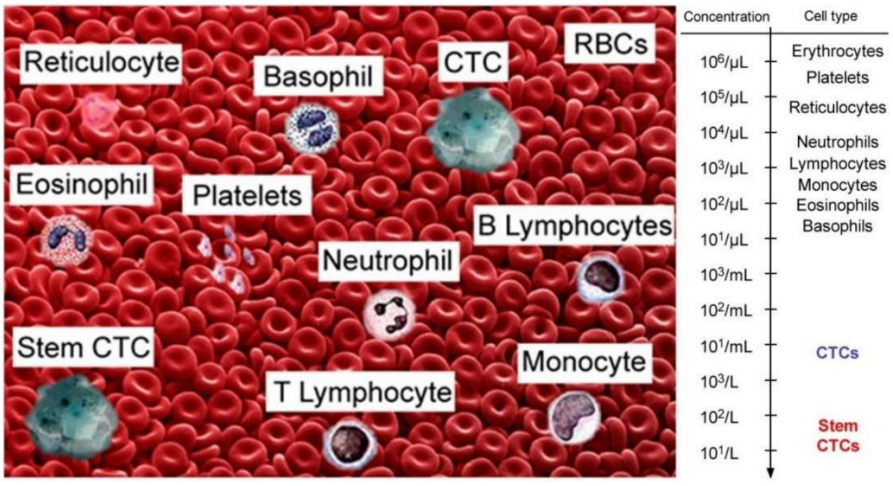

Figure 40. Typical blood composition and concentration levels of bulk and stem CTCs in blood cells [292].

The central hypothesis of this dissertation is the attachment of CTCs and not the WBCs to the nanotube surface resulting in very high enrichment of CTCs. To validate this hypothesis, we spiked breast cancer cells in blood and used these samples for testing this hypothesis. This chapter has discussed these experiments in details.

4.2. Experimental setup

4.2.1. Device fabrication

Five 4" glass wafers were fabricated by transferring 100 µg HiPco SWCNT dispersed in IPA on each as it was discussed in chapter 2. The devices were diced after electrode and isolation layer fabrication. It should be noted that in order to protect the CNT film on each device during dicing, a protective layer of S1813 photoresist was spinned and deposited as it was described in chapter 2. The devices were protected in a vacuum desiccator from any surface chemical change. A day before their use, the photoresist was washed away using acetone, methanol and DI water. The devices were dried using an air gun and kept under UV light overnight.

4.2.2. Cell culture

M.D. Anderson metastasis breast 231 (MDA-MB-231) is a breast adenocarcinoma cell line that is highly aggressive, invasive, and poorly differentiated. This cell line is not expressing estrogen receptor (ER), progesterone receptor (PR), and HER2 (human epidermal growth factor receptor 2) amplification and that is why it is called triple negative breast cancer (TNBC) cell line. This cell line was purchased in a condition that

it has Luciferase/Green Fluorescent Protein (GFP) dual-labeled and this means that they will exhibit bright green fluorescence when exposed to light in the blue to ultraviolet range. Figure 41 shows the excitation and emission spectra of GFP.

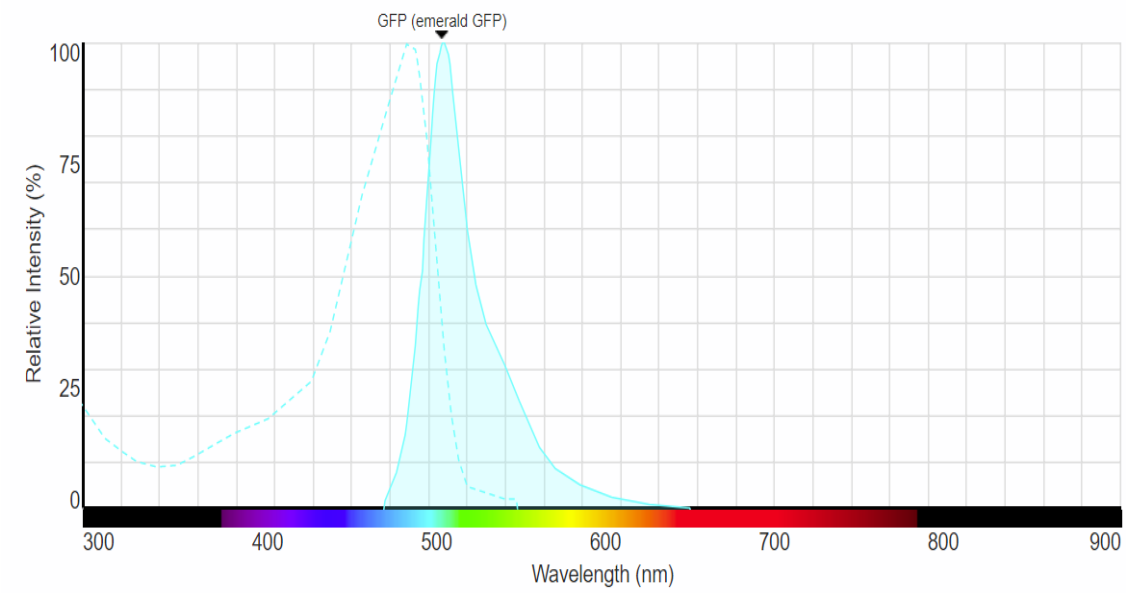

Figure 41. Excitation and emission spectra of GFP (taken from ThermoFisher website).

MDA-MB-231 in RPMI-1640 growth medium was cultured per their suggested protocol by the manufacturer (GenTarget Cat# SC044). Its media contains 10% Fetal Bovine Serum and 1% penicillin-streptomycin. The cells were incubated at 37ºC and 5% CO_2 condition. For resuspension of cells, 0.25% EDTA-trypsin solution was used. Figure 42 shows cultured MDA-MB-231 cells attached to the nano surface.

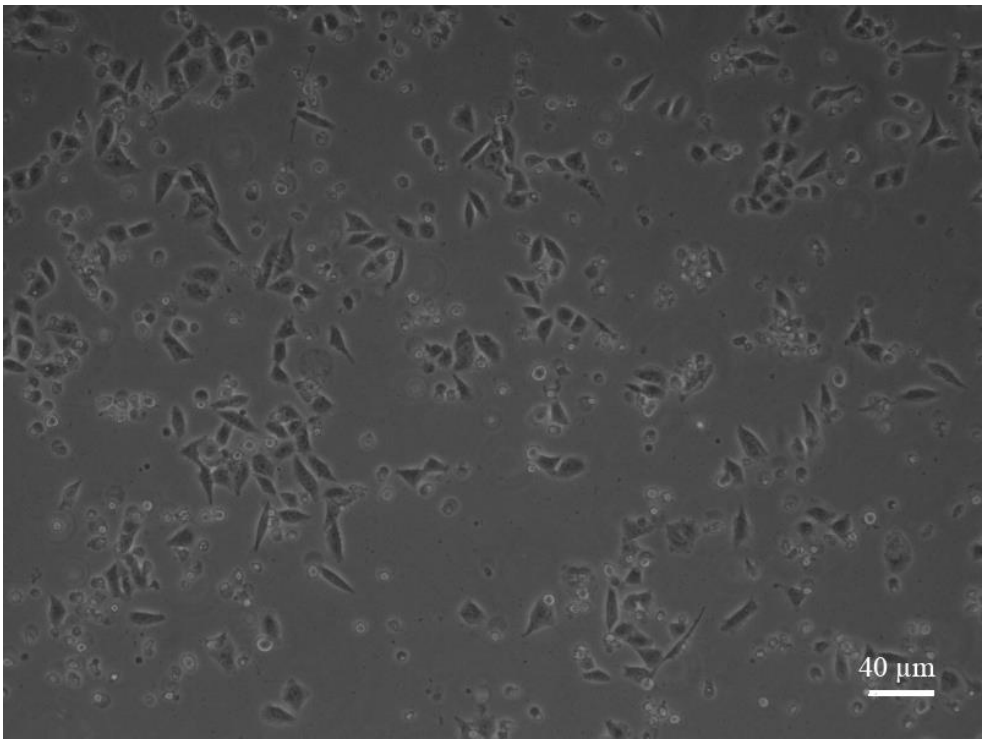

Figure 42. Optical images of MDA-MB-231 triple negative breast cancer cell line.

4.2.3. Spiking the cultured cells in blood

Cells were grown to reach ~80% confluence, and then they were washed with PBS and detached from the culture dish using Gibco™ Trypsin-EDTA (Cat No. 25200056). Next, they were centrifuged and suspended in specific culture media volume. Hemocytometer was used to count the cells and calculate its concentration in each tube. To be able to track differentiate the tumor cells in blood from normal cells, GFP labeled cancer cells were used. The fluorescent microscope was used for counting and calculating the capture efficiency of the devices. During counting and adjustment of cells concentration, their temperature was reduced to 4 ^{o}C in order to avoid any thermal shock when they are mixed with blood.

Safe-T-Fill™ Capillary Blood Collection tubes: Lithium Heparin, 125 µL (RAM Scientific Catalog# 07 6101) were used in these experiments. The advantage of using capillary tubes is that it reduces hemolysis, tissue contamination, and re-draws and it does not need "scooping" or "milking."

After blood collection from wild mice, the capillary tip was removed, the cap was sealed, and the blood sample was kept in a 4 ^{o}C refrigerator inside a biohazard Specimen Transport Bag before it was used. Ten µl of wild mice blood was mixed with 10 µl of culture media containing the required number of cells in 1.5 ml tube.

It should be mentioned that using healthy human blood for spiking experiments will complicate the experiments significantly. In cancer patient blood samples, CTCs are already have overcome the immune system, but when the culture cells are mixed with healthy human blood, there is a high chance that the remaining immune system of the donor in the donated blood attacks the cultured cells and harm them. As a separate experiment, we isolated 1 ml of healthy donor blood plasma using high-speed centrifugation, and we added it to a culture dish that contained adherent HeLa cells with more than 80% confluency in 10 ml of culture media. In 30 minutes, almost all of the cells were died floating in the culture media, and the cell viability assay confirmed this result.

4.2.4. Immunofluorescence microscopy

Due to the novel design of the most recent generation of CTC Nanotube chip devices and transparency of the glass substrate, it is possible to carry on the microscopy and

identification of cells directly on the chip without further transfer. For immunofluorescent analysis, after washing the devices with PBS, they were fixed in 4% paraformaldehyde for 15 minutes. After that, specimen was blocked with blocking medium (1X PBS / 5% goat normal serum / 0.3% Triton™ X-100, CellSignal Inc.).

For this chapter, since we are using GFP labeled cells, we only used DAPI for staining the nuclei. The final step of staining in this chapter was washing the sample with PBS, staining the sample with DAPI for 5 minutes and mount it on cover slip. Three separate images were obtained for each event through separate channels of DAPI, GFP, and bright field accordingly. Merged images were created using ImageJ software. Therefore, the cells that are only stained with blue under the fluorescent microscope are WBCs while the cells that are emitting GFP and DAPI are target cells. NIKON Eclipse TE300 microscope was used for tracking and characterizing the cells in this chapter.

4.3. Tracking single cells using the nanotube-CTC chip

In our previous work on the nanotube-CTC-chip, we observed that the cells inside the blood start to settle immediately due to the forces of gravity, and density gradients resulting in cells coming in contact and interacting with the base substrate surface along with RBCs [178]. The initial observations on the optical microscope of cancer cell spiked blood sample droplets on top of the devices showed that the spiked cancer cells and RBCs as a part of the settling process, tend to go to the bottom of the device compared to WBCs which settle on top [178]. Knowing this, we decided to track the individual cells from a blood droplet.

To track the cells, we used a TNBC cell line (MDA-MB-231; $EpCAM^-$) that were transduced by lentivirus to actively express a green fluorescent protein (GFP) marker [293]. Typically, CTC technologies such as CELLSEARCH® use Epithelial Cell Adhesion Molecule (EpCAM) to identify CTCs from hematological cells. It is now realized that CTCs are highly heterogeneous and actively change their shape and even downregulate EpCAM during epithelial-mesenchymal transition (EMT) [294]. Thus, the inadequacy of EpCAM as a universal marker for CTCs detection seems unquestionable and alternative methods able to recognize a broader spectrum of CTC phenotypes are needed and as presented here [294]. With this in mind, we used an $EpCAM^-$ and TNBC basal-like cell line MDA-MB-231 for our spiked cell line studies.

The GFP transduced triple-negative breast cancer cells were spiked in blood and were observed under a fluorescent microscope. For these experiments, blood was diluted to 10% that enabled us to track all the GFP cells in the droplet. Figure 43 presents the fluorescent image of the GFP tracked cells at a different depth of focus by changing the focal plane in the microscope. This image was taken after 5 minutes of droplet deposition on the chip.

As it can be observed in Figure 43.a, not all the cancer cells are settled down on the nano surface, and there are still cells that floating in the droplet. This can be because some cancer cells are not viable because of their collision with other cells in blood or they are smaller than other cultured cells in the sample. In contrast, in Figure 43.c which is focused on the surface of CNT film, there is a brighter cell in the middle that is directly

sitting on the CNTs and one in the bottom left corner that is sitting on RBCs and because RBCs are scattering the emitted light, its image is not sharp.

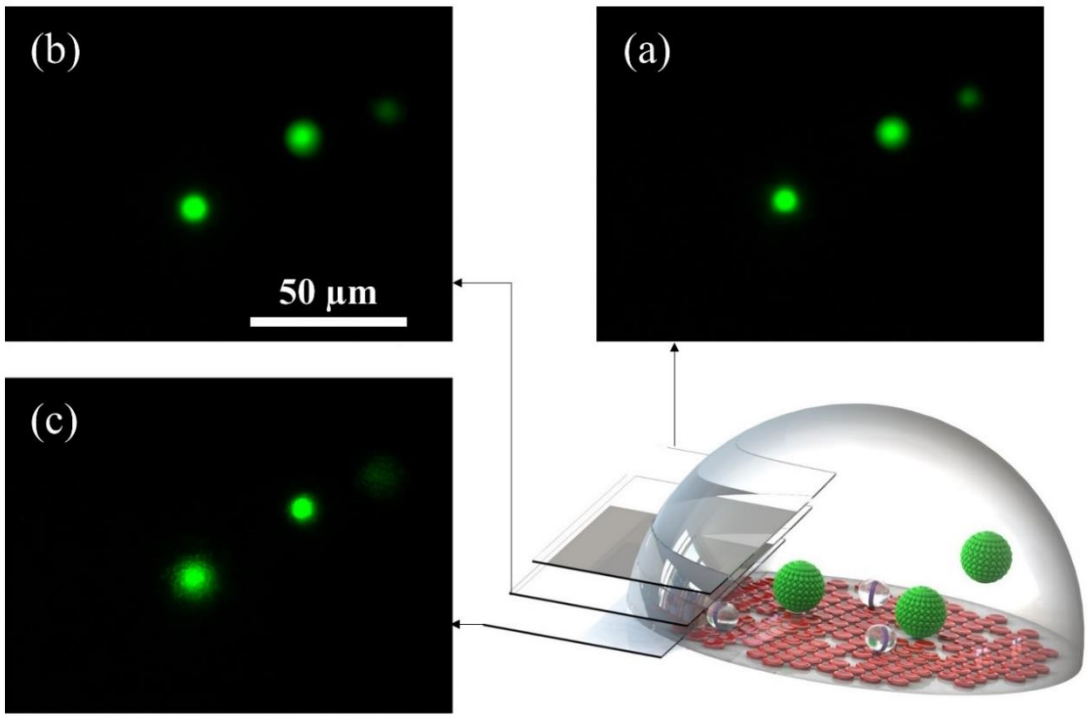

Figure 43. Fluorescent image of the GFP tracked cells at a different depth of focus by changing the focal plane in microscope.

In our previous spiking experiments, it was observed that when a droplet of blood was placed on the nanotube device surface, the cancer cells and RBCs went to the bottom as a part of the settling process [178]. The RBCs were seen to cover most of the nanosurface which is not desirable for preferential cell adherence strategy. This problem was resolved with diluting the blood in PBS 3-fold in our previous work [178]. However, this procedure increases the sample volume significantly and makes it more challenging and time-consuming to process it. Also, a high concentration of blood droplets with small volumes are vulnerable to dry faster in air or incubator, and this is also a challenge in

microscopy. Having the cells exposed to the nanosurface is desirable as it enables the cells to attach to the nanoscale topography. In many mechanobiology studies, microfabricated topographic features with specific dimensions have been fabricated to mimic the architecture and orientation of the extracellular matrix (ECM) in vitro [283]. The nanotube surface enables topographic anisotropy for cellular attachment due to the collection of nanometer scale tubes on the surface.

Before investigating the adherence of cancer cells to CNTs and isolating them using this strategy, we conducted a set of experiments to see if we can count and track all the cells that we are spiking in blood. Seven samples were prepared based on the protocol that was described in the previous section and 1, 10, 100, 300, 500, 800, and 1000 cells were spiked in blood. Each of these samples was prepared in 6 µl media+6 µl wild mice blood+48 µl PBS in 7 different 1.5 ml centrifuge tubes. Each tube was divided on six different CNT device, and the cells inside each droplet were counted under a fluorescent microscope within 30 minutes of placing droplet on each device. Figure 44 shows the number of spiked cells versus some GFP observations. Figure 45 is the entire image of a droplet with MDA-MB-231-GFP cells marked by arrows. Figure 46 presents the spiked cell counts in blood for 1, 10, 100, 300, 500, and 1000 spiked GFP cells in the blood for each device. We observed 87% to 100% of the cells. Slight error in cell counts is as a result of counting the cells using a hemocytometer and is seen in many spiked cell experiments [6]. Also, since some the cells may float inside the droplet, they will not be seen due to the focus of microscope on the surface of the sensor.

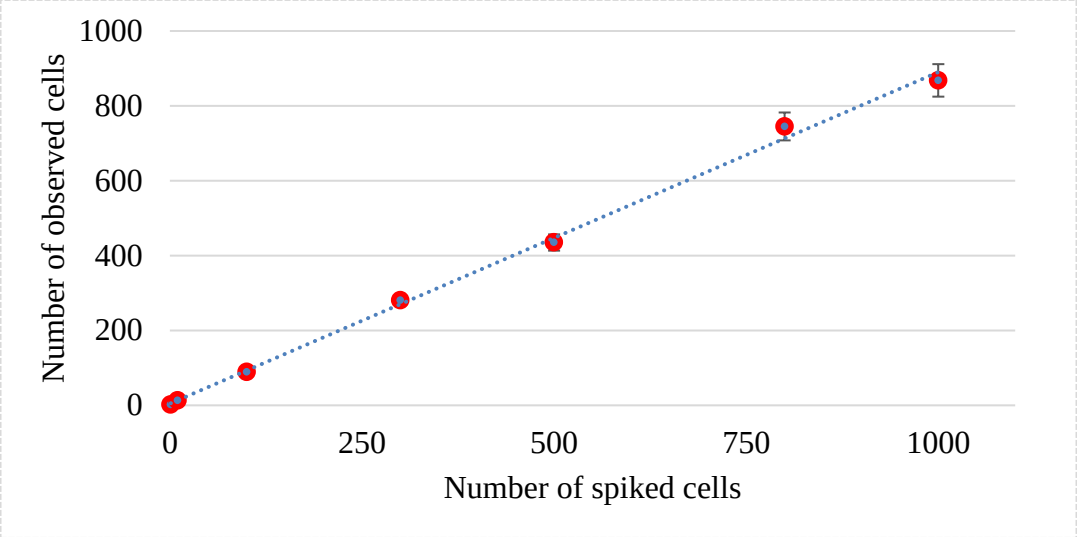

Figure 44. Number of spiked cells versus some GFP observations.

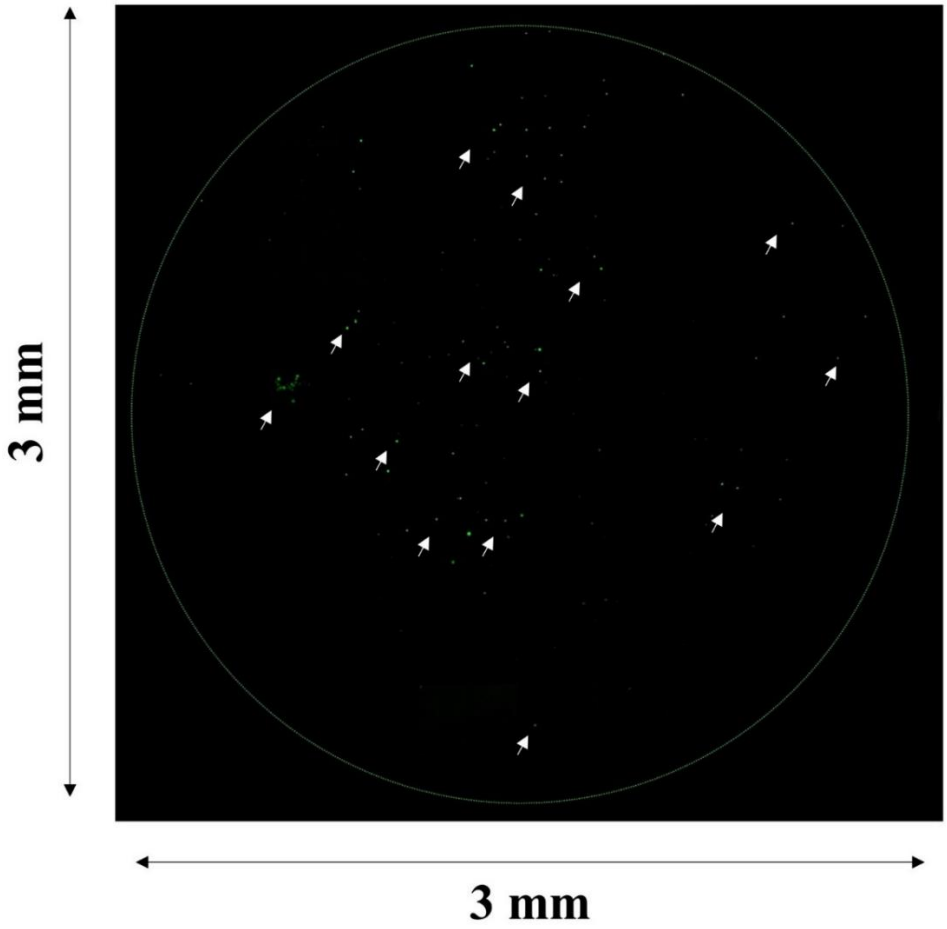

Figure 45. The entire image of a droplet with MDA-MB-231-GFP cells marked by arrows.

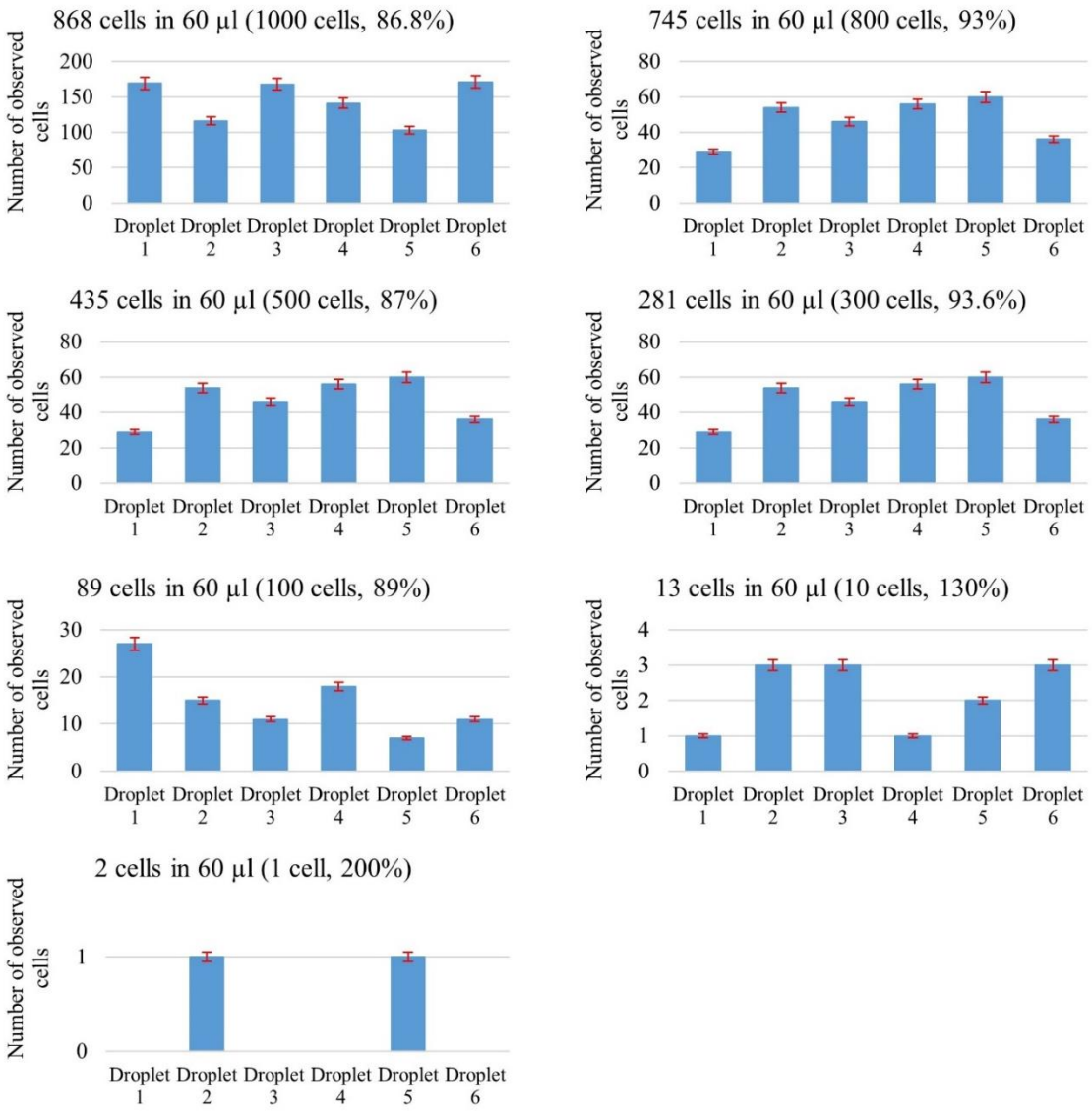

Figure 46. The observed spiked cell counts in blood for 1, 10, 100, 300, 500, and 1000 spiked GFP cells in the blood for each device.

Although we gave 48 hours the samples that were prepared for observation inside the incubator to in culture condition, less than 1% of the samples adhered to the surface of devices. Most of the target cells were not adhering to nanosurface, and RBCs interference could be the most important element in this failure. These results encouraged us to consider lysing the RBCs in blood for higher capture efficiency.

4.4. RBC Lysis

For CTC isolation based on such topographic features, RBC lysis is necessary as this enables more exposure of the cells to the surface. While there is a section of CTC community that is of the understanding RBC lysis can lead to loss of CTCs and lead to false positives and negatives [295], this work has successfully shown that RBC lysis can be beneficial to enable viable CTCs of high quality.

Further, CTC cultures will not be possible on the nanotube surface without RBC lysis process. There are many ways to lyse RBCs, and any of them may work if it does not damage CTCs or lose them in the process. Here, Hypotonic NaCl solution was used to break the membrane of RBC. Low concentration solution of NaCl drive more water into RBCs and put more pressure on its membrane. By neutralizing the low concentration NaCl solution with a higher concentration and pipetting the RBCs, their membrane will break while CTCs will not be affected due to having a different membrane structure. When RBCs explode, they lose their mass, and after centrifugation at low g-forces, CTCs will settle down while RBCs will be removed from the supernatant. The advantage of this method is that it does nott use any chemicals to harm the CTCs. Figure 47 presents the RBC lysis protocol.

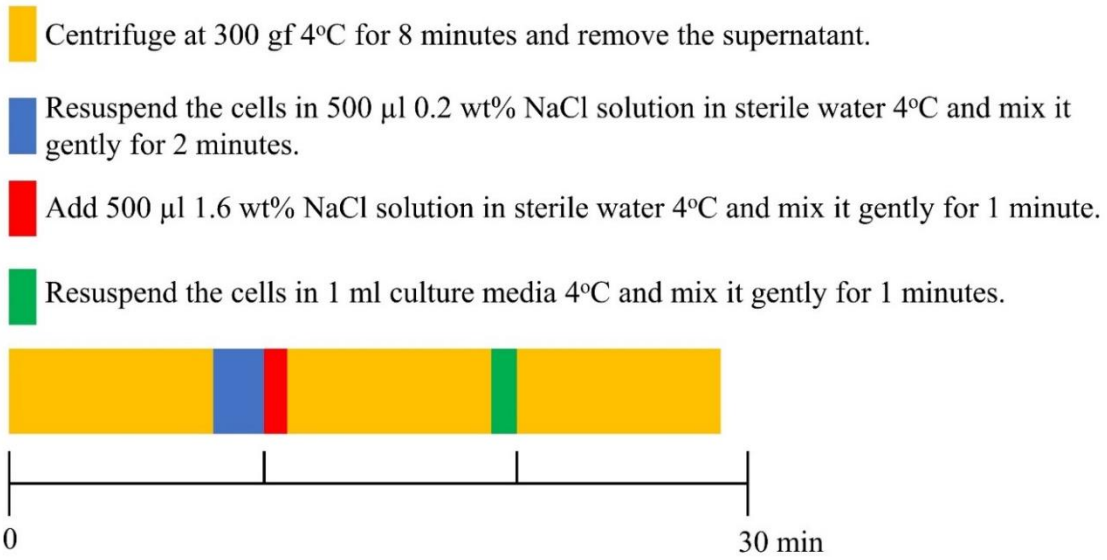

Figure 47. RBC lysis protocol for removing the RBCs from spiked cancer cell samples in blood.

Hypotonic NaCl solution was used for RBC lysis. The sample of spiked cells in blood was centrifuged at 300 gf at 4 °C for 8 minutes, and the supernatant was removed. The cells were resuspended in 500 µl 0.2 wt.% NaCl solution in sterile water at 4°C, and it was mixed gently for 2 minutes. Then 500 µl, 1.6 wt% NaCl solution in sterile water at 4°C was added, and it was mixed gently for 1 minute. The solution was centrifuged at 300 gf at 4°C for 8 minutes, and the supernatant was removed. The cells were resuspended in 1 ml culture media at 4°C, and it was centrifuged at 300 gf (4°C) for 8 minutes, and the supernatant was removed. In the end, cells were resuspended in 60 µl culture media, and it was transferred into six different chips each containing ten µl of the processed sample. Figure 48 presents the optical image of control blood (from a healthy volunteer) before and after lysis. None of the RBCs, but the WBCs are observed after the lysis procedure.

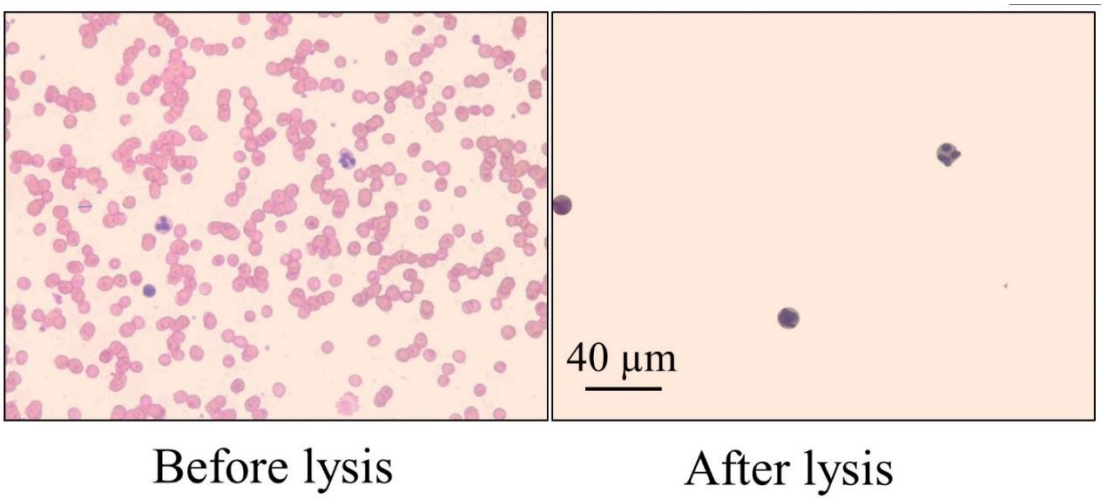

Figure 48. The colorful optical image of control blood sample (from a healthy volunteer) before and after lysis.

Figure 49 presents the cells that are attached to the surface versus non-adhered cells using the RBC lysis protocol. The attached cells have different shape and morphology, looking elongated/mechanically stretched as presented in the fluorescent images. Three stages characterize the process of static in vitro cell adhesion: attachment of the cell body to its substrate (initial stage), flattening and spreading of the cell body, and the organization of the actin skeleton network with the formation of focal adhesion between the cell and its substrate [289]. The deformation, mechanical stretching, and flattening are observed in Figure 49.

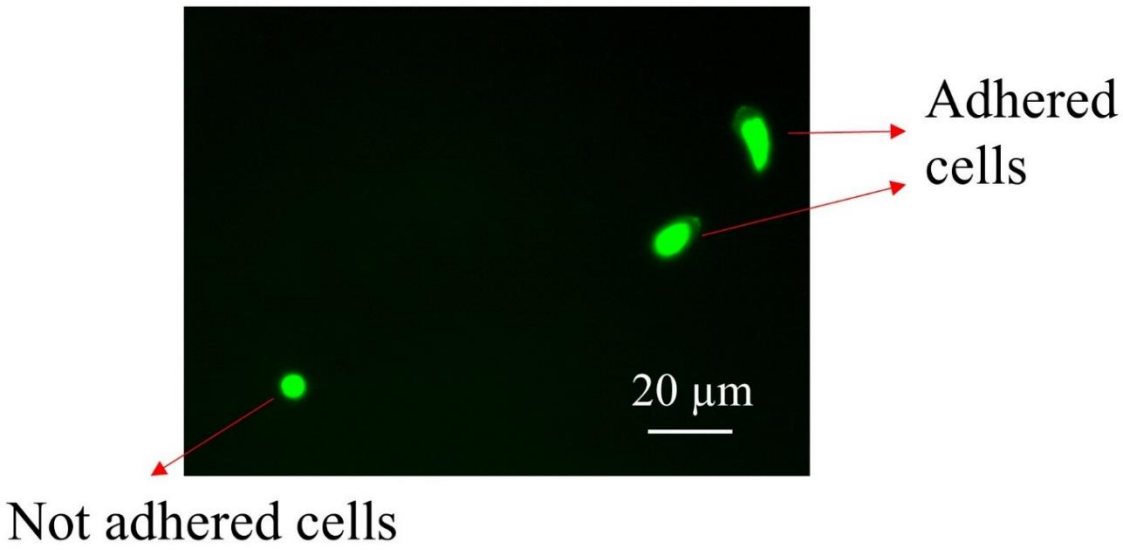

Figure 49. Attached to the nanosurface versus non-adhered cells using the RBC lysis protocol.

4.5. Preferential adherence of spiked cancer cells using nanotube-CTC-chip

One of the major questions regarding the adherence of tumor cells to surface is how much time they need to adhere to the CNT film. Obviously, the shorter time they adhere, the better technology it would be since this makes it possible to process the sample faster and get access to the results that we are looking for. But on the other hand, if we do not give them enough time, there is a good chance that the target cells may not adhere and get lost in the process. It should be noted that extremely long times necessarily would not help the process to adhere the cells to nanosurface. The reason is that there might be some debris or contamination from RBC lysis or blood sample that can affect and harm cells if we give them enough time. Therefore, an optimized time should be found to have the highest adherence efficiency.

To determine if all the spiked cancer cells would survive the RBC lysis process, we undertook several experiments. GFP positive, EpCAM^{-}, MDA-MB-231 breast cancer cells were spiked in mice blood, and the lysis protocol was used to determine the adherence/non-adherence of cells on the carbon nanotube surface.

Three different samples containing 50 cells of the MDA-MB-231-GFB-Luc cell line was mixed with 10 µl wild mice blood inside a 1.5 ml tube and lysed. Each of these three samples was placed on three separate CNT devices as a 10 µl droplet, and they were given 12, 24, and 48 hours for attachment. After this time, the removed droplet was then placed on another new CNT device surface and they were kept in culture condition inside the incubator till the total time including initial step reaches to 72 hours. These experiments were conducted to observe if any of the non-attached cells could be attached to a new CNT device surface. The results are presented in Figure 50.

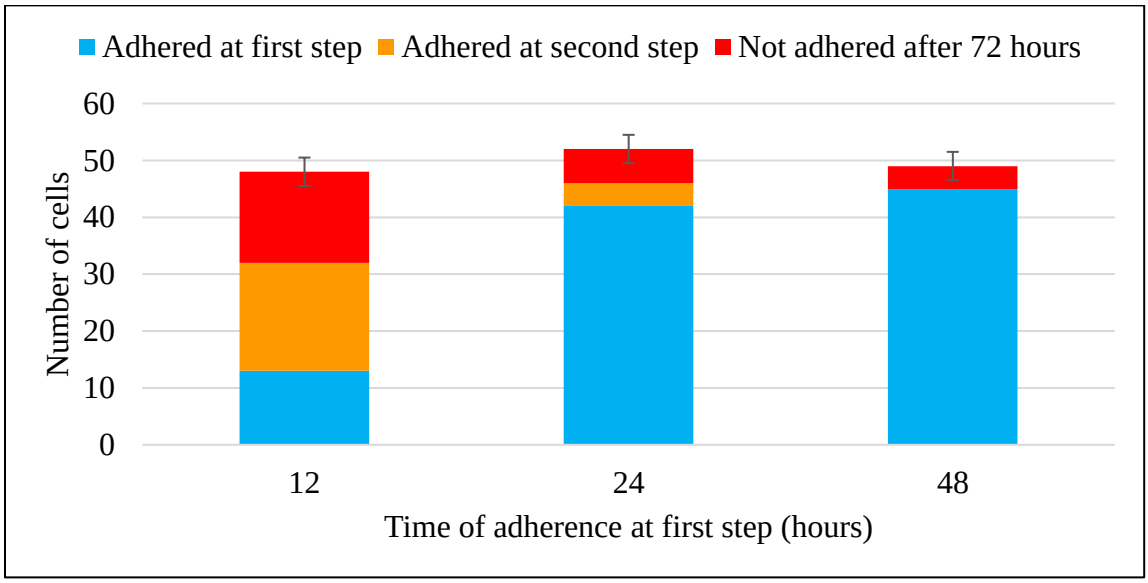

Figure 50. The time of adherence versus the captured number of cells.

It is seen that for the first sample that was incubated for 12 hours, less than 30% of the cells attached at the first step. An additional 50% attach after 72 hours, and some do not attach. However, when the time of first step adherence is increased to 48 hours, more than 90% of the cells attached, suggesting the increase in adhesion strength with time.

The strength of adhesion of the nanotube matrix to the cell is muscular as witnessed with the increased number of captured cells on the surface with time. The initial adhesive interaction between the cells and the substrate are driven by the specific integrin-mediated adhesion and starts with the binding of single receptor-ligand pairs [296]. This will initiate the following receptor-ligand bonds and quickly enhance in number, thus increasing the total adhesion strength in 48 hours.

The advantage of small adherence time is that only 7 WBCs (less than 0.005%) adhered to first CNT device from our observations. For the second sample, 42 cancer cells out of 52 cancer cells (80%) adhered to CNT surface after 24 hours. 4 cells adhered on the secondary device after 48 hours and 6 cells (11%) were not captured eventually. For the third sample, 45 cells out of 49 cells (92%) adhered to CNT film. The rest of the cells did not adhere to the second device. The number of WBCs that adhered to CNT surface for the second and third sample was counted as 21 and 24 (0.02%), respectively in these small volumes. From these experiments, we concluded that 48 hours is the optimum time to have the highest capture efficiency while the number of WBCs attached to CNT was negligible.

After optimizing the lysis protocol and time for isolating the tumor cell using preferential adherence strategy, a new set of experiments were conducted to find out the

capture efficiency of this method. Five samples containing 1, 10, 100, 500, and 1000 MDA-MB-231 cells in 10 µl culture media were spiked into 10 µl blood from wild type mice in 5 different 1.5 micro-centrifuge tubes. After each sample was lysed, the volume of the lysed sample was adjusted to 60 µl. The cells were resuspended in culture medium, and it was divided into six CNT chips, having 10 µl volume each. Fluorescent microscopy was done to observe the captured GFP cells. They were kept inside a sterile culture dish containing PBS to stop droplets from being dried in a 5% CO_2 incubator at 37°C. After 48 hours, samples were taken out from the incubator, and the droplet was removed and transferred into the second device to count the number of non-adhered cells from the first device. The first device was then washed with PBS, fixed and stained with DAPI. Both the primary and secondary devices were examined under a fluorescent microscope to count the cells on each device. The number of cells on the primary device was labeled "Adhered" while the ones on the secondary device were labeled "Not Adhered". Figure 51 presents the capture efficiency which suggests 87-100% of the cells adhered on the primary device at all spiked concentrations.

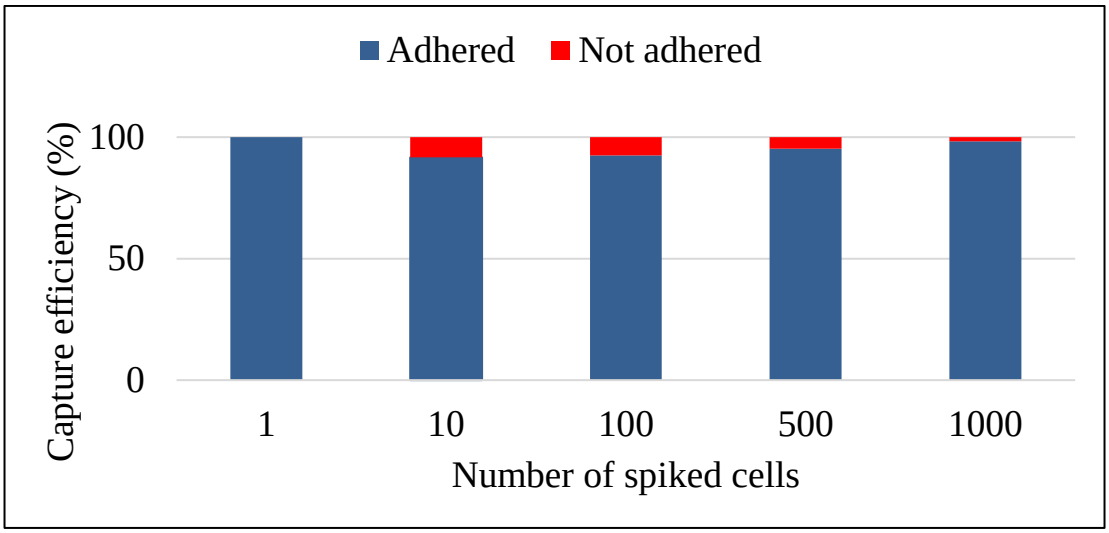

Figure 51. The capture efficiency of spiked breast cancer cells in blood using RBC lysis and preferential adherence to nanotube surface.

By using two devices from the array, we captured both adhered and non-adhered cells or tracked all the spiked cells. Figure 52 presents the number of cells counted in each droplet across all spike concentrations. Our method is a new way to enumerate cells using droplets, having a standard volume and a standard number of devices from the array. Since the volumes are quite small, one can ensure highly accurate counts. The standard 6 droplets can also be used for staining cells with 6 different markers, enabling multi-marker analysis of captured cells.

Figure 53 presents the fluorescence image of the captured cells after RBC lysis and preferential attachment in spiked blood experiments. The difference in MDA-MB-231-GFP-Luc cells that are attached versus WBCs (DAPI only) on the same surface is observed. The cells that attached changed shape and morphology looking elongated/mechanically stretched as presented in the fluorescent images. The deformation, mechanical stretching, and flattening are observed in Figure 53.

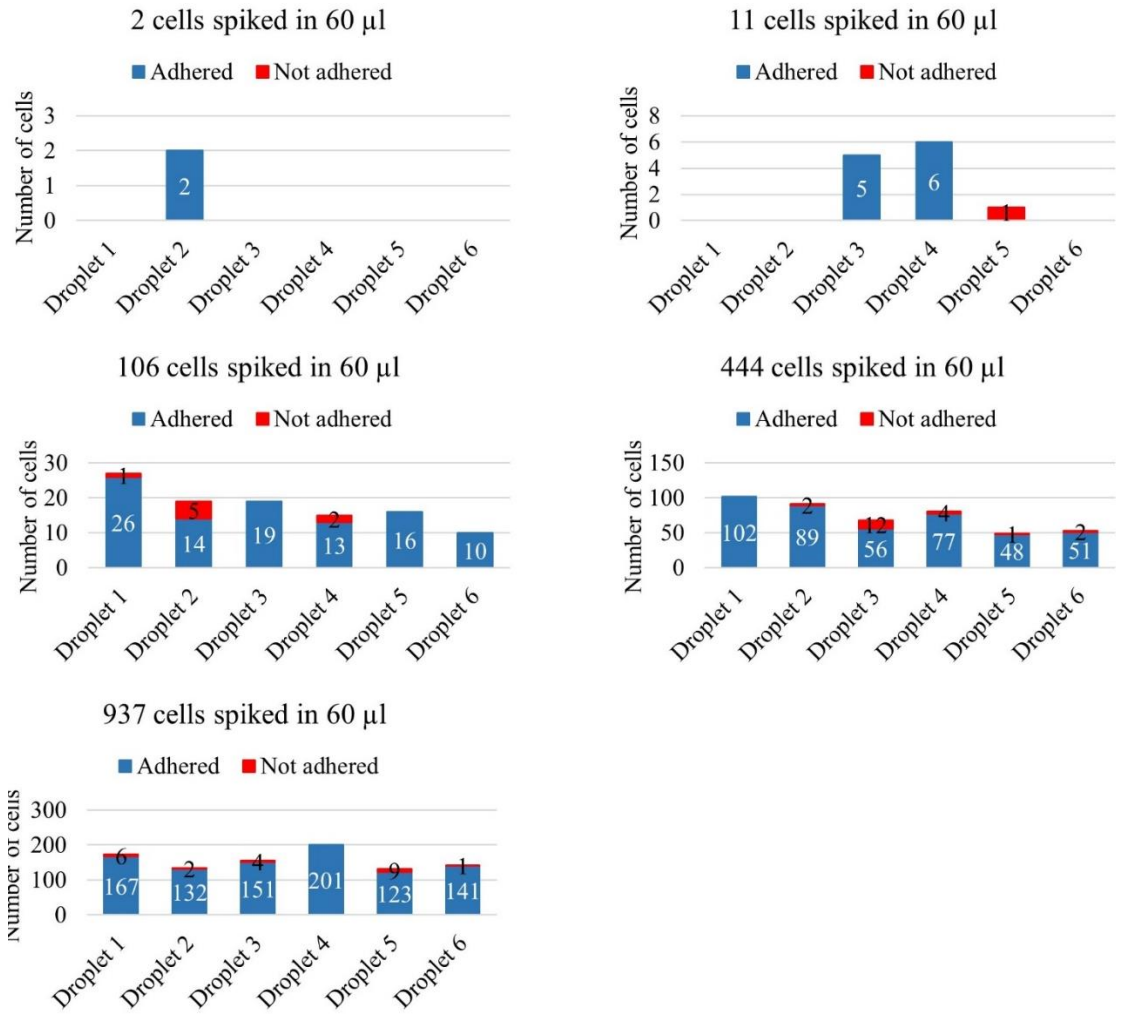

Figure 52. The number of cells counted in each droplet across all spike concentrations. The blue columns are for the number of cells that adhered on the first device while the red columns are for the observed GFP cells on the secondary device.

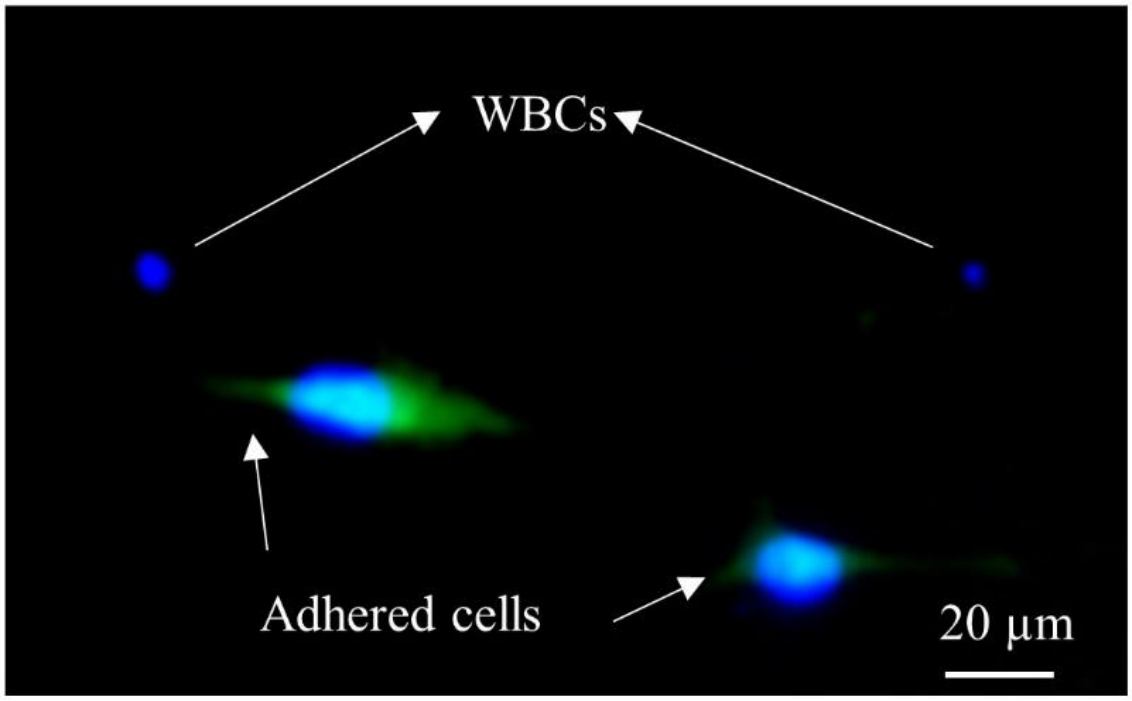

Figure 53. The fluorescence image of the captured cells after RBC lysis and preferential attachment in spiked blood experiments stained with DAPI. The cells that attached changed shape and morphology looking elongated/mechanically stretched.

While all the experiments were done using GFP positive MDA-MB-231 triple negative cells, this technique is not limited to specific cancer types, and therefore could potentially capture any type of epithelial cancer cell which constitutes the four significant cancers (breast, colon, lung, and prostate) using the method of preferential adherence. Other epithelial cancer cell lines including HeLa (Cervix), U-251 (Glioblastoma), MCF7 (Breast), LN-291 (brain) were also tested using this method, and the yield of adherence was more than 90% as it was described in Chapter 3.

Further, our method is currently the only one to track both adherent and non-adherent cells on the CNT chip, thus effectively tracking all the cells, a task that is of high value in CTC capture especially in early-stage cancers where the cell numbers may be meager.

With suitable functionalization protocol, one can also capture non-epithelial cells such as lymphoma and sarcomas.

The mechanism of adherence for MDA-MB-231 cells to CNT film is similar to what has been explained in chapter 3. Figure 54 shows two of these cells adhered to nanotube-CTC chip after spiking and microtentacles are visible at high magnification and GFP excitation.

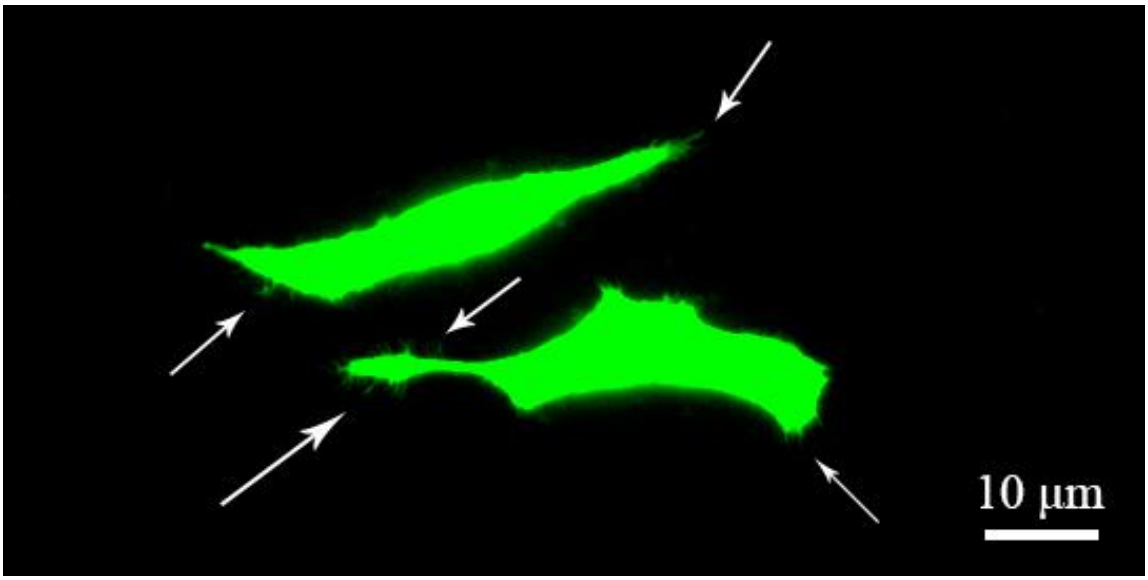

Figure 54. Local adhesion of MDA-MB-231 cells to CNTs using under fluorescent microscope.

4.6. Preferential adherence using collagen adhesion matrix (CAM) on the Nanotube- CTC chip

We compared our cancer cell attachment strategy on carbon nanotubes with that of collagen adhesion matrix (CAM) scaffolding for the capture of CTCs. The capture of CTCs based on CAM strategy (Vita assay) is a unique strategy and is a method of adherence [95]. The proclivity of a tumor cell to invade collagenous matrices is one of

the hallmarks of metastasis. In the past, it was hypothesized that populations of CTCs that adhere and invade collagenous matrices would be invasive and exhibit the propensity of progenitor cells to metastasize [95].

CAM was deposited on the surface of CNTs, and cell spiking experiments in blood were conducted. During these tests, the surface of the sensor was covered with collagen to improve and speed up the adhesion of target cells to the surface, similar to metastatic invasion by digesting the collagen. We used collagen from calf skin Type I (0.1% solution in 0.1 M acetic acid), aseptically processed, suitable for cell culture. Based on the suggested protocol by the manufacturer, collagen solution (Sigma Aldrich Cat. No. C8919) was used to coat devices with 6-10 μg/cm2 with a 10 μl droplet. The CAM droplet on the device was kept at 4°C refrigerator overnight to allow the proteins to bond with CNTs. The excess droplet was removed from the coated surface the next day. The device was dried overnight and simultaneously allowed to sterilize through exposure to UV light in a sterile biosafety cabinet. Next day before using the device, it was rinsed with PBS and used for the cellular attachment studies.

Five samples containing 1, 10, 100, 400, and 1000 cells were spiked in 10 μl wild mice blood in 5 different 1.5 μl micro-centrifuge tube. After each sample was lysed, the cells were resuspended in culture medium, and it was divided into six CNT chips, each having 10 μl volume. Incubation condition and time was the same as previous spiking experiments on bare CNT surface (48 hours at 37 ^{o}C 5% CO_2). Same counting strategy was utilized to count the cells that were adhered to the primary device and not adhered on the secondary devices based on CAM strategy.

Figure 55 presents the overall capture efficiency for CAM devices. The adherence efficiency of CAM strategy is observed to be only 50%, which is consistent with what has been reported previously [95]. The 50% of cells did not adhere on the primary CAM device even after 48 hours incubation, although we were able to track all the cells both adhered and non-adhered by counting the number of cells in the secondary device. Repeating these experiments three times enabled us similar values for capture rate. It is possible that CAM devices need more time for the cells to digest the collagen, although it should be noted that some of the cells may not attach to the CAM. A study based on CAM coated tubes in Stage I-III breast cancer (Vita-assay) only were able to detect CTCs in 28/54 patients which is only 52% sensitivity [95]. The CAM strategy needs optimization regarding collagen type, the deposition technique, and concentration. This method has a lower yield compared to bare SWCNT film under the same conditions for preferential adherence using our microarrays. Figure 56 shows the number of cells (both adhered and non-adhered) for each device for the CAM strategy.

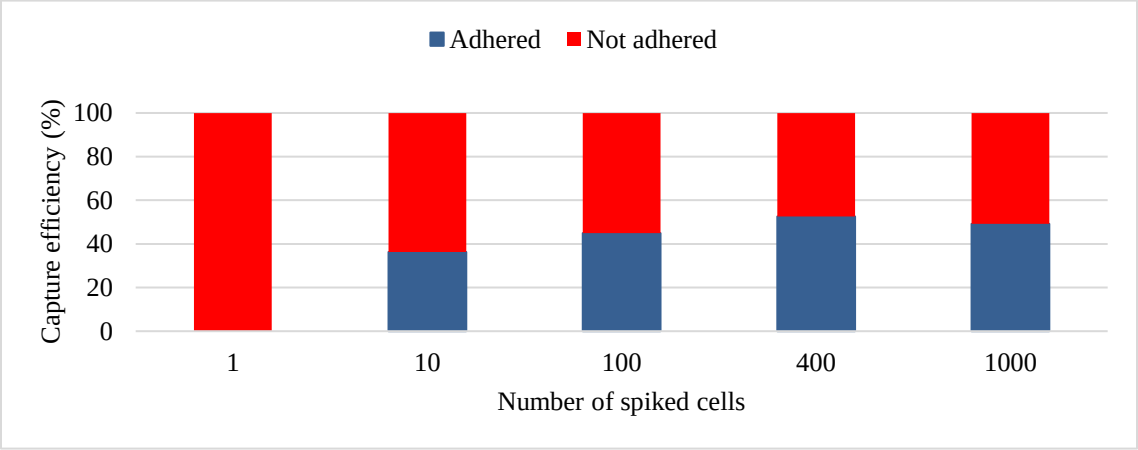

Figure 55. Overall capture efficiency for CAM devices.

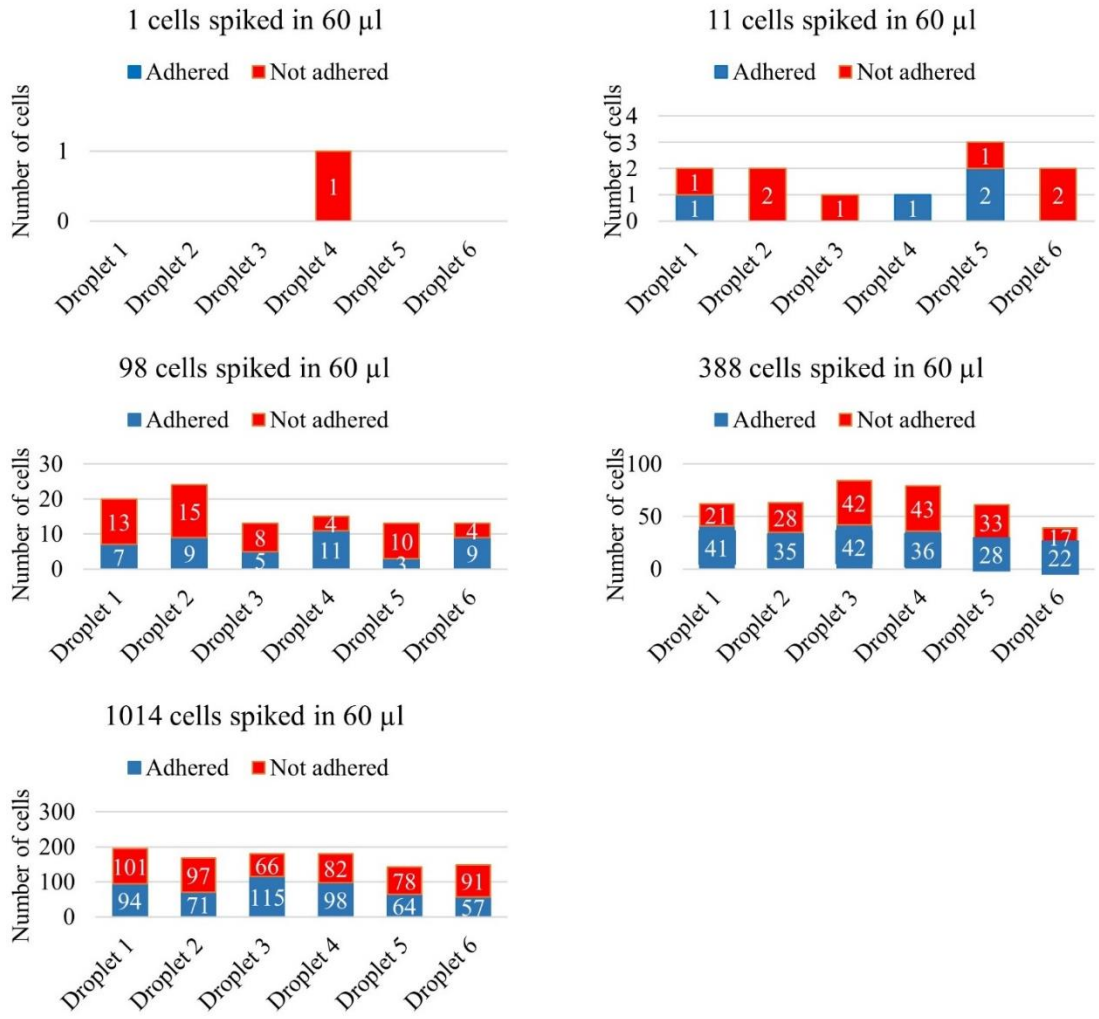

Figure 56. The number of cells (both adhered and non-adhered) for each device for the CAM strategy.

4.7. Downstream analysis

Although the focus of this study is to enumerate CTC with high specification. Any isolated cell needs to be proved a CTC, and that is the first step toward benefiting from CTC capture. Immunoflourescent technic is a simple and easy way to identify the CTCs, and it is the golden standard used in CELLSEARCH®, the only FDA approved cancer prognosis based on CTC enumeration. However, more important information that can be

extracted from isolated CTC including diagnosis of cancer type at early stages, CTC subtype, determination of treatment eligibility, progress in individualized cancer therapy, real-time monitoring of treatment and predicting the site of the future metastatic lesion are lost due to the insufficiency of immunofluorescent approach. Nowadays that most of the technologies are getting better in capture efficiency of CTCs, new demands are rising from such technology and providing a guide for the physician toward the right path for treating the patient is what oncologist are looking for. Performing downstream process and genomics is one of the best methods for identifying the genetics and properties of cancer type and aggression and providing such capability would be a plus for any CTC isolation technology. Polymerase chain reaction (PCR) is a method widely used in molecular biology to make copies of a DNA sequence. Using PCR, one copy (or more) of a DNA segment is amplified exponentially to generate millions of more copies of that particular DNA segment. Using PCR, we are going to demonstrate an effective and easy way to extract genomic information from isolated cancer cells adhered to CNT film.

PCR experiments were performed using Platinum Taq DNA Polymerase according to a protocol from the manufacturer (Thermofisher Catalog#10966026). In summary, after DNA extraction from the cells attached to each device based on The Jackson Laboratory protocol, they were mixed with PCR buffer, dNTP mix, platinum Taq DNA Polymerase, Forward primer (5'-AAGGTACCATGGTG AGCAAGGGCGAGGAG-3'), and reverse primer (5'-AAGGTACCCTTGTACAGCTC GTCCATGCC-3'). The PCR volume for each sample was 12.5 µl, and PCR steps are as follow: after heating at 95^{o}C for 3 minutes, 40 cycles of 95^{o}C for 20 seconds, 65^{o}C for 30 seconds, and 72^{o}C for 1 minute was

repeated, and at the end, the samples were kept at 72^{o}C for 10 minutes and then they were cooled to 4^{o}C until they are being used. After PCR, they were analyzed using 1% agarose gel electrophoresis.

To show the capability of nanotube surface, 100000 cells were spiked in 10 µl RPMI-1640 culture medium and 10 µl wild mice blood, and they were captured using lysis and Nanotube-CTC chip. Next, they were trypsinized and separated from CNT film, and they were transferred into a micro centrifuge tube. DNA was extracted from the cells based on the Jackson Laboratory protocol. From this tube, 4 different dilutions including the DNA for 10, 100, 1000, and 10000 cells were prepared. Each of these samples was processed based on the explained PCR method earlier. Figure 57 shows the band 753 Bp which is an indication of the GFP gene and as demonstrated, the band is getting stronger by increasing the number of cells. Each cell has two chromosomes and usually for regular PCR this is not enough. However, since the artificially induced GFP genes are targeted in this study and they are abundant in each cell, our simple PCR experiment could detect and show the GFP sequence even for 10 cells. In the patient samples which do not have these artificially induced genes, more precise methods like single-cell sequencing can be used for genotyping.

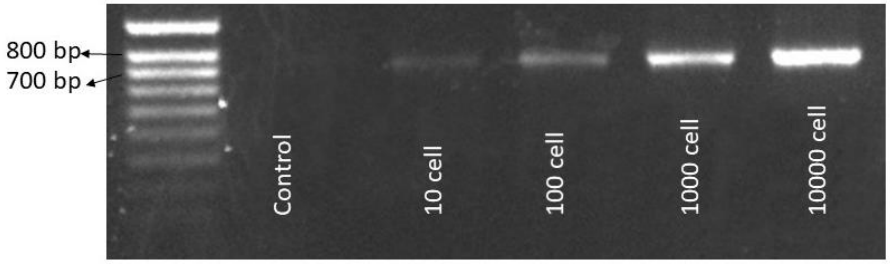

Figure 57. PCR results showing 753 Bp band for targeted GFP genes in MDA-MB-231-GFP-Luc cell line cells.

4.8. WBC depletion

The main challenge for capturing CTCs is their low concentration compared to the other cell types in the peripheral blood. As it was mentioned in the first chapter, there are only a few CTCs among 4.7 billion RBCs and 7.5 million WBCs in each milliliter of blood. In almost all of CTC enumeration technologies that do not lose CTCs based on false assumption, there are always WBC contamination in the final product. The reason is the overlap in physical and in some cases biological properties of WBCs and CTCs. Therefore, having minimum WBC contamination is an advantage for every technology in this field.

Purity describes the ability of the device under evaluation to specifically capture CTCs within a background of contaminating cells (such as leukocytes). Purity is the one metric that can be measured from clinical samples [91]. The log depletion formula can be used to assess CTC purity and is given as:

$$Depletion = \log_{10} \frac{Initial\ number\ of\ WBCs}{Final\ number\ of\ WBCs\ after\ enumeration} \qquad \text{Equation 2}$$

Table 12 has summarized the final number of WBCs after using the nanotube-CTC chip for spiked experiments. Assuming 75000 WBCs for 10 µl of mice blood, it is possible to calculate the WBC depletion in each experiment. It can be observed that for spiking experiments, average WBC log depletion of 3.73 has obtained and this number is one of the highest WBC depletions among cutting edge CTC isolation techniques [99, 297-299].

Table 12. Summary of isolated CTCs and WBCs on a nanotube-CTC chip for spiking experiments.

Sample	Number of captured CTCs	Number of captured WBCs	Log10 Depletion
1000 cells spiked in 10 µl mice blood	937	12	3.79
500 cells spiked in 10 µl mice blood	444	14	3.72
100 cells spiked in 10 µl mice blood	106	21	3.55
10 cells spiked in 10 µl mice blood	12	9	3.92
1 cell spiked in 10 µl mice blood	2	16	3.67

4.9. Conclusion

We have demonstrated the capture of 1-1000 spiked breast cancer cells. Spiking experiments were performed using a MDA-MB-231 expressing green fluorescent protein and analyzed using a fluorescent microscope, counted using a hemocytometer and in line with many published reports including ours. We also counted the GFP cells under a fluorescent microscope as a function of dilution.

The method of preferential adherence is the hypothesis that CTCs preferentially attach to the nanotube surface and not the other blood components including WBCs. In the recent past, the nano-roughened adhesion-based capture of CTCs with heterogeneous expression and metastatic characteristics was reported [283]. With the nano-roughened glass microfluidic CTC capture device, they were able to achieve capture yields of > 80% for both EpCAM+ (MCF-7, SUM-149, A549) and EpCAM- (MDA-MB-231) cancer cell lines spiked in blood samples [283]. We have independently discovered this effect on carbon nanotubes in our microarray, and our capture efficiencies are more substantial with very high purity (5-log depletion), partially due to RBC lysis.

Typically, CTC technologies such as CELLSEARCH use EpCAM to identify CTCs from hematological cells. It is now realized that CTCs are highly heterogeneous and actively change their shape and even downregulate EpCAM during EMT [23]. Thus, the inadequacy of EpCAM as a universal marker for CTCs detection seems unquestionable and alternative methods able to recognize a broader spectrum of CTC phenotypes are needed and as presented here [23]. With this in mind, we used an EpCAM- and triple negative basal-like cell line MDA-MB-231 for our spiked cell line studies.

Our previous publication was a demonstration in diluted spiked blood experiments and with a low volume of samples [178]. However, in this dissertation, we have shown a new antigen-independent method of capture in large volumes using Lysis. This strategy will help us reduce the large volume of blood into a concentrated mixture of WBCs and CTCs. Our work utilizes RBCs lysis and centrifugation to reduce the blood sample volume into one or a few small droplets. By giving time to these droplets, CTCs adhere to nanosurface while WBCs will not adhere and gently washing the surface results in the enumeration of CTCs.

Chapter 5

CLINICAL STUDIES: THE CAPTURE OF HUMAN CTCS USING NANOTUBE-CTC-CHIP FROM BREAST CANCER PATIENTS

5.1. Introduction

The ultimate goal for utilizing CNTs toward isolation of CTCs is creating a point of care diagnosis product for detecting cancer at early stages of cancer using a simple blood test. Blood tests are noninvasive, and that is a considerable advantage for diagnosis. Blood screening is a gold standard to assess the status of numerous systems in the body including cardiovascular risk factors, blood sugar levels, liver and kidney function, immune system wellness, and optimal hormone balance. However, a cancer diagnosis is still not possible using CTCs as a biomarker after 150 years of their discovery in blood [12]. Furthermore, isolating CTCs in a blood sample can provide a valuable opportunity for precise prognosis and personalized medicine in cancer treatment.

In the previous chapter, the idea of preferential adherence of CTCs to CNT film was described, and this concept was proved using spiked cultured cancer cells in blood samples and mice model blood samples. However, it is important to independently establish the clinical relevance and utility of the Nanotube-CTC chip through clinical trials. In spiking experiments and mice model, we have a lot of information already about the tumor cells that we are looking for in blood, and it provides us a chance to optimize our methodology. Here in this chapter, we are evaluating this our approach with patient

samples which have higher blood volume and the status of tumor cells in blood is unknown. This provide a great challenge and opportunity at the same time.

5.2. Experimental setup

5.2.1. Device fabrication

Two 4" glass wafers were fabricated by transferring 20 µg HiPco SWCNT dispersed in NMP on each as it was discussed in chapter 2. The devices we diced after electrode and isolation layer fabrication. It should be noted that in order to protect the CNT film on each device during dicing, a protective layer of S1813 photoresist was spun and deposited as it was described in chapter 2. The devices were protected in a vacuum desiccator from any surface chemical change.

There were 12 CNT devices ready for each patient sample. The day before the experiment, diced devices were washed with acetone, methanol, and DIW. Then they were dried with Nitrogen gun and they were kept under UV light overnight.

5.2.2. Ethical Considerations:

We investigated the ability of nanotube-CTC-chip to isolate CTCs with high purity from breast cancer patients. De-identified 8.5 ml blood samples were obtained from the University of Louisville under IRB (IRB#18.0828). De-identified 4 ml blood samples were also obtained from UMASS tissue bank, to determine the numbers of CTCs captured using the nanotube-CTC-chip from these two sources of different volumes. Blood Safety Measures should be followed for patient's blood samples.

5.2.3. Preserving the blood samples

When the blood is extracted from its natural environment, it should be preserved from any constraints for further processing. This includes hemolysis and platelet activation which can cause damage to the blood sample. Here is the protocol for collecting, shipping and maintaining the blood sample before processing it:

1- The blood sample should be collected in BD Medical #367874 Vacutainer® Plus Plastic Heparin Blood Collection Tubes with Sodium Heparin for Plasma Determination, 16 x 100mm, 10mL Draw Volume, Paper Label, and Green Conventional Closure.

2- Tirofiban is very slightly soluble in water. A stock solution of 0.1 mg/ml tirofiban in sterile PBS should be prepared. After collecting the blood, 0.5 µg tirofiban should be added to each ml of the blood sample. For an 8.5 ml blood sample, 42.5 µl of tirofiban stock solution should be added.

3- The sample should be kept in a $4^{o}C$ refrigerator inside a biohazard Specimen Transport Bag before it is ready to be used or shipped out.

4- In the case of shipping, an appropriate packaging should be considered for preserving the sample at 2-8 oC. As an example, Nanocool box from FedEx can maintain the desired temperature up to 96 hours.

5- When the setup is ready to start the experiments, the blood sample should be tested. No clumps should be seen while pipetting blood. Also, a blood smear sample should be prepared for further analysis. Place an approximately 4 mm

diameter drop of blood on one end of the slide and smear it with another slide and let it dry for 5 minutes.

6- Giemsa staining protocol can be used for blood smear sample analysis. Dip the smeared blood on a glass slide in methanol for 7 min. Dry it with an air gun. Dilute Giemsa stain (Sigma Aldrich #GS500) 1:20 with DI water. Dip the slide in diluted Giemsa solution for 40 min. Rinse the slide with DI water thoroughly and dry it with an air gun. Coat the slide with xylene and protect it with a cover slip.

Figure 58 and Figure 59 show Giemsa stained sample from a first patient sample. Unfortunately, this protocol was not used for the first patient sample, and as it can be observed, there are Echinocytes, Platelet cloaking, and broken Lymphocyte. For more detailed guidance, other references can be used [300].

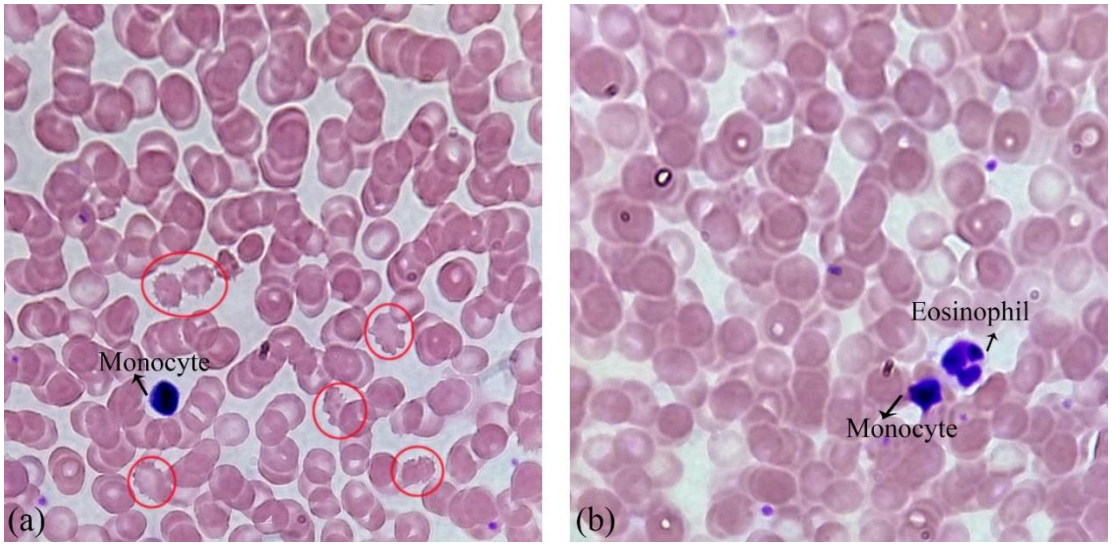

Figure 58. Echinocytes are the result of inappropriate handling and storing of the blood sample in room temperature for 48 hours. (b) A healthy blood sample that was kept at 4 ºC for 48 hours.

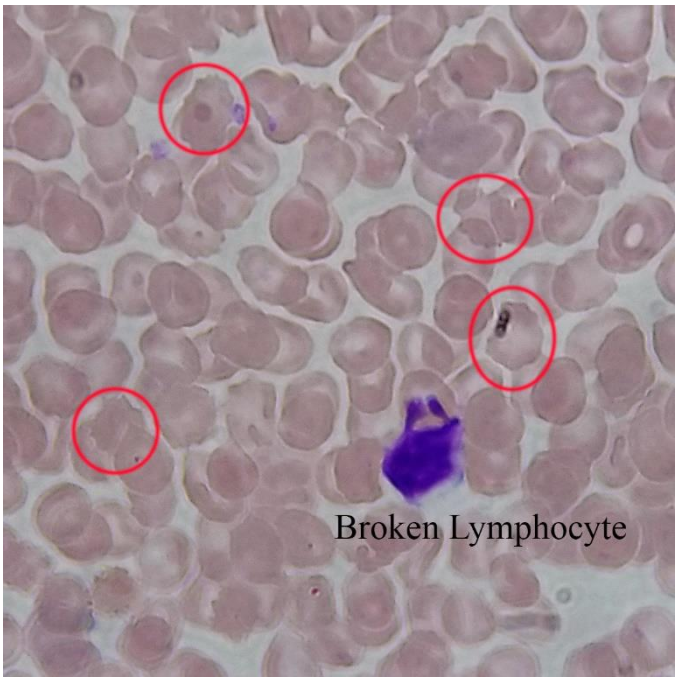

Figure 59. Several Echinocytes and a broken Lymphocyte due to storing the sample in room temperature for 48 hours.

5.2.4. RBC Lysis and Processing the patient's blood sample

Previously, hypotonic low NaCl concentration solution was used for lysing spiked and PDX blood samples. For those experiments, the volume was up to 0.8 ml, and after removing the plasma, it was possible to lyse the RBCs with 15 ml of lysed sample. However, for the first patient sample, we had to repeat the lysing more than once to remove most of the RBCs. There was a learning curve associated with processing large volumes of blood for patient samples. Therefore, we updated the RBC lysis protocol. RPMI-1640 medium (GlutaMAX™ Supplement) was mixed with EGF (20ng/ml), basic FGF (20ng/ml), B27 (10ml), 50 ml FBS and 1x Antibiotic as the culture media for patient samples.

4 ml of he collected blood sample was transferred from the original tube to a 15 ml centrifuge tube, and then it was centrifuged at 300 g force for 5 minutes. The blood plasma was removed from the supernatant. The cells pellet at the bottom of the tube were re-suspended in 12 ml lysis buffer (G-Bioscience #786650). After mixing for 3 minutes, the tube was centrifuged at 130 g for 5 minutes. The supernatant of the lysed sample was transferred to another tube (waste tube). Using 1 ml of culture media, the cells were resuspended at the bottom of the tube and then they were transferred to a 1.5 ml microcentrifuge tube. Cells were centrifuged at 130g for 5 minutes, and then the supernatant was transferred to waste bottle. The remaining cells were resuspended in 120 µl culture media, and they were divided into 12 CNT devices. These devices were kept in a larger petri dish containing PBS for creating a moist environment, inside an incubator at 37ºC 5% CO2. After 48 hours, the droplets on the devices were removed, and the devices were washed once with PBS. The isolated cells on the device are then used for immunofluorescence studies. Figure 60 compares the patient sample before and after lysis.

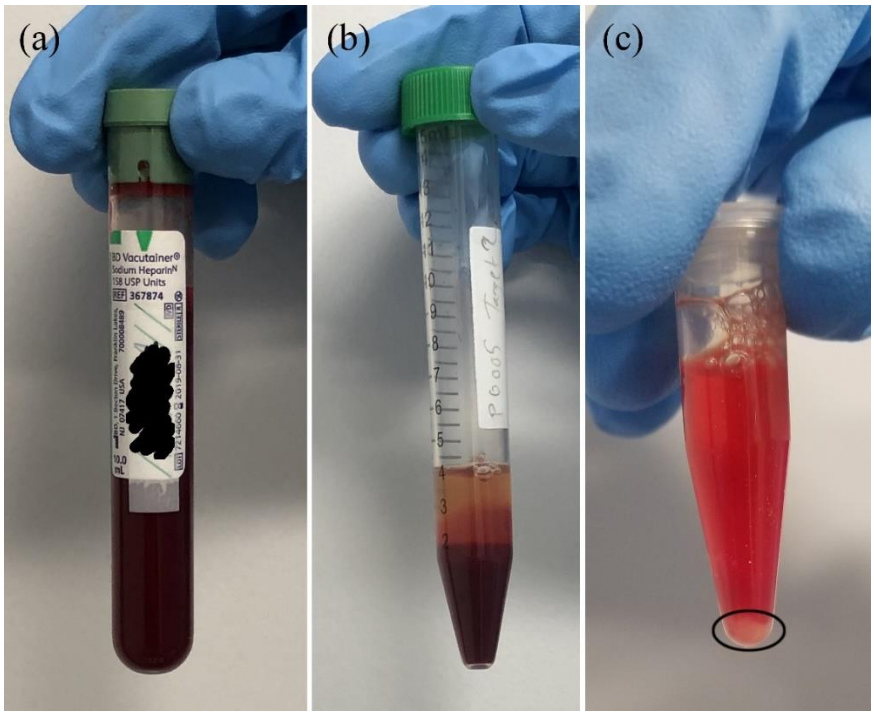

Figure 60. (a) Collected blood from a breast cancer patient in a BD Medical #367874 Vacutainer® Plus Plastic Heparin Blood Collection Tube, (b) Separated plasma for a 4 ml blood sample after the first centrifuge, (c) Lysed sample, WBCs and CTCs palette at the bottom of micro centrifuge tube is circled.

5.2.5. Immunofluorescence microscopy

We were able to do the microscopy and identification of captured cells directly on the chip without further transfer. For immunofluorescent analysis, after washing the devices with PBS once, they were fixed with 4% paraformaldehyde for 10 minutes. The sample was washed with PBS and then blocked with Image-iT™ FX Signal Enhancer, and immunofluorescence locking buffer (cell signal #12411) for 1 hour each at room temperature. The primary antibody was diluted based on the suggested concentration by the manufacturer, and then the sample was covered with it, incubated at 4^{o}C overnight. The sample was washed with PBS 3 times. The secondary antibody was diluted to 1 µg/ml, and the sample was covered for 1 hour at room temperature in a dark container.

The final step was to stain the nucleus with DAPI, wash the devices and mount the sample with a coverslip. Table 13 has listed the antibodies that have been used in this chapter. Except for the DAPI, the other primary antibodies are reactive only to human cells.

Table 13. Utilized antibodies for immunofluorescent identification of captured CTCs in mice model.

Antibody	Manufacturer	Host	Clone	Used dilution (µg/ml)
Cytokeratin 8/18	Thermofisher (#180213)	Mouse	Zym5.2 (UCD/PR.10-11)	1:100
EGFR	CellSignal (#4267S)	Rabbit	D38B1	1:50
ITGB4	Thermofisher (#14-1049-82)	Rat	439-9B	1:100
DAPI	CellSignal (#4083S)	-------	-------	µg/ml
Her2	Thermofisher (#MA5-14057)	Mouse	e2-4001, 3B5	1:100
CD45	Thermofisher (#MA5-17687)	Rat	YAML501.4	1:500

5.2.6. Patients characteristics

As it was mentioned in the first chapter, the golden standard for cancer diagnosis is pathology and the most commonly used tool that doctors use to describe the stage is the TNM system. In this chapter, we have compared our results with the pathology report on the same patient to understand the population of CTCs better. It should be mentioned that the pathology report was received after fully processing the blood sample. The CTC isolation and identification experiments were handled in WPI while the pathology tests were handled where the blood samples were provided in University of Louisville Cancer Center or UMASS medical school.

TNM is the abbreviation of the tumor, node, and metastasis. For breast cancer patients, there are five stages: stage 0 (zero), which is noninvasive ductal carcinoma in situ (DCIS), and stages I through IV (1 through 4), which are used for invasive breast cancer. The stage provides a common way of describing cancer, so doctors can work together to plan the best treatments.

These results are combined to identify the stage of cancer for each patient. Staging can be clinical or pathological. Clinical staging is based on the results of tests done before surgery, which may include physical examinations, mammogram, ultrasound, and MRI scans. Pathologic staging is based on what is found during surgery to remove breast tissue and lymph nodes. The results are usually available several days after surgery. In general, pathological staging provides the most information to determine a patient's prognosis.

6.2.6.1 Tumor (T)

The report should contain the tumor information including its size and location. Using the TNM system, the "T" plus a letter or number (0 to 4) is used to describe the size and location of the tumor. Tumor size is measured in centimeters (cm).

6.2.6.2 Node (N)

The "N" in the TNM staging system stands for lymph nodes. The TNM report also should indicate whether the tumor has spread to the lymph nodes and if so, where and how many nodes are there. Regional lymph nodes include Lymph nodes located under the arm called the axillary lymph nodes, Above and below the collarbone, and Under the

breastbone called the internal mammary lymph nodes. Lymph nodes in other parts of the body are called distant lymph nodes.

6.2.6.3 Metastasis (M)

Also, such report should make it clear if cancer has spread to other parts of the body and if so, where and how much. This is no longer considered early-stage or locally advanced cancer.

Overall, we have processed seven breast cancer patients with different staging and conditions and two healthy controls. In the next section, we will discuss the obtained results from these samples.

5.3. Results

5.3.1. The sensitivity of Nanotube-CTC chip

Figure 61 is the composite, and optical images of CTCs captured from breast cancer patients using preferential adherence in 4 ml and 8.5 ml blood. We captured CTCs in n=7/7 samples in patients suggesting 100% sensitivity. Healthy controls (n=2/2) showed no presence of CTCs in blood. CTCs of different phenotypes were captured based on CK8/18+, Her2+, DAPI+, CD45-, and EGFR+ stains. Both healthy control 1 and 2, were CK8/18-, CD45+, and DAPI+.

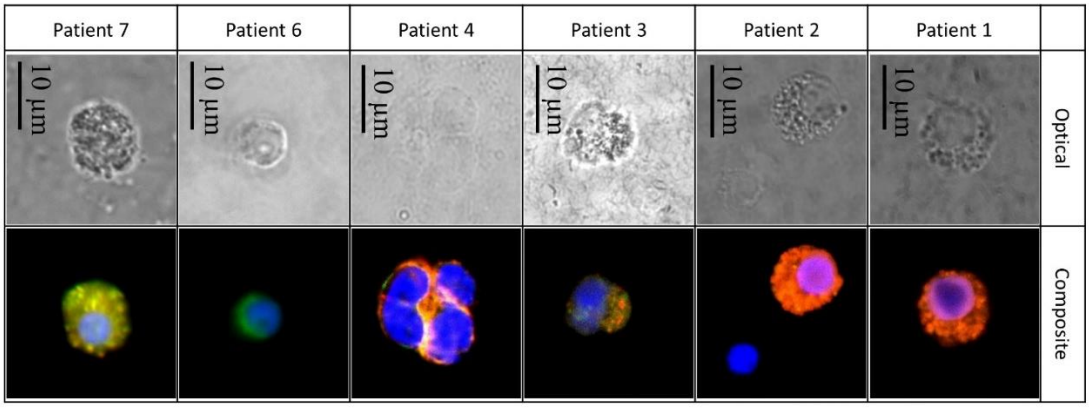

Figure 61. Optical images and merge images of patient samples.

Table 14 presents the TNM staging, a number of CTCs and number of heterogeneous CTCs captured using nanotube-CTC-chip. Patient 1 (stage 4) was an outlier as the lysis procedure did not work the first time (due to platelet aggregation) and we had to do the lysis more than once. However, we still captured 8 CTCs expressing Her2 and EGFR.

As Table 14 suggests, anywhere from 8-238 CTCs per were captured in 4 ml/8.5 ml blood. CTCs were captured in patients that were lymph node positive and negative. In general, using TNM staging and number of CTCs counted we infer, patients who were staged between stage 1-3 (patient 2, patient 3, patient 5 and patient 6) had a lower number of CTCs (4-39 CTCs in 4 ml and 8.5 ml blood or 0.5 to 10 CTCs per ml). Patient 4 was stage 4 cancer with an elevated level of CTCs (238 in 8.5 ml blood or 28 CTCs per ml). There is an apparent spread in CTC counts between early stage (stage 1-3) and advanced disease (stage 4) using the nanotube-CTC-chip. The CTCs were positive for both Her2 and EGFR suggesting aggressive disease. Finally, in patient 7, blood was only obtained after radiation therapy (although the patient was chemo naïve). Surprisingly, we captured only 9 CTCs in 8.5 ml blood (1 CTC/ml) suggesting that the number of CTCs may have

receded in this stage 4 patient after radiation. Comparing this patient 7 to patient 4 (treatment naïve), we believe the nanotube-CTC-chip can predict the treatment response based on CTC enumeration. More patients need to be tested, but the number of CTCs, the range of CTCs in early stage versus metastatic disease suggests the potential predictive powers of the chip. Figure 62, Figure 63, and Figure 64 show the level of expression for the captured CTCs and WBCs.

Table 14. Patient characteristics, TNM staging, CTC numbers, and stable/progressive disease

Patient	TNM staging& Source	# CTC captured	#CTC per ml	#Heterogeneous CTCs	Notes
Patient 1	PT4N2M1; treatment naïve; Stage 4; UofL;	8 in 8.5 ml blood	N/A	8 based on Her2/EGFR	Lysis used more than once. A criterion cannot be established
Patient 2	PT1CN0; Stage 1B; UMASS;	39 in 4 ml blood;	9.75 CTC/ml	36 CK+ and 3 EGFR+	Stable disease; lymph node invasion
Patient 3	PT2N0M0; Stage 2 UMASS;	21 in 4 ml blood	5.25 CTC/ml	19 CK+, 2 EGFR+	Stable disease; tumor >20 mm
Patient 4	PT1BN1M1; Stage 4; UofL; treatment naïve;	238 in 8.5 ml blood	28 CTC/ml	Her2+ and EGFR+	2 CTC clusters; progressive disease
Patient 5	PT1N1M0; treatment naïve; Stage 2A; UofL	27 in 8.5 ml blood	3 CTC/ml	3 EGFR+ and 26 CK+	Stable disease
Patient 6	PT2N2A; Stage 3A; UMASS	4 CTCs in 4 ml blood	1 CTC/ml	only CK+	Stable disease
Patient 7	PT4BN1M1; treated with radiation; UofL	9 CTCs in 8.5 ml blood	1 CTC/ml	1 EGFR; 8 CK+	Metastasis to bone and lung; CTCs still exist after radiation therapy

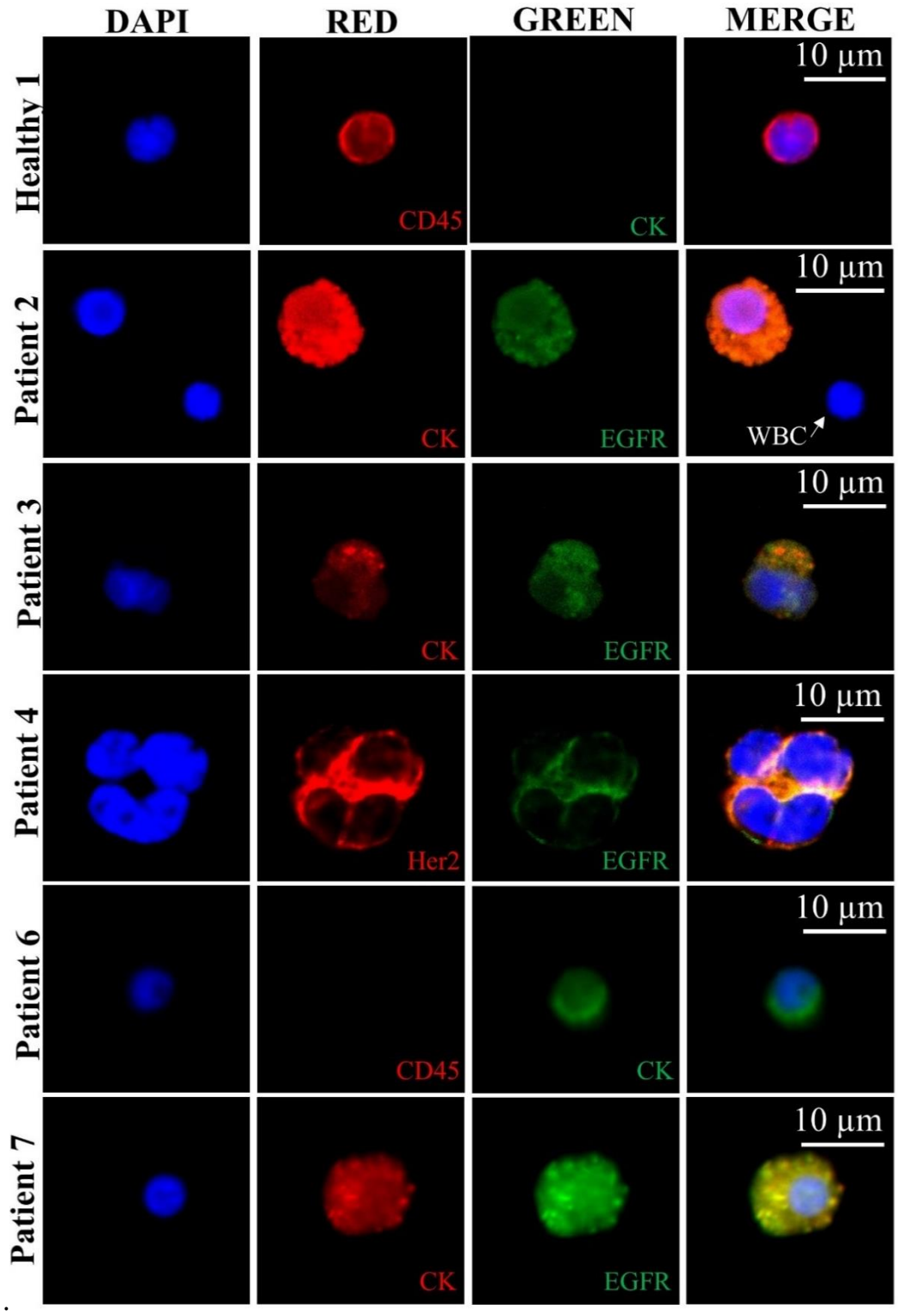

Figure 62. Heterogeneous CTCs isolated from breast cancer patients based on CK, Her2, and EGFR. No CTCs were found in healthy controls. The volume of blood: 4 ml and 8.5 ml blood. CK+, CD45- and DAPI+ was identified as CTCs, while CD45+ and DAPI+ were identified as WBC.

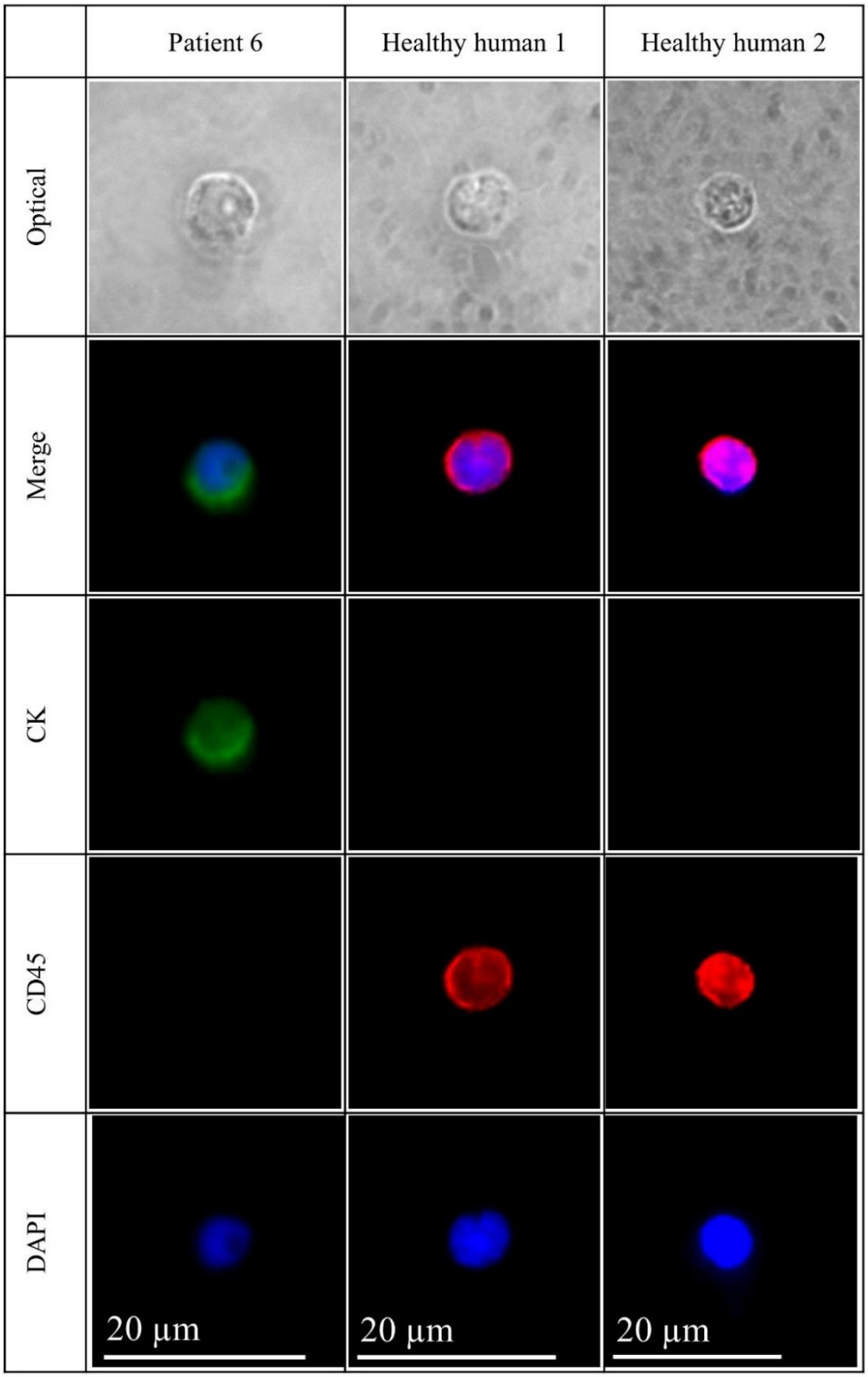

Figure 63. CTC versus WBC; CTCs were CK+, CD45- and DAPI+; WBCs were CK-, CD45+ and DAPI+.

5.3.2. Capture of CTCs of various phenotypes using nanotube-CTC-chip in breast cancer patients:

One of the objectives of our study in patients was to investigate the presence of single CTCs of various phenotypes (Her2+/EGFR+ CTC subclones in breast cancer). The EGFR family is comprised of four structurally similar receptors including EGFR (ErbB-1, HER1), HER2 (ErbB-2), HER3 (ErbB-3), and HER4 (ErbB-4) [301]. There is significant interest in EGFR and HER2 because of their frequent overexpression in breast carcinomas [301]. In our analysis of all patients, apart from CK (8/18)+ cells, we were able to capture 2-3 cells that were strongly EGFR positive in stage 1-3 cancer. This suggests various CTC phenotypes exist in patients even in early-stage cancers. However, advanced stage cancers (patient 4) showed both Her2 and EGFR positive CTCs with large numbers of CTCs (Table 14). This may suggest the combination of CTC numbers, and the heterogeneity of CTCs determines the aggressiveness of the disease in breast cancer.

To distinguish between CTCs of different phenotypes, we further investigated whether different types of CTCs could exist on the same patient. Figure 64 provides dynamic views of epithelial and mesenchymal states of CTCs captured from patient 5. In Figure 64, one can see WBC (DAPI only), epithelial CTCs (positive only for CK8/18) and EMT related CTC (CK8/18 and EGFR). Figure 64 (b-d) show the different CTC from the same sample. In Figure 64 (b), the spindle cell with both EGFR and CK8/18 suggest activation of the EMT process. CTCs often change morphology on EMT activation and the presence of EGFR and the morphology of the CTC can be a positive

confirmation. In Figure 64 (c-d) shows the presence of both epithelial and mesenchymal CTCs. Epithelial CTCs were only positive for CK8/18 and not EGFR, but the more aggressive mesenchymal state was also strongly positive for EGFR and lacked CK8/18 expression (Figure 64(c)). Overall, we found 3 EGFR+ CTCs and 26 CK8/18+ CTCs in patient 5, suggesting we can track CTC of various phenotypes at the single cell level.

Further details can be found in Figure 65 and Figure 66 showing the difference between epithelial, mesenchemal, and EMT CTCs. Our analysis of phenotype heterogeneity can also inform decision making as we have focused mainly on 3 markers namely CK (8/18), Her2, and EGFR for which treatment options are available. Overall, the nanotube-CTC-chip enabled a high level of success in analyzing CTCs, CTC enumeration, the capture of heterogeneous CTCs and the ability to distinguish between epithelial, mesenchymal, and EMT related CTCs in breast cancer patients.

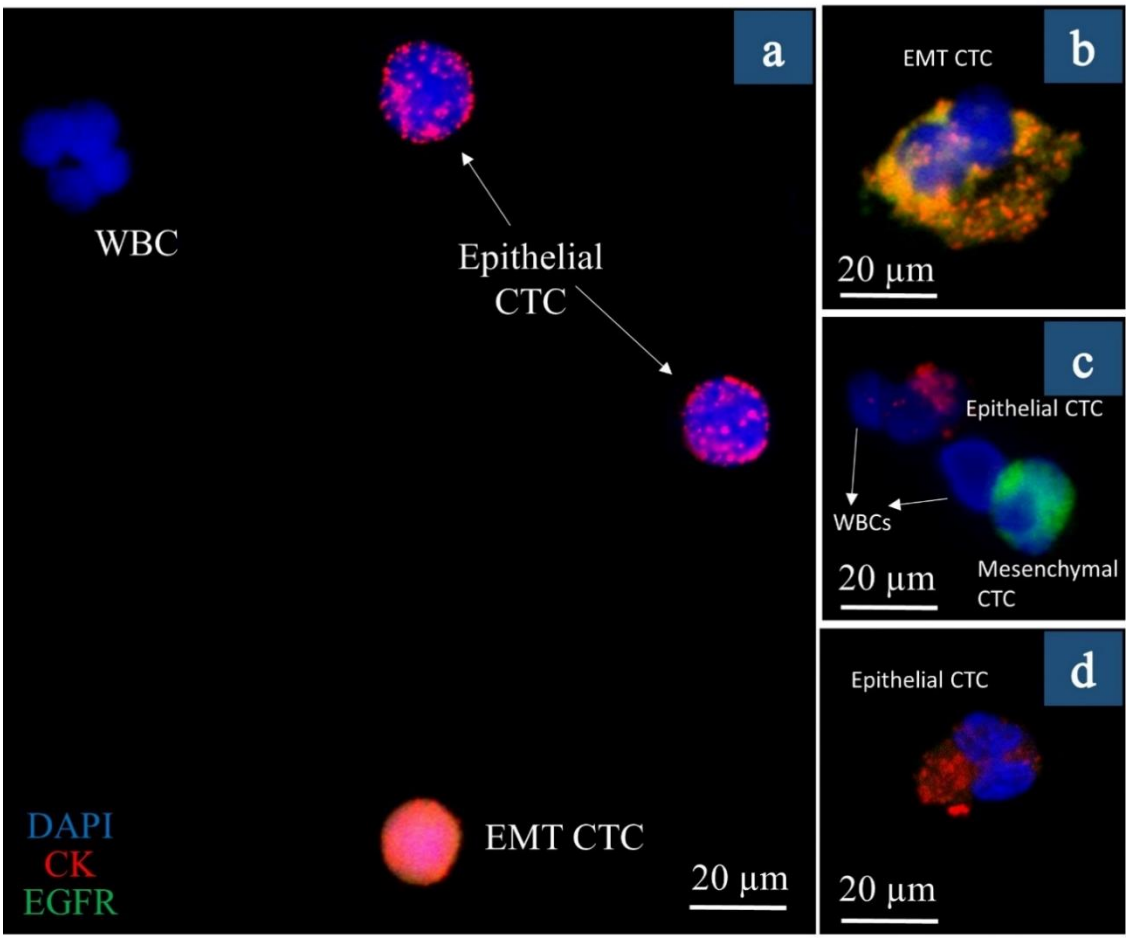

Figure 64. Epithelial, Mesenchymal, and EMT CTCs captured from a single patient: (a) Merge image of CK+, EGFR+ and DAPI+ cells on the same chip; the cell at the bottom is a single cell expressing CK, EGFR and nuclear stain DAPI; (b) Spindle-shaped partial epithelial and partial mesenchymal cell expressing both CK and EGFR; (c) Fully epithelial CTC, WBC and mesenchymal CTCs (expressing only EGFR); (d) Epithelial CTC expressing no EGFR and only CK.

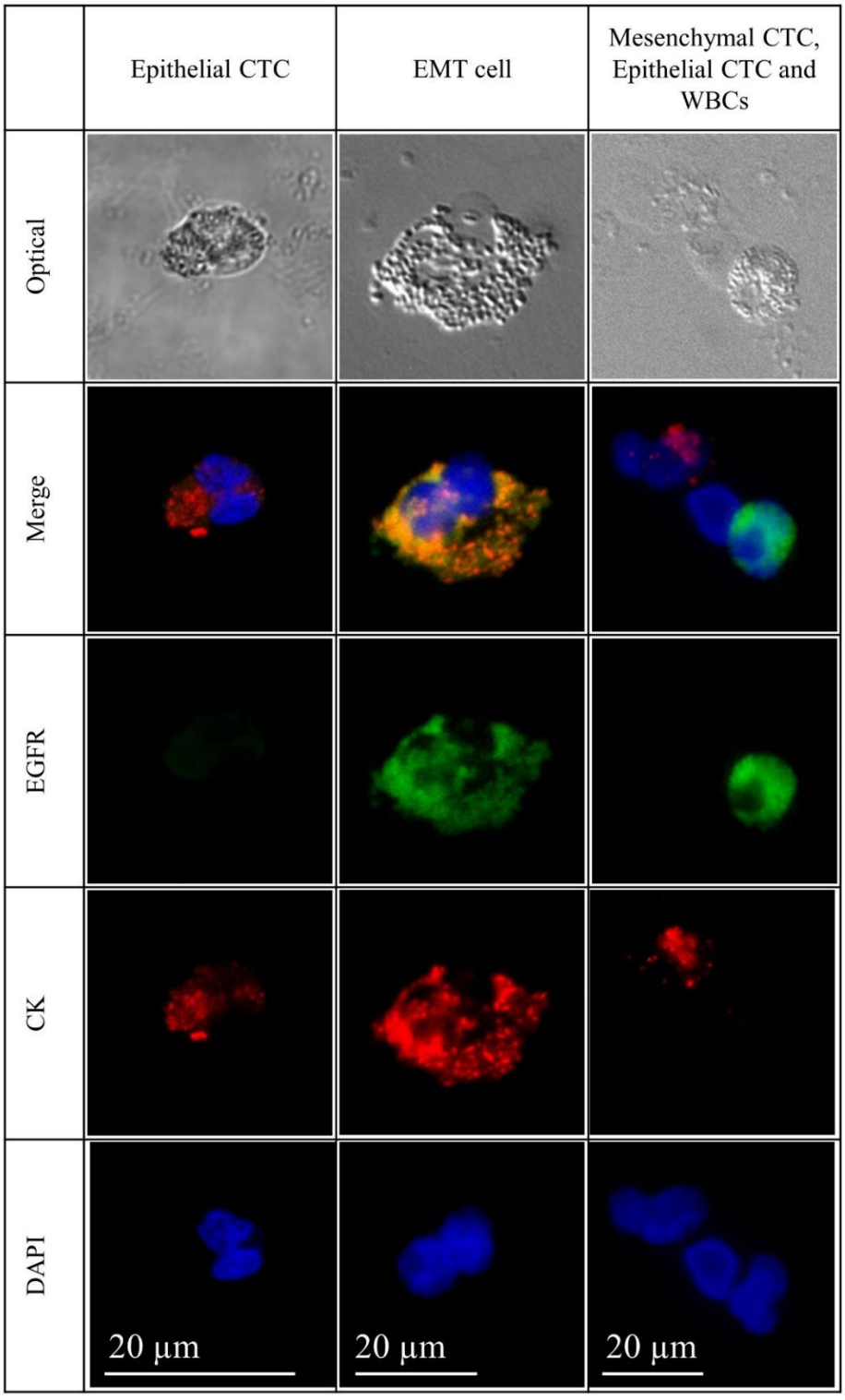

Figure 65. Epithelial, mesenchymal and EMT related CTCs along with WBCs (DAPI only) distinguished using the surface protein expression of different antibodies.

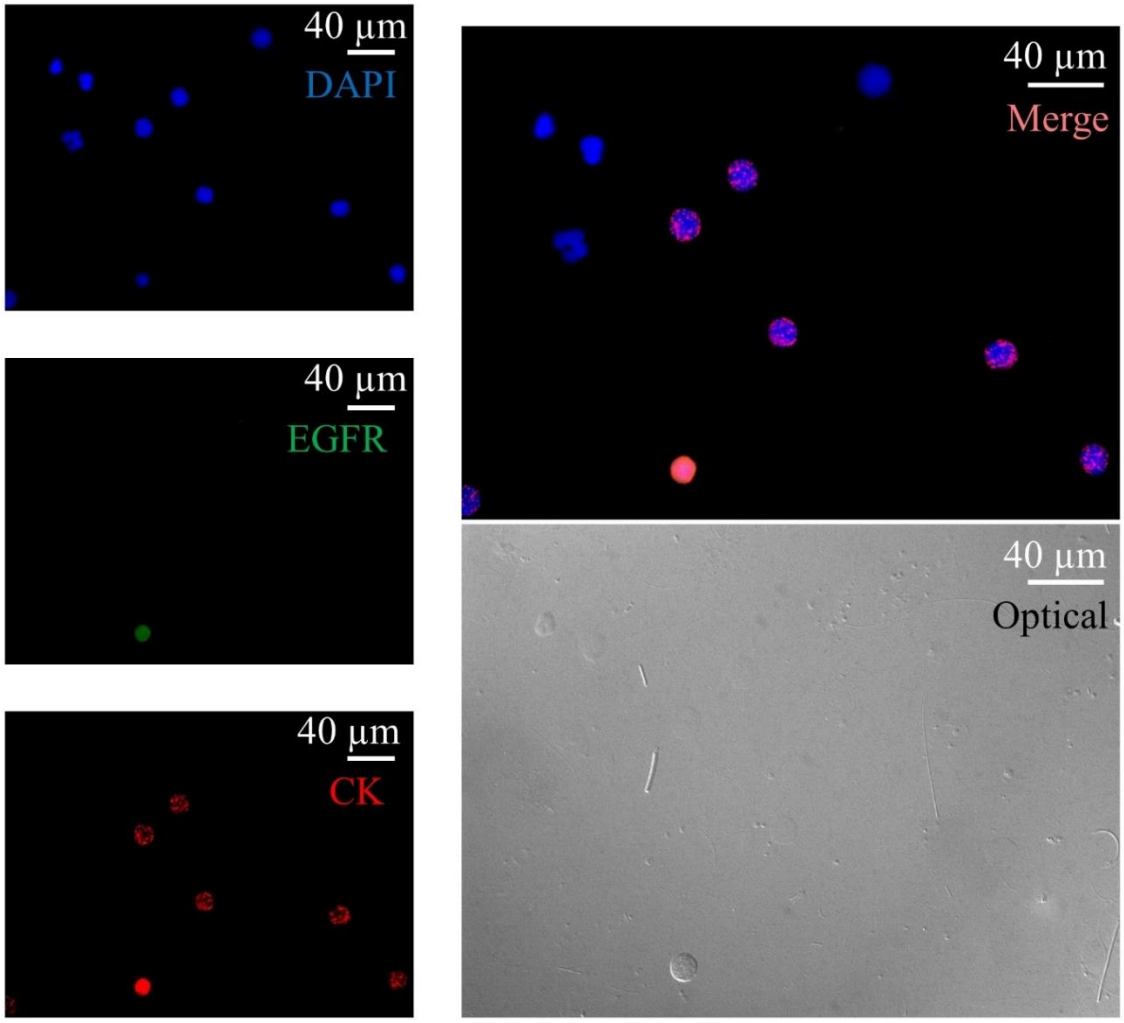

Figure 66. Heterogenous CTCs and WBCs on the same nanotube-CTC chip; optical, DAPI, EGFR, CK and merge images. A single CTC is seen at the bottom of each image suggesting this CTC was positive for DAPI, CK, EGFR indicating multiple phenotypes on the same cell.

Figure 66 shows a single CTC at the bottom of the image exhibiting multiple phenotypes (both EGFR and CK(8/18)), while the majority of CTCs were only positive for CK8/18. This suggests a small clone exist among primary tumor CTCs that can have metastatic (EMT) phenotype. Brain metastatic breast cancer (BMBC), can express both Her2 and EGFR [302, 303], suggesting such populations are at high risk for metastatic

disease. The high CTC numbers and the presence of both Her2/EGFR pathological features can trigger EMT, metastasis and determine future survival.

The mechanism of adherence for patients derived CTCs has been explored and hypothosized in Chapter 3. Figure 67.a shows the microtentacles that could be observed due to extensive excitation of nuclei stained with DAPI. It was possible to stain the microtentacles using tubulin-based antibodies [271]. However, the focus of this study was on confirmation of isolated cells and their characteristics and surface protein expressions that are being used in breast cancer patient treatments.

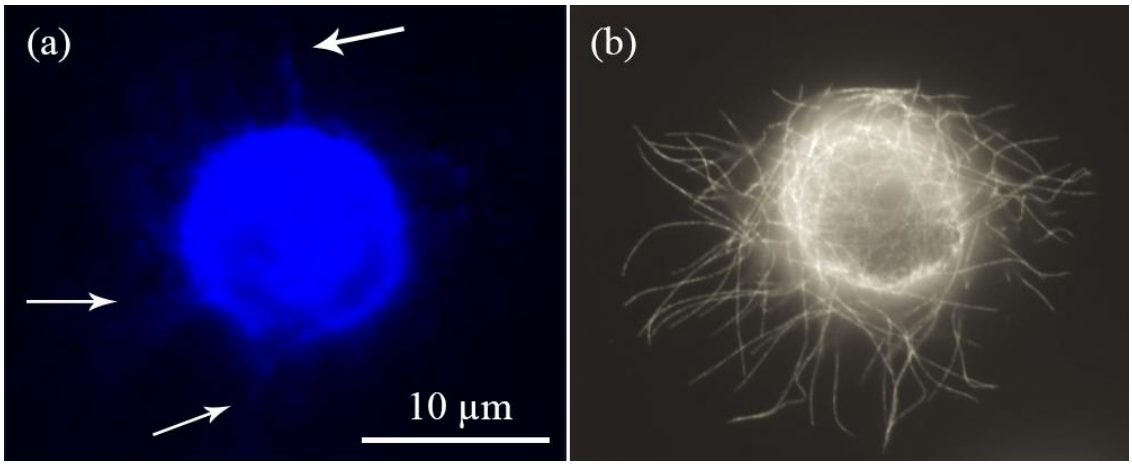

Figure 67. (a) Extreme excitation of DAPI stained nuclei in one of the captured CTCs in breast cancer patient 2 resulted in slight presentation of the microtentacles. (b) A STEM breast cancer CTC stained for tubulin and identification of microtentacles [271].

The number of captured CTCs and WBCs were quantified to investigate CTC: WBC ratio in processed patient samples. The DAPI only cells were counted as WBCs in patients 1-5 and seven while in Patient 6 sample and two healthy controls, WBCs were identified with DAPI+ and CD45+. Table 15 presents the number of CTCs, WBCs, and contamination levels in patient samples. We can observe that anywhere from 4-238 CTCs

were captured in patient samples while there was no CTCs in healthy controls. The number of WBCs captured were between 151-771. For calculation of WBC contamination and log depletion, we took a median of 7,500 WBCs per micro-liter. The log10 depletion for WBC contamination was calculated as it was described in chapter 4 equation 4.

Table 15. A number of CTCs and WBCs captured from the patient and healthy blood samples.

Sample	Number of captured CTCs	Number of captured WBCs	Log10 Depletion	Initial number of WBCs
Patient 1 (8.5 ml)	8	31	6.31	63,750,000
Patient 2 (4 ml)	39	637	4.67	30,000,000
Patient 3 (4 ml)	21	479	4.79	30,000,000
Patient 4 (8.5 ml)	238	277	5.36	63,750,000
Patient 5 (8.5 ml)	27	549	5.06	63,750,000
Patient 6 (4 ml)	4	151	5.29	30,000,000
Patient 7 (8.5 ml)	9	771	4.91	63,750,000
Healthy control 1 (8.5 ml)	0	643	4.99	63,750,000
Healthy control 2 (8.5 ml)	0	652	4.99	63,750,000

Patient 1 is an outlier due to lysis procedure done more than once. It can be seen in both healthy controls we got the same log- depletion suggesting high controllability and uniformity of the process. The range of log-depletion was between 4.6 to 5.3 suggesting this number could be useful as a calibration marker for suggesting process control in routine clinical practice. However, narrowing this distribution even further in future samples can be highly beneficial to enable comparison across multiple cancer types. Figure 68 presents the distribution of the number of captured CTCs based on breast cancer patient staging and treatment condition.

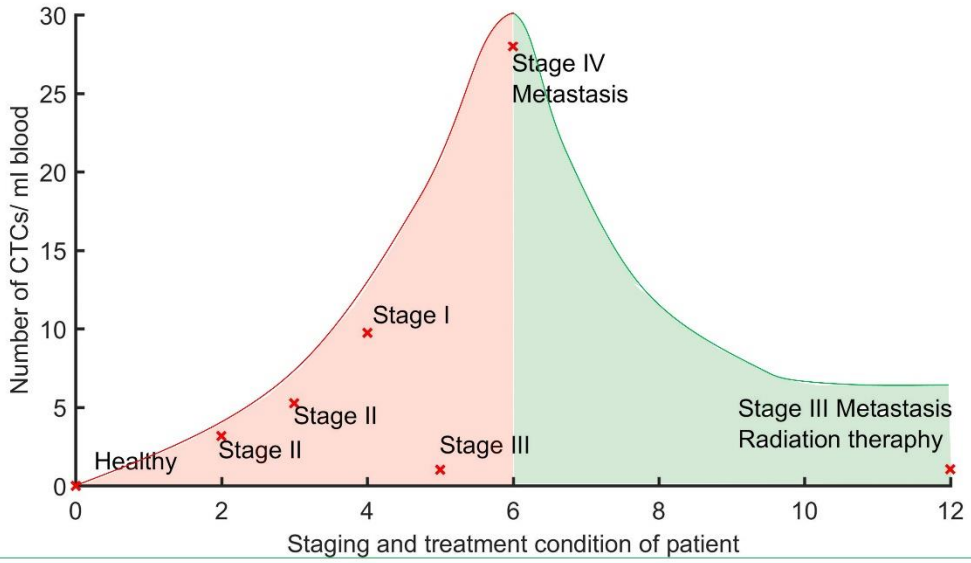

Figure 68. Distribution of the number of captured CTCs based on patient staging and treatment condition.

5.4. Conclusion

We have successfully demonstrated that we can capture CTCs in all of breast cancer patients with different cancer staging and treatment condition. This is a great achievement, and it shows the clinical relevance of the ideology of capturing CTCs in blood sample not based on their physical or biological properties but rather based on their mechanical functionality.

For many years, the concept of using biomarkers on the surface of tumor cells is dominating the field of CTC isolation and identification. The only FDA approved tool for isolating CTCs in blood samples for partial prognosis of cancer patients is the highlighted technology of such approach. However, many studies have proven that Immunoaffinity approach in general and CELLSEARCH in specific is suffering from

low sensitivity. This is due to the heterogeneous nature of CTCs, and using single biomarker is inadequate to capture all the CTCs

In contrast, here in this chapter, we were able to show that isolating CTCs solely based on their mechanical functionality and behavior is enabling us to have 100% sensitivity. We also have proven that Nanotube-CTC chip have the capability of isolating CTCs with different phenotypes and aggressiveness. This shows that Nanotube-CTC chip has the potential to be used for diagnosis, prognosis and treatment plan for different cancer types and different staging. For example, in this chapter, CNT film enumerated CTCs in all blood samples from breast cancer patients with various staging condition. In chapter 3, we reported similar results for breast, cervix, and brain cancer cells. As another example, comparing Patient #4 and #7 samples with similar staging condition show that the number of CTCs in Patient 7 has significantly lower than Patient 4. This is an indication of successful radiation therapy in Patient 7.

Another important outcome of this chapter is that our protocol can process large volume of blood in a very short time. This add up to the fact that using the preferential adherence of CTCs to CNT film will result in removing more than 99% of WBC. Consistent WBC log depletion of 5 for all of the healthy and breast cancer patients is one the highest products in CTC isolation technologies and these results is another important advantage of Nanotube-CTC chip.

Chapter 6

CONCLUSIONS AND FUTURE DIRECTIONS

6.1. Conclusions

CTCs are rare, comprising as few as 1-100 cells per 10^9 to 10^{10} hematological cells and CTC shedding from a solid tumor into the bloodstream is a highly discontinuous process. Thus, the isolation of CTCs with high purity is still a very significant challenge. The high mortality in cancer patients is mainly attributable to metastasis and to the fact that tumors in many cancers are generally detected at advanced, inoperable stages of the disease.

Early detection of cancer before it metastasizes to other organs is crucial for its treatment and patient survival. Identifying those small subclones of CTCs that can have metastatic potential in early stage cancer can potentially save lives through suitable intervention. Therefore, minimally invasive liquid biopsies for early detection and diagnosis, especially from a blood sample, have been a significant goal of cancer research for many years. Tissue biopsy is the standard of care in the diagnosis and treatment of cancer. It is possible that the genomic characterization of CTCs based on liquid biopsies may prove useful as a substitute for tissue biopsies, especially when tumor tissues from metastatic breast cancer patients become unavailable for different reasons [299]. However, current CTC detection and capture techniques suffer from one or many problems such as sensitivity, specificity, size and deformability of cells through filters,

dependence on immunohistochemistry, non-viability of captured fixed cells, WBC contamination, and mass production related issues due to complexities.

The isolation, capture, and enumeration of CTCs of different phenotypes using the nanotube-CTC-chip can be broadly classified into four steps as presented in Figure 69. In step 1, 8.5 ml blood consisting of approximately 40 billion erythrocytes, 64 million leukocytes and 1-10 CTCs of different phenotypes are removed from a patient. In step 2, the red blood cells (RBCs) are depleted through an RBC lysis protocol [304]. The entire contents are centrifuged, and nucleated cell fractions consisting of CTCs & WBCs pelleted. In step 3, the nucleated cells consisting of CTCs & WBCs are added as standard 10 µl droplets on 6-12 individual nanotube devices (total 60-120 µl; each device is 3 mm x 3 mm). The hypothesis being CTCs attach to the nanotube substrate and not the other nucleated cells including WBCs. Also called, antigen-independent CTC capture, this strategy represents an approach to the enrichment of CTCs with high purity that is not biased by the selection of potentially variably expressed markers on tumor cells. In step 4, the attached CTCs on the nanotube surface are immunostained on-chip using antibodies to identify and enumerate CTCs of different phenotypes. DAPI (4′,6-diamidino-2-phenylindole) is used as the nuclear stain and cytokeratin (CK8/18), and other antibodies (ex: Her2, EGFR) identify CTCs. CD45 and only DAPI identify WBCs.

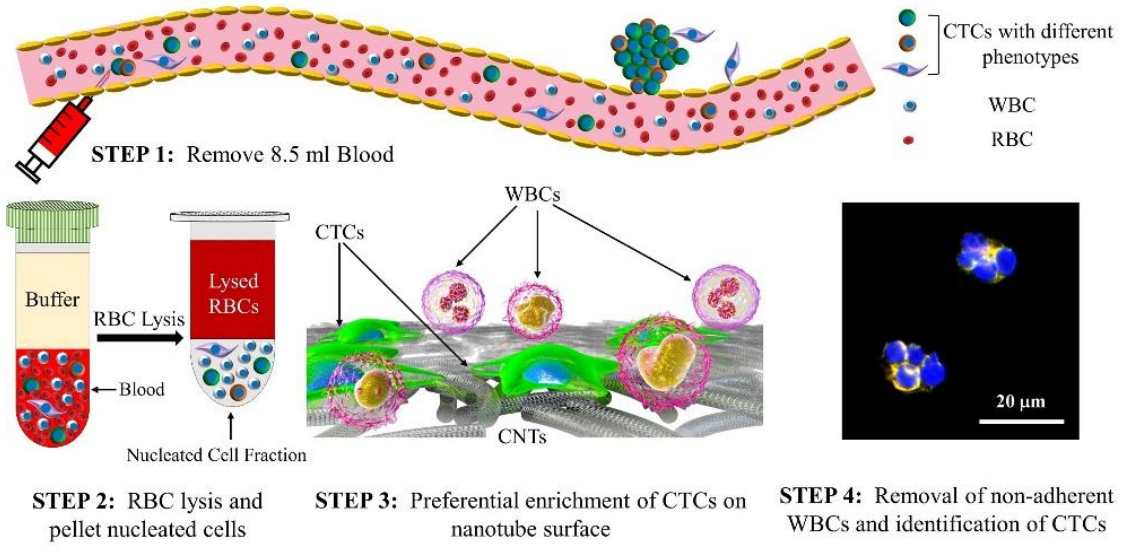

Figure 69. Steps in isolation and enumeration of CTCs using nanotube-CTC-Chip.

There are several advantages to the nanotube-CTC-chip as mentioned before including size independent and antigen-independent capture, surface/planar architecture and ability to capture CTCs of different phenotypes. We found that RBC lysis does not affect the target cells and CTCs were found in every patient. We captured 0.5-10 CTCs per ml in early stage (patient 2, 3, 5 & 6) cancer versus >10 CTCs per ml in advanced stages (patient 4; 28 CTC per ml). The number of CTCs in initially diagnosed advanced disease (patient 7; stage 4 metastasized to lung and bone) was seen to be low with radiation therapy (1 CTC per ml). This suggests, our chip has predictive capabilities and can monitor therapy induced CTC numbers, similar to CELLSEARCH®; except we capture more CTCs due to the antigen-independent method and our baseline numbers are expected to be higher compared to CELLSEARCH®, which captures CTCs based on EpCAM/CK8/18.

Using this chip, we have overcome technical issues affecting the CTC community, namely the issue of cellular retrieval experienced in most fluidic devices by using a surface architecture in our microarrays that is amenable to surface chemistry modifications [91]. We have surmounted the issue of mass production by using semiconductor batch fabrication techniques, with the ability to create 76-element arrays in silicon and glass with >99 % yield. We have overcome the issue of WBC contamination, by using a combination of RBC lysis and preferential adherence on a nanotube surface, that results in the capture of CTCs and 5-log depletion of WBCs. The transparency of glass devices can enable imaging from either side of the device for CTC capture, and that lends itself to manufacturing. The presented nanotube-CTC chip is also gentle and allows for the isolation of viable cells for future CTC culture, whereas magnetic-bead-based approaches such as CELLSEARCH® can only isolate fixed, non-viable cells [305].

Over the past decade, researchers have highlighted the importance of matrix stiffness, topography, compressive and shear stresses, and deformation on cells in influencing tumor growth and proliferation [306]. CTCs, in order to survive and travel to a distant site, should develop the ability to attach in an environment that is not conducive to attachment. We exploit the ability of CTCs to attach preferentially to a nanotube surface to enrich them. One exciting aspect of our study is that RBC lysis affects neither target cells nor their clusters. The ability to successfully use RBC lysis along with a method of preferential adherence using a CNT microarray suggests that our new route is simple and easy to capture CTCs, EMT related cells, and rare clusters.

The most significant aspect of our study is that we successfully identified single CTCs and exhibiting multiple phenotypes in early stage (CK8/18, EGFR) and advanced breast cancer patient (Her2, EGFR) samples using our chip. Such dynamic views are not obtained by most CTC technologies currently based on EpCAM and CK8/18 enumeration. While we used immunofluorescence to identify pathological features in captured cells, future capture can directly investigate many other characterization techniques (ex: FISH, NGS). Dynamic views of cancer genomes to understand evolutionary pathways during the process of metastasis are needed [307-309]. For this to happen, high-quality CTCs using elegant and straightforward surface techniques without WBC contamination is needed, which we have shown using this proof-of-concept study in patients. Therefore, the nanotube-CTC-chip is a highly versatile technique for clinical diagnostics and monitoring therapeutic response in human cancers.

6.2. Comparison of Nanotube-CTC-chip micro-array with existing CTC capture techniques and the technical impact of Nanotube-CTC chip

Table 16 and Table 19 compare some of the existing CTC capture methods with that of the nanotube-CTC-Chip. The CELLSEARCH® a technique based on immunomagnetic enrichment was the first to arrive in the market based on EpCAM antigen-dependent capture [99]. A decade of research on CTC capture based on CELLSEARCH® has only yielded modest results. In the recent German SUCCESS study based on the CELLSEARCH® system involving 2026 breast cancer patients before chemotherapy, CTCs were detected in only 21.5% of patients (n = 435 of 2026),

following surgical removal of primary tumor [297]. Another study in comparison of CELLSEARCH® and ISET (filtration system) for circulating tumor cell detection in patients with metastatic carcinomas yielded consistent results only in 55% (11 out of 20) of the patients with breast cancer, in 60% (12 out of 20) of the patients with prostate cancer and in only 20% (4 out of 20) of lung cancer patients [46]. Both techniques have discrepancies between the number of CTCs enumerated using both techniques [46].

Microfluidic technologies such as CTC-Chip [298], Herringbone chip [113] and CTC-iChip [71] are essential concepts and fluidic platforms. CTC-chip with micro-posts is challenging to manufacture and functionalize the surface, and no CTC clusters were captured using this device [71]. The Herringbone chip has surface characteristics also yielded only 2 clusters [113]. The CTC-iChip has low WBC contamination and can capture antigen-independent and dependent CTCs [71]. But an array with 20 μm gaps on the iChip cannot capture CTC clusters and thus is reduced to size-dependent capture [71]. Therefore, newer devices with asymmetry and size-based separation are being developed [310]. Most of the filtration/size-based techniques such as ScreenCell [150], MOFF [311] and ISET [146] seem to isolate CTCs. However, RBC saturation and clogging are a problem in these devices. Similarly, microfabricated filters also isolate CTCs [85, 155]. The problem with most size-based technologies is that the CTCs are highly deformable unless fixed chemically and EMT related CTCs might not be retained. CAM is another unique strategy where only CTCs are captured through digesting the collagen, with 52% sensitivity in stage 1-3 breast cancer [95].

Table 16. Comparison of dominant CTC technology with nanotube-CTC-chip.

Method/Device	Number of CTCs	Number of WBCs	Notes
CELLSEARCH®	5-1000 CTCs in 7.5 ml blood; >5 CTCs is bad prognosis	No information	21.5% capture rate for breast cancer; chemically fixed cells [99, 312].
CTC-Chip	5-1281 CTCs/ml	50% purity	Micro-post, not surface technique; no clusters [298].
Herringbone Chip	12-3,167 CTCs/ml	No information	2 clusters each about 4-12 cells [113].
CTC-iChip	1-30 cells/7.5 ml blood in patients	1188/ml; median, 352/ml; range, 58 to 9249/ml	Has a cutoff for cells larger than 21 μm [71].
NanoVelcro	1-99 CTCs/ml in patients;	No Information	CTCs are captured in 1 ml blood [313]
Vortex	25-300 CTCs/ml	57-94% purity; more recent studies show 5-44% purity ; >20-500 WBCs per ml [305]	Size based collection, deformability of cells, CTC collection depends on aspect ratio [87, 305].
MOFF, SCREEN CELL, ISET, microfabricated portable filters (filtration)	1-100 cells, capture of EGFR based cells; 51/57 patients had CTCs.	Possibly both CTCs/WBCs will be retained.	RBC clogging; deformability of cells are issues. High pressures can damage cells [85, 146, 150, 155, 311]
Collagen Adhesion Matrix	10-1000 CTCs/ml	No information.	52% sensitivity in Stage1-3 cancers. Not all cancer cells adhere to collagen. Culturing over 33 days is necessary [95].
Parsotrix System	Cell lines (66-92% capture); clinical studies ongoing	No information	The blood samples are spiked and processed ~18–36 h after collection, and the number of pre-labeled cells are captured in each cassette [314].
Nanotube-CTC-Chip	8-238 CTCs per 8.5 ml or 4 ml blood; 7/7 patients with stage 1c to stage 4 cancers had CTCs	5 to 6 log depletion of WBCs in patients; 31-652 WBCs in 8.5 ml	Preferential adherence; Antigen-independent and size independent strategy; 5-6 log depletion of WBCs; CTC of multiple phenotypes. Present Work

Table 17. Comparison of dominant CTC technology parameters and outcome with nanotube-CTC-chip.

Technology	**Scalability/ Device Complexity**	**Notes**	**Processed blood volume (ml)**
CELLSEARCH®	Scalable; complex box which has everything automated	Cannot perform subsequent tests on CTCs [107, 297, 315]	7.5
CTC-Chip	Scalable; Complex micro-posts; sealed chambers	Difficult to manufacture reliably	3
Herringbone Chip	Scalable; Complex; sealed chambers	Difficult to manufacture reliably	4
CTC-iChip	Scalable; Complex; hydrodynamic cell sorting; inertial focusing and magnetophoresis in a single chip	cumbersome and production difficult	7.5
Nanovelcro	Scalable; Silicon nanowire; capture efficiency 80% at 0.5 ml/hr; slow; complex microfluidic device	They only do 1 ml; takes 6 hours to capture [11]; Slow; CTCs are difficult to remove for further processing	1
Vortex	Scalable; Device geometry is complex requiring vortex generation	Blood has to be diluted. Even at 40 X dilution, capture reliability is 35% [10]	7.5
Filtration	Scalable; Simple design; RBC clogging is a problem; blood has to be diluted to 50 X	Blood has to be diluted. RBC clogging and not all CTCs are captured [12-16];	
Collagen Adhesion Matrix	Scalable to large volumes; there is no device	Culturing over 33 days; they lose 50% CTCs [17]	3
Parsotrix System	Scalable to large volumes; Complex device with specific critical gaps in channels to capture CTCs	Critical gap is 6.5 μm [18]	2-4.2
EPIC platform	Scalable; microscopy on a glass slide; but need sophisticated laser scanning microscopes	Huge files associated with imaging every cell; seems time consuming. [19]	
Nanotube-CTC-chip; Our work	Simple; micro-array geometry; scalable to larger arrays; handheld device	Uses CTCs own mechanics to attach to nanotubes [20]; Easy to remove CTCs and do post-processing such as NGS	8.5

Compared to all these essential techniques from the past, the nanotube-CTC-chip has advantages. This is a new antigen-independent capture technique based on the mechanobiology of tumor cells on nanotube surfaces, not described before. The preferential adherence strategy enables 5-log WBC depletion which is one of the best today. 100% capture yield at low levels of spiked triple-negative breast cancer cells (1, 10, 100) suggests that the RBC lysis and preferential attachment is a highly competitive strategy. We had high success in capturing CTCs of different heterogeneity in 4 ml and 8.5 ml patient samples of different stages of breast cancer. The clear capture of CTCs in breast cancer patients and no capture of CTCs in healthy controls suggest this chip is ready for a prospective clinical trial. Many clinical trials today are mainly doing CTC enumeration [316]. However, CTC biology, phenotypes, and other pathological features are also relevant in the clinical decision making. In a single microarray, we have been able to demonstrate the correlation between advanced disease, high CTC numbers, CTC pathological features, and ability to track a single CTC with multiple phenotypes.

Currently, the only FDA-approved system (CELLSEARCH®) enumerates merely a total number of chemically-fixed CTCs and cannot capture CTC clusters. Microfluidics is an active field of research for isolation of CTCs. Microfluidic technologies such as CTC-Chip, Herringbone chip, CTC-iChip, Vortex, Rarecyte, Fluxion, NanoVelcro, DEP-Array, and JETTA are leading fluidic devices. Although promising, there are inherent constraints in large-scale production of complex microfluidic-based devices and surface functionalization for targeted capture. Further, the rare CTC clusters could potentially be damaged in fluidic devices due to turbulence, vortices and shear forces.

Very few devices have been able to successfully capture CTC clusters with 30-40% sensitivity in metastatic patients. Further, some of the leading microfluidic technology has only 5-44% purity which makes genomic sequencing difficult.

By engineering nanomaterials namely carbon nanotubes, and microarray manufacturing techniques, we have been able to successfully develop the world's first microarray for CTC capture. Advantages of our microarrays include: 1) microarray format enabling large volume of blood to be fractionated into smaller portion that enables better capture sensitivity; 2) no transfer of cells is necessary to do microscopy, and one can do confocal/optical microscopy on chip; 3) surface architecture lends itself to a variety of surface functionalization and instant CTC isolation for further analysis unlike microfluidics where CTCs have to be recovered from sealed chambers and could be lost; and 4) mature manufacturing process resulting in a 99% yield; 5) Nanotube-CTC chip isolates CTCs solely based on their mechanobiology regardless of their size, biological aspects and expressed biomarkers on their surface, and their phenotype.

Using the mentioned advantages of microarrays, we have demonstrated the capture of spiked breast cancer cells in blood using independent capture with >90% capture rate and elimination of 99% contaminating leukocytes. Further, using donated blood from breast cancer patients from Stage 1 to Stage 4, we have demonstrated the capture of highly invasive CTCs and the very rare CTC clusters which are metastasis-initiating cells. In volumes up to 8.5 ml blood from breast cancer patients, we have shown the capture of up to 238 CTCs of different morphologies. The combination of materials engineering,

microarray manufacturing, biochemical surface functionalization, and cancer biology has led to this new microarray technology that will help in the fight against cancer.

6.3. Socioeconomic impact of Nanotube-CTC chip

It has been estimated that only in US during 201, there would be about 4800 new patients diagnosed with cancer every day [1]. Unfortunately, the survival rate for cancer is not high and two of the main reasons for such low survival rate are absent of a universal product to diagnose cancer at early stages and changing the course of cancer from a local disease into a systematic problem in body named metastasis. Since Circulating Tumor Cells may be present in blood stream and they have valuable information about the primary and potential metastasis tumors, isolating and identifying CTCs would help significantly toward create a clinically relevant medical tool to diagnose cancer at early stages. The goal of this work was to present a new technology to isolate CTC in blood sample regardless of the cancer type, stage, CTCs' size, and their phenotype.

Individual-level socioeconomic data are not routinely reported by cancer registries in the United States because they are not available in patient's hospital records [317]. However, several studies were able to investigate socioeconomic status (SES) on cancer survival based on limited number of cases [317-321]. It has been suggested that SES differences affecting tumor stage at diagnosis may be the most important explanatory factor for this topic [317, 319, 320]. Level of education, disability, and body mass index are a few target criteria for determination of SES and their effect on tumor stage at diagnosis. These studies were able to establish that having lower level of education,

having disability, and high body mass index are associated with an increased risk of advanced tumor stage at diagnosis [317, 319]. These conditions are also associated with low income individual and families which also do not have access to expensive cancer checkups and advance diagnosis tools.

Nanotube-CTC chip is an effective, efficient, and affordable technology that has been able to isolate CTCs in all breast cancer patients with staging 1 to 4. This promising result showing the potential of this technic to be used for early stage cancer diagnosis. A congressional legislation in 2000 (Public Law 106-525) requested the establishment of the NIH National Center for Minority Health and Health Disparities and a strategic plan in health disparities research. While some of the forementioned disparities are in cancer incidence, some other are mostly on their access to proper diagnosis at early stages. Unfortunately, most of the current technologies for isolating CTCs are not able to deliver high sensitivity and most of them are expensive methods.

In a study, Yarboff et al. reported the socioeconomic burden on 1870 ovarian cancer patients with different staging at diagnosis. As it has been presented in U-shape graphs of Figure 70, most of the cost for cancer patients are at the beginning for initial diagnosis and choosing the treatment procedure or at the end if cancer when it leads to death. With an efficient and cost-effective diagnosis technology like Nanotube-CTC chip, the initial cost for cancer treatment will be reduced significantly. If cancer is diagnosed at early stages with a sensitive technology like Nanotube-CTC chip, there is a very good chance that cancer does not lead to extreme condition and death and the significant cost at the final stage of cancer before death will be avoided.

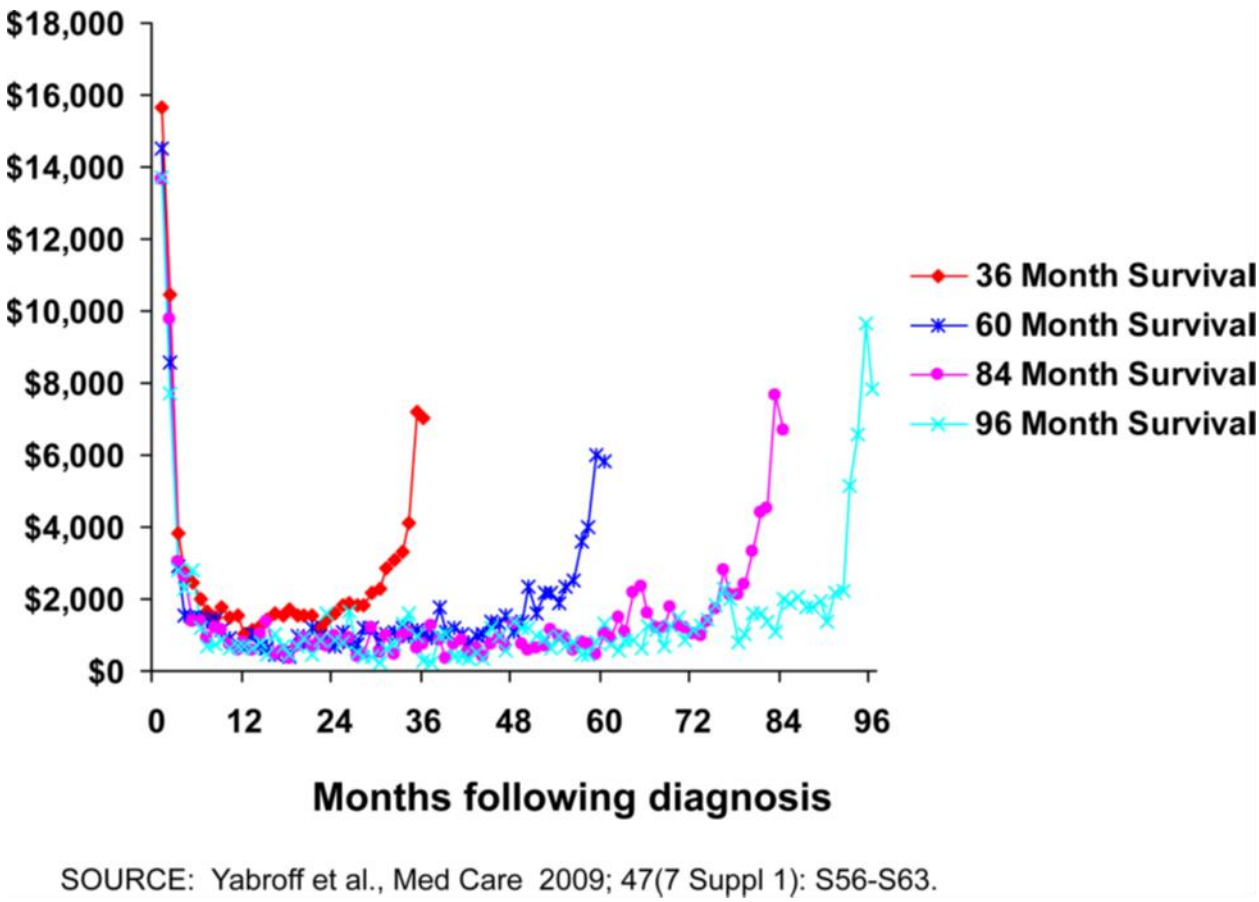

Figure 70. Monthly Costs of Care for Colorectal Cancer Patients by Length of Survival [319].

Cancer and its treatment result in the financial loss, morbidity, reduced quality of life, and premature death. The Agency for Healthcare Research and Quality estimates that the direct medical costs (total of all health care expenditures) for cancer in the US in 2015 were $80.2 billion [1].The loss of economic resources and opportunities for patients, families, employers, and society overall can be reduced significantly if a sensitive and cost-effective diagnosis tool is available that can diagnose cancer at early stages and Nanotube-CTC chip has a lot to offer toward this goal.

6.4. Future directions

We were able to process large blood sample volumes from breast cancer patients up to 8.5 ml using RBC lysis and preferential adherence strategy. Nanotube-CTC chip has shown 100% sensitivity by isolating CTCs in all 7 patients. This achievement has opened a new avenue in the CTC isolation research field showing its clinical relevance, and it can be explored in several directions. More sophisticated statistical analysis can give us a deeper understanding of the results. More robust design of experiment will be led to better statistical power. More experiments can be conducted by testing more breast cancer blood samples, increase the replicates of spiking experiments, and more mice models with better control. Narrowing this distribution even further in future samples can be highly beneficial to enable comparison across multiple cancer types. It also helps us have a better understanding of WBC contamination distribution for different conditions and identify the outlaw samples more efficient.

One of the most interesting aspects of preferential adherence strategy using CNT film is that it is a label-free technic and it makes it possible to use the exact same product for different cancer types. Therefore, testing other types of cancer patient blood samples including lung, prostate, and colon is going to shed more light onto the similarities and differences in CTCs and their adhesion mechanism to CNTs.

While we used immunofluorescence to identify pathological features in captured cells, FISH, NGS or other characterization techniques can be used directly on the chip in future experiments. Dynamic views of cancer genomes to understand evolutionary pathways during the process of metastasis are needed. Expanding the captured CTCs directly on

the Nanotube-CTC chip is providing the option for easier and less expensive genomic methods and also testing personalized treatment and medicine based on captured CTCs. The advantage of our platform is that each microarray device is a separate unit and one can use different identification technics and biomarkers for characterization of CTCs.

Investigation of fundamental aspects of preferential adherence mechanism is an interesting aspect of this technology which can be explored further. Using biomarkers to label the McTNs and filopodia will provide us with a better sense of their contribution in adhesion mechanism. It is possible to monitor how these cells grow or shrink their microtubules and McTNs in order to adhere, move or proliferate. Measuring the forces that adhered cells are applying to CNT film is another interesting investigation that can provide a deeper understanding of the bond between CTCs and CNTs.. Tracking the change in conductance of the chips due to adherence of tumor cells is going to determine the alteration of CNT surface chemistry due to the bonding with CTCs.

Last but not least, making the whole process more autonomous is going to provide a chance for everyone to use this technology. It is possible to use proper machinery to perform RBC lysis, staining, and microscopy faster, more efficient and easier. This also will improve the sensitivity and specificity of the technology. Investigating the size of the device is another path for improving the process as well.

It has been observed that most of the WBCs are accumulated around the device where they are stuck to corners during droplet removal. Designing a larger size device and creating an autonomous approach for depositing and removing the droplet can provide a better understanding of why WBCs are mostly around the walls of the device. An

interesting experiment to conduct in near future is to create new masks to change the geometry of the devices for having larger size device with thicker containing layer of PDMS. Comparing the results of such device with what has been reported may shed light on why WBCs are found on the Nanotube-CTC chip in current design.

CellSearch is the only FDA approved cancer prognosis technology that has shown a model to present clinical relevant outcome for breast, prostate, and colorectal cancer patient. However, it isot applicable to patients with lung cancer. Conducting a series of experiments on lung patients blood samples can show the potential of Nanotube-CTC chip regardless of the type of cancer.

One of the topics that was not covered in this work is that why CNT film facilitates the absorption of serum and cell secreted adhesive proteins. Conducting a series of experiments using AFM on measuring the roughness and stiffness of the fabricated device with different concentration and dispersion parameter can shed light on the effect of the morphology and CNT coverage on cell adhesion. It may be also possible to measure the adhesion forces between cells and CNTs using AFM force spectroscopy.

Another topic that may have an effect on enhancing focal adhesion is the chemical interaction of CNTs and CTCs. Chemical properties of dispersed CNTs should be investigated in a detailed series of experiments. Different dispersion and debundling processes that will result in various surface chemistry, adsorbents and defects could be investigated in more details. The bath sonicator that was used in this work has a control on sonication parameters including power (0-160 W), sonication time, and temperature

(20-60 ^{o}C) of sonication. Investigating the effect of sonication parameters on the quality of CNT film and enhancing the focal adhesion of tumor cells is feasible in near future.

Chemical characterization of CNTs after adhesion is another approach for investigating the chemical interaction of CNTs and cells. It is possible to use X-ray Photoelectron spectroscopy (XPS) to understand if rehybridization of carbon atoms from sp2 to sp3 is taking place due to attachment of oxygen of hydrogen the C-C π-bonds. Another approach is to track the electrical properties of Nanotube-CTC chip (e.g. resistance) with and without cell adhesion. Since the electrical properties of CNTs are depending on its surface properties, changing the electrical properties of the CNT film due to cell adhesion can be an indication of chemical interaction between cells and CNTs.

It is highly suggested that a series of experiments will be conducted to explore the effect of surface morphology and topography on capture efficiency in a controlled manner. Quantitative values including the $I_{G/D}$, roughness, pocket size between CNT bundles, and bundle size can be used to compare the effect of surface topography on enhancing the focal adhesion.

Comparing different functionalized surfaces with Nanotube-CTC chip for enhancing the focal adhesion of tumor cells would be an interesting study. We already compared collagen adhesion matrix with CNT film for this purpose. Functionalizing the surface with other materials including fibronectin and cadherin in order to compare their capture efficiency with of Nanotube-CTC chip for different cancer type cell lines will be an interesting study to have a better understanding of focal adhesion of tumor cells.

Appendix A

ELECTRON MICROSCOPY IMAGES OF ADHERED SKBR3 BREAST CANCER CELLS TO CNT FILM

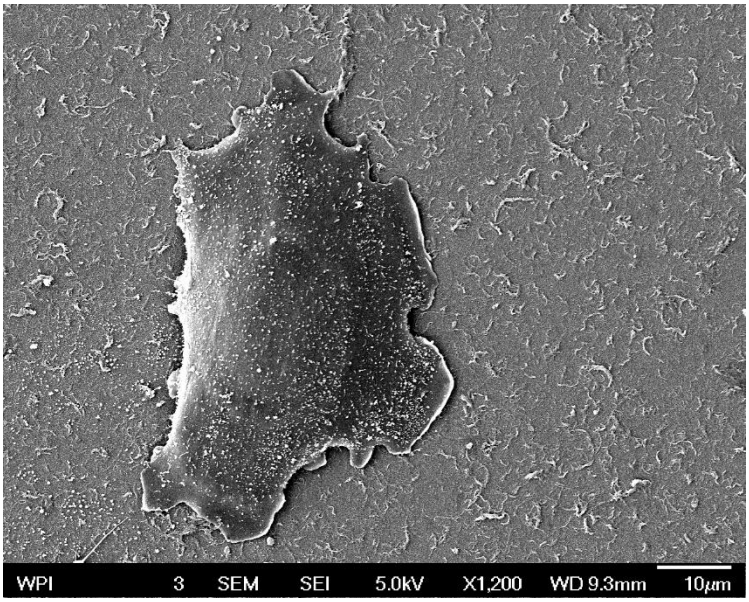

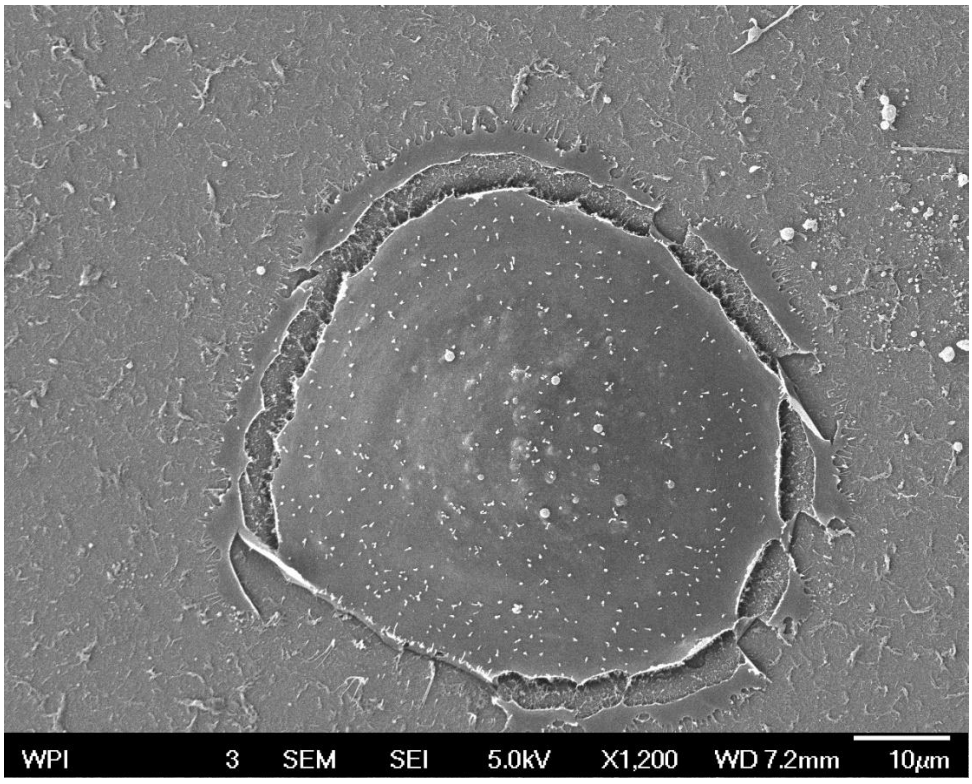
WPI 3 SEM SEI 5.0kV X1,200 WD 7.2mm 10μm

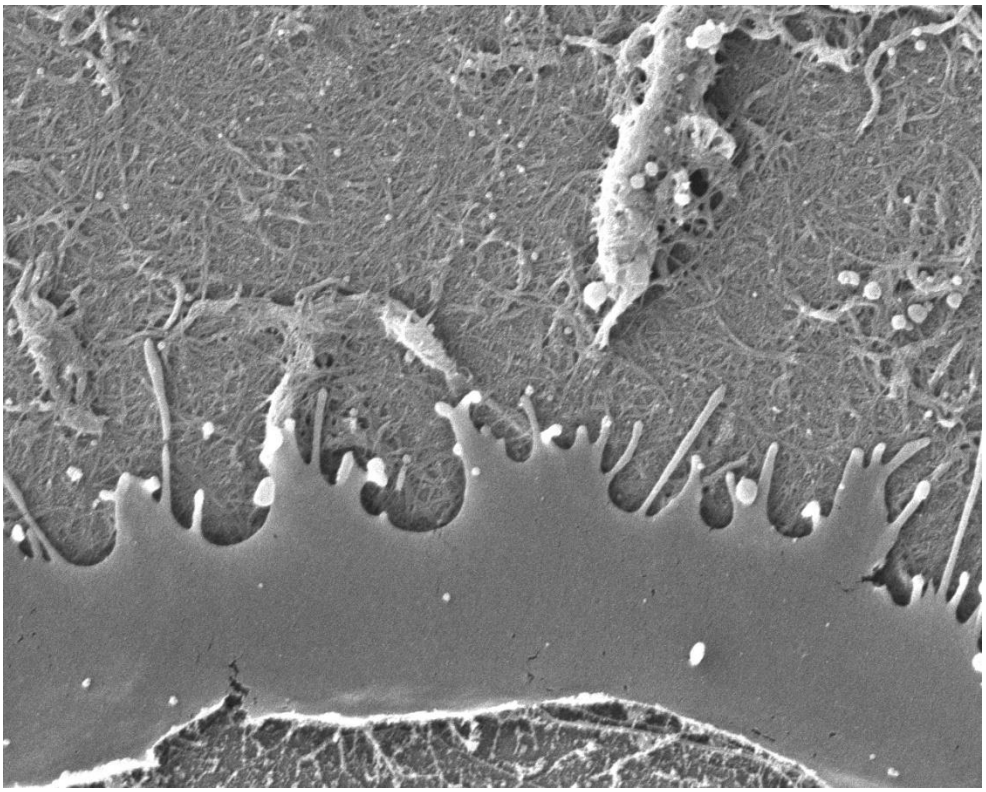

REFERENCES

[1] A. C. Society, "Cancer Facts & Figures 2019," *Atlanta: American Cancer Society*, 2019.

[2] R. L. Siegel, K. D. Miller, and A. Jemal, "Cancer statistics, 2019," *CA Cancer J Clin*, vol. 69, no. 1, pp. 7-34, Jan 2019.

[3] C. Palmieri, E. Bird, and R. Simcock, *ABC of cancer care* (ABC series). Chichester, West Sussex, UK Hoboken, NJ: Wiley-Blackwell : BMJ Books, 2013, pp. xiii, 86 pages.

[4] G. H. Wu, R. H. Datar, K. M. Hansen, T. Thundat, R. J. Cote, and A. Majumdar, "Bioassay of prostate-specific antigen (PSA) using microcantilevers," (in English), *Nature Biotechnology*, vol. 19, no. 9, pp. 856-860, Sep 2001.

[5] J. Phallen *et al.*, "Direct detection of early-stage cancers using circulating tumor DNA," (in English), *Science Translational Medicine*, vol. 9, no. 403, Aug 16 2017.

[6] S. A. Joosse, T. M. Gorges, and K. Pantel, "Biology, detection, and clinical implications of circulating tumor cells," *EMBO Mol Med*, vol. 7, no. 1, pp. 1-11, Jan 2015.

[7] K. Naxerova and R. K. Jain, "Using tumour phylogenetics to identify the roots of metastasis in humans," *Nature reviews Clinical oncology*, vol. 12, no. 5, p. 258, 2015.

[8] A. D. Rhim *et al.*, "EMT and Dissemination Precede Pancreatic Tumor Formation," (in English), *Cell*, vol. 148, no. 1-2, pp. 349-361, Jan 20 2012.

[9] A. F. Chambers, A. C. Groom, and I. C. J. N. R. C. MacDonald, "Metastasis: dissemination and growth of cancer cells in metastatic sites," vol. 2, no. 8, p. 563, 2002.

[10] S. Paget, "The distribution of secondary growths in cancer of the breast. 1889," *Cancer Metastasis Rev,* vol. 8, no. 2, pp. 98-101, Aug 1989.

[11] M. J. M. Magbanua and J. W. Park, *Isolation and Molecular Characterization of Circulating Tumor Cells*. Springer, 2017.

[12] T. R. Ashworth, "A case of cancer in which cells similar to those in tumors were seen in the blood after death," *Medical Journal of Australia*, vol. 14, p. 4, 1869.

[13] D. Hanahan and R. A. Weinberg, "Hallmarks of Cancer: The Next Generation," (in English), *Cell,* vol. 144, no. 5, pp. 646-674, Mar 4 2011.

[14] S. A. Joosse and K. Pantel, "Biologic Challenges in the Detection of Circulating Tumor Cells," (in English), *Cancer Res,* vol. 73, no. 1, pp. 8-11, Jan 1 2013.

[15] S. P. H. Chiang, R. M. Cabrera, and J. E. Segall, "Tumor cell intravasation," (in English), *American Journal of Physiology-Cell Physiology,* vol. 311, no. 1, pp. C1-C14, Jul 1 2016.

[16] D. Kong, Y. Li, Z. Wang, and F. H. Sarkar, "Cancer Stem Cells and Epithelial-to-Mesenchymal Transition (EMT)-Phenotypic Cells: Are They Cousins or Twins?," *Cancers (Basel),* vol. 3, no. 1, pp. 716-29, Feb 21 2011.

[17] R. Kalluri and R. A. Weinberg, "The basics of epithelial-mesenchymal transition," (in English), *Journal of Clinical Investigation,* vol. 119, no. 6, pp. 1420-1428, Jun 2009.

[18] M. Bockhorn, R. K. Jain, and L. L. Munn, "Active versus passive mechanisms in metastasis: do cancer cells crawl into vessels, or are they pushed?," (in English), *Lancet Oncology,* vol. 8, no. 5, pp. 444-448, May 2007.

[19] D. M. McDonald and P. Baluk, "Significance of blood vessel leakiness in cancer," (in English), *Cancer Res,* vol. 62, no. 18, pp. 5381-5385, Sep 15 2002.

[20] P. Friedl and K. Wolf, "Proteolytic interstitial cell migration: a five-step process," (in English), *Cancer and Metastasis Reviews,* vol. 28, no. 1-2, pp. 129-135, Jun 2009.

[21] S. Douma, T. van Laar, J. Zevenhoven, R. Meuwissen, E. van Garderen, and D. S. Peeper, "Suppression of anoikis and induction of metastasis by the neurotrophic receptor TrkB," (in English), *Nature,* vol. 430, no. 7003, pp. 1034-1040, Aug 26 2004.

[22] C. Alix-Panabieres, S. Riethdorf, and K. Pantel, "Circulating tumor cells and bone marrow micrometastasis," (in English), *Clin Cancer Res,* vol. 14, no. 16, pp. 5013-5021, Aug 15 2008.

[23] K. Pantel, R. H. Brakenhoff, and B. Brandt, "Detection, clinical relevance and specific biological properties of disseminating tumour cells," (in English), *Nature Reviews Cancer,* vol. 8, no. 5, pp. 329-340, May 2008.

[24] B. J. Bain, *Blood cells : a practical guide,* Fifth edition. ed. Chichester, West Sussex ; Hoboken, NJ: John Wiley & Sons Ltd., 2015, p. p.

[25] C. Alix-Panabieres and K. Pantel, "Circulating Tumor Cells: Liquid Biopsy of Cancer," (in English), *Clinical Chemistry,* vol. 59, no. 1, pp. 110-118, Jan 2013.

[26] K. Pantel, C. Alix-Panabieres, and S. Riethdorf, "Cancer micrometastases," (in English), *Nature Reviews Clinical Oncology*, vol. 6, no. 6, pp. 339-351, Jun 2009.

[27] S. Braun *et al.*, "A pooled analysis of bone marrow micrometastasis in breast cancer," (in English), *New England Journal of Medicine,* vol. 353, no. 8, pp. 793-802, Aug 25 2005.

[28] K. Pantel and R. H. Brakenhoff, "Dissecting the metastatic cascade," (in English), *Nature Reviews Cancer,* vol. 4, no. 6, pp. 448-456, Jun 2004.

[29] Z. Candar, A. C. Ritchie, J. F. Hopkirk, and R. C. Long, "The prognostic value of circulating tumor cells in patients with breast cancer," *Surg Gynecol Obstet,* vol. 115, pp. 291-4, Sep 1962.

[30] G. Wuest and G. Birk, "[Demonstration and incidence of tumor cells in circulating human blood]," *Med Welt,* vol. 17, pp. 922-8, Apr 28 1962.

[31] S. Riethdorf, H. Wikman, and K. Pantel, "Review: Biological relevance of disseminated tumor cells in cancer patients," *Int J Cancer,* vol. 123, no. 9, pp. 1991-2006, Nov 1 2008.

[32] J. K. Wilson, "The detection of tumor cells in circulating blood," *Bull Tulane Univ Med Fac,* vol. 18, pp. 171-82, Aug 1959.

[33] H. Saito, "Studies on cancer cells in the circulating blood. II. Experimental study on the fate of intraportally injected tumor cells and metastasis formation," *Acta Med Biol (Niigata),* vol. 9, pp. 151-73, Sep 1961.

[34] H. J. Soost, "[On the incidence of tumor cells in the circulating blood]," *Dtsch Med Wochenschr,* vol. 85, pp. 893-9, May 13 1960.

[35] M. D. Romsdahl, E. W. Chu, R. Hume, and R. R. Smith, "The time of metastasis and release of circulating tumor cells as determined in an experimental system," *Cancer,* vol. 14, pp. 883-8, Jul-Aug 1961.

[36] M. M. Romsdahl, J. F. Potter, R. A. Malmgren, E. W. Chu, C. O. Brindley, and R. R. Smith, "A clinical study of circulating tumor cells in malignant melanoma," *Surg Gynecol Obstet,* vol. 111, pp. 675-81, Dec 1960.

[37] C. Alix-Panabieres and K. Pantel, "OPINION Challenges in circulating tumour cell research," (in English), *Nature Reviews Cancer,* vol. 14, no. 9, pp. 623-631, Sep 2014.

[38] P. T. Went *et al.,* "Frequent EpCam protein expression in human carcinomas," (in English), *Human Pathology,* vol. 35, no. 1, pp. 122-128, Jan 2004.

[39] Y. F. Sun, X. R. Yang, J. Zhou, S. J. Qiu, J. Fan, and Y. Xu, "Circulating tumor cells: advances in detection methods, biological issues, and clinical relevance," (in English), *Journal of Cancer Research and Clinical Oncology,* vol. 137, no. 8, pp. 1151-1173, Aug 2011.

[40] C. Alix-Panabieres *et al.,* "Full-length cytokeratin-19 is released by human tumor cells: a potential role in metastatic progression of breast cancer," (in English), *Breast Cancer Research,* vol. 11, no. 3, 2009.

[41] I. Baccelli *et al.,* "Identification of a population of blood circulating tumor cells from breast cancer patients that initiates metastasis in a xenograft assay," (in English), *Nature Biotechnology,* vol. 31, no. 6, pp. 539-U143, Jun 2013.

[42] J. M. Hou *et al.*, "Clinical Significance and Molecular Characteristics of Circulating Tumor Cells and Circulating Tumor Microemboli in Patients With Small-Cell Lung Cancer," (in English), *Journal of Clinical Oncology,* vol. 30, no. 5, pp. 525-532, Feb 10 2012.

[43] A. J. Armstrong *et al.*, "Circulating Tumor Cells from Patients with Advanced Prostate and Breast Cancer Display Both Epithelial and Mesenchymal Markers," (in English), *Molecular Cancer Research,* vol. 9, no. 8, pp. 997-1007, Aug 2011.

[44] C. G. Rao *et al.*, "Expression of epithelial cell adhesion molecule in carcinoma cells present in blood and primary and metastatic tumors," (in English), *Int J Oncol,* vol. 27, no. 1, pp. 49-57, Jul 2005.

[45] K. Hoshino *et al.*, "Microchip-based immunomagnetic detection of circulating tumor cells," (in English), *Lab on a Chip,* vol. 11, no. 20, pp. 3449-3457, 2011.

[46] F. Farace *et al.*, "A direct comparison of CellSearch and ISET for circulating tumour-cell detection in patients with metastatic carcinomas," (in English), *British Journal of Cancer,* vol. 105, no. 6, pp. 847-853, Sep 6 2011.

[47] M. Herlyn, Z. Steplewski, D. Herlyn, and H. Koprowski, "Colorectal Carcinoma-Specific Antigen - Detection by Means of Monoclonal Antibodies," (in English), *Proceedings of the National Academy of Sciences of the United States of America,* vol. 76, no. 3, pp. 1438-1442, 1979.

[48] D. P. Edwards *et al.*, "Monoclonal-Antibody Identification and Characterization of a Mr 43,000 Membrane Glycoprotein Associated with Human-Breast Cancer," (in English), *Cancer Res,* vol. 46, no. 3, pp. 1306-1317, Mar 1986.

[49] D. Sansonno and F. Dammacco, "Expression and Distribution of a Human Colon-Carcinoma-Associated Antigen in Normal and Diseased Liver-Tissue," (in English), *Pathobiology,* vol. 61, no. 3-4, pp. 193-196, May-Aug 1993.

[50] R. P. Takes *et al.*, "Markers for assessment of nodal metastasis in laryngeal carcinoma," (in English), *Archives of Otolaryngology-Head & Neck Surgery,* vol. 123, no. 4, pp. 412-419, Apr 1997.

[51] C. J. de Boer, J. H. van Krieken, C. M. Janssen-van Rhijn, and S. V. Litvinov, "Expression of Ep-CAM in normal, regenerating, metaplastic, and neoplastic liver," *J Pathol,* vol. 188, no. 2, pp. 201-6, Jun 1999.

[52] K. Chang *et al.*, "Combination of circulating tumor cell enumeration and tumor marker detection in predicting prognosis and treatment effect in metastatic castration-resistant prostate cancer," (in English), *Oncotarget,* vol. 6, no. 39, pp. 41825-41836, Dec 8 2015.

[53] C. V. Pecot *et al.*, "A novel platform for detection of CK+ and CK- CTCs," *Cancer Discov,* vol. 1, no. 7, pp. 580-6, Dec 2011.

[54] S. Nagrath *et al.*, "Isolation of rare circulating tumour cells in cancer patients by microchip technology," *Nature,* vol. 450, no. 7173, pp. 1235-9, Dec 20 2007.

[55] S. Kumble, M. B. Omary, L. F. Fajardo, and G. Triadafilopoulos, "Multifocal heterogeneity in villin and Ep-CAM expression in Barrett's esophagus," *Int J Cancer,* vol. 66, no. 1, pp. 48-54, Mar 28 1996.

[56] M. Munz *et al.*, "Side-by-side analysis of five clinically tested anti-EpCAM monoclonal antibodies," (in English), *Cancer Cell International,* vol. 10, Nov 2 2010.

[57] R. Moll, M. Divo, and L. Langbein, "The human keratins: biology and pathology," (in English), *Histochemistry and Cell Biology,* vol. 129, no. 6, pp. 705-733, Jun 2008.

[58] S. D. Mikolajczyk *et al.*, "Detection of EpCAM-Negative and Cytokeratin-Negative Circulating Tumor Cells in Peripheral Blood," *J Oncol,* vol. 2011, p. 252361, 2011.

[59] G. Galletti *et al.*, "Isolation of breast cancer and gastric cancer circulating tumor cells by use of an anti HER2-based microfluidic device," (in English), *Lab on a Chip,* vol. 14, no. 1, pp. 147-156, 2014.

[60] S. L. Stott *et al.*, "Isolation and Characterization of Circulating Tumor Cells from Patients with Localized and Metastatic Prostate Cancer," (in English), *Science Translational Medicine,* vol. 2, no. 25, Mar 31 2010.

[61] H. Iinuma *et al.*, "Clinical Significance of Circulating Tumor Cells, Including Cancer Stem-Like Cells, in Peripheral Blood for Recurrence and Prognosis in Patients With Dukes' Stage B and C Colorectal Cancer," (in English), *Journal of Clinical Oncology,* vol. 29, no. 12, pp. 1547-1555, Apr 20 2011.

[62] A. Stathopoulou *et al.*, "Molecular detection of cancer cells in the peripheral blood of patients with breast cancer: Comparison of CK-19, CEA and maspin as

detection markers," (in English), *Anticancer Res,* vol. 23, no. 2c, pp. 1883-1890, Mar-Apr 2003.

[63] S. Lankiewicz, E. Rother, S. Zimmermann, C. Hollmann, F. Korangy, and T. F. Greten, "Tumour-associated transcripts and EGFR deletion variants in colorectal cancer in primary tumour, metastases and circulating tumour cells," (in English), *Cellular Oncology,* vol. 30, no. 6, pp. 463-471, 2008.

[64] R. E. Payne *et al.*, "Measurements of EGFR expression on circulating tumor cells are reproducible over time in metastatic breast cancer patients," (in English), *Pharmacogenomics,* vol. 10, no. 1, pp. 51-57, Jan 2009.

[65] T. Dragovich and C. Campen, "Anti-EGFR-Targeted Therapy for Esophageal and Gastric Cancers: An Evolving Concept," *J Oncol,* vol. 2009, p. 804108, 2009.

[66] M. Kitago *et al.*, "mRNA expression and BRAF mutation in circulating melanoma cells isolated from peripheral blood with high molecular weight melanoma-associated antigen-specific monoclonal antibody beads," *Clin Chem,* vol. 55, no. 4, pp. 757-64, Apr 2009.

[67] A. El-Heliebi *et al.*, "In Situ Detection and Quantification of AR-V7, AR-FL, PSA, and KRAS Point Mutations in Circulating Tumor Cells," (in English), *Clinical Chemistry,* vol. 64, no. 3, pp. 536-546, Mar 2018.

[68] J. E. Hardingham *et al.*, "Molecular detection of blood-borne epithelial cells in colorectal cancer patients and in patients with benign bowel disease," (in English), *International Journal of Cancer,* vol. 89, no. 1, pp. 8-13, Jan 20 2000.

[69] S. M. O'Hara, J. G. Moreno, D. R. Zweitzig, S. Gross, L. G. Gomella, and L. W. Terstappen, "Multigene reverse transcription-PCR profiling of circulating tumor cells in hormone-refractory prostate cancer," *Clin Chem,* vol. 50, no. 5, pp. 826-35, May 2004.

[70] A. Satelli *et al.*, "Universal Marker and Detection Tool for Human Sarcoma Circulating Tumor Cells," (in English), *Cancer Res,* vol. 74, no. 6, pp. 1645-1650, Mar 15 2014.

[71] E. Ozkumur *et al.*, "Inertial Focusing for Tumor Antigen-Dependent and -Independent Sorting of Rare Circulating Tumor Cells," (in English), *Science Translational Medicine,* vol. 5, no. 179, Apr 3 2013.

[72] L. Y. Yang *et al.*, "Optimization of an Enrichment Process for Circulating Tumor Cells From the Blood of Head and Neck Cancer Patients Through Depletion of Normal Cells," (in English), *Biotechnology and Bioengineering,* vol. 102, no. 2, pp. 521-534, Feb 1 2009.

[73] O. Lara, X. D. Tong, M. Zborowski, and J. J. Chalmers, "Enrichment of rare cancer cells through depletion of normal cells using density and flow-through, immunomagnetic cell separation," (in English), *Experimental Hematology,* vol. 32, no. 10, pp. 891-904, Oct 2004.

[74] Z. A. Liu *et al.*, "Negative enrichment by immunomagnetic nanobeads for unbiased characterization of circulating tumor cells from peripheral blood of cancer patients," (in English), *Journal of Translational Medicine,* vol. 9, May 19 2011.

[75] C. Alix-Panabieres and K. Pantel, "Technologies for detection of circulating tumor cells: facts and vision," (in English), *Lab on a Chip,* vol. 14, no. 1, pp. 57-62, 2014.

[76] H. Iinuma *et al.,* "Detection of tumor cells in blood using CD45 magnetic cell separation followed by nested mutant allele-specific amplification of p53 and K-ras genes in patients with colorectal cancer," (in English), *International Journal of Cancer,* vol. 89, no. 4, pp. 337-344, Jul 20 2000.

[77] U. Bilkenroth, H. Taubert, D. Riemann, U. Rebmann, H. Heynemann, and A. Meye, "Detection and enrichment of disseminated renal carcinoma cells from peripheral blood by immunomagnetic cell separation," (in English), *International Journal of Cancer,* vol. 92, no. 4, pp. 577-582, May 15 2001.

[78] M. Partridge, E. Phillips, R. Francis, and S. R. Li, "Immunomagnetic separation for enrichment and sensitive detection of disseminated tumour cells in patients with head and neck SCC," (in English), *Journal of Pathology,* vol. 189, no. 3, pp. 368-377, Nov 1999.

[79] S. Miltenyi, W. Muller, W. Weichel, and A. Radbruch, "High-Gradient Magnetic Cell-Separation with Macs," (in English), *Cytometry,* vol. 11, no. 2, pp. 231-238, 1990.

[80] N. M. Karabacak *et al.,* "Microfluidic, marker-free isolation of circulating tumor cells from blood samples," (in English), *Nat Protoc,* vol. 9, no. 3, pp. 694-710, Mar 2014.

[81] E. E. van der Toom, J. E. Verdone, M. A. Gorin, and K. J. Pienta, "Technical challenges in the isolation and analysis of circulating tumor cells," (in English), *Oncotarget,* vol. 7, no. 38, pp. 62754-62766, Sep 20 2016.

[82] H. G. Sun, W. H. Tan, and Y. L. Zu, "Aptamers: versatile molecular recognition probes for cancer detection," (in English), *Analyst,* vol. 141, no. 2, pp. 403-415, 2016.

[83] R. A. Potyrailo, A. J. Murray, N. Nagraj, A. D. Pris, J. M. Ashe, and M. Todorovic, "Towards maintenance-free biosensors for hundreds of bind/release cycles," *Angew Chem Int Ed Engl,* vol. 54, no. 7, pp. 2174-8, Feb 9 2015.

[84] P. Zhang *et al.,* "Using an RNA aptamer probe for flow cytometry detection of CD30-expressing lymphoma cells," (in English), *Laboratory Investigation,* vol. 89, no. 12, pp. 1423-1432, Dec 2009.

[85] H. K. Lin *et al.,* "Portable Filter-Based Microdevice for Detection and Characterization of Circulating Tumor Cells," (in English), *Clin Cancer Res,* vol. 16, no. 20, pp. 5011-5018, Oct 15 2010.

[86] H. W. Hou *et al.,* "Isolation and retrieval of circulating tumor cells using centrifugal forces," (in English), *Scientific Reports,* vol. 3, Feb 12 2013.

[87] E. Sollier *et al.,* "Size-selective collection of circulating tumor cells using Vortex technology," (in English), *Lab on a Chip,* vol. 14, no. 1, pp. 63-77, 2014.

[88] D. L. Adams *et al.,* "The systematic study of circulating tumor cell isolation using lithographic microfilters," (in English), *Rsc Advances,* vol. 4, no. 9, pp. 4334-4342, 2014.

[89] P. R. C. Gascoyne, J. Noshari, T. J. Anderson, and F. F. Becker, "Isolation of rare cells from cell mixtures by dielectrophoresis," (in English), *Electrophoresis,* vol. 30, no. 8, pp. 1388-1398, Apr 2009.

[90] S. D. Meng *et al.*, "Circulating tumor cells in patients with breast cancer dormancy," (in English), *Clin Cancer Res,* vol. 10, no. 24, pp. 8152-8162, Dec 15 2004.

[91] M. M. Ferreira, V. C. Romani, and S. S. Jeffrey, "Circulating tumor cell technologies," (in English), *Molecular Oncology,* vol. 10, no. 3, pp. 374-394, Mar 2016.

[92] S. E. Cross, Y. S. Jin, J. Rao, and J. K. Gimzewski, "Nanomechanical analysis of cells from cancer patients," (in English), *Nature Nanotechnology,* vol. 2, no. 12, pp. 780-783, Dec 2007.

[93] D. R. Gossett *et al.*, "Hydrodynamic stretching of single cells for large population mechanical phenotyping," (in English), *Proceedings of the National Academy of Sciences of the United States of America,* vol. 109, no. 20, pp. 7630-7635, May 15 2012.

[94] R. M. Vazquez *et al.*, "An optofluidic constriction chip for monitoring metastatic potential and drug response of cancer cells," (in English), *Integrative Biology,* vol. 7, no. 4, pp. 477-484, Apr 2015.

[95] J. Lu *et al.*, "Isolation of circulating epithelial and tumor progenitor cells with an invasive phenotype from breast cancer patients," (in English), *International Journal of Cancer,* vol. 126, no. 3, pp. 669-683, Feb 1 2010.

[96] S. H. Au *et al.*, "Clusters of circulating tumor cells traverse capillary-sized vessels," (in English), *Proceedings of the National Academy of Sciences of the United States of America,* vol. 113, no. 18, pp. 4947-4952, May 3 2016.

[97] A. Lebeau *et al.*, "HER-2/neu analysis in archival tissue samples of human breast cancer: Comparison of immunohistochemistry and fluorescence in situ hybridization," (in English), *Journal of Clinical Oncology,* vol. 19, no. 2, pp. 354-363, Jan 15 2001.

[98] H. Nitta *et al.*, "Development of automated brightfield double in situ hybridization (BDISH) application for HER2 gene and chromosome 17 centromere (CEN 17) for breast carcinomas and an assay performance comparison to manual dual color HER2 fluorescence in situ hybridization (FISH)," *Diagn Pathol,* vol. 3, p. 41, Oct 22 2008.

[99] M. Cristofanilli *et al.*, "Circulating tumor cells, disease progression, and survival in metastatic breast cancer," (in English), *New England Journal of Medicine,* vol. 351, no. 8, pp. 781-791, Aug 19 2004.

[100] D. F. Hayes *et al.*, "Circulating tumor cells at each follow-up time point during therapy of metastatic breast cancer patients predict progression-free and overall survival," (in English), *Clin Cancer Res,* vol. 12, no. 14, pp. 4218-4224, Jul 15 2006.

[101] D. C. Danila *et al.*, "Circulating tumor cell number and prognosis in progressive castration-resistant prostate cancer," (in English), *Clin Cancer Res,* vol. 13, no. 23, pp. 7053-7058, Dec 1 2007.

[102] S. J. Cohen *et al.*, "Relationship of circulating tumor cells to tumor response, progression-free survival, and overall survival in patients with metastatic colorectal cancer," (in English), *Journal of Clinical Oncology,* vol. 26, no. 19, pp. 3213-3221, Jul 1 2008.

[103] A. Truini *et al.*, "Clinical Applications of Circulating Tumor Cells in Lung Cancer Patients by CellSearch System," *Front Oncol,* vol. 4, p. 242, 2014.

[104] A. A. Powell *et al.*, "Single Cell Profiling of Circulating Tumor Cells: Transcriptional Heterogeneity and Diversity from Breast Cancer Cell Lines," (in English), *Plos One,* vol. 7, no. 5, May 7 2012.

[105] A. H. Talasaz *et al.*, "Isolating highly enriched populations of circulating epithelial cells and other rare cells from blood using a magnetic sweeper device," (in English), *Proceedings of the National Academy of Sciences of the United States of America,* vol. 106, no. 10, pp. 3970-3975, Mar 10 2009.

[106] E. Andreopoulou *et al.*, "Comparison of assay methods for detection of circulating tumor cells in metastatic breast cancer: AdnaGen AdnaTest BreastCancer Select/Detect (TM) versus Veridex CellSearch (TM) system," (in English), *International Journal of Cancer,* vol. 130, no. 7, pp. 1590-1597, Apr 1 2012.

[107] V. Muller *et al.*, "Prognostic impact of circulating tumor cells assessed with the CellSearch System (TM) and AdnaTest Breast (TM) in metastatic breast cancer patients: the DETECT study," (in English), *Breast Cancer Research,* vol. 14, no. 4, 2012.

[108] S. J. Gendler, "MUC1, the renaissance molecule," (in English), *Journal of Mammary Gland Biology and Neoplasia,* vol. 6, no. 3, pp. 339-353, Jul 2001.

[109] S. Kasimir-Bauer, O. Hoffmann, D. Wallwiener, R. Kimmig, and T. Fehm, "Expression of stem cell and epithelial-mesenchymal transition markers in primary breast cancer patients with circulating tumor cells," (in English), *Breast Cancer Research,* vol. 14, no. 1, 2012.

[110] D. Pluim, L. A. Devriese, J. H. Beijnen, and J. H. M. Schellens, "Validation of a multiparameter flow cytometry method for the determination of phosphorylated extracellular-signal-regulated kinase and DNA in circulating tumor cells," (in English), *Cytom Part A,* vol. 81a, no. 8, pp. 664-671, Aug 2012.

[111] C. M. Earhart *et al.*, "Isolation and mutational analysis of circulating tumor cells from lung cancer patients with magnetic sifters and biochips," (in English), *Lab on a Chip,* vol. 14, no. 1, pp. 78-88, 2014.

[112] S. Nagrath *et al.*, "Isolation of rare circulating tumour cells in cancer patients by microchip technology," (in English), *Nature,* vol. 450, no. 7173, pp. 1235-U10, Dec 20 2007.

[113] S. L. Stott *et al.*, "Isolation of circulating tumor cells using a microvortex-generating herringbone-chip," (in English), *Proceedings of the National Academy of Sciences of the United States of America,* vol. 107, no. 43, pp. 18392-18397, Oct 26 2010.

[114] J. P. Gleghorn *et al.*, "Capture of circulating tumor cells from whole blood of prostate cancer patients using geometrically enhanced differential

immunocapture (GEDI) and a prostate-specific antibody," (in English), *Lab on a Chip,* vol. 10, no. 1, pp. 27-29, 2010.

[115] W. Harb *et al.*, "Mutational Analysis of Circulating Tumor Cells Using a Novel Microfluidic Collection Device and qPCR Assay," (in English), *Translational Oncology,* vol. 6, no. 5, pp. 528-+, Oct 2013.

[116] A. E. Saliba *et al.*, "Microfluidic sorting and multimodal typing of cancer cells in self-assembled magnetic arrays," (in English), *Proceedings of the National Academy of Sciences of the United States of America,* vol. 107, no. 33, pp. 14524-14529, Aug 17 2010.

[117] S. Park *et al.*, "Morphological Differences between Circulating Tumor Cells from Prostate Cancer Patients and Cultured Prostate Cancer Cells," (in English), *Plos One,* vol. 9, no. 1, Jan 8 2014.

[118] R. A. Harouaka, M. Nisic, and S. Y. Zheng, "Circulating Tumor Cell Enrichment Based on Physical Properties," (in English), *Jala,* vol. 18, no. 6, pp. 455-468, Dec 2013.

[119] M. E. Warkiani *et al.*, "Slanted spiral microfluidics for the ultra-fast, label-free isolation of circulating tumor cells," (in English), *Lab on a Chip,* vol. 14, no. 1, pp. 128-137, 2014.

[120] B. L. Khoo *et al.*, "Clinical Validation of an Ultra High-Throughput Spiral Microfluidics for the Detection and Enrichment of Viable Circulating Tumor Cells," (in English), *Plos One,* vol. 9, no. 7, Jul 7 2014.

[121] J. S. Sun *et al.*, "Double spiral microchannel for label-free tumor cell separation and enrichment," (in English), *Lab on a Chip*, vol. 12, no. 20, pp. 3952-3960, 2012.

[122] J. S. Sun *et al.*, "Size-based hydrodynamic rare tumor cell separation in curved microfluidic channels," (in English), *Biomicrofluidics*, vol. 7, no. 1, Jan 2013.

[123] F. F. Becker, X. B. Wang, Y. Huang, R. Pethig, J. Vykoukal, and P. R. C. Gascoyne, "Separation of Human Breast-Cancer Cells from Blood by Differential Dielectric Affinity," (in English), *Proceedings of the National Academy of Sciences of the United States of America*, vol. 92, no. 3, pp. 860-864, Jan 31 1995.

[124] V. Gupta *et al.*, "ApoStream (TM), a new dielectrophoretic device for antibody independent isolation and recovery of viable cancer cells from blood," (in English), *Biomicrofluidics*, vol. 6, no. 2, Jun 2012.

[125] F. F. Becker, X. B. Wang, Y. Huang, R. Pethig, J. Vykoukal, and P. R. C. Gascoyne, "The Removal of Human Leukemia-Cells from Blood Using Interdigitated Microelectrodes," (in English), *Journal of Physics D-Applied Physics*, vol. 27, no. 12, pp. 2659-2662, Dec 14 1994.

[126] S. Shim, K. Stemke-Hale, A. M. Tsimberidou, J. Noshari, T. E. Anderson, and P. R. C. Gascoyne, "Antibody-independent isolation of circulating tumor cells by continuous-flow dielectrophoresis," (in English), *Biomicrofluidics*, vol. 7, no. 1, Jan 2013.

[127] N. Manaresi *et al.*, "A CMOS chip for individual cell manipulation and detection," (in English), *Ieee Journal of Solid-State Circuits,* vol. 38, no. 12, pp. 2297-2305, Dec 2003.

[128] F. Fabbri *et al.*, "Detection and recovery of circulating colon cancer cells using a dielectrophoresis-based device: KRAS mutation status in pure CTCs," (in English), *Cancer Letters,* vol. 335, no. 1, pp. 225-231, Jul 10 2013.

[129] P. Augustsson, C. Magnusson, M. Nordin, H. Lilja, and T. Laurell, "Microfluidic, Label-Free Enrichment of Prostate Cancer Cells in Blood Based on Acoustophoresis," (in English), *Analytical Chemistry,* vol. 84, no. 18, pp. 7954-7962, Sep 18 2012.

[130] M. Poudineh, E. H. Sargent, K. Pantel, and S. O. Kelley, "Profiling circulating tumour cells and other biomarkers of invasive cancers," (in English), *Nature Biomedical Engineering,* vol. 2, no. 2, pp. 72-84, Feb 2018.

[131] I. Y. Wong *et al.*, "Collective and individual migration following the epithelial-mesenchymal transition," (in English), *Nature Materials,* vol. 13, no. 11, pp. 1063-1071, Nov 2014.

[132] Y. Zhang, W. Zhang, and L. Qin, "Mesenchymal-mode migration assay and antimetastatic drug screening with high-throughput microfluidic channel networks," *Angew Chem Int Ed Engl,* vol. 53, no. 9, pp. 2344-8, Feb 24 2014.

[133] A. F. Sarioglu *et al.*, "A microfluidic device for label-free, physical capture of circulating tumor cell clusters," (in English), *Nature Methods,* vol. 12, no. 7, pp. 685-+, Jul 2015.

[134] S. J. Tan, L. Yobas, G. Y. H. Lee, C. N. Ong, and C. T. Lim, "Microdevice for the isolation and enumeration of cancer cells from blood," (in English), *Biomedical Microdevices,* vol. 11, no. 4, pp. 883-892, Aug 2009.

[135] S. J. Tan, R. L. Lakshmi, P. F. Chen, W. T. Lim, L. Yobas, and C. T. Lim, "Versatile label free biochip for the detection of circulating tumor cells from peripheral blood in cancer patients," (in English), *Biosens Bioelectron,* vol. 26, no. 4, pp. 1701-1705, Dec 15 2010.

[136] S. H. Seal, "Silicone flotation: a simple quantitative method for the isolation of free-floating cancer cells from the blood," *Cancer,* vol. 12, no. 3, pp. 590-5, May-Jun 1959.

[137] J. Weitz *et al.,* "Dissemination of tumor cells in patients undergoing surgery for colorectal cancer," (in English), *Clin Cancer Res,* vol. 4, no. 2, pp. 343-348, Feb 1998.

[138] M. Balic *et al.,* "Comparison of two methods for enumerating circulating tumor cells in carcinoma patients," (in English), *Cytometry Part B-Clinical Cytometry,* vol. 68b, no. 1, pp. 25-30, Nov 2005.

[139] V. Muller *et al.,* "Circulating tumor cells in breast cancer: Correlation to bone marrow micrometastases, heterogeneous response to systemic therapy and low proliferative activity," (in English), *Clin Cancer Res,* vol. 11, no. 10, pp. 3678-3685, May 15 2005.

[140] E. Obermayr *et al.*, "Assessment of a six gene panel for the molecular detection of circulating tumor cells in the blood of female cancer patients," (in English), *Bmc Cancer*, vol. 10, Dec 3 2010.

[141] R. Rosenberg *et al.*, "Comparison of two density gradient centrifugation systems for the enrichment of disseminated tumor cells in blood," (in English), *Cytometry*, vol. 49, no. 4, pp. 150-158, Dec 1 2002.

[142] R. Harouaka, Z. G. Kang, S. Y. Zheng, and L. Cao, "Circulating tumor cells: Advances in isolation and analysis, and challenges for clinical applications," (in English), *Pharmacology & Therapeutics*, vol. 141, no. 2, pp. 209-221, Feb 2014.

[143] W. He *et al.*, "Quantitation of circulating tumor cells in blood samples from ovarian and prostate cancer patients using tumor-specific fluorescent ligands," (in English), *International Journal of Cancer*, vol. 123, no. 8, pp. 1968-1973, Oct 15 2008.

[144] D. E. Campton *et al.*, "High-recovery visual identification and single-cell retrieval of circulating tumor cells for genomic analysis using a dual-technology platform integrated with automated immunofluorescence staining," (in English), *Bmc Cancer*, vol. 15, May 6 2015.

[145] G. Vona *et al.*, "Isolation by size of epithelial tumor cells - A new method for the immunomorphological and molecular characterization of circulating tumor cells," (in English), *American Journal of Pathology*, vol. 156, no. 1, pp. 57-63, Jan 2000.

[146] G. Vona *et al.*, "Impact of cytomorphological detection of circulating tumor cells in patients with liver cancer," (in English), *Hepatology,* vol. 39, no. 3, pp. 792-797, Mar 2004.

[147] V. De Giorgi *et al.*, "Application of a Filtration- and Isolation-by-Size Technique for the Detection of Circulating Tumor Cells in Cutaneous Melanoma," (in English), *Journal of Investigative Dermatology,* vol. 130, no. 10, pp. 2440-2447, Oct 2010.

[148] V. Hofman *et al.*, "Preoperative Circulating Tumor Cell Detection Using the Isolation by Size of Epithelial Tumor Cell Method for Patients with Lung Cancer Is a New Prognostic Biomarker," (in English), *Clin Cancer Res,* vol. 17, no. 4, pp. 827-835, Feb 15 2011.

[149] C. L. Chen *et al.*, "Single-cell analysis of circulating tumor cells identifies cumulative expression patterns of EMT-related genes in metastatic prostate cancer," (in English), *Prostate,* vol. 73, no. 8, pp. 813-826, Jun 2013.

[150] I. Desitter *et al.*, "A new device for rapid isolation by size and characterization of rare circulating tumor cells," *Anticancer Res,* vol. 31, no. 2, pp. 427-41, Feb 2011.

[151] M. B. Freidin *et al.*, "An assessment of diagnostic performance of a filter-based antibody-independent peripheral blood circulating tumour cell capture paired with cytomorphologic criteria for the diagnosis of cancer," (in English), *Lung Cancer,* vol. 85, no. 2, pp. 182-185, Aug 2014.

[152] D. L. Adams *et al.*, "Cytometric Characterization of Circulating Tumor Cells Captured by Microfiltration and Their Correlation to the CellSearch (R) CTC Test," (in English), *Cytom Part A,* vol. 87a, no. 2, pp. 137-144, Feb 2015.

[153] R. A. Harouaka *et al.*, "Flexible Micro Spring Array Device for High-Throughput Enrichment of Viable Circulating Tumor Cells," (in English), *Clinical Chemistry,* vol. 60, no. 2, pp. 323-333, Feb 2014.

[154] J. T. Kaifi *et al.*, "Circulating tumor cell isolation during resection of colorectal cancer lung and liver metastases: a prospective trial with different detection techniques," (in English), *Cancer Biology & Therapy,* vol. 16, no. 5, pp. 699-708, May 2015.

[155] S. Zheng *et al.*, "Membrane microfilter device for selective capture, electrolysis and genomic analysis of human circulating tumor cells," (in English), *Journal of Chromatography A,* vol. 1162, no. 2, pp. 154-161, Aug 31 2007.

[156] S. Y. Zheng *et al.*, "3D microfilter device for viable circulating tumor cell (CTC) enrichment from blood," (in English), *Biomedical Microdevices,* vol. 13, no. 1, pp. 203-213, Feb 2011.

[157] M. D. Zhou *et al.*, "Separable Bilayer Microfiltration Device for Viable Label-free Enrichment of Circulating Tumour Cells," (in English), *Scientific Reports,* vol. 4, Dec 9 2014.

[158] X. Qin *et al.*, "Size and deformability based separation of circulating tumor cells from castrate resistant prostate cancer patients using resettable cell traps," (in English), *Lab on a Chip,* vol. 15, no. 10, pp. 2278-2286, 2015.

[159] N. Saucedo-Zeni *et al.*, "A novel method for the in vivo isolation of circulating tumor cells from peripheral blood of cancer patients using a functionalized and structured medical wire," (in English), *Int J Oncol*, vol. 41, no. 4, pp. 1241-1250, Oct 2012.

[160] D. Marrinucci *et al.*, "Fluid biopsy in patients with metastatic prostate, pancreatic and breast cancers," (in English), *Physical Biology*, vol. 9, no. 1, Feb 2012.

[161] E. H. Cho *et al.*, "Characterization of circulating tumor cell aggregates identified in patients with epithelial tumors," (in English), *Physical Biology*, vol. 9, no. 1, Feb 2012.

[162] D. C. Lazar *et al.*, "Cytometric comparisons between circulating tumor cells from prostate cancer patients and the prostate-tumor-derived LNCaP cell line," (in English), *Physical Biology*, vol. 9, no. 1, Feb 2012.

[163] J. Nieva *et al.*, "High-definition imaging of circulating tumor cells and associated cellular events in non-small cell lung cancer patients: a longitudinal analysis," (in English), *Physical Biology*, vol. 9, no. 1, Feb 2012.

[164] K. G. Phillips *et al.*, "Optical quantification of cellular mass, volume, and density of circulating tumor cells identified in an ovarian cancer patient," *Front Oncol*, vol. 2, p. 72, 2012.

[165] M. Wendel *et al.*, "Fluid biopsy for circulating tumor cell identification in patients with early-and late-stage non-small cell lung cancer: a glimpse into lung cancer biology," (in English), *Physical Biology*, vol. 9, no. 1, Feb 2012.

[166] D. Issadore *et al.*, "Ultrasensitive Clinical Enumeration of Rare Cells ex Vivo Using a Micro-Hall Detector," (in English), *Science Translational Medicine,* vol. 4, no. 141, Jul 4 2012.

[167] S. L. Werner *et al.*, "Analytical Validation and Capabilities of the Epic CTC Platform: Enrichment-Free Circulating Tumour Cell Detection and Characterization," *J Circ Biomark,* vol. 4, p. 3, Jan-Dec 2015.

[168] K. M. Yamada and E. Cukierman, "Modeling tissue morphogenesis and cancer in 3D," (in English), *Cell,* vol. 130, no. 4, pp. 601-610, Aug 24 2007.

[169] A. M. Weaver, "Cortactin in tumor invasiveness," (in English), *Cancer Letters,* vol. 265, no. 2, pp. 157-166, Jul 8 2008.

[170] T. W. Friedlander *et al.*, "Detection and Characterization of Invasive Circulating Tumor Cells Derived from Men with Metastatic Castration- Resistant Prostate Cancer," (in English), *International Journal of Cancer,* vol. 134, no. 10, pp. 2284-2293, May 15 2014.

[171] C. Alix-Panabieres, "EPISPOT assay: detection of viable DTCs/CTCs in solid tumor patients," *Recent Results Cancer Res,* vol. 195, pp. 69-76, 2012.

[172] L. Cayrefourcq *et al.*, "Establishment and Characterization of a Cell Line from Human Circulating Colon Cancer Cells," (in English), *Cancer Res,* vol. 75, no. 5, pp. 892-901, Mar 1 2015.

[173] M. A. Dobrovolskaia and S. E. Mcneil, "Immunological properties of engineered nanomaterials," (in English), *Nature Nanotechnology,* vol. 2, no. 8, pp. 469-478, Aug 2007.

[174] S. D. Puckett, P. P. Lee, D. M. Ciombor, R. K. Aaron, and T. J. Webster, "Nanotextured titanium surfaces for enhancing skin growth on transcutaneous osseointegrated devices," (in English), *Acta Biomaterialia,* vol. 6, no. 6, pp. 2352-2362, Jun 2010.

[175] W. G. Lee, U. Demirci, and A. Khademhosseini, "Microscale electroporation: challenges and perspectives for clinical applications," (in English), *Integrative Biology,* vol. 1, no. 3, pp. 242-251, Mar 2009.

[176] A. Solanki, J. D. Kim, and K. B. Lee, "Nanotechnology for regenerative medicine: nanomaterials for stem cell imaging," (in English), *Nanomedicine,* vol. 3, no. 4, pp. 567-578, Aug 2008.

[177] F. Khosravi, P. Trainor, S. N. Rai, G. Kloecker, E. Wickstrom, and B. Panchapakesan, "Label-free capture of breast cancer cells spiked in buffy coats using carbon nanotube antibody micro-arrays," (in English), *Nanotechnology,* vol. 27, no. 13, Apr 1 2016.

[178] F. Khosravi *et al.*, "Static micro-array isolation, dynamic time series classification, capture and enumeration of spiked breast cancer cells in blood: the nanotube-CTC chip," (in English), *Nanotechnology,* vol. 27, no. 44, Nov 4 2016.

[179] G. D. Chen, F. Fachin, M. Fernandez-Suarez, B. L. Wardle, and M. Toner, "Nanoporous Elements in Microfluidics for Multiscale Manipulation of Bioparticles," (in English), *Small,* vol. 7, no. 8, pp. 1061-1067, Apr 18 2011.

[180] H. J. Yoon *et al.*, "Sensitive capture of circulating tumour cells by functionalized graphene oxide nanosheets (vol 8, pg 735, 2013)," (in English), *Nature Nanotechnology,* vol. 8, no. 11, Nov 2013.

[181] S. Wang *et al.*, "Three-dimensional nanostructured substrates toward efficient capture of circulating tumor cells," *Angewandte Chemie,* vol. 121, no. 47, pp. 9132-9135, 2009.

[182] S.-K. Lee *et al.*, "Nanowire substrate-based laser scanning cytometry for quantitation of circulating tumor cells," *Nano letters,* vol. 12, no. 6, pp. 2697-2704, 2012.

[183] N. Zhang *et al.*, "Electrospun TiO2 nanofiber-based cell capture assay for detecting circulating tumor cells from colorectal and gastric cancer patients," *Advanced Materials,* vol. 24, no. 20, pp. 2756-2760, 2012.

[184] H. J. Yoon *et al.*, "Sensitive capture of circulating tumour cells by functionalized graphene oxide nanosheets," *Nature nanotechnology,* vol. 8, no. 10, p. 735, 2013.

[185] M. Abdolahad, M. Taghinejad, H. Taghinejad, M. Janmaleki, and S. Mohajerzadeh, "A vertically aligned carbon nanotube-based impedance sensing biosensor for rapid and high sensitive detection of cancer cells," *Lab on a Chip,* vol. 12, no. 6, pp. 1183-1190, 2012.

[186] G. D. Chen, F. Fachin, E. Colombini, B. L. Wardle, and M. Toner, "Nanoporous micro-element arrays for particle interception in microfluidic cell separation," *Lab on a Chip,* vol. 12, no. 17, pp. 3159-3167, 2012.

[187] F. Khosravi, S. M. Loeian, and B. Panchapakesan, "Ultrasensitive label-free sensing of IL-6 based on PASE functionalized carbon nanotube micro-arrays with RNA-aptamers as molecular recognition elements," *Biosensors,* vol. 7, no. 2, p. 17, 2017.

[188] F. Khosravi, "Carbon nanotubes micro-arrays: characterization and application in biosensing of free proteins and label-free capture of breast cancer cells," 2016.

[189] S. Iijima, "Helical Microtubules of Graphitic Carbon," (in English), *Nature,* vol. 354, no. 6348, pp. 56-58, Nov 7 1991.

[190] J.-M. Bonard, T. Stöckli, O. Noury, and A. Châtelain, "Field emission from cylindrical carbon nanotube cathodes: possibilities for luminescent tubes," *Applied Physics Letters,* vol. 78, no. 18, pp. 2775-2777, 2001.

[191] Y. Saito, S. Uemura, and K. Hamaguchi, "Cathode ray tube lighting elements with carbon nanotube field emitters," *Japanese Journal of Applied Physics,* vol. 37, no. 3B, p. L346, 1998.

[192] Y. Wang and J. T. Yeow, "A review of carbon nanotubes-based gas sensors," *Journal of Sensors,* vol. 2009, 2009.

[193] R. H. Baughman, A. A. Zakhidov, and W. A. De Heer, "Carbon nanotubes--the route toward applications," *science,* vol. 297, no. 5582, pp. 787-792, 2002.

[194] P. Liu *et al.*, "Fast High-Temperature Response of Carbon Nanotube Film and Its Application as an Incandescent Display," *Advanced Materials,* vol. 21, no. 35, pp. 3563-3566, 2009.

[195] H. Sugie, M. Tanemura, V. Filip, K. Iwata, K. Takahashi, and F. Okuyama, "Carbon nanotubes as electron source in an x-ray tube," *Applied Physics Letters,* vol. 78, no. 17, pp. 2578-2580, 2001.

[196] Y. Lin, F. Lu, Y. Tu, and Z. Ren, "Glucose biosensors based on carbon nanotube nanoelectrode ensembles," *Nano letters,* vol. 4, no. 2, pp. 191-195, 2004.

[197] X. Tang, S. Bansaruntip, N. Nakayama, E. Yenilmez, Y.-l. Chang, and Q. Wang, "Carbon nanotube DNA sensor and sensing mechanism," *Nano letters,* vol. 6, no. 8, pp. 1632-1636, 2006.

[198] K. Kempa *et al.*, "Photonic crystals based on periodic arrays of aligned carbon nanotubes," *Nano Letters,* vol. 3, no. 1, pp. 13-18, 2003.

[199] G. Liu, Y. Lin, Y. Tu, and Z. Ren, "Ultrasensitive voltammetric detection of trace heavy metal ions using carbon nanotube nanoelectrode array," *Analyst,* vol. 130, no. 7, pp. 1098-1101, 2005.

[200] S. Lu and B. Panchapakesan, "Nanotube micro-optomechanical actuators," *Applied Physics Letters,* vol. 88, no. 25, p. 253107, 2006.

[201] J. Loomis and B. Panchapakesan, "Dimensional dependence of photomechanical response in carbon nanostructure composites: a case for carbon-based mixed-dimensional systems," *Nanotechnology,* vol. 23, no. 21, p. 215501, 2012.

[202] Y. Tian *et al.*, "Analysis of the size distribution of single-walled carbon nanotubes using optical absorption spectroscopy," *The Journal of Physical Chemistry Letters,* vol. 1, no. 7, pp. 1143-1148, 2010.

[203] H. Zhu, C. Xu, D. Wu, B. Wei, R. Vajtai, and P. Ajayan, "Direct synthesis of long single-walled carbon nanotube strands," *Science,* vol. 296, no. 5569, pp. 884-886, 2002.

[204] O. V. Kharissova and B. I. Kharisov, "Variations of interlayer spacing in carbon nanotubes," *Rsc Advances,* vol. 4, no. 58, pp. 30807-30815, 2014.

[205] H. Dai, "Carbon nanotubes: opportunities and challenges," *Surface Science,* vol. 500, no. 1-3, pp. 218-241, 2002.

[206] J. Hass, W. De Heer, and E. Conrad, "The growth and morphology of epitaxial multilayer graphene," *Journal of Physics: Condensed Matter,* vol. 20, no. 32, p. 323202, 2008.

[207] A. Krishnan, E. Dujardin, T. Ebbesen, P. Yianilos, and M. Treacy, "Young's modulus of single-walled nanotubes," *Physical review B,* vol. 58, no. 20, p. 14013, 1998.

[208] M.-F. Yu, O. Lourie, M. J. Dyer, K. Moloni, T. F. Kelly, and R. S. Ruoff, "Strength and breaking mechanism of multiwalled carbon nanotubes under tensile load," *Science,* vol. 287, no. 5453, pp. 637-640, 2000.

[209] D. V. Smitherman Jr, "Technology Development and Demonstration Concepts for the Space Elevator," 2004.

[210] C. Journet *et al.,* "Large-scale production of single-walled carbon nanotubes by the electric-arc technique," *Nature,* vol. 388, no. 6644, p. 756, 1997.

[211] D. Bethune *et al.,* "Cobalt-catalysed growth of carbon nanotubes with single-atomic-layer walls," *Nature,* vol. 363, no. 6430, p. 605, 1993.

[212] A. Thess *et al.*, "Crystalline ropes of metallic carbon nanotubes," *Science,* vol. 273, no. 5274, pp. 483-487, 1996.

[213] A. M. Cassell, J. A. Raymakers, J. Kong, and H. Dai, "Large scale CVD synthesis of single-walled carbon nanotubes," *The Journal of Physical Chemistry B,* vol. 103, no. 31, pp. 6484-6492, 1999.

[214] Y. Zhan, Z. Liu, S. Najmaei, P. M. Ajayan, and J. Lou, "Large-area vapor-phase growth and characterization of MoS2 atomic layers on a SiO2 substrate," *Small,* vol. 8, no. 7, pp. 966-971, 2012.

[215] J. W. Suk *et al.*, "Transfer of CVD-grown monolayer graphene onto arbitrary substrates," *ACS nano,* vol. 5, no. 9, pp. 6916-6924, 2011.

[216] K. Novoselov, A. Mishchenko, A. Carvalho, and A. C. Neto, "2D materials and van der Waals heterostructures," *Science,* vol. 353, no. 6298, p. aac9439, 2016.

[217] Q. Cao and J. A. Rogers, "Ultrathin films of single-walled carbon nanotubes for electronics and sensors: a review of fundamental and applied aspects," *Advanced Materials,* vol. 21, no. 1, pp. 29-53, 2009.

[218] K. Hata, D. N. Futaba, K. Mizuno, T. Namai, M. Yumura, and S. Iijima, "Water-assisted highly efficient synthesis of impurity-free single-walled carbon nanotubes," *Science,* vol. 306, no. 5700, pp. 1362-1364, 2004.

[219] T. Hiraoka *et al.*, "Synthesis of single-and double-walled carbon nanotube forests on conducting metal foils," *Journal of the American Chemical Society,* vol. 128, no. 41, pp. 13338-13339, 2006.

[220] C. L. Cheung, J. H. Hafner, and C. M. Lieber, "Carbon nanotube atomic force microscopy tips: Direct growth by chemical vapor deposition and application to high-resolution imaging," *Proceedings of the National Academy of Sciences,* vol. 97, no. 8, pp. 3809-3813, 2000.

[221] D.-m. Sun *et al.*, "Flexible high-performance carbon nanotube integrated circuits," *Nature nanotechnology,* vol. 6, no. 3, p. 156, 2011.

[222] W. Qian *et al.*, "The evaluation of the gross defects of carbon nanotubes in a continuous CVD process," *Carbon,* vol. 41, no. 13, pp. 2613-2617, 2003.

[223] J. Kong, H. T. Soh, A. M. Cassell, C. F. Quate, and H. Dai, "Synthesis of individual single-walled carbon nanotubes on patterned silicon wafers," *Nature,* vol. 395, no. 6705, p. 878, 1998.

[224] J. H. Hafner *et al.*, "Catalytic growth of single-wall carbon nanotubes from metal particles," *Chemical Physics Letters,* vol. 296, no. 1-2, pp. 195-202, 1998.

[225] P. Nikolaev *et al.*, "Gas-phase catalytic growth of single-walled carbon nanotubes from carbon monoxide," *Chemical physics letters,* vol. 313, no. 1-2, pp. 91-97, 1999.

[226] D. A. Heller, P. W. Barone, J. P. Swanson, R. M. Mayrhofer, and M. S. Strano, "Using Raman spectroscopy to elucidate the aggregation state of single-walled carbon nanotubes," *The Journal of Physical Chemistry B,* vol. 108, no. 22, pp. 6905-6909, 2004.

[227] H. Liu, D. Nishide, T. Tanaka, and H. Kataura, "Large-scale single-chirality separation of single-wall carbon nanotubes by simple gel chromatography," *Nature communications,* vol. 2, p. 309, 2011.

[228] O. Lourie, D. Cox, and H. Wagner, "Buckling and collapse of embedded carbon nanotubes," *Physical Review Letters,* vol. 81, no. 8, p. 1638, 1998.

[229] A. M. Heintz, J. Cafmeyer, J. D. Elhard, and B. R. Vijayendran, "Methods of dispersing carbon nanotubes," ed: US Patent App. 12/282,304, 2018.

[230] L. Vaisman, H. D. Wagner, and G. Marom, "The role of surfactants in dispersion of carbon nanotubes," *Advances in colloid and interface science,* vol. 128, pp. 37-46, 2006.

[231] X.-L. Xie, Y.-W. Mai, and X.-P. Zhou, "Dispersion and alignment of carbon nanotubes in polymer matrix: a review," *Materials science and engineering: R: Reports,* vol. 49, no. 4, pp. 89-112, 2005.

[232] H. T. Ham, Y. S. Choi, and I. J. Chung, "An explanation of dispersion states of single-walled carbon nanotubes in solvents and aqueous surfactant solutions using solubility parameters," *Journal of Colloid and Interface Science,* vol. 286, no. 1, pp. 216-223, 2005.

[233] M. S. Loeian, D. A. Ziolkowska, F. Khosravi, J. B. Jasinski, and B. Panchapakesan, "Exfoliated WS 2-Nafion Composite based Electromechanical Actuators," *Scientific reports,* vol. 7, no. 1, p. 14599, 2017.

[234] H. Pathangi, P. M. Vereecken, A. Klekachev, G. Groeseneken, and A. Witvrouw, "Quantifying the aggregation factor in carbon nanotube dispersions by absorption spectroscopy," *Journal of Nanoscience,* vol. 2014, 2014.

[235] M. J. Green, "Analysis and measurement of carbon nanotube dispersions: nanodispersion versus macrodispersion," *Polymer International,* vol. 59, no. 10, pp. 1319-1322, 2010.

[236] F. Khosravi, B. King, B. Panchapakesan, S. Rai, G. Kloecker, and E. Wickstrom, "Nanotube devices for digital profiling of cancer biomarkers and circulating tumor cells," in *The 7th IEEE International Conference on Nano/Molecular Medicine and Engineering*, 2013: IEEE, pp. 107-112.

[237] K. Sivakumar and B. Panchapakesan, "Electric Field–Assisted Deposition of Nanowires on Carbon Nanotubes for Nanoelectronics and Sensor Applications," *Journal of nanoscience and nanotechnology*, vol. 5, no. 2, pp. 313-318, 2005.

[238] B. C. King *et al.*, "Electrical detection of specific versus non-specific binding events in breast cancer cells," in *Biosensing and Nanomedicine V*, 2012, vol. 8460: International Society for Optics and Photonics, p. 84600S.

[239] J. Yu, N. Grossiord, C. E. Koning, and J. Loos, "Controlling the dispersion of multi-wall carbon nanotubes in aqueous surfactant solution," *Carbon,* vol. 45, no. 3, pp. 618-623, 2007.

[240] J. Liu *et al.*, "Fullerene pipes," *Science,* vol. 280, no. 5367, pp. 1253-1256, 1998.

[241] H. Kataura *et al.*, "Optical properties of single-wall carbon nanotubes," (in English), *Synthetic Met,* vol. 103, no. 1-3, pp. 2555-2558, Jun 1999.

[242] S. H. Jeong, K. K. Kim, S. J. Jeong, K. H. An, S. H. Lee, and Y. H. Lee, "Optical absorption spectroscopy for determining carbon nanotube concentration in solution," (in English), *Synthetic Met,* vol. 157, no. 13-15, pp. 570-574, Jul 2007.

[243] S. Giordani *et al.*, "Debundling of single-walled nanotubes by dilution: Observation of large populations of individual nanotubes in amide solvent dispersions," (in English), *J Phys Chem B,* vol. 110, no. 32, pp. 15708-15718, Aug 17 2006.

[244] M. Ouyang, J. L. Huang, and C. M. Lieber, "Fundamental electronic properties and applications of single-walled carbon nanotubes," (in English), *Accounts of Chemical Research,* vol. 35, no. 12, pp. 1018-1025, Dec 2002.

[245] S. D. Bergin *et al.*, "Large populations of individual nanotubes in surfactant-based dispersions without the need for ultracentrifugation," (in English), *J Phys Chem C,* vol. 112, no. 4, pp. 972-977, Jan 31 2008.

[246] M. J. O'connell *et al.*, "Band gap fluorescence from individual single-walled carbon nanotubes," *Science,* vol. 297, no. 5581, pp. 593-596, 2002.

[247] W. Kern, "Cleaning solution based on hydrogen peroxide for use in silicon semiconductor technology," *RCA review,* vol. 31, pp. 187-205, 1970.

[248] B. King and B. Panchapakesan, "Vacuum filtration based formation of liquid crystal films of semiconducting carbon nanotubes and high performance transistor devices," *Nanotechnology,* vol. 25, no. 17, p. 175201, 2014.

[249] S. Costa, E. Borowiak-Palen, M. Kruszynska, A. Bachmatiuk, and R. Kalenczuk, "Characterization of carbon nanotubes by Raman spectroscopy," *Materials Science-Poland*, vol. 26, no. 2, pp. 433-441, 2008.

[250] L. Kavan, P. Rapta, L. Dunsch, M. J. Bronikowski, P. Willis, and R. E. Smalley, "Electrochemical tuning of electronic structure of single-walled carbon nanotubes: in-situ Raman and Vis-NIR study," *The Journal of Physical Chemistry B*, vol. 105, no. 44, pp. 10764-10771, 2001.

[251] L. Alvarez *et al.*, "Resonant Raman study of the structure and electronic properties of single-wall carbon nanotubes," *Chemical Physics Letters*, vol. 316, no. 3-4, pp. 186-190, 2000.

[252] M. Dresselhaus, G. Dresselhaus, A. Jorio, A. Souza Filho, M. Pimenta, and R. Saito, "Single nanotube Raman spectroscopy," *Accounts of Chemical Research*, vol. 35, no. 12, pp. 1070-1078, 2002.

[253] F. Khosravi, P. Trainor, S. N. Rai, G. Kloecker, E. Wickstrom, and B. Panchapakesan, "Label-free capture of breast cancer cells spiked in buffy coats using carbon nanotube antibody micro-arrays," *Nanotechnology*, vol. 27, no. 13, p. 13LT02, 2016.

[254] M. S. Dresselhaus, G. Dresselhaus, R. Saito, and A. Jorio, "Raman spectroscopy of carbon nanotubes," *Physics reports*, vol. 409, no. 2, pp. 47-99, 2005.

[255] Y. Tian, H. Jiang, P. Laiho, and E. I. Kauppinen, "Validity of Measuring Metallic and Semiconducting Single-Walled Carbon Nanotube Fractions by Quantitative Raman Spectroscopy," *Analytical chemistry*, vol. 90, no. 4, pp. 2517-2525, 2018.

[256] A. R. Harutyunyan *et al.*, "Preferential growth of single-walled carbon nanotubes with metallic conductivity," *Science,* vol. 326, no. 5949, pp. 116-120, 2009.

[257] L. Qu, F. Du, and L. Dai, "Preferential syntheses of semiconducting vertically aligned single-walled carbon nanotubes for direct use in FETs," *Nano letters,* vol. 8, no. 9, pp. 2682-2687, 2008.

[258] E. Bragina, J. M. Vasiliev, and I. Gelfand, "Formation of bundles of microfilaments during spreading of fibroblasts on the substrate," *Experimental cell research,* vol. 97, no. 2, pp. 241-248, 1976.

[259] Z. Qin, L. Kreplak, and M. J. Buehler, "Hierarchical structure controls nanomechanical properties of vimentin intermediate filaments," *PloS one,* vol. 4, no. 10, p. e7294, 2009.

[260] M. A. Goldstein and M. L. Entman, "Microtubules in mammalian heart muscle," *The Journal of cell biology,* vol. 80, no. 1, pp. 183-195, 1979.

[261] M. Pilhofer, M. S. Ladinsky, A. W. McDowall, G. Petroni, and G. J. Jensen, "Microtubules in bacteria: ancient tubulins build a five-protofilament homolog of the eukaryotic cytoskeleton," *PLoS biology,* vol. 9, no. 12, p. e1001213, 2011.

[262] A. J. Tobin and J. Dusheck, *Asking about life*. Cengage Learning, 2005.

[263] A. Infante, M. Stein, Y. Zhai, G. Borisy, and G. Gundersen, "Detyrosinated (Glu) microtubules are stabilized by an ATP-sensitive plus-end cap," *Journal of Cell Science,* vol. 113, no. 22, pp. 3907-3919, 2000.

[264] D. Pastre, M. Cailleret, P. Curmi, and B. Mirela, "Methods and tools for detecting interactions in eukaryotic cells using microtubule structures and dynamics," ed: Google Patents, 2017.

[265] M. J. Dalby, M. O. Riehle, D. S. Sutherland, H. Agheli, and A. S. Curtis, "Use of nanotopography to study mechanotransduction in fibroblasts–methods and perspectives," *European journal of cell biology,* vol. 83, no. 4, pp. 159-169, 2004.

[266] A. D. Bershadsky, N. Q. Balaban, and B. Geiger, "Adhesion-dependent cell mechanosensitivity," *Annual review of cell and developmental biology,* vol. 19, no. 1, pp. 677-695, 2003.

[267] R. A. Whipple, A. M. Cheung, and S. S. Martin, "Detyrosinated microtubule protrusions in suspended mammary epithelial cells promote reattachment," *Experimental cell research,* vol. 313, no. 7, pp. 1326-1336, 2007.

[268] D. Taichman *et al.*, "Tumor cell surface alpha 4 beta 1 integrin mediates adhesion to vascular endothelium: demonstration of an interaction with the N-terminal domains of INCAM-110/VCAM-1," *Cell regulation,* vol. 2, no. 5, pp. 347-355, 1991.

[269] Y. Li *et al.*, "Antibody-Modified Reduced Graphene Oxide Films with Extreme Sensitivity to Circulating Tumor Cells," *Advanced Materials,* vol. 27, no. 43, pp. 6848-6854, 2015.

[270] P. K. Mattila and P. Lappalainen, "Filopodia: molecular architecture and cellular functions," *Nature reviews Molecular cell biology,* vol. 9, no. 6, p. 446, 2008.

[271] M. Charpentier and S. Martin, "Interplay of stem cell characteristics, EMT, and microtentacles in circulating breast tumor cells," *Cancers,* vol. 5, no. 4, pp. 1545-1565, 2013.

[272] A. N. Killilea *et al.*, "Cytoskeletal organization in microtentacles," *Experimental cell research,* vol. 357, no. 2, pp. 291-298, 2017.

[273] K. Margaris and R. A. Black, "Modelling the lymphatic system: challenges and opportunities," *Journal of the Royal Society Interface,* vol. 9, no. 69, pp. 601-612, 2012.

[274] A. S. Popel and P. C. Johnson, "Microcirculation and hemorheology," *Annu. Rev. Fluid Mech.,* vol. 37, pp. 43-69, 2005.

[275] L. Antiga and D. A. Steinman, "Rethinking turbulence in blood," *Biorheology,* vol. 46, no. 2, pp. 77-81, 2009.

[276] K. A. Rejniak, "Investigating dynamical deformations of tumor cells in circulation: predictions from a theoretical model," *Frontiers in oncology,* vol. 2, p. 111, 2012.

[277] L. Weiss, "Deformation-Driven, lethal damage to cancer cells," *Cell biophysics,* vol. 18, no. 2, p. 73, 1991.

[278] B. Wehrle-Haller, "Assembly and disassembly of cell matrix adhesions," *Current opinion in cell biology,* vol. 24, no. 5, pp. 569-581, 2012.

[279] G. F. Weber, M. A. Bjerke, and D. W. DeSimone, "Integrins and cadherins join forces to form adhesive networks," *J Cell Sci,* vol. 124, no. 8, pp. 1183-1193, 2011.

[280] R. Rathinam and S. K. Alahari, "Important role of integrins in the cancer biology," *Cancer and Metastasis Reviews,* vol. 29, no. 1, pp. 223-237, 2010.

[281] C. M. Kraning-Rush, J. P. Califano, and C. A. Reinhart-King, "Cellular traction stresses increase with increasing metastatic potential," *PloS one,* vol. 7, no. 2, p. e32572, 2012.

[282] G. Giannone and M. P. Sheetz, "Substrate rigidity and force define form through tyrosine phosphatase and kinase pathways," *Trends in cell biology,* vol. 16, no. 4, pp. 213-223, 2006.

[283] W. Chen *et al.*, "Nanoroughened adhesion-based capture of circulating tumor cells with heterogeneous expression and metastatic characteristics," *BMC cancer,* vol. 16, no. 1, p. 614, 2016.

[284] M. Imaninezhad, J. Schober, D. Griggs, P. Ruminski, I. Kuljanishvili, and S. P. Zustiak, "Cell Attachment and Spreading on Carbon Nanotubes Is Facilitated by Integrin Binding," *Frontiers in bioengineering and biotechnology,* vol. 6, 2018.

[285] S.-R. Ryoo, Y.-K. Kim, M.-H. Kim, and D.-H. Min, "Behaviors of NIH-3T3 fibroblasts on graphene/carbon nanotubes: proliferation, focal adhesion, and gene transfection studies," *ACS nano,* vol. 4, no. 11, pp. 6587-6598, 2010.

[286] L. Rodriguez-Fernandez, R. Valiente, J. Gonzalez, J. C. Villegas, and M. n. L. Fanarraga, "Multiwalled carbon nanotubes display microtubule biomimetic properties in vivo, enhancing microtubule assembly and stabilization," *ACS nano,* vol. 6, no. 8, pp. 6614-6625, 2012.

[287] K. Webb, V. Hlady, and P. A. Tresco, "Relationships among cell attachment, spreading, cytoskeletal organization, and migration rate for anchorage-dependent cells on model surfaces," *Journal of Biomedical Materials Research: An Official Journal of The Society for Biomaterials and The Japanese Society for Biomaterials*, vol. 49, no. 3, pp. 362-368, 2000.

[288] L. Chou, J. D. Firth, V.-J. Uitto, and D. M. Brunette, "Substratum surface topography alters cell shape and regulates fibronectin mRNA level, mRNA stability, secretion and assembly in human fibroblasts," *Journal of cell science*, vol. 108, no. 4, pp. 1563-1573, 1995.

[289] A. Khalili and M. Ahmad, "A review of cell adhesion studies for biomedical and biological applications," *International journal of molecular sciences*, vol. 16, no. 8, pp. 18149-18184, 2015.

[290] L. Chen *et al.*, "Aptamer-mediated efficient capture and release of T lymphocytes on nanostructured surfaces," *Advanced materials*, vol. 23, no. 38, pp. 4376-4380, 2011.

[291] X. Liu *et al.*, "Bio-inspired soft polystyrene nanotube substrate for rapid and highly efficient breast cancer-cell capture," *NPG Asia Materials*, vol. 5, no. 9, p. e63, 2013.

[292] E. Galanzha and V. Zharov, "Circulating tumor cell detection and capture by photoacoustic flow cytometry in vivo and ex vivo," *Cancers*, vol. 5, no. 4, pp. 1691-1738, 2013.

[293] K. Wang, S. Xie, Y. Ren, H. Xia, X. Zhang, and J. He, "Establishment of a bioluminescent MDA-MB-231 cell line for human triple-negative breast cancer research," *Oncology reports,* vol. 27, no. 6, pp. 1981-1989, 2012.

[294] C. Raimondi, C. Nicolazzo, and A. Gradilone, "Circulating tumor cells isolation: the “post-EpCAM era”," *Chinese Journal of Cancer Research,* vol. 27, no. 5, p. 461, 2015.

[295] S. A. Joosse, T. M. Gorges, and K. Pantel, "Biology, detection, and clinical implications of circulating tumor cells," *EMBO molecular medicine,* vol. 7, no. 1, pp. 1-11, 2015.

[296] S. Hong, E. Ergezen, R. Lec, and K. A. Barbee, "Real-time analysis of cell–surface adhesive interactions using thickness shear mode resonator," *Biomaterials,* vol. 27, no. 34, pp. 5813-5820, 2006.

[297] B. Rack *et al.*, "Circulating tumor cells predict survival in early average-to-high risk breast cancer patients," *Journal of the National Cancer Institute,* vol. 106, no. 5, p. dju066, 2014.

[298] S. Nagrath *et al.*, "Isolation of rare circulating tumour cells in cancer patients by microchip technology," *Nature,* vol. 450, no. 7173, p. 1235, 2007.

[299] H. E. Liu *et al.*, "Workflow optimization of whole genome amplification and targeted panel sequencing for CTC mutation detection," *NPJ genomic medicine,* vol. 2, no. 1, p. 34, 2017.

[300] K. H. Wong *et al.*, "Whole blood stabilization for the microfluidic isolation and molecular characterization of circulating tumor cells," *Nature communications,* vol. 8, no. 1, p. 1733, 2017.

[301] S. R. Sirkisoon, R. L. Carpenter, T. Rimkus, L. Miller, L. Metheny-Barlow, and H.-W. Lo, "EGFR and HER2 signaling in breast cancer brain metastasis," *Frontiers in bioscience (Elite edition),* vol. 8, p. 245, 2016.

[302] N. L. Grupka, K. C. Lear-Kaul, B. K. Kleinschmidt-DeMasters, and M. Singh, "Epidermal growth factor receptor status in breast cancer metastases to the central nervous system: comparison with HER-2/neu status," *Archives of pathology & laboratory medicine,* vol. 128, no. 9, pp. 974-979, 2004.

[303] J. Gaedcke *et al.*, "Predominance of the basal type and HER-2/neu type in brain metastasis from breast cancer," *Modern Pathol,* vol. 20, no. 8, p. 864, 2007.

[304] B. L. Khoo, G. Grenci, Y. B. Lim, S. C. Lee, J. Han, and C. T. Lim, "Expansion of patient-derived circulating tumor cells from liquid biopsies using a CTC microfluidic culture device," (in English), *Nat Protoc,* vol. 13, no. 1, pp. 34-58, Jan 2018.

[305] W. J. Allard *et al.*, "Tumor cells circulate in the peripheral blood of all major carcinomas but not in healthy subjects or patients with nonmalignant diseases," (in English), *Clin Cancer Res,* vol. 10, no. 20, pp. 6897-6904, Oct 15 2004.

[306] P. K. Chaudhuri, B. C. Low, and C. T. Lim, "Mechanobiology of Tumor Growth," (in English), *Chem Rev,* vol. 118, no. 14, pp. 6499-6515, Jul 25 2018.

[307] M. J. Magbanua *et al.*, "Comprehensive genomic characterization of circulating tumor cells (CTCs) in metastatic breast cancer (MBC) sheds light on the biology of blood-borne metastasis," (in English), *Cancer Res,* vol. 77, Feb 2017.

[308] S. Gkountela, B. Szczerba, C. Donato, and N. Aceto, "Recent advances in the biology of human circulating tumour cells and metastasis," (in English), *Esmo Open,* vol. 1, no. 4, Jul 2016.

[309] K. Pantel and M. R. Speicher, "The biology of circulating tumor cells," (in English), *Oncogene,* vol. 35, no. 10, pp. 1216-1224, Mar 10 2016.

[310] S. H. Au *et al.*, "Microfluidic Isolation of Circulating Tumor Cell Clusters by Size and Asymmetry," (in English), *Scientific Reports,* vol. 7, May 26 2017.

[311] K. A. Hyun, K. Kwon, H. Han, S. I. Kim, and H. I. Jung, "Microfluidic flow fractionation device for label-free isolation of circulating tumor cells (CTCs) from breast cancer patients," (in English), *Biosens Bioelectron,* vol. 40, no. 1, pp. 206-212, Feb 15 2013.

[312] B. Rack *et al.*, "Circulating Tumor Cells Predict Survival in Early Average-to-High Risk Breast Cancer Patients," (in English), *Jnci-J Natl Cancer I,* vol. 106, no. 5, May 14 2014.

[313] Y. T. Lu *et al.*, "NanoVelcro Chip for CTC enumeration in prostate cancer patients," (in English), *Methods,* vol. 64, no. 2, pp. 144-152, Dec 1 2013.

[314] M. C. Miller, P. S. Robinson, C. Wagner, and D. J. O'Shannessy, "The Parsortix (TM) Cell Separation System-A versatile liquid biopsy platform," (in English), *Cytom Part A,* vol. 93a, no. 12, pp. 1234-1239, Dec 2018.

[315] T. M. Gorges *et al.*, "Improved detection of circulating tumor cells in metastatic colorectal cancer by the combination of the CellSearch® system and the AdnaTest®," *PloS one*, vol. 11, no. 5, p. e0155126, 2016.

[316] D. S. Micalizzi, S. Maheswaran, and D. A. Haber, "A conduit to metastasis: circulating tumor cell biology," (in English), *Gene Dev*, vol. 31, no. 18, pp. 1827-1840, Sep 15 2017.

[317] L. X. Clegg *et al.*, "Impact of socioeconomic status on cancer incidence and stage at diagnosis: selected findings from the surveillance, epidemiology, and end results: National Longitudinal Mortality Study," *Cancer causes & control*, vol. 20, no. 4, pp. 417-435, 2009.

[318] S. K. Lau *et al.*, "Impact of Socioeconomic Status on Pretreatment Weight Loss and Survival in Non–Small-Cell Lung Cancer," *Journal of oncology practice*, vol. 14, no. 4, pp. e211-e220, 2018.

[319] K. R. Yabroff, J. Lund, D. Kepka, and A. Mariotto, "Economic burden of cancer in the United States: estimates, projections, and future research," *Cancer Epidemiology and Prevention Biomarkers*, vol. 20, no. 10, pp. 2006-2014, 2011.

[320] B. R. Park, S. Y. Kim, D. W. Shin, H. K. Yang, and J. H. Park, "Influence of Socioeconomic Status, Comorbidity, and Disability on Late-stage Cancer Diagnosis," *Osong public health and research perspectives*, vol. 8, no. 4, p. 264, 2017.

[321] C. Præstegaard *et al.*, "The association between socioeconomic status and tumour stage at diagnosis of ovarian cancer: A pooled analysis of 18 case-control studies," *Cancer epidemiology,* vol. 41, pp. 71-79, 2016.